Year : 2017

FUNCTIONAL AND STRUCTURAL TOPOGRAPHY WITHIN CORTICO- SUBCORTICAL LOOPS IN PARKINSON'S DISEASE USING MAGNETIC RESONANCE IMAGING

Marquis Renaud

UNIL | Université de Lausanne
Faculté de biologie
et de médecine

Département des Neurosciences Cliniques

FUNCTIONAL AND STRUCTURAL TOPOGRAPHY WITHIN CORTICO-SUBCORTICAL LOOPS IN PARKINSON'S DISEASE USING MAGNETIC RESONANCE IMAGING

Thèse de doctorat en Neurosciences

présentée à la

Faculté de Biologie et de Médecine
de l'Université de Lausanne

par

Renaud MARQUIS

Neuroscientifique diplômé de l'Université de Genève, Suisse

Jury

Prof. Kim Do Cuénod, Président
Prof. Bogdan Draganski, Directeur
Dr. Ferath Kherif, Co-Directeur
Prof. Stéphane Lehéricy, Expert
Dr. Thilo Van Eimeren, Expert

Thèse n° 208

Lausanne 2017

Programme doctoral interuniversitaire en Neurosciences des Universités de Lausanne et Genève

LEMANIC NEURO SCIENCE DOCTORAL SCHOOL

UNIL | Université de Lausanne

UNIVERSITÉ DE GENÈVE

UNIL | Université de Lausanne

UNIVERSITÉ DE GENÈVE

Programme doctoral interuniversitaire en Neurosciences
des Universités de Lausanne et Genève

Imprimatur

Vu le rapport présenté par le jury d'examen, composé de

Président·e	Madame Prof. Kim **Do Cuénod**
Directeur·trice de thèse	Monsieur Prof. Bogdan **Draganski**
Co-directeur·trice de thèse	Monsieur Dr Ferath **Kherif**
Expert·e·s	Monsieur Prof. Stéphane **Lehéricy**
	Monsieur Dr Thilo **Van Eimeren**

le Conseil de Faculté autorise l'impression de la thèse de

Monsieur Renaud Marquis

Master interdisciplinaire en Neurosciences, Genève

intitulée

FUNCTIONAL AND STRUCTURAL TOPOGRAPHY WITHIN CORTICO-SUBCORTICAL LOOPS IN PARKINSON'S DISEASE USING MAGNETIC RESONANCE IMAGING

Lausanne, le 3 juillet 2017

pour Le Doyen
de la Faculté de Biologie et de Médecine

Prof. Kim Do Cuénod

Source: https://en.wikipedia.org/wiki/File:Phrenology-journal.jpg

De ces prémisses incontroversables il déduisit que la Bibliothèque est totale, et que ses étagères consignent toutes les combinaisons possibles des vingt et quelques symboles orthographiques (nombre, quoique très vaste, non infini), c'est-à-dire tout ce qu'il est possible d'exprimer, dans toutes les langues. Tout: l'histoire minutieuse de l'avenir, les autobiographies des archanges, le catalogue fidèle de la Bibliothèque, des milliers et des milliers de catalogues mensongers, la démonstration de la fausseté de ces catalogues, la démonstration de la fausseté du catalogue véritable, l'évangile gnostique de Basilide, le commentaire de cet évangile, le commentaire du commentaire de cet évangile, le récit véridique de ta mort, la traduction de chaque livre en toutes les langues, les interpolations de chaque livre dans tous les livres; le traité que Beda ne put écrire (et n'écrivit pas) sur la mythologie des Saxons, ainsi que les livres perdus de Tacite.

Jorge Luis Borges, *La Bibliothèque de Babel (1941)*.

Œuvres complètes, tome 1 (1993) pour la traduction française.

À mon épouse Eléonore et mon fils Caleb, qui ont toujours été présents, dans mon cœur et mon esprit, et m'ont aidé à traverser ce labyrinthe, même dans les plus sombres recoins.

Acknowledgments

I would like to thank my thesis director, Prof. Bogdan Draganski, and my thesis supervisor, Dr. Ferath Kherif, for their continuous support and guidance throughout this thesis work. I learned a lot during my PhD thanks to your amazing mentoring and suggestions.

I would like also to sincerely thank the external experts of my thesis committee, Prof. Stéphane Lehéricy and Dr. Thilo Van Eimeren, as well as the jury president, Prof. Kim Do Cuénod.

I am also very grateful to the medical doctors and colleagues in the Clinique des Mouvements Anormaux at CHUV for their generous help for the recruitment of patients and her constructive suggestions, especially Dr. Deepa Pothalil for her help with motor examinations and for her professionalism.

I would like to thank Kay Corday and coworkers from the Atelier CES-Brico at Cery, who made the wood part of the custom device we used in this study.

I am very grateful to the Swiss National Science Foundation, Foundation Parkinson Switzerland, Foundation Synapsis, Roger De Spoelberch and Partridge Foundations as well as the European Union Seventh Framework Programme for their generous financial support. I want also to express my gratitude to the Clinical Neuroscience Department at CHUV for providing the research infrastructure.

I want to give special thanks to all my colleagues and friends at LREN. I want to thank Estelle Dupuis for her support with scanning, Rémi Castella for his help building the custom device, and Dr. Sara Lorio for the fruitful collaboration and support for writing. I want to thank also Dr. Antoine Lutti, who helped me a lot for improving my writing and understanding of MRI physics. I want to thank also Dr. Sandrine Muller and David Slater for the passionate exchanges we had and their support for performing analyses with cutting-edge tools. Many thanks also to Dr. Elisabeth Roggenhofer for her help with motor examinations and sharing insights in Parkinson's disease from a neuroscientific and clinical perspective. I will miss all the fascinating discussions I had with you, Dr. Anne Ruef and Dr. Lester Mélie Garcia in particular.

I especially want to express my immense gratitude to my family for her continuous support and help during these exhausting years. In particular, I want to thank Charlotte for having reviewed the writing of this thesis, Sylviane and Daniel for having taken care of Caleb so that I could finish it. I want to thank all of you for your encouragement.

I want also to thank my son, Caleb, who helped me to take a step back when I was too much involved. Last but not least, I will never thank my wife enough. Eléonore, you endured it

with me, you supported me, you encouraged me, you helped me, you took care of Caleb without me so many times, you had to do everything I should have normally do, so that I could finally finish this thesis. Thanks for reminding me of childhood memories where everything was as fresh as the bright blue sky.

Abstract

Parkinson's disease (PD) is a debilitating neurodegenerative disorder due to loss of dopamine producing cells in the substantia nigra. Given the fact that clinical symptoms emerge after a long preclinical period with gradual decline in dopamine production, there is pressing need to advance our understanding about the progression of motor and non-motor symptoms in symptomatic phase of PD. Recent theoretical work and animal models suggest a link between dopamine-dependent loss of neuronal specificity (LOS) in the basal ganglia (BG) and a broad range of symptoms in movement disorders. The overall goal of my thesis project was to test and validate this hypothesis *in vivo* using non-invasive magnetic resonance imaging (MRI). In a preparatory study for my main experiment, I evaluate how the spatial resolution of different MRI protocols impacts BGs motor somatotopy mapping. The second study tests the LOS hypothesis in PD patients and how functional segregation of motor somatotopy is affected by dopamine substitution. In a following study I expand the LOS hypothesis on the insular cortex, which shares major connections with the BG. My last experiment extends these findings to structural connectivity patterns of projections between thalamus, BG and cortex. I am truly convinced that my thesis project will contribute to advance our understanding of PD pathophysiology that helps monitoring and predicting clinical outcome.

Résumé

La maladie de Parkinson (MP) est une maladie neurodégénérative débilitante résultant de la perte des cellules dopaminergiques dans la substance noire. Etant donné l'émergence de symptômes cliniques après une longue période préclinique caractérisée par un déclin progressif de la production de dopamine, il est urgent de faire avancer notre compréhension de la progression des symptômes moteurs et non-moteurs dans la phase symptomatique de la MP. De récents travaux théoriques et modèles animaux suggèrent un lien entre une perte de la spécificité neuronale (PDS) dans les ganglions de la base (GB) dépendant de la dopamine et un large éventail de symptômes dans les troubles du mouvements. L'objectif général de mon projet de thèse était de tester et valider cette hypothèse *in vivo* en utilisant l'imagerie par résonance magnétique (IRM) non-invasive. Dans une étude préliminaire, j'ai évalué l'impact de la résolution spatiale de différents protocoles IRM sur la cartographie de la somatotopie motrice dans les GB. La deuxième étude teste l'hypothèse de la PDS chez des patients atteints de la MP et comment la ségrégation fonctionnelle de la somatotopie motrice est affectée par la substitution de dopamine. Dans l'étude suivante j'étends l'hypothèse de la PDS au cortex insulaire, qui partage d'importantes connections avec les GB. Ma dernière expérience étend ces découvertes aux patterns de connectivité structurelle entre le thalamus, les GB et le cortex. Je suis sincèrement convaincu que mon projet de thèse contribuera à l'avancée de notre compréhension de la pathophysiologie de la MP qui aide au suivi et à la prédiction de l'issue clinique.

Table of Contents

List of common abbreviations

AADC: amino acid decarboxylase

ACh: acetylcholine

AD: Alzheimer's disease

ADC: apparent diffusion coefficient

ADHD: attention deficit hyperactivity disorder

BG: basal ganglia

BOLD: blood-oxygen-level dependent

CBD: corticobasal degeneration

CSF: cerebrospinal fluid

DA: dopamine

DBS: deep brain stimulation

DMS: dorsomedial striatum

DLPFC: dorsolateral prefrontal cortex

DLS: dorsolateral striatum

DTI: diffusion tensor imaging

DWI: diffusion-weighted imaging

ECT: electroconvulsive therapy

EEG: electroencephalography

EMG: electromyography

EPI: echo planar imaging

ET: essential tremor

FA: fractional anistotropy

FDR: false discovery rate

fMRI: functional MRI

FOG: freezing of gait

FSI: fast-spiking interneurons

FTD: frontotemporal dementia

FWER: family-wise error rate

GABA: γ -aminobutyric acid

GDNF: glial cell line-derived neurotrophic factor

GLM: general linear model

GMV: grey matter volume

GPe: globus pallidus pars externa

GPi: globus pallidus pars interna

GTP: guanosine triphosphate

GTS: Gilles de la Tourette's syndrome

IoS: index of specificity

HC: healthy control

HD: Huntington's disease

LB: Lewy bodies

LIDs: levodopa-induced dyskinesias

LOS: loss of specificity

LTD: long-term depression

LTP: long-term potentiation

LTS: low-threshold spiking

M1: primary motor cortex

MAO: monoamine oxidase

MD: mean diffusivity

MNI: Montreal Neurologic Institute

MRI: magnetic resonance imaging

MS: multiple sclerosis

MSA: multiple system atrophy

MSNs: medium spiny neuron

MT: magnetization transfer

MVB: multivariate Bayes

NAcc: nucleus accumbens

NMDA: N-methyl-D-aspartate

NMS: non-motor symptoms

NPY: neuropeptide Y

OCD: obsessive compulsive disorders

PANs: phasically active neurons

PCA: principal component analysis

PCM: pattern component model

PD: Parkinson's disease

PET: positron emission tomography

PFC: prefrontal cortex

PNS: peripheral nervous system

PPN: pedunculopontine nucleus

PSP: progressive supranuclear palsy

RBD: rapid eye movement sleep behaviour disorder

RD: radial diffusivity

RL: reinforcement learning

RLS: restless legs syndrome

ROI: region of interest

RSA: representational similarity analysis

rTMS: repetitive transcranial magnetic stimulation

SMA: supplementary motor area

SN: substantia nigra

SNc: substantia nigra pars compacta

SNr: substantia nigra pars reticulata

SPECT: single-photon emission computed tomography

SPNs: spiny projection neurons

STN: subthalamic nucleus

T2*WI: T2*-weighted magnitude imaging

TANs: tonically active neurons

TMS: transcranial magnetic stimulation

VBM: voxel-based morphometry

VEGF: vascular endothelial growth factor

VTA: ventral tegmental area

1. Theoretical framework

In this introductory section, I define the core features of Parkinson's disease (PD) from a clinical and pathophysiological perspective by providing the current view on its pathogenesis from the perspective of structural and functional characteristics of cortico-subcortical loops. I also review the existing models explaining basal ganglia (BG) dysfunction in PD and other brain disorders. Finally, I emphasize on several different *in vivo* imaging approaches aiming to characterize its complex manifestations, monitoring its progression, providing clues into its pathophysiology and highlighting potential new venues for therapeutic strategies. Given the fact that I used functional MRI throughout the entire project, I focus on its methodological description. Research questions and general hypotheses are formulated for the experimental work section. Specific hypotheses and methodological procedures regarding data acquisition and analysis are demonstrated separately for each study in section 2.

1.1. Parkinson's disease

In the following section I review current knowledge of PD accumulated over the last decades. After a very brief history of research on PD, the latter is defined from the clinical point of view, in terms of symptoms and in regard to other neurological diseases. Following subsections provide an overview of PD epidemiology, risk and protective factors, as well as insights into its pathophysiology and etiology. The last subsection attempts to summarize treatment options available for patients, from conventional medical practices to experimental treatments undergoing pre-clinical studies.

1.1.1. A brief history

200 years after the publication of James Parkinson's essay (1817), there is still no cure for PD, the second most common neurodegenerative disorder after Alzheimer's disease (AD) (Dauer and Przedborski, 2003; De Virgilio et al., 2016), despite considerable progress achieved in the past decades. In the late 1950's, the main neurotransmitter lost in PD was localized in the brain and the first pharmacological model of PD was developed (Goetz, 2011). Later, Langston and colleagues (1983) observed that a self-administered narcotic derivative, 1-méthyl-4-phényl-1,2,3,6-tétrahydropyridine (MPTP), induced symptoms strikingly similar to that of PD. One of the most influential animal models of PD was born (Dauer and Przedborski, 2003). The discovery of this neurotoxin triggered an exponential increase of studies on PD (**Figure 1**). Nevertheless, the causes of PD remain unknown. The discrepancy between research investments and the puzzle of PD pathogenesis has recently led some researchers to question the existence of the disease entity itself and propose the usage of the term "syndrome" rather than "disease" (Titova et al., 2017).

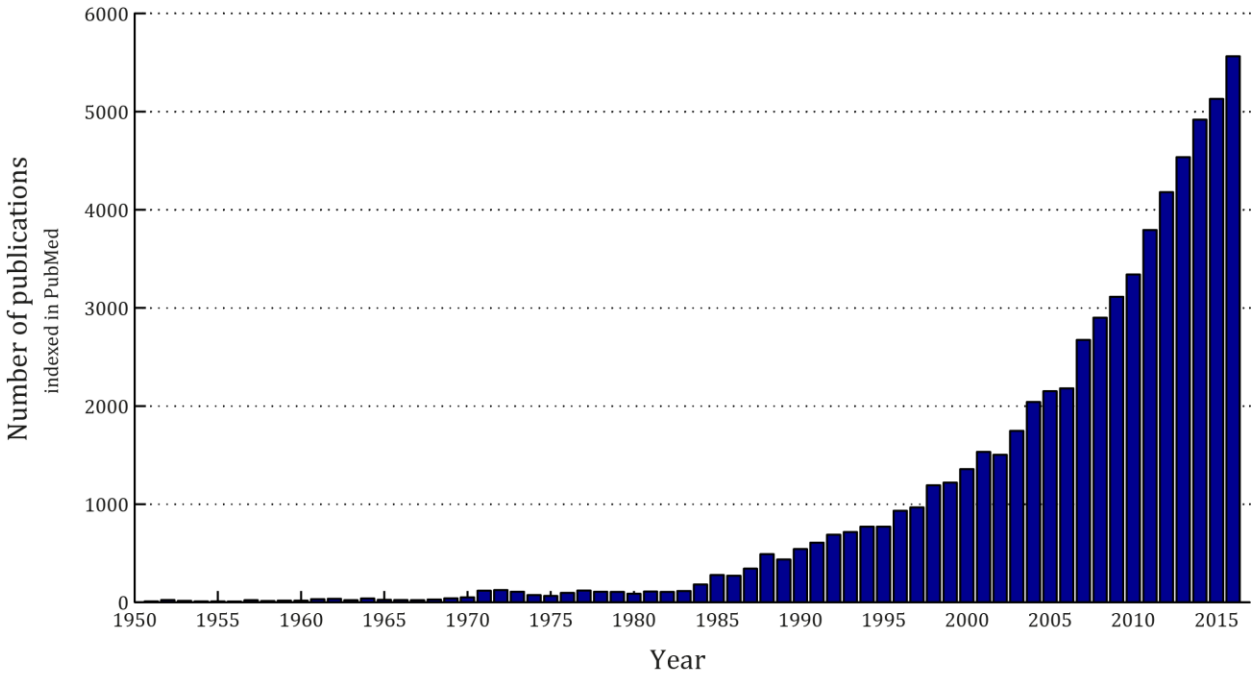

Figure 1: Number of publications referenced in the U.S. National Library of Medicine MEDLINE. A query was performed at http://dan.corlan.net/medline-trend.html using the keywords "Parkinson's disease".

1.1.2. Definition and symptoms

PD is a debilitating progressive neurodegenerative disease characterized by the following cardinal symptoms: generalized slowing of movements in the absence of weakness (bradykinesia), increased muscle tone (rigidity), postural instability and rest tremor, whose typical frequency lies between 4 and 6 Hz (Jankovic, 2008; Mazzoni et al., 2012). The terms "akinesia" and "hypokinesia" refer to specific aspects of motor symptoms, though their usage may vary: the former denotes the delayed initiation and the poverty or paucity of movements, whereas the latter designates the reduction of movement amplitude, force, or both (Dauer and Przedborski, 2003; Mazzoni et al., 2012). Other clinical signs resulting from the cardinal features include hypomimia, dysarthria, hypophonia, sialorrhoea, dysphagia, decreased arm swing, shuffling gait, festination, difficulty arising from a chair or turning in a bed, micrographia, striatal position of fingers and toes, glabellar tap reflex, blepharospasm, dystonia, scoliosis and camptocormia (Dauer and Przedborski, 2003; Jankovic, 2008; Moustafa et al., 2016).

According to the UK Parkinson's Disease Society Brain Bank's clinical criteria, a diagnosis of probable PD can be made when bradykinesia and at least one of the other three cardinal symptoms are present (Hughes et al., 1992). While the National Institute of Neurological Disorders and Stroke proposes slightly different diagnosis criteria (Gelb et al., 1999), a unilateral disease onset with later persistent asymmetry, a progressive disorder course

lasting 10 years or more, and an excellent response to dopamine (DA) replacement therapy leading to severe dyskinesias are all supportive criteria (Jankovic, 2008). It has to be noted however that tremor is a peculiar symptom: it does not progress at the same rate as other cardinal symptoms, responds less well to DAergic treatment, can occur on the body side contralateral to the one most affected by other symptoms, is absent in up to one out of four patients, and its severity does not correlate with other symptoms (Helmich et al., 2012; Lang and Lozano, 1998a).

In addition, non-motor symptoms (NMS) are frequent in PD and gained recently more attention because they may precede classical motor abnormalities and the hallmark of the neurodegenerative process (De Virgilio et al., 2016; Miller and O'Callaghan, 2015). NMS comprise bradyphrenia, cognitive impairment, depression, apathy, anhedonia, fatigue, hyposmia, ageusia, deafness, pain, paraesthesias, weight loss, hallucinations, delusion, psychiatric symptoms such as psychosis and paranoia, disturbance of sleep and wakefulness such as excessive daytime sleepiness or rapid eye movement sleep behaviour disorder (RBD), and disorders of the autonomic nervous system such as constipation, hypotension, urinary frequency, impotence and sweating (Bosboom et al., 2004; Burn, 2002a, 2002b; Chaudhuri et al., 2006; Davie, 2008; De Virgilio et al., 2016; Jankovic, 2008; Kaji and Hirata, 2011; Kalia and Lang, 2015; Kirsch-Darrow et al., 2011; Lang and Lozano, 1998a; Mizuno et al., 2008; Postuma and Berg, 2016; Robbins and Cools, 2014; Sharma et al., 2013). NMS in PD are not negligible: cognitive impairment leads to dementia in 83% of patients with a disease duration of 20 year, depression affects 25% to 50% of patients and psychosis can occur in up to 30% of patients. Although neuro-behavioural measures may be confounded, interesting analogies between NMS and motor symptoms can be made, for example between apathy and akinesia, bradyphrenia and bradykinesia, difficulties in movement sequences and shifting set in learning situations (Mandir and Vaughan, 2000).

Objective tests can measure various symptomatic aspects of PD. For example, tremor can be quantified using muscle action potentials, hyposmia can be measured with the University of Pennsylvania's Smell Identification Test (UPSIT) and polysomnography can detect RBD (De Virgilio et al., 2016; Kalia and Lang, 2015; Sharma et al., 2013). Most importantly, PD diagnosis mostly relies on the clinical picture. Disease severity is typically assessed by the Unified Parkinson's Disease Rating Scale (UPDRS; Fahn et al., 1987). The latter has been recently revised by the Movement Disorder Society (Goetz et al., 2008) and comprises different subscales that aim at capturing cognitive, behavioural, motivational and psychiatric symptoms (UPDRS I), the impairment during activities of daily living (UPDRS II), motor symptoms (UPDRS III) and complications (UPDRS IV). Other scales of disease progression or disability, such as the Hoehn and Yahr staging (Hoehn and Yahr, 1967) or the Schwab and England activities of daily living scale (Schwab and England, 1969), are sometimes referred to as UPDRS V and VI respectively. While the premotor phase can last 12 to 14 years, NMS, motor complications due to DAergic therapy and

treatment-resistant motor symptoms such as choking, freezing of gait (FOG) and falls prevail in late-stage PD (Baas, 2000; Bargiotas and Konitsiotis, 2013; De Virgilio et al., 2016; Tinazzi, 2006). Besides a decreased quality of life, mortality increases considerably with PD, reported as being 1.5 to 2.7 times as high as age-matched healthy individuals, up to a hazard ratio of 5 (Lang and Lozano, 1998a; de Lau and Breteler, 2006). However PD is marked by heterogeneity (Obeso et al., 2010), in terms of age of onset, rate of disease progression and clinical symptoms (Kempster et al., 2010; Lotharius and Brundin, 2002). These factors will vary noticeably as a function of the precise form of parkinsonian syndrome (Williams and Litvan, 2013).

Indeed, the diagnosis of PD is a clinical one that besides resembling essential tremor (ET) due to the presence of tremor (Deuschl and Bergman, 2002; Jankovic, 2008), is sometimes difficult to differentiate from other disorders with distinct pathophysiology - multiple system atrophy (MSA), progressive supranuclear palsy (PSP) and corticobasal degeneration (CBD). Additionally, there are a number of other differential diagnoses including vascular parkinsonism, dystonia, frontotemporal dementia (FTD), Niemann-Pick disease type C, and prion disease (Williams and Litvan, 2013). Another terminology frequently used to avoid misdiagnosis refers to "atypical" or "secondary" parkinsonism (Martí and Tolosa, 2013).

Most PD cases are sporadic – i.e. not linked to a known genetic factor, hence called also "idiopathic" PD. The genetic forms of PD account for only 5-10% of the cases (Calì et al., 2011; Dauer and Przedborski, 2003; Lill, 2016; Pan and Yue, 2013; Spatola and Wider, 2013; Thenganatt and Jankovic, 2014; Winklhofer and Haass, 2010; Wood-Kaczmar et al., 2006). Additionally, recent studies suggested that several subtypes can be identified in PD patients (Marras and Chaudhuri, 2016; Moustafa and Poletti, 2013; Thenganatt and Jankovic, 2014). This heterogeneity poses important issues for the diagnosis of PD: underdiagnosis is not rare, and misdiagnosis has been reported in 24% of the cases (Lang and Lozano, 1998a). As a consequence, an *in vivo* biomarker of PD onset, progression and prognosis is urgently needed, as its definitive diagnosis still relies on neuropathological examination at autopsy (Lang and Lozano, 1998a; Miller and O'Callaghan, 2015). Supportive diagnostic criteria do not suffice: asymmetric onset may be seen in CBD and hemiparkinsonism-hemiatrophy, and the response to DAergic therapy can be initially encouraging in patients with MSA (Lang and Lozano, 1998a).

1.1.3. Epidemiology

With an incidence of 8 to 18 per 100'000 person-years, PD affects 0.3% of the entire population (de Lau and Breteler, 2006; Sveinbjornsdottir, 2016), in all ethnic groups, with only a little predominance among males (Lang and Lozano, 1998a; de Lau and Breteler, 2006). Other surveys consider gender as an established factor and report a male-to-female ratio of 3:2 (De Virgilio et al., 2016). This general prevalence increases exponentially with

age, with 1-2% of the population over 65 years old and 3-5% after 85 years old (Alves et al., 2008; Lang and Lozano, 1998a; de Lau and Breteler, 2006). Although estimates might vary depending on the methodology (de Lau and Breteler, 2006), it is believed that the number of people with PD will increase by more than 50% by 2030 (De Virgilio et al., 2016) and that PD could surpass cancer by becoming the second most common cause of death in elderly by the year 2040 (Lilienfeld and Perl, 1994).

1.1.4. Risk- and protective factors

Age represents the biggest risk factor for PD (De Virgilio et al., 2016; Reeve et al., 2014). The links between age and PD is so strong that Rodriguez et al. (2015) suggested that there might be a common aetiology for ageing and PD, and that PD can be interpreted in the context of accelerated ageing triggered by insufficient mitochondrial homeostasis and compensatory mechanisms. Several environmental risk factors, such as the use of beta-blocker and prior head injury, have been proposed (De Virgilio et al., 2016; Kalia and Lang, 2015). Although subject to controversy and despite the lack of data implicating a specific toxin in PD, living in a rural environment, agricultural occupation, drinking from a water well and exposure to pesticides, herbicides, plant-derived toxins, organic solvents, carbon monoxide, carbon disulfide, bacterial and viral infection have been generally considered to increase the risk of developing PD (Dauer and Przedborski, 2003; De Virgilio et al., 2016; Kalia and Lang, 2015; Lang and Lozano, 1998a; Schapira and Jenner, 2011). Nevertheless, the fact that the proportion of patients with PD exposed to pesticides has been estimated to only 10% spreads doubts on the importance of rural environment as a risk factor, and even if an important causative role of exogenous toxins might be inferred from the fact that the first formal description of the disease occurred during the Industrial Revolution, descriptions of akinetic and tremulous symptoms strikingly similar to PD were found between 4500 and 1000 B.C. (Lang and Lozano, 1998a). Other factors such as alcohol consumption, cancer and dietary habits – including fat, fatty acids, iron and nutriments influencing homocysteine concentration – led to inconclusive results but drinking coffee had protective effects, and smoking has been shown to drastically reduce the risk of PD by half (Lang and Lozano, 1998a; de Lau and Breteler, 2006).

More recently, vagotomy, the use of anti-inflammatory drugs, antihypertensives, antilipidaemics and physical activity were associated with a decreased risk of developing PD, whereas olfactory disturbances, risk-avoiding personality type, depression and anxiety were linked to a higher risk of future PD (De Virgilio et al., 2016; de Lau and Breteler, 2006; Petzinger et al., 2013; Schapira and Jenner, 2011; Svensson et al., 2015). Although the significance of antioxidants has been the matter of controversy (Filograna et al., 2016; de Lau and Breteler, 2006), latest studies also suggest that these may have protective effects in relation to the possible role of reactive oxygen species in PD pathogenesis (Ataie et al., 2016; Magalingam et al., 2015). Coenzyme Q10, mitochondrial ubiquinone-NADH

173 oxidoreductase, melatonin, metallothioneins, N-acetyl-aspartate, and superoxide dismutase
174 may also have neuroprotective effects (Sharma et al., 2013).

Gene	**OMIM[1] entry**	**Function**
PTEN-induced putative kinase 1 (*PINK1*; *PARK6)*	608309	Mitochondrial function and mitophagy
DJ-1 (*PARK7*)	602533	
Coiled-coil-helix-coiled-coil-helix domain-containing protein 2 (*CHCHD2)*	616244	
POLG1	174763	
Sterol regulatory element-binding transcription factor 1 (*SREBF1)*	184756	
Parkin (PRKN, PARK2)	602544	Mitochondrial function and mitophagy, UPS
F-box only protein 7 (*FBXO7*; *PARK15)*	605648	Ubiquitin–proteasome system (UPS)
Ataxin 3 (*ATXN3*	607047	
RAB39B	300774	Regulation of protein membrane and trafficking
Cyclin G-associated kinase (*GAK)*	602052	
RAB7L1	603949	
Vacuolar protein sorting-associated protein 35 (*VPS35*; *PARK17)*	601501	Regulation of protein membrane and trafficking, lysosome autophagy pathway
DNAJC13	614334	
Leucine-rich repeat kinase 2 (*LRRK2*; *PARK8)*	609007	Regulation of protein membrane and trafficking, lysosome autophagy pathway, neurite structure, synaptic function and DA neurotransmission
Synuclein α (*SNCA*; *PARK1*; *PARK4)*	163890	Protein aggregation, synaptic vesicle formation, prion-like transmission, synaptic function and DA neurotransmission
Microtubule-associated protein tau (*MAPT)*	157140	Protein aggregation, synaptic vesicle formation, neurite structure
ATP13A2 (*PARK9*	610513	Lysosome autophagy pathway
Glucosylceramidase beta (*GBA)*	606463	
SCARB2	602257	
Synaptojanin-1 (*SYNJ1*; *PARK20)*	604297	Synaptic function and DA neurotransmission
Syntaxin-1B (STX1B)	601485	
guanosine triphosphate (*GTP) cyclohydrolase 1* (*GCH1)*	600225	

175 **Table 1**: Genes involved in PD.

[1] Online Mendelian Inheritance in Man (OMIM®); www.omim.org

Alternatively, neurodegeneration in PD might be triggered by a combination of inherited and environmental factors (Dauer and Przedborski, 2003; De Virgilio et al., 2016; Kalia and Lang, 2015; Lill, 2016; Schapira, 2006; Thomas and Beal, 2007). Genetic factors provided an important contribution to the understanding of PD, though as mentioned above inheritance accounts for only 5-10% of PD cases, at utmost 15% (Mochizuki, 2009; Wider et al., 2010). More specifically, genetic influence seems determinant in 2–3% of the late-onset forms and ~50% of early-onset cases (Obeso et al., 2010). Genes identified as playing a role in PD (**Table 1**) influence various molecular pathways (Abou-Sleiman et al., 2006; Feany, 2004; Haelterman et al., 2014; Kalia and Lang, 2015; de Lau and Breteler, 2006; Moore et al., 2005; Pan and Yue, 2013; Thenganatt and Jankovic, 2014; Valadas et al., 2014), which will be discussed in detail in section 1.1.6.

Mutations in *ATP13A2*, *FBXO7*, *POLG1*, *ATXN3* and *SYNJ1* are usually found in atypical forms of parkinsonism with juvenile onset and presenting pyramidal signs, gait disturbance, ophthalmologic abnormalities and cognitive impairments (Kalia and Lang, 2015). While *SNCA*, *LRRK2*, *VPS35*, *EIF4G1*, *DNAJC13* and *CHCHD2* are associated with autosomal dominant forms of PD, *PRKN*, *PINK1* and *DJ-1* seem to mediate autosomal recessive forms with early age of onset and slow disease course (Abou-Sleiman et al., 2006; Bonifati, 2013; Gandhi, 2005; Kalia and Lang, 2015; Mizuno et al., 2008; Schapira, 2006; Steece-Collier et al., 2002; Surmeier et al., 2011a; Winklhofer and Haass, 2010; Wood-Kaczmar et al., 2006). Other genes possibly involved in PD include *eukaryotic translation initiation factor 4 gamma 1* (*EIF4G1*; *PARK18*; OMIM 600495), *chromosome 9 open reading frame 72* (*C9ORF72*; OMIM 614260), *phospholipase A2 group VI* (*PLA2G6*; *PARK14*; OMIM 603604), *ubiquitin carboxy-terminal hydrolase L1* (*UCH-L1*; *PARK5*; OMIM 191342), *fibroblast growth factor 20* (*FGF20*; OMIM 605558), *HtrA serine peptidase 2* (*HTRA2*; *OMI*; *PARK13*; OMIM 606441), *nuclear receptor subfamily 4 group A member 2* (*NURR1*; *NR4A2*; OMIM 601828), *GRB10 interacting GYF protein 2* (*GIGYF2*; *PARK11*; OMIM 612003), *granulin precursor* (*GRN*; OMIM 138945), *dynactin 1* (*DCTN1*; OMIM 601143), *FBXO2* (OMIM 607112), *DNAJC6* (OMIM 608375), *ataxin 2* (*ATXN2*; OMIM 601517), *spatacsin* (*SPG11*; OMIM 610844) and *RAB39B* (OMIM 300774) (Bose and Beal, 2016; Hardy, 2010; Kalia and Lang, 2015; Lill, 2016; Moore et al., 2005; Obeso et al., 2010; Schapira, 2006; Thenganatt and Jankovic, 2014; Wider et al., 2010). Several genes linked to PD are also involved in other disease phenotypes. Variants of *SNCA* have been associated to MSA (Stefanis, 2012). Mutations to *ATXN2* and *ATXN3* cause spinocerebellar ataxia (SCA). *GBA* is notably known for its role in Gaucher's disease (Obeso et al., 2010). FTD and CBD are linked to mutations in *GRN* and *MAPT*. While *UCH-L1*, *HTRA2* and *GIGYF2* would be involved in autosomal dominant PD, *ATP13A2*, *PLA2G6*, *DNAJC6* and *FBXO7* would be implicated in autosomal recessive forms (Spatola and Wider, 2013; Thenganatt and Jankovic, 2014). Common genetic models used in mammals manipulate *SNCA*, *LRRK2*, *PRKN*, *DJ-1*, *PINK1* (Dawson et al., 2010; Jagmag et

al., 2016). Unfortunately, none of the animal models provide insights into selective SNc cells vulnerability (Dawson et al., 2010).

1.1.5. Pathophysiology

Between 5 and 15 years before the onset of clinical symptoms, neuromelanin containing DAergic neurons in the substantia nigra pars compacta (SNc) begin to die and α-synuclein, a small and flexible monomeric 140 amino acid protein characterized by a lack of secondary structure, starts to abnormally accumulate (Braak et al., 2004; Fearnley and Lees, 1991; Forno, 1996; Golbe, 1999; Miller and O'Callaghan, 2015; Postuma and Berg, 2016; Ross and Pickart, 2004; Stefanis, 2012). When the first motor symptoms appear, 60% of DAergic cells have been lost and about 80% of DA in the putamen is depleted (Dauer and Przedborski, 2003; Miller and O'Callaghan, 2015).

Together with the severe loss of DA in the striatum, the presence of eosinophillic intracytoplasmatic proteinaceous inclusions termed Lewy bodies (LB), and dystrophic Lewy neurites in surviving neurons has been reported primarily in the SNc, but also in regions thought to be involved in NMS, including the locus cœruleus, pedunculo-pontine nucleus, raphe nucleus, dorsal motor nucleus of the vagal nerve, hypothalamus, olfactory bulb, substantia innominata, parasympathetic and sympathetic post-ganglionic neurons, Meynert nucleus, amygdala and cerebral cortex – particularly the cingulate and entorhinal cortex (Dauer and Przedborski, 2003; Lang and Lozano, 1998a; Mizuno et al., 2008; Thomas and Beal, 2007). However LB are especially abundant in late-onset disease forms and their role in cell death remains unclear (Obeso et al., 2010). Furthermore, LB are not only found in PD but also in AD and in elderly people, in which they are even found at a greater frequency (Dauer and Przedborski, 2003).

Other neuronal systems comprising catecholaminergic – notably norepineprehine – and serotoninergic nuclei, as well as mesolimbic DAergic neurons in the ventral tegmental area (VTA), are considered less affected (Dauer and Przedborski, 2003; Lang and Lozano, 1998a; Lotharius and Brundin, 2002). This might explains the lesser DA depletion in the caudate, site of VTA neurons projection, as well as the greater dependence of synaptic DA clearance in the striatum on DA active transporter as compared to the prefrontal cortex (PFC), another critical projection site of VTA neurons where DA is modulated by other monoaminergic transporters and the synaptic enzyme catechol-O-methyltransferase (Dauer and Przedborski, 2003). It has to be noted that VTA neurons also project to the hippocampus and amygdala (Broussard et al., 2013; Shohamy and Adcock, 2010), the latter projecting further to the ventromedial striatum (Fudge et al., 2002), thereby increasing the complexity of DA circuitry. Therefore, patients with PD exhibit progressive, nonlinear loss of serotonergic function, which starts in the caudate, thalamus, hypothalamus and anterior

cingulate cortex and expands into other areas in the basal ganglia, limbic system and cortex with disease progression.

The levels of decline between the serotonergic and DAergic systems are similar in the caudate (reduction of 30–40%), but there is attenuated serotonergic loss (20–30%) compared with profound DAergic dysfunction (70–80%) in the putamen (Politis, 2014). Some evidence suggest that tremor might be related to serotoninergic rather than DAergic dysfunction (Politis, 2014). Serotonergic function is mainly affected in the raphe nuclei and several other brain regions involved in the regulation of sleep, arousal, satiety and emotion (Politis, 2014).

Falls in PD are related to decreased cholinergic innervation in the thalamus (Politis, 2014). FOG is associated with cortical grey matter loss and with decreased activity signal in striatal and extra-striatal regions (Politis, 2014). Limbic noradrenergic and DAergic function are reduced in patients with PD experiencing depression compared with those without depression. These decreases correlate with the severity of anxiety and apathy. Studies also showed a reduced striatal and thalamic serotonergic function and reduced DA capacity in the caudate of patients with PD who experience fatigue compared with those who do not (Politis, 2014). Patients with hallucinations show increased serotonin availability in the ventral visual pathway and other cortical regions, as well as increased glucose metabolism in the frontal cortex in those with psychosis (Politis, 2014). Patients with ICDs exhibit an abnormal increase in DA release in the ventral release (Stoessl et al., 2014). Similarly, increased activity in brain networks controlling reward and decreased activity in areas associated with behavioural inhibition is seen in patients with hypersexuality (Politis, 2014).

Cognitive dysfunctions are induced by a greater medial nigral cell loss, involving projections to the caudate (Lang and Lozano, 1998a). Dementia, gait dysfunction and falls in late-stage PD are thought to reflect the degeneration of hippocampal structures and cholinergic cortical inputs (Dauer and Przedborski, 2003; Kalia and Lang, 2015). However, degeneration in the Meynert nucleus, locus cœruleus, and cerebral cortex might also contribute to cognitive symptoms (Lang and Lozano, 1998a), although serotonergic and noradrenergic systems are not as well documented as those related to DA system (Dauer and Przedborski, 2003). Similarly, hyposmia, depression and dysautonomia are frequently linked to neurodegeneration in the olfactory bulb, brainstem serotoninergic and noradrenergic nuclei, and intermediolateral nucleus of the spinal cord as well as sympathetic and parasympathetic ganglia respectively (Lang and Lozano, 1998a). The amygdala might be involved in both behavioural and autonomic nervous system dysfunctions (Lang and Lozano, 1998a). More generally, dysfunctions in DAergic, cholinergic, glutamatergic, noradrenergic and serotoninergic systems are thought to contribute to symptoms in PD, and recent accounts suggest that the different motor and non-motor manifestations of the PD, which typically have a poor response to DAergic

medication in late-stage PD, might be linked to different patterns of neurodegeneration (Kalia and Lang, 2015; Lima et al., 2012; Tremblay et al., 2015).

Most importantly, the DA depletion follows a specific topology, different from the one observed in normal ageing: whereas the cell loss affects the ventrolateral tier and caudal aspects of the SNc in PD, it concentrates on the dorsomedial portion in healthy ageing (Dauer and Przedborski, 2003; Lang and Lozano, 1998a). The process underlying the death of DA neurons in PD is therefore different from the ones observed in striato-nigral degeneration, PSP and ageing, despite age being the most important risk factor for developing PD (Dauer and Przedborski, 2003; Lang and Lozano, 1998a). It results in a regionally specific pattern of striatal DA loss, starting in the dorsal putamen and considered to be responsible of akinesia and rigidity (Cools, 2006; Lang and Lozano, 1998a; Vaillancourt et al., 2013). Surprisingly, the majority of DAergic cells in the substantia nigra (SN) resides in the neuropil, a calbindin-rich area, while neurons most susceptible to PD seem to be found in calbindin-poor regions of the SNc (Dauer and Przedborski, 2003). Interestingly, the loss of striatal synaptic terminals seems more remarkable than SNc DA cell death. The protection of terminals in MPTP-treated mice prevents cell death in the SNc, indicating that abnormal neurite function and integrity in the striatum possibly precede somatic cell death in the SNc – i.e. a "dying back" process (Dauer and Przedborski, 2003), which as been considered as possibly resulting from alterations in structural functions of neurofilaments in axonal connections from the SNc to the striatum by LB (Lang and Lozano, 1998a).

Neurotoxin based models of PD attempt to mimic the pathophysiology and symptoms of PD using chemical compounds such as MPTP, a precursor of 1-methyl-4-phenylpyridinium (MPP+), 6-hydroxydopamine (6-OHDA), rotenone, N,N'dimethyl-4,4'-bipyridinium dichloride (Paraquat) and methamphetamine (Beal, 2001; Jagmag et al., 2016). While these models greatly improved our understanding of PD, most of them do not reproduce all features of PD or lack a detailed understanding of the causal chains of chemical events. The exception might be rotenone, which imitates successfully almost all features of PD, but has a low reproducibility due to high mortality in rats (Jagmag et al., 2016). Similarly, studies using actacystin, epoxomicin, or PSI (Z-lle-Glu(O*t*Bu)-Ala-Leu-al) raised hope for realistic models of PD. However, not only the neurotoxic effects are not as remarkable as initially reported, but also the reproducibility of these models is low (Schapira and Jenner, 2011).

1.1.6. Etiology

The common view on PD is that it results from a multi-factorial pathogenic process that explains the heterogeneity of PD clinical manifestations (Vila et al., 2008) and underlines the need for multiple biomarkers (De Virgilio et al., 2016; Kalia and Lang, 2015; Miller and O'Callaghan, 2015). The causes underlying PD pathophysiology are debated though several

potential culprits have been considered, such as mitochondrial dysfunction (Amano et al., 2014; Schapira and Gegg, 2011), Ca^{2+} dyshomeostasis (Calì et al., 2011; Surmeier et al., 2011a), neuroinflammation (Dias et al., 2013), α-synuclein aggregation (Brundin et al., 2016; Mizuno et al., 2008; Sidhu et al., 2004; Spillantini et al., 1997), iron dysregulation (Mochizuki and Yasuda, 2012), oxidative and nitrosative stress induced by DA toxicity (Hare and Double, 2016), as well as altered protein handling, accumulation and phosphorylation (Eriksen et al., 2005). Other factors could be implicated in PD, including lipid peroxidation, decrease in glutathione, increase in hydroxynonenal-modified proteins, increase in 8-hydroxy-deoxy guanine, abnormalities in the endolysosomal compartment, chaperone-mediated autophagy, excitotoxicity and autoimmune-mediated mechanisms. τ proteins, as well as β-amyloid plaques, are rather associated to cognitive impairments in PD (Halliday et al., 2014; Irwin et al., 2013). The possible interactions between these mechanisms raised the view of PD etiology as a network rather than a cascade of events (Haelterman et al., 2014; Schapira, 2006; Sulzer, 2007).

Based on the aforementioned agents, several biomarkers of PD were proposed. While pathological markers such as confirm the diagnosis after death, other markers only support the clinical diagnosis and are non-specific to PD (Sharma et al., 2013). Pathological markers include death of DAergic neurons in the SNc, α-synuclein index, the presence of LB and Charnol bodies, which are formed following mitochondrial dysfunction, as well as iron accumulation. Pyridoxal kinase and lysosomal ATPase have been identified as potential additional markers of PD. Other biomarkers use samples in the cerebrospinal fluid (CSF), blood, serum, plasma, and urine. They include quantification of α-synuclein, DJ-1, tau (τ) proteins, β-amyloid, β-glucocerebrosidase, glutathione-SH, neuromelanin antibody, platelet complex I activity, urinary 8-OH-2dG, parkin, ubiquitin, brain-derived neuronal factor (BDNF), cytokines, monoamines, endogenously synthesized tetrahydroisoquinolines, salsolinol, and plasma homocysteine, monoamine oxidase-B (MAO-B) and osteopontin (Chahine and Stern, 2011; Chahine et al., 2013; De Virgilio et al., 2016; Kalia and Lang, 2015; Sharma et al., 2013). Additionally, epidermal growth factor might be characteristic of dementia in PD, and interleukin-8 might discriminate β-glucocerebrosidase mutation carriers. Furthermore, ApoA1 could be linked to motor disease severity and age at disease onset (Chahine et al., 2013).

Nonetheless, recent meta-analyses considering cross-sectional and longitudinal studies including biomarkers provided by electrophysiology, transcranial duplex ultrasound, cardiac 123I-MIBG scintigraphy, brain MRI, magnetic resonance spectroscopy (MRS), positron emission tomography (PET) and single-photon emission computed tomography (SPECT), as well as other biomarkers found mainly in the CSF, serum, urine, plasma and blood, revealed the lack of sufficient evidences to recommend the use of any biomarker to measure motor or non-motor disease progression in PD clinical trials (McGhee et al., 2013).

Further, several inconsistencies were raised concerning most of the proposed causal mechanisms leading to nigral cell death in PD.

Abnormal iron levels are more generally associated with other disorders, such as AD, Huntington's disease (HD), multiple sclerosis (MS), MSA, PSP, CBD, restless legs syndrome (RLS), neurodegeneration with brain iron accumulation (NBIA) and other diseases (Dušek et al., 2012; Ke and Ming Qian, 2003; Rouault, 2013; Sian-Hülsmann et al., 2011; Zecca et al., 2004). Despite the existing comorbidity between PD and RLS (Rijsman et al., 2013; Tan et al., 2002), iron levels in the SN seem reduced in the latter whereas they appear to be increased in the former. This raises questions regarding the specific role of iron in PD pathogenesis. Furthermore, even if iron chelation and overexpression of iron-sequestering ferritin are advanced as potential neuroprotective strategies (Benarroch, 2009; Zecca et al., 2004), reports about the stage at which iron deposition reaches an abnormal level in the parkinsonian SN are conflicting, especially concerning the prodromal phase (Sian-Hülsmann et al., 2011). The role of mitochondrial dysfunction in PD etiopathogenesis poses the issue of the selective vulnerability of the SNc, as mitochondria and endoplasmic reticulum are not different across neuronal cell types (Surmeier et al., 2011a). Despite the links between the pathogenic processes suggested for PD and the free radical theory of ageing (Wickens, 2001), ventrolateral SNc cells do not specifically exhibit a regionally different DA metabolism that could lead to an increased toxicity, and their vulnerability is unrelated to the amount of neuromelanin within each cell (Obeso et al., 2010). Moreover, although SNc neurons show diminished calcium buffering capacity and greater dependence on L-type Ca^{2+} channels in SNc neurons, they do not exhibit pacemaking activity and are associated with levels of DA way below the toxicity threshold (Obeso et al., 2010), yet opinions on the later statement are divergent (Surmeier et al., 2005). Furthermore, DAergic therapy does not seem to accelerate disease progression (Surmeier et al., 2011a). The amount of LB does not correlate with clinical severity, disease duration, nigral cell loss and α-synuclein deposition (Jellinger, 2009). Moreover, LB are found in other neurodegenerative diseases (Lang and Lozano, 1998a; Schapira and Jenner, 2011).

The neuropathologist Heiko Braak contested the brain-centred view by claiming that the PD pathology affects primarily the olfactory bulb, the anterior olfactory nucleus, autonomic neurons of the peripheral nervous system (PNS), and the dorsal motor nuclei of vagal and glossopharyngeal nerves in the medulla of the brainstem. The neurodegenerative process further propagates through the brain, affecting the spinal cord grey matter and pons – including the locus cœruleus, magnecellular portions of the reticular formation and the posterior raphe nuclei –, leading to stage 2. In stage 3, the pedunculopontine nucleus, SNc, central subnucleus of amygdala and magnocellular nuclei in the basal forebrain such as the nucleus basalis of Meynert would be reached. In stage 4, the interstitial nucleus of stria terminalis, ventral claustrum, intralaminar thalamic nuclei, anteromedial temporal

mesocortex, CA2 hippocampal subfield, as well as accessory cortical and basolateral nuclei of the amygdala would be affected. In final stages 5 and 6, neurodegeneration would harm multiple cortical regions, including insular, associative and primary cortices (Goedert et al., 2012; Jellinger, 2011; Kalia and Lang, 2015). Braak and colleagues (2003) used α-synuclein immunohistochemistry and suggested that PD was the consequence of infectious agents likely entering in the body through the guts (Braak et al., 2003b; Del Tredici and Braak, 2008; Hawkes et al., 2009). Although supported by recent findings (Sampson et al., 2017; Svensson et al., 2015), the Braak staging hypothesis does not explain the asymmetry of clinical symptoms and has been criticized (Burke et al., 2008). It has to be noted that subjects without clinical manifestations have shown widespread α-synuclein aggregates (Stefanis, 2012) and that the latter fail to reproduce entirely clinical and neuropathological features of PD (Corti et al., 2005).

1.1.7. Treatment

The currently available treatment for PD are symptomatic – meaning that they alleviate some of the symptoms rather than curing the disease (Dauer and Przedborski, 2003; De Virgilio et al., 2016). The main therapeutic strategy includes DA substitution (Kalia and Lang, 2015; Lang and Lozano, 1998b), deep brain stimulation (DBS) (Bittar et al., 2005; Hickey and Stacy, 2016; Lozano et al., 2002; Perlmutter and Mink, 2006) and surgical ablation (Davie, 2008). DA replacement therapy consists of the administration of various pharmaceutical compounds, including levodopa, ergoline and non-ergoline DA agonists, monoamine oxidase type B (MAO-B) inhibitors, catechol-O-methyltransferase (COMT) inhibitors, amantadine, clozapine and anticholinergics, the latter comprising notably benztropine, ethopropazine and trixyphenidyl (Blandini and Armentero, 2014; Davie, 2008; Fernandez and Chen, 2007; Hauser, 2009; Kaakkola, 2010; Kalia and Lang, 2015; Lang and Lozano, 1998b; LeWitt and Fahn, 2016; Tomlinson et al., 2010). Levodopa is often used in combination with inhibitors of dopa decarboxylase (or amino acid decarboxylase (AADC) inhibitors) such as carbidopa or benserazide. Each drug class targets the treatment of motor symptoms and acts on a particular component of DA synthesis and metabolism (Bainbridge et al., 2008; Hauser, 2009; Kalia and Lang, 2015; Koller and Rueda, 1998; Youdim et al., 2006).

DA agonists work by stimulating post-synaptic DA receptors. Ergot-derived DA agonists comprise bromocriptine, cabergoline, pergolide and lisuride. Non-ergot-derived DA agonists include apomorphine, piribedil, pramipexole, ropinirole and rotigotine. MAO-B inhibitors such as rasagiline and selegiline prolong DA activity by preventing its metabolic break down and disinhibiting its neuronal uptake. Besides the prescription of pramipexole and clozapine for depression and psychosis respectively, other drugs can counteract NMS such as cognitive impairment, depression, psychosis, RBD, constipation, gastrointestinal motility, urinary dysfunction, orthostatic hypotension, sialorrhoea and fatigue, although

treatment options and responses are more limited than in the case of motor symptoms (Chaudhuri et al., 2006; Kalia and Lang, 2015; Rascol et al., 2003).

For example, cholinesterase inhibitors rivastigmine and donepezil appear to partially alleviate cognitive, gait and balance dysfunction (Kalia and Lang, 2015). DA substitution is considered as the most common and effective symptomatic treatment for motor dysfunction in PD (Lang and Lozano, 1998b). Given the lack of evidence for both neurotoxic and neuroprotective effects of DAergic drugs (Davie, 2008; Kalia and Lang, 2015; Lang and Lozano, 1998b; Surmeier et al., 2011a), it is generally considered that treatment should not be delayed and rather be oriented towards preserving independence, safety, function and quality of life of patients (De Virgilio et al., 2016; Lang and Lozano, 1998b; Magrinelli et al., 2016). However, symptoms such as tremor, abnormal posture, FOG, postural instability and dysarthria frequently do not improve with DA replacement therapy (De Virgilio et al., 2016; Helmich et al., 2012; Lang and Lozano, 1998b; Rascol et al., 2003). These treatment-resistant symptoms are considered to be due to neurodegeneration in non-DAergic structures (Kalia and Lang, 2015; Nonnekes et al., 2016).

Additionally, *de novo* patients typically experience at first the so-called "honeymoon" period and develop later motor complications (Dauer and Przedborski, 2003; Davie, 2008; Müller, 2002; Rascol et al., 2003; Stocchi et al., 2010; Valadas et al., 2014). During the "honeymoon" period, DAergic therapy abolishes most motor symptoms without severe side effects. This phase lasts 5 years for half of the patients, up to 10 years at utmost in general and only 6 in young patients. On one hand, late-stage PD patients suffer from motor fluctuations such as the "wearing-off phenomenon" – consisting of a gradual shortening of the effect individual levodopa doses – and the "on-off phenomenon" – characterized by abrupt and unpredictable phases of motor inability and stiffness dissociated from levodopa supply –, resulting in periods of good ("on-time") and bad ("off-time") control of motor symptoms (Davie, 2008; Kalia and Lang, 2015; Lees, 1989). Likewise, fluctuations can occur in NMS (Kalia and Lang, 2015). Pre- and postsynaptic changes occurring in the DAergic nigrostriatal system and glutamatergic striatopallidal projections were advanced as contributing to the shortening of levodopa effects (Lang and Lozano, 1998b). On the other hand, long-term levodopa intake induces dykinesias – i.e. choreiform dystonic involuntary movements – at a rate of 10% per year after starting the treatment (Davie, 2008; Kalia and Lang, 2015).

Levodopa-induced dyskinesias (LIDs) typically include "off" period dystonia, "peak dose" dyskinesias and "diphasic" dyskinesias (Davie, 2008; Voon et al., 2009). While motor fluctuations are mostly associated with quantity of levodopa and disease duration, dyskinesias are strongly linked to the duration of treatment (Davie, 2008). With a half-life of 60-90 minutes, current recommendations tend towards using frequent and small doses of levodopa, as both oscillating levels of levodopa and PD progression are thought to contribute to the appearance of motor complications (Davie, 2008; Lees, 1989). Despite

strategies to ameliorate motor fluctuations and the potential efficacy of amantadine and clozapine to alleviate LIDs, the treatment of motor complications – especially of "wearing-off phenomenon" and LIDs – remains unsatisfying (Davie, 2008; Kalia and Lang, 2015; Müller, 2015).

The pathophysiology of motor complications remains poorly understood but may involve fluctuating stimulation of DAergic receptors subtype D1 – inducing an increase in dynorphine/substance P –, glutamatergic overactivity, as well as interactions between D1- and D2-mediated striato-pallidal pathways and colocalization of neuropeptides, N-methyl-D-aspartate (NMDA) receptors and γ-aminobutyric acid (GABA) receptors (Baas, 2000; Bargiotas and Konitsiotis, 2013). Similarly to PD pathogenesis, the multifactorial aspect of LIDs pathogenesis inspired novel therapeutic approaches based on drugs interfering with glutamatergic, serotonergic, adenosine, adrenergic, and cholinergic neurotransmission (Bargiotas and Konitsiotis, 2013), as well as technical advances aiming at delivering drugs in a continuous fashion such as continuous delivery of subcutaneous apomorphine, transdermal rotigotine administration, intraduodenal or intrajejunal levodopa infusion, but also DBS, which will be covered later in the text (Davie, 2008; Nyholm, 2012; Timpka et al., 2016; Voon et al., 2009). Nonetheless, motor complications are less frequent with DA agonists, which commonly have a selective affinity for D2 receptors, albeit the latter are associated with a lower efficacy and higher risk of side effects as compared to levodopa (Baas, 2000; Davie, 2008; Kalia and Lang, 2015). Indeed, LIDs and motor fluctuations are not the only disadvantages of DAergic medication. If nausea, vomiting, anorexia, vivid dreams, nightmares and sleep disorders have been reported (Hauser, 2009; Lang and Lozano, 1998b; LeWitt and Fahn, 2016), DA agonists are particularly renowned for being associated with such side effects but also with psychotic symptoms such as illusions, delusions and paranoia, as well as presence or passage hallucinations, well-formed visual hallucinations, and less frequently auditory, tactile or olfactory hallucinations (Calabresi et al., 2015; Kalia and Lang, 2015).

Psychiatric symptoms were regarded as possibly related to the stimulation of DA receptors in the mesolimbic and mesocortical systems (Lang and Lozano, 1998b). Moreover, impulse control disorders (ICDs) – which occur in 13.6% of patients and include pathological gambling, hypersexuality, mania, punding (hobbyism), compulsive shopping, eating and medication use –, are associated with the use of DA agonists and high doses of levodopa but not with DA agonists dose (Davie, 2008; Voon et al., 2009, 2011).

Other risk factors for ICDs are known, such as younger age, being unmarried and a family history of gambling problems (Voon et al., 2009), and the DA overdose hypothesis states that ICDs in PD might result, apart from genetic factors, from the mismatch between the selective and progressive caudorostral pattern of striatal denervation and the lack of spatial selectivity of DAergic treatment, which leads to a DA overdose in striatal regions initially spared by the disease, such as the ventral striatum (Cools, 2006; Vaillancourt et al.,

2013). In any event, ICDs and psychotic symptoms contraindicate the use of DA agonists in patients with history of addiction, obsessive-compulsive disorder and impulsive personality, as well as in elderly patients, especially those with cognitive impairment (Kalia and Lang, 2015). MAO-B inhibitors can be effective in addition to levodopa in advanced PD or as monotherapy in early disease stage by hampering DA enzymatic metabolism, although their potential neuroprotective and neurotoxic effects are a matter of controversy and their mechanisms of action leading to alleviate clinical symptoms in PD remain to be elucidated (Bargiotas and Konitsiotis, 2013; Davie, 2008; Fernandez and Chen, 2007; Youdim et al., 2006). In combination with AADC inhibitors, COMT inhibitors – which include entacapone, tolcapone and nebicapone – prevent a set of enzymes to metabolize DA, increasing thereby the availability and the steadiness of the latter in the plasma and the brain (Davie, 2008). However, despite probable neuroprotective effects through reduced production of free radicals via DA deamination (Müller, 2015), the efficacy of this drug class could be improved as COMT inhibition with current pharmaceutical compounds does not reach 90% (Kaakkola, 2010).

The widespread acknowledgment of LIDs and DAergic therapy shortfalls encouraged clinicians and surgeons to reconsider ablative surgery, introduced back in the early 1950s, as a therapeutic alternative for PD (Davie, 2008; Wagle Shukla and Okun, 2013). Current irreversible procedures include pallidotomy and thalamotomy (Mandir and Vaughan, 2000). With the introduction of stimulators, a new therapeutic approach, termed deep brain stimulation (DBS), emerged (Davie, 2008). DBS consists of implanting electrodes of varying technical complexity (Hickey and Stacy, 2016) via surgery in predefined deep brain nuclei to induce electrical stimulation via a implantable pulse generator similar to a pacemaker (Bittar et al., 2005; Hickey and Stacy, 2016; Lozano et al., 2002). Notable advantages of DBS over surgical ablation are its reversibility, programmability and safety of bilateral surgery (Davie, 2008; Lang and Lozano, 1998b; Wagle Shukla and Okun, 2013). Despite its effectiveness, precise mechanisms of action of DBS remain largely unclear (Hickey and Stacy, 2016; Kalia and Lang, 2015; Lang and Lozano, 1998b; Lozano et al., 2002; Perlmutter and Mink, 2006) and are apparently more complex than the original suggestion of long-term inhibition within the defective motor circuit via depolarization blockade of aberrant neuronal firing, as DBS seems to inhibit soma while concurrently activating axons, change neurotransmitter release, and could improve PD symptoms by normalization of global functional networks or selective stimulation of white matter tracts (Hickey and Stacy, 2016; Lang and Lozano, 1998b; Lozano et al., 2002; Perlmutter and Mink, 2006). The specific pathology leading to indication for DBS defines the precise nucleus to be targeted as well as the settings of the implantable pulse generator, including amplitude, pulse width and frequency of stimulation, based also on the type of electrode implanted (Bittar et al., 2005; Hickey and Stacy, 2016).

Similarly to early ablative procedures, common target nuclei include the subthalamic nucleus (STN) and internal part of the globus pallidus (GPi) for the global treatment of motor symptoms in PD, as well as the motor thalamus – notably the Vim nucleus – for the specific treatment of tremor in PD (Bittar et al., 2005; Lang and Lozano, 1998b; Lozano et al., 2002; Perlmutter and Mink, 2006). While STN DBS allows the diminution of DAergic medication, GPi DBS can reduce LIDs (Perlmutter and Mink, 2006). Beyond this difference, both targets are comparable in terms of motor symptoms improvement (Perlmutter and Mink, 2006; Wagle Shukla and Okun, 2013). DBS can also improve NMS such as sleep disorders and behavioural abnormalities, although further studies are needed to disentangle the effects specific to DBS and the reduction of DAergic medication that accompanies it (Kalia and Lang, 2015).

Notwithstanding the average delay of 10-13 years between PD diagnosis and DBS surgery, recent findings suggest that early DBS intervention might better improve quality of life of patients as compared to any other therapy (Kalia and Lang, 2015). DBS targets currently under investigation are the spinal cord, to treat chronic pain, and the pedunculopontine nucleus (PPN), for axial symptoms such as balance and gait dysfunction (Rowland et al., 2016). Other DBS targets such as the zona incerta (ZI), periventricular gray matter (PVG), fornix, subcallosal cingulate, lateral habenula, ventral capsule, ventral striatum, nucleus accumbens, inferior thalamic peduncle, centromedian-parafascicular thalamic complex, external part of the globus pallidus (GPe), medial forebrain bundle, ventralis oralis posterior (Vop), ventroposterior lateral (VPL) and medial (VPM) thalamic nuclei are currently used or studied to treat AD, dystonia, ET, pain – including neuropathic, phantom-limb, failed low back, and cluster-headache pain –, depression, anorexia, obsessive compulsive disorders (OCD), addiction, Gilles de la Tourette's syndrome (GTS), rubral, proximal and MS tremor (Bittar et al., 2005; Cleary et al., 2015; Lipsman et al., 2013; Perlmutter and Mink, 2006; Rowland et al., 2016). However one cannot exclude the possibility that structures adjacent to the targeted nuclei are additionally stimulated (Bittar et al., 2005).

Nowadays, computed tomography (CT) and magnetic resonance imaging (MRI) are fundamental to improve the accuracy of DBS electrodes placement, as well as in the use of focused ultrasound and gamma knife radiosurgery (Bittar et al., 2005; Higuchi et al., 2016; Rowland et al., 2016). However, despite considerable technical progresses and the possible postoperative adjustment of electrical stimulation settings, risks of irreversible complications exist (Lang and Lozano, 1998b). Some of the latter are related to surgery itself or device failures: cable discomfort, buzzing sound, lead fracture, dislocation of device, headache, mental status change, confusional state, paresthesia, pain, delirium, impaired wound healing, infection, infraclavicular hematoma, air embolus, intracerebral abscess, cerebral hemorrhage, stroke and death (Wagle Shukla and Okun, 2013). Yet adverse effects can also be induced by electrical stimulation and affect worsening of

mobility, gait and balance disturbance, falls, speech disorders, visual field defect, emotional lability, anxiety, depression, impulse control disorder, obsessive–compulsive disorder, mania, changes in personality, cognitive symptoms, psychiatric disturbance, psychosis, hallucinations, suicide (Cyron, 2016; Davie, 2008; Wagle Shukla and Okun, 2013).

There is evidence suggesting that DBS might impair spatial delayed recall and response inhibition (Cavanagh et al., 2011; Frank et al., 2007; Perlmutter and Mink, 2006). DBS is therefore limited to PD patients presenting no contraindications such as depression, cognitive impairment or other comorbid neuropsychological and neuropsychiatric factors. DBS further requires careful screening of the surgical candidates depending on age, disease duration and levodopa responsiveness, with apparently 30% of DBS failures being due to surgical candidacy issues (Davie, 2008; Rowland et al., 2016; Wagle Shukla and Okun, 2013). Some of these complications may cumulate over time (Perlmutter and Mink, 2006). While benefits from surgery appear to last for at least 4 years, patients often experience a "second honeymoon" during which symptoms improvements are lost (di Biase and Fasano, 2016; Perlmutter and Mink, 2006). This shortcoming, together with the suboptimal efficacy of DBS for the treatment of axial symptoms, incited trials of low-frequency DBS, typically around 60-80 Hz, as an alternative to high-frequency DBS, which is generally above 100 Hz (di Biase and Fasano, 2016). Apart from detrimental effects of very-low-frequency DBS, these studies suggest notably that the different cardinal symptoms of PD might respond differently to each stimulation frequency, although further investigations are needed, experimental designs being largely variable and inconsistent across studies (di Biase and Fasano, 2016). Future technical developments for DBS might include closed-loop stimulation systems, which would deliver electrical stimulation pulses based on the detection of physiological signals (Rowland et al., 2016). However, the development of such adaptive DBS systems would require a deeper understanding of the links between PD pathophysiology and symptomatology.

Other stimulation techniques, such as repetitive transcranial magnetic stimulation (rTMS) and electroconvulsive therapy (ECT), are commonly used for the treatment of depression in patients without PD (Kalia and Lang, 2015). In PD, psychotherapy and electroconvulsive therapy (ECT) are therapeutic alternatives to medication for the treatment of depression (Veazey et al., 2005) and recent reports suggest that repetitive transcranial magnetic stimulation (rTMS) alleviates symptoms on lower limb and improve gait (Chung and Mak, 2016).

Rehabilitation strategies might be considered as motor relearning methods, possibly acting at the basal ganglia (BG) level (Magrinelli et al., 2016). These comprise nonspecific physiotherapy, occupational therapy, dance, martial arts therapy, treadmill and robotic training, speech and cognitive therapy, motor imagery, action observation therapy, virtual reality and telerehabilitation. Studies on the effects of rehabilitation procedures have

shown significant improvement in PD symptoms, especially gait and balance, though PD neurodegenerative processes are not blocked by such approaches.

Other approaches in the experimental phase such as neural transplantation for DA transmission restoration, gene therapy, immunomodulatory therapy using for instance minocycline, anti-inflammatory treatments, as well as recent local and systemic drug delivery systems for administration of DA, levodopa, agonists, neuroprotectors, antioxidants, protein inhibitors, peptides and neurotrophic factors using micro- and nanoparticles are currently under study and may hold promising future therapeutic applications for patients with PD. Some gene therapy approaches combine tricistronic vector encoding tyrosine hydroxylase, AADC and GTP cyclohydrolase hydroxylase, while others aim at delivering neurturin, AADC or glutamic acid decarboxylase (GAD) through adeno-associated viral vector serotype 2 (AAV2). To date, none of the recent gene therapy approaches demonstrate a clinical efficacy leading to a consistent improvement in PD symptoms in clinical trials (Bartus et al., 2013; Feng and Maguire-Zeiss, 2010).

Anti-inflammatory treatments include fibrates, rosiglitazone, metformin, pyrroloquinoline quinone, 5-aminoimidazole-4-carboxamide ribonucleotide (AICAR) and resveratrol (Sirt1). Neuroprotectors comprise anti-apoptotic agents (TCH346, CEP-1347), glutamate antagonists, promitochondrial drugs (coenzyme Q10, creatine) or calcium channel blockers (isradipine). Typical neurotrophic factors are glial cell line-derived neurotrophic factor (GDNF) and vascular endothelial growth factor (VEGF). Still, further knowledge of the relationships between PD etiopathogenesis and pathophysiology are necessary, as most of these approaches still do not surpass the benefits of DAergic medication or DBS (De Virgilio et al., 2016; Garbayo et al., 2013; Lang and Lozano, 1998b; Miller and O'Callaghan, 2015; Obeso et al., 2010; Rodríguez-Nogales et al., 2015; Rowland et al., 2016).

1.2. Segregation and integration of information in cortico-subcortical loops

The pathogenesis of PD is multifactorial and remains unclear. Cortico-subcortical loops represent a key element in PD pathophysiology. In this section I focus on cortico-subcortical circuits: what are their constituents and organization in terms of structure and function, as well as theoretical models attempting to explain their role in disease, notably in PD.

1.2.1. Structural and functional architecture of cortico-basal ganglia-thalamic circuitry

The BG are a phylogenetically ancestral set of interconnected subcortical structures (**Figure 2**; **Figure 3**) that receive connections from essentially the whole cortex and contribute to multiple behavioural functions (Alexander et al., 1989; DeLong and Wichmann, 2009;

Grillner and Robertson, 2016; Haber, 2003; Utter and Basso, 2008). The main input nucleus of the BG is the striatum, the other being the STN. The two major output stations of the BG are the substantia nigra pars reticulata (SNr) and the GPi, whose activity pathologically increases in PD (Lang and Lozano, 1998b). The dorsal striatum, which comprises the putamen and caudate nucleus, as well as the ventral striatum, project to the dorsal pallidum, which includes the GPi and GPe, as well as the ventral pallidum. The term "ventral striatum" encompasses the nucleus accumbens (NAcc) – wherein two regions, the shell and the core, can be identified – and striatal cells of the olfactory tubercle (Afifi, 1994a; Haber, 2003; van der Meer and Redish, 2011). Features of the shell are similar to those of the limbic structures, whereas the core resembles more to regions in the dorsal striatum (Clarke and Adermark, 2015). Another frequent terminology divides the dorsal striatum into dorsolateral striatum (DLS), implicated in stimulus-response learning, and dorsomedial striatum (DMS), involved in goal-directed learning (Clarke and Adermark, 2015; Devan et al., 2011).

The ventral pallidum lies in the sub-commissural part of the substantia innominata (Lanciego et al., 2012; Root et al., 2015). While the GPi sends back information to the cortex via the thalamus and projects to brainstem nuclei and the habenula, the GPe projects to all BG nuclei but principally to GPi, SNr and STN, as well as SNc (Chan et al., 2006; Parent et al., 1999, 2001). The STN projects back to GPe and sends further connections to the pedunculo-pontine nucleus (PPN), GPi and SNr (Joel and Weiner, 1997; Lenglet et al., 2012; Martinez-Gonzalez et al., 2011; Nakano, 2000). Apart from excitatory inputs from the STN, cerebral cortex and thalamus (Kita, 2007), most afferent to the GPe are inhibitory inputs from the striatum. However there are also feedback projections from the STN and thalamus to the striatum, from the thalamus to the striatum, as well as from the GPi to GPe (Afifi, 1994a; Haber and Calzavara, 2009; Joel and Weiner, 1997; Smith et al., 2004).

The SNc is reciprocally connected to the striatum, modulating cortico-striatal inputs through long-term potentiation and depression by means of phasic and tonic DA signals of various intensities, and sends also projections to the GPi and STN (Calabresi et al., 2007; Goto et al., 2007; Lenglet et al., 2012; Redgrave et al., 2011). Striatal DA elevates in regions innervated by nigrostriatal projections that are activated, while it reduces in adjacent zones, as evidenced by DA reinforcement of specific sets of corticostriatal connections and concurrent inhibition of other inputs (Lanciego et al., 2012). Studies show that striato/pallidal neurons receive greater input from pyramidal tract (PT) cortical neurons, whereas striatonigral neurons preferentially receive input from intratelencephalic (IT) cortical neurons (Lei, 2004).

The thalamus, a complex including several nuclei and situated in the diencephalon, receives inputs from the GPi/SNr and projects back to the cerebral cortex (Herrero et al., 2002). The main type of neurons found in the thalamus are relay cells, whose morphology is exceptionally constant, and intrinsic interneurons (Sherman, 2004). Despite being often

seen as a simple relay nucleus, the thalamus receives also direct inputs from the cortex, as well as inputs from the cerebellum, and projects back to the striatum and cerebral cortex by integrating these various excitatory and inhibitory inputs (Goldberg et al., 2013; Graybiel, 2008; Guillery and Sherman, 2002; Haber, 2003; Haber and Calzavara, 2009; Haber et al., 2000; Pelzer et al., 2016; Smith et al., 2004).

The cerebellum can also modulate motor commands sent through the spinal cord notably via the red nucleus, the latter being possibly involved in ET (Ramnani, 2006; Sharifi et al., 2010; Telford and Vattoth, 2014) conversely to neighbouring retrorubral area A8 which may be implicated in PD resting tremor according to the dimmer-switch model (Helmich et al., 2012). Although the role of the cortico-cebellar network has been recently proposed to underlie pathophysiological changes in PD (Martinu and Monchi, 2013), the latter circuit is largely viewed as playing a compensatory role that occasionally favour cortico-BG dysfunction.

Both the SNr and SNc project to the PPN, but in addition the SNr sends connections to the reticular formation and superior colliculus, which projects back to thalamic nuclei (Lenglet et al., 2012; McHaffie et al., 2005; Tykocki et al., 2011). Afferent and efferent connections as well as neurotransmitter types in the PPN are topographically organized (Martinez-Gonzalez et al., 2011; Mena-Segovia et al., 2008). The striatum principally receives afferent connections from VTA and SNc, the loss of the latter being considered as the pathological hallmark of PD as discussed in section 1.1.5. Despite asymmetry in DAergic nigrostriatal projections in PD, the latter pathway is generally symmetrical in healthy subjects, while the meso-striatal projections from the VTA to the striatum are asymmetrical at baseline (Molochnikov and Cohen, 2014). A third pathway, termed "meso-cortical", sends DAergic projection from the VTA to the PFC (Seamans and Yang, 2004). Nigro-cortical projections are more diffuse (Haber and Knutson, 2009).

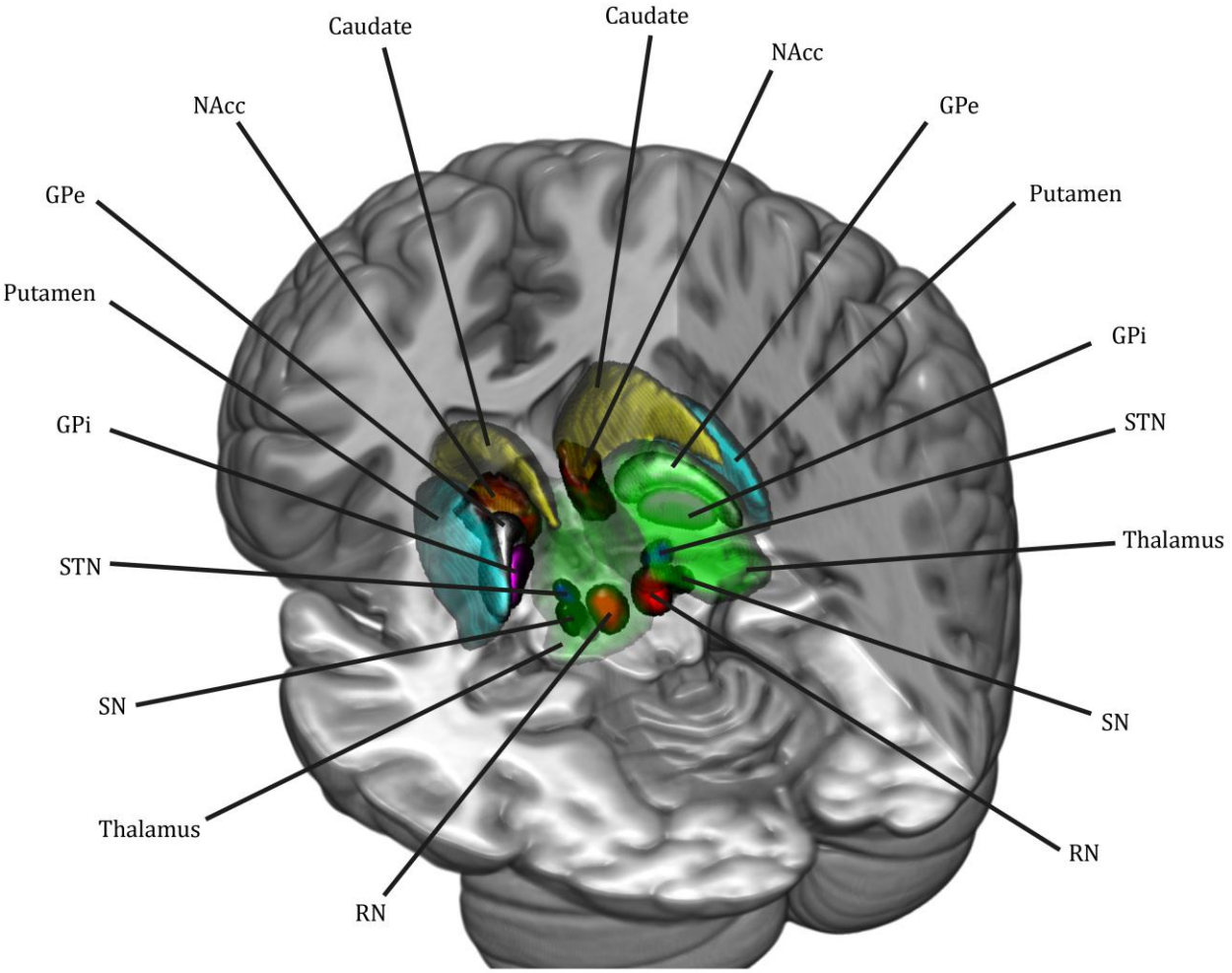

Figure 2: Anatomy of basal ganglia, thalamus and midbrain nuclei rendered on a canonical T1-weighted image . The thalamus (light green) is rendered in a semi-transparent fashion to make apparent the STN, SN and RN. The Harvard-Oxford atlas provided with FSL (https://fsl.fmrib.ox.ac.uk/fsl/fslwiki/Atlases) is used to represent the putamen, caudate, NAcc and thalamus. The GPe, GPi, STN, SN and RN are rendered using the ATAG atlas (Keuken et al., 2014).

Striatal neuronal cells predominantly consist of inhibitory GABAergic medium spiny neurons (MSNs), which are also named spiny projections neurons (SPNs) and likely correspond to phasically active neurons (PANs) (Kreitzer, 2009; Smith et al., 2014). The latter have massive dendritic arborisation to integrate inputs from virtually the whole cortex, hippocampus and amygdala while sending axons collaterals to neighbouring MSNs (Parent et al., 2000; Surmeier et al., 2010). Electrophysiologically, MSNs have a bimodal distribution of membrane potentials, hence the terms "up" and "down" characterizing these two states (Nicola et al., 2000). Consistent with the hypothesis that striatal MSNs receive converging cortical inputs firing in a correlated but not entirely synchronous fashion, the up states correlate among MSNs (Kreitzer, 2009). The "up" and "down" states in MSNs

become bistable with DA innervation (Gruber, 2003) and long-term potentiation is consolidated via a 3-factor learning rule, which uses a reward-predicting signals from DA neurons (Houk et al., 1995). Besides astrocytes, other striatal cells comprise interneurons (Clarke and Adermark, 2015). Large interneurons likely correspond to tonically active neurons (TANs) and are cholinergic (Lim et al., 2014). They spread dense connections throughout the striatum despite representing only 1-2% of striatal cells (Lim et al., 2014). It is worth mentioning that striatal levels of ACh are outstanding compared to other brain regions. Some neurotransmitters used by small aspiny neurons are GABA, somatostatin, neuropeptide Y (NPY), neurotensin and thyrotropin-releasing hormone (Tepper and Bolam, 2004). GABAergic interneurons have been further subdivided into low-threshold-spiking (LTS) and fast-spiking interneurons (FSIs). The latter, also designated as GABAergic interneurons, are parvalbumin-positive and interconnected by dendritic gap junctions (Berke, 2011; Kreitzer, 2009), which may cause synchronous activity in the striatum (Hjorth et al., 2009). Furthermore, FSIs project preferentially to MSNs, can be depolarized directly by cholinergic interneurons via nicotinic receptors and might be play a particularly important role in the DLS, as they are distributed along a postero-ventro-median to antero-dorsolateral gradient of increasing density (Clarke and Adermark, 2015). LTS interneurons express NPY, somatostatin and nitric oxide synthetase (Clarke and Adermark, 2015). Other GABAergic interneurons express tyrosine hydroxylase (TH) or the calcium binding protein calretinin. Striatal cholinergic interneurons can reduce glutamatergic input to striatal neurons by activating muscarinic receptors and modulate FSIs by releasing both glutamate and ACh. Further, when synchronously activated, they enhance GABA co-release at DA terminals and mediate thereby considerable inhibitory signals in MSNs by acting on nicotinic receptors (Clarke and Adermark, 2015; Nelson et al., 2014).

It has been reported that neuropeptides such as substance P, enkephalin, and dynorphin are differentially involved in each efferent striatal connection (Afifi, 1994a; Calabresi et al., 2000; Haber, 2003). Additionally, muscarinic and opioid receptors in striatal interneurons regulate DA release (Rice et al., 2011). GABAergic interneurons in general have been considered to influence spike timing of MSNs, whereas cholinergic interneurons are thought to modulate sub- and supra-threshold MSNs responses (Tepper and Bolam, 2004). Besides neurotransmitters modulating striatal function via afferent connections, striatal output is therefore modulated by its local microcircuitry via several mechanisms. Other intra-striatal mechanisms include "feedback inhibition", which is supported by a weak lateral inhibitory network between competing MSNs at pre- and postsynaptic levels (Houk et al., 2007; Plenz, 2003), and a forceful control over striatal excitability allowing "feed-forward inhibition" by GABAergic and cholinergic interneurons, both of which are involved in the induction of synaptic plasticity (Clarke and Adermark, 2015). Intrastriatal circuitry is therefore strongly influenced by GABAergic and cholinergic interneurons, as well as DAergic input, in terms of spiking activity as well as synaptic plasticity (Calabresi et al.,

2014; Reynolds and Wickens, 2002; Shen et al., 2008; Surmeier et al., 2007). Furthermore, DA alters both voltage-dependent conductance and synaptic transmission in the striatum (Nicola et al., 2000). Recent studies showed that the apparently antagonistic behaviour of DA and ACh might be revised because synchronous activation of cholinergic interneurons seems to promote striatal DA release via activation of presynaptic nicotinic ACh receptors (Surmeier and Graybiel, 2012).

Concerning DA receptors, two major types were reported in the striatum: D_1 and D_2 (Afifi, 1994a; Missale et al., 1998; Surmeier et al., 2010). Though striatal subregions cytoarchitectonics appear similar, each of these is associated with different cellular morphologies, receptor localization, as well as afferent and efferent circuitry (Clarke and Adermark, 2015). While PD neurodegeneration seems to affect D_1 rather than D_2 receptors, the former are preferentially found in striosomes, or "patch" striatal compartment, whereas the latter are more frequently detected in matrisomes, also termed "matrix" compartment of the striatum (Afifi, 1994a; Graybiel, 1990; Lanciego et al., 2012). An imbalance between these two intermingled compartments has been argued to play a role in basal ganglia disorders (Crittenden and Graybiel, 2011; Graybiel, 2008). Cholinergic modulation takes place mostly in the extra-striosomal compartment (Clarke and Adermark, 2015; Nakano et al., 2000). While the ventral tier of the SNc and ventral SNr are preferentially connected to striosomes, the VTA and dorsal SNc neurons project to matrisomes. In thalamo-striatal circuits, the centromedian and parafascicular thalamic nuclei – considered as more susceptible to PD neurodegeneration – are interconnected with the striatal matrix, while the rest of the thalamus shows no clear preference for any compartment (Smith et al., 2014). Furthermore, MSNs expressing D_1 receptors mostly forward cortical inputs to GPi, forming the so-called "direct" pathway (Gerfen and Surmeier, 2011; Parent and Hazrati, 1995a; Smith et al., 1998; Surmeier et al., 2011b). On the contrary, D_2-expressing MSNs convey cortical signals to GPi by passing through GPe and STN. The term "indirect" pathway designates this detour.

However, it has to be noted that further distinction can be made between "short" and "long" indirect pathways. The first connects the striatum to GPi via GPe, whereas in the second striatal output goes through the GPe and STN before ending in the GPi (Schroll and Hamker, 2013). However some projections terminate in both pallidal segments and there are MSNs co-expressing D_1 and D_2 receptors, suggesting that the separation between direct and indirect pathways may not be complete (Bergman and Deuschl, 2002; Calabresi et al., 2007; Wichmann and Dostrovsky, 2011). Thalamostriatal projections seem to innervate preferentially striatal neurons of the direct pathway (Smith et al., 2004). However recent studies suggest that they may equally project to both pathways, like specific cortical layers (Wall et al., 2013). On the contrary, motor cortex would have a higher affinity for the indirect pathway and sensory cortex as well as limbic structures were reported to project mainly to the direct pathway (Wall et al., 2013). A third pathway is referred to as the

"hyperdirect" pathway, across which the cortex reaches the GPi/SNr via the STN, without transiting through the striatum (Nambu et al., 2002). Nevertheless, there exist other cortico-subcortical loops (Afifi, 1994b; Parent and Hazrati, 1995b).

Other DA receptors include D_3 and D_4 in the D_2-like family as well as D_5 in the D_1-like family. D_1 is the most prevalent receptor and is mainly expressed in the dorsal and ventral striatum, limbic system, hypothalamus and thalamus (Missale et al., 1998). D_5 is weakly expressed compared to D_1 and has been found in the hippocampus, lateral mammillary nucleus, diagonal band area, substantia nigra, striatum as well as in parafascicular, medial and lateral nuclei of the thalamus. D_1 and D_5 receptors are also expressed in prefrontal, premotor, cingulate and entorhinal cortex, as well as in the dentate gyrus. D_2 is principally found in the dorsal and ventral striatum, but also in the amygdala, hypothalamus, SNc, VTA and granule cells of the hippocampal formation, as well as in prefrontal, cingulate, temporal and entorhinal cortices. D_3 is especially found in limbic areas, such as the ventromedial shell of the NAcc, the olfactory tubercle and the islands of Calleja, but also in the hippocampus, cerebellum and medial temporal lobe. It is rarely found in the dorsal striatum, SNc and VTA. Levels of D_4 are low in the pallidum, SNr and reticular thalamic nucleus, but high in the frontal cortex, amygdala, hippocampus, hypothalamus and mesencephalon. It is worth mentioning that DA receptors are also found in blood vessels, adrenal gland, kidney, sympathetic ganglia and heart. While the role of D_3 and D_4 receptors was less studied, D_1, D_2, D_3 and D_5 receptors are likely to play a role in motor activity, learning and memory (Missale et al., 1998).

Apart from the rostro-medial tegmental area (RMTg) in the tail of the VTA, which contains GABAergic interneurons and seems involved in aversion, DAergic neurons in the VTA are more heterogeneous than initially thought and participate differently to rewarding and aversive stimuli (Russo and Nestler, 2013). Following DA depletion, the number of striatal D_1 and D_2 receptors increases and a shift from long-term depression (LTD) to long-term potentiation (LTP) is observed in the indirect pathway (Kreitzer and Malenka, 2008). Both the firing and membrane resistance of MSNs of the indirect pathway increase as well, while the latter cells lose dendritic spines. Additionally, DA depletion might increase the propensity of oscillatory activity in cortex and thalamus. The recurrent GPe-STN circuit may then further amplify synchronous activity in striatal outputs to GPe. Therefore, although GABA remains the prominent neurotransmitter within the BG, signals within the latter are notably modulated by DAergic and serotonin inputs mainly from the midbrain and hindbrain, cholinergic striatal interneurons and excitatory glutamatergic neurotransmission from the cortex, thalamus and STN (Conn et al., 2005). GABA allows striato-pallidal pathways exerting tonic inhibitory control over the thalamus, using henceforth disinhibition as one of its main physiological mechanism (Chevalier and Deniau, 1990).

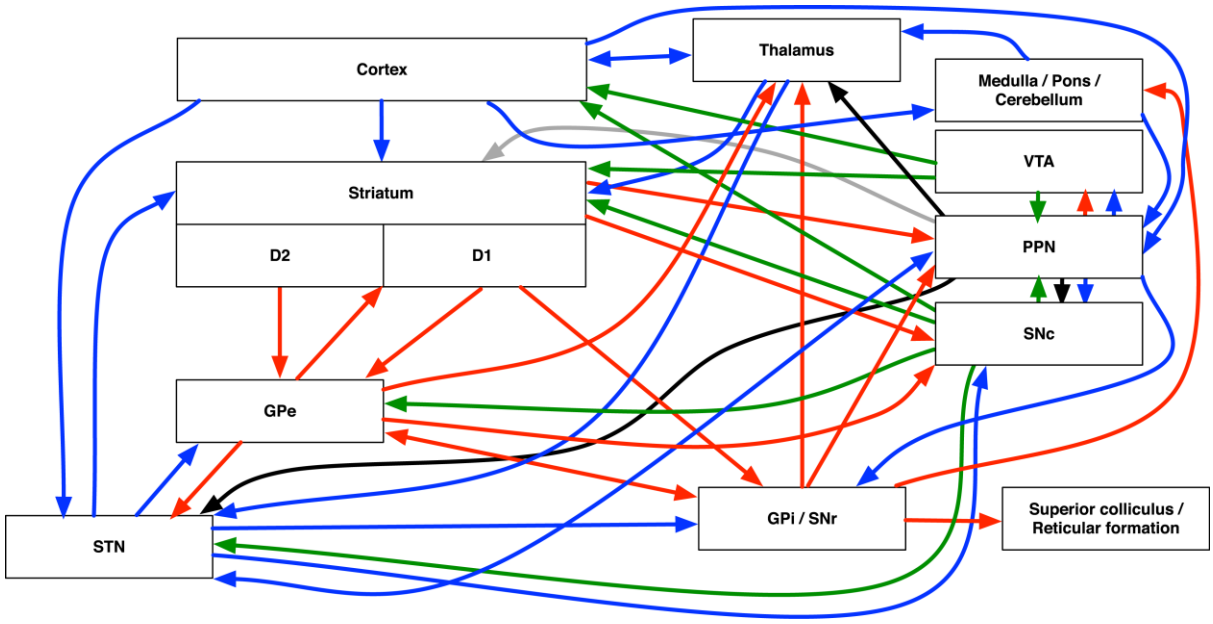

Figure 3: Simplified schematic of BG circuitry based on the reviewed literature, focusing on main BG intrinsic connections, as well as its afferents from and efferents to the thalamus, cortex, midbrain and hindbrain. DAergic, GABAergic, glutamatergic and cholinergic projections are shown in green, red, blue and black respectively. Neurotransmitter in play for connections in grey is unknown. Some projections may involve multiple neurotransmitters, which are not thoroughly shown. Reciprocal connections are shown with double-headed arrows. Additional references to original research articles supporting some of the depicted connections are available at http://www.frontiersin.org/files/cognitiveconsilience/index.html (Solari and Rich Stoner, 2014). For an alternative schematic including raphe nuclei, locus cœruleus and nucleus basalis of Meynert, see Weingarten and colleagues (2015).

Functionally, BG nuclei are organized topographically into several open and closed loops subserving different brain functions (**Figure 4**). This topographical organization mirrors to a certain extent the one found in the cerebral cortex (Accolla et al., 2014; Afifi, 1994b; Alexander and Crutcher, 1990; Alexander et al., 1986, 1989; Draganski et al., 2008; Galvan et al., 2015; Graybiel, 2008; Haber, 2016; Haber et al., 2000; Haegelen et al., 2009; Iwamuro, 2011; Joel and Weiner, 1997, 2000; Lambert et al., 2012; Nakano et al., 2000; Nambu, 2008, 2011, Obeso et al., 2008, 2014, Redgrave et al., 2010, 2011; Romanelli et al., 2005; Seger and Spiering, 2011). While major functional territories are the limbic, associative and sensorimotor subdivisions, experimental evidences support the notion of further detailed topographical organization within the BG such as somatotopy (Alexander and Crutcher, 1990; Iwamuro, 2011; Nambu, 2011; Obeso et al., 2008; Romanelli et al., 2005). Segregation at the level of cerebellothalamic, pallidothalamic and nigrothalamic projections to the cortex, between oculomotor and skeletomotor functions, but also between various cognitive functions (Middleton and Strick, 2000) has been advanced, as well as the existence of distinct visual, parietal, premotor and cingulate corticostriatal loops

(Seger, 2013; Seger and Peterson, 2013; Takada et al., 1998, 2001; Utter and Basso, 2008). Retinotopic and tonotopic organization might also be partially preserved across corticostriatal projections (Updyke, 1993; Xiong et al., 2015). The putamen, STN, GPe, GPi, SNr as well as oral parts of the ventrolateral and ventro-postero-lateral nuclei of the thalamus are thought to embed somatotopically-organized representations, yet the SNr is often considered to play a role in eye movements (Basso and Sommer, 2011). Somatotopically organized representations found in the primary motor cortex (M1) and the supplementary motor area (SMA) are both preserved at the BG level, although M1 and SMA representations of the same body part are more difficult to distinguish, especially in the pallidum and STN (Iwamuro, 2011). Somatotopy in the SNc is regarded as weaker and its existence is unclear (Nambu, 2011; Rommelfanger, 2010), although topographic arrangement is observed in the SN and VTA (Haber, 2016; Haber et al., 2000). A fractured somatotopy is found in the cerebellum, which is apparently involved not only in motor function but also in emotional and executive functions (Apps and Hawkes, 2009; Bernard and Mittal, 2014; Bostan et al., 2013; Manni and Petrosini, 2004; Ramnani, 2006; Stoodley and Schmahmann, 2009, 2010; Stoodley et al., 2012).

The insula, which shares massive connections with the striatum, is a distinctive part of the cerebral cortex as it intrinsically embeds a topographic gradient from social-emotional to sensorimotor functions (Christopher et al., 2014; Kurth et al., 2010). There are also reports of somatotopic organization in the insular cortex, at least for somatosensory function but possibly also for pure motor function (Baumgartner et al., 2010; Brooks et al., 2005; Fink et al., 1997; Henderson et al., 2007, 2010). DA neurons in the SNc and VTA also integrate sensory, motor and cognitive information from multiple afferents to modulate BG signalling, notably through their intimate link with the striatum (Haber et al., 2000; Morikawa and Paladini, 2011). Interestingly, spinal neurons preserve the topography of muscle effectors found in the motor cortex to a certain extent, although the representation is probably best described as "musculotopic" instead of somatotopic (Levine et al., 2012).

Functional topography does not solely concern striato-pallido-thalamic but also thalamo-striatal and thalamo-cortical projections (Herrero et al., 2002; Smith et al., 2004, 2009). Thus, the previous concept of serial processing across BG has been mostly replaced by the one of parallel channels (Afifi, 1994a), which converge across nuclei to a certain degree (Haber, 2003; Utter and Basso, 2008). While earlier debates on BG functional organization focused on two opposite views (Bergman et al., 1998a; Nambu, 2011; Parent and Hazrati, 1995a), namely the parallel (or segregated) processing (Alexander et al., 1986; Hoover and Strick, 1993) hypothesis and the information convergence (or funnelling) hypothesis (Bolam et al., 1993; Kolomiets et al., 2001, 2003; Percheron and Filion, 1991), it is nowadays generally accepted that parallel circuits subject to relative overlap form topographical gradients along different spatial axes depending on the brain structure considered (**Figure 4**). Borders between functional territories are not strict, and

interactions between cortico-subcortical loops are promoted by striato-nigro-striatal, thalamo-cortical and striato-pallidal pathways (Seger, 2008).

Alternatively, in regard to the organization of the striatum into patch and matrix compartments, a pattern of divergence-reconvergence across cortico-striato-pallidal pathways has been proposed (Graybiel et al., 1994). While the notion of topographical organization mirroring – at least partially – the organization of the cerebral cortex in the BG, thalamus and related nuclei is now widely accepted, the very existence of maps parallelizing high granularity topographies found in the cortex (Badre and D'Esposito, 2009; Conant et al., 2014; Grill-Spector and Malach, 2004; Kanold et al., 2014) remains uncertain. Furthermore, the extent to which topographic maps found in BG might be modified through experience-dependent plasticity as shown in the cortex (Ejaz et al., 2015; Stoeckel et al., 2009; Wiestler and Diedrichsen, 2013) remains unknown at present.

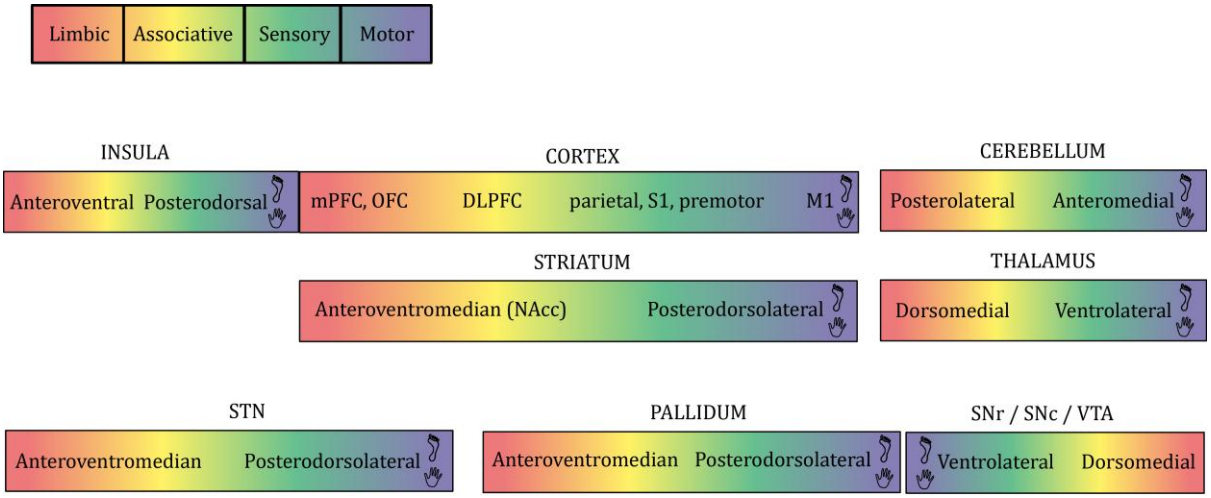

Figure 4: Functional topography in cortico-BG-thalamo-cerebellar circuits following the concept of parallel channels. Legend on the upper left shows the colour codes for the different functional territories. Symbols of hand and foot designate the presence of somatotopy. For the simplicity of the schematic, multiple nuclei are grouped into single entities and the presence of somatotopy is not mentioned for each nucleus separately but rather for the whole entity.

1.2.2. Theoretical models of basal ganglia function and dysfunction

The classical "box and arrow" model (Albin et al., 1989; DeLong, 1990; Wichmann and DeLong, 1996; Wichmann and Dostrovsky, 2011) is probably the most influential model of BG function and dysfunction. It postulates that an imbalance between the direct and indirect pathways is at the origin of movement disorders such as PD and possibly later motor complications following DA replacement therapy (Zhuang et al., 2013). This model focuses on neuronal firing rates and is based on the presumed different contributions of D_1 and D_2 striatal MSNs to locomotion and hypoactivity respectively (Kreitzer and Berke,

2011; Lang and Lozano, 1998b). According to this model, DA depletion in PD leads to hypoactivity in D_1-mediated direct pathway and hyperactivity in D_2-mediated indirect pathway. The increased inhibition of the GPe leads to a disinhibition of the STN, which further accentuates activity in the GPi and supresses activity in thalamus and motor centres in the brainstem, causing PD (Obeso et al., 2014). This view greatly contributed to our understanding of BG function and dysfunction by generating a wealth of studies (DeLong and Wichmann, 2009).

Although recent evidence found support for the "box and arrow" model (Macpherson et al., 2014) it has a number of limitations that have been extensively discussed in the literature (Nambu, 2008; Nelson and Kreitzer, 2014; Obeso et al., 2000). First, studies using MPTP reported loss of recurrent lateral connections between striatal MSNs and selective eradication of glutamatergic synapses on MSNs of the indirect pathway instead of hyperactivity in the GPi (Nambu, 2008). Even if the ratio between GPi neurons increasing and decreasing activity during movements elevates after MPTP treatment, the simplistic view stating that the direct and indirect pathways are involved in movement facilitation and inhibition can be regarded as reductionist, as both pathways are activated during movement execution (Calabresi et al., 2014) and several BG circuits are involved in inhibitory control (Jahanshahi et al., 2015). Furthermore, this model is incomplete, as it does not account for thalamo-striatal connections, projections from GPe to striatum, GPi and reticular nucleus of the thalamus, but also from the cortex to the STN, as well as the role of DA outside of the striatum (Bergman and Deuschl, 2002; Lang and Lozano, 1998b). Also, this model does not account for information processing within each "box" (Bronfeld and Bar-Gad, 2011). Similarly, the increased firing rate of the GPe was questioned by physiological and metabolic studies (Bergman and Deuschl, 2002). Its predictions regarding therapeutic interventions are problematic: thalamotomy should worsen PD and pallidotomy should produce hemiballism, but the first alleviates efficiently tremor and the second eliminates levodopa-induced dyskinesias (Lang and Lozano, 1998b).

There is also a lack of consensus on reports about the decreased GPi activity in dystonia and hemiballism (Bergman and Deuschl, 2002; Nambu, 2008). GPi lesions have been shown to improve symptoms in dystonia, chorea and LIDs, while the "box and arrow" model predict that the latter should aggravate (Ellens and Leventhal, 2013). The fact that this model only accounts for firing rates and not firing patterns might partly explain these inaccurate predictions. For example, intraoperative microelectrode recordings of STN neurons showed that neuronal spiking activity parameters, including oscillatory activity around beta and gamma frequencies, intra-burst rate and ratio of interspike intervals below/above 10ms, could explain more than 60% of variance in motor scores in late-stage PD patients (Sharott et al., 2014). However, this recent study did not find any activity parameter correlated with tremor. The "box and arrow" model has been extended to incorporate the idea of temporal scaling to explain the convergence of the direct and

indirect pathways on the same pallidal neurons (Darbin et al., 2006, 2013a, 2013b). Contrasting with the classical association with direct and indirect pathways, recent models emphasized the crucial role of intra-striatal connections (Calabresi et al., 2014) or proposed that D_1- and D_2-expressing striatal pathways "prepare" and "select" actions respectively (Keeler et al., 2014).

Each of the subsequent models highlights particular functional contributions of the BG (Gillies and Arbuthnott, 2000; Joel et al., 2002; Schroll and Hamker, 2013; Seo et al., 2012). The first category comprises models focusing on serial processing and motor sequencing. These models are based on the idea that each single response of a motor sequence is a stimulus for the following one and that the BG link the different elements of a sequence in a stimulus-response fashion, leading ultimately to the formation of habits (Berns and Sejnowski, 1998; Marsden and Obeso, 1994; Matsumoto et al., 1999). While some of these views underlined the role of BG in the execution of well-learned and automatized motor plans (Marsden, 1982), others emphasized their importance in motor learning (Doyon, 2008; Doyon et al., 2009) or the formation of habits (Graybiel, 2008).

The thalamus is considered as a gate in the "vector integration" model (Gillies and Arbuthnott, 2000). Perspectives similar to motor sequencing models focus on the modulation of response "vigor" according to motivational factors (Dudman and Krakauer, 2016; Mazzoni et al., 2007; Turner and Desmurget, 2010; Wang et al., 2013). One of the mechanisms accounted for in models of serial processing is "chunking", a mechanism by which sequences of motor commands are concatenated into "chunks" (Graybiel, 1998; Wymbs et al., 2012). These perspectives attempts to explain the impairment of motor sequence learning, more specifically of chunking, in PD (Doyon, 2008; Tremblay et al., 2010), as well as the impairment of PD patients in procedural learning and the appearance of stereotypies in some cases (Graybiel, 2008). However these models do not account for other motor and non-motor symptoms observed in PD.

The next group of models considers the BG as pivotal for action selection and represents one of the most widely accepted current views on the topic (Gurney et al., 2001a, 2001b; Humphries et al., 2006; Redgrave et al., 1999). The action selection hypothesis has been originally proposed by Denny-Brown and Yanagisawa Denny-Brown and Yanagisawa (1976). These models include occasionally also the cerebellum (Houk, 2005; Houk et al., 2007) and the hyperdirect pathway (Nambu, 2004, 2005; Nambu et al., 2002). In a typical action selection model, the presumed "surround inhibition" mechanism, often represented as a two-dimensional response function having the form of a "Mexican hat", is considered to underlie the selection of appropriate responses based on the environmental context (Mink, 1996, 2003). This concept, originally borrowed from sensory physiology to explain enhanced contrast for visual stimuli, refers initially to reduced corticospinal excitability of non-active neighbouring muscles. While intra-cortical and intra-striatal mechanisms of inhibition – notably lateral inhibition between MSNs – have been proposed to subserve

motor surround inhibition, the neuronal correlates of surround inhibition remain unknown (Beck and Hallett, 2011; Bronfeld and Bar-Gad, 2011; Kassavetis et al., 2014).

However, surround inhibition is not systematically observed and does not correlate with electromyography (EMG) at adjacent muscles (Kassavetis et al., 2014). While reduced surround inhibition has been proposed to contribute to pathophysiology of dystonia, counter-intuitive observations show that it is reduced in musicians (Shin et al., 2012). If the latter finding may potentially explain why musicians develop dystonic symptoms in rare cases, this type of activity usually requires dexterous individuated fingers movements. Nevertheless, action selection models generally assume that the striatum generates focused inhibition in a subset of GPi neurons through the direct pathway and that diffuse GPi excitation is induced by projections from the STN and GPe through the hyperdirect and indirect pathways. The combination of signals from these pathways produces the "Mexican hat" activation pattern, wherein focused centre of GPi inhibition is surrounded by diffused excitation (Schroll and Hamker, 2013). While action selection models originally apply to motor function, an extension to any kind of cortical input has been proposed (Trapp et al., 2012). Further, action selection has been also thought to extend to stimulus-response-outcome associations (Redgrave and Gurney, 2006).

The "competition between verbal and implicit system" (COVIS) model emphasises on bringing together both motor and cognitive impairment resulting from BG dysfunction (Ashby et al., 1998; Hélie et al., 2011). Experimental evidence invalidated some of the predictions made by action selection models. In action selection models, PD would be due to an inability to disinhibit the desired motor program and, most importantly, to inhibit competing motor programs (Mink, 1996). Instead, the potential for cortical disinhibition seems preserved in PD, as GPi neurons still exhibit a combination of firing rate increases and decreases comparable to that of the normal state (Bronfeld and Bar-Gad, 2011). Action selection models predict that motor tics are caused by aberrant inhibition of a limited number of GPi neurons. Instead, localized motor tics were associated with inhibition of the majority of GPi neurons, which would normally lead to simultaneous activation of multiple motor programs (Bronfeld and Bar-Gad, 2011).

The third category emphasizes the role of BG in reinforcement learning (RL), which is assumed in many models of BG function (Schroll and Hamker, 2013). In this framework, BG adapt behaviour by promoting actions, emotions and cognitive processes that maximize reinforcements (Amemori et al., 2011; Belin et al., 2009; Dayan and Daw, 2008; Doya, 2000; Frank, 2005; Gläscher et al., 2010; Guthrie et al., 2009; Hikosaka et al., 2014; Kamali Sarvestani et al., 2011; Mannella et al., 2013; Parush et al., 2011; Wolpert and Landy, 2012). Unexpected rewards (Ashby et al., 2007; Brown et al., 2004; Suri et al., 2001; Vitay and Hamker, 2010), punishments (Bromberg-Martin et al., 2010; Frank, 2004; Palminteri et al., 2012) and more generally any unexpected sensory event (Redgrave and Gurney, 2006) are thought to induce learning in BG. This is not only supported by the role of DA in modulating

synaptic plasticity at the BG level, but also by phasic DA signals from possibly distinct neuronal systems encoding reward prediction (Hollerman and Schultz, 1998), salient unexpected events (Horvitz et al., 1997), earlier learning-induced BG activity in the BG as compared to PFC (Antzoulatos and Miller, 2011; Pasupathy and Miller, 2005), differential recruitment of brain regions in instrumental conditioning and in the prediction of immediate and future rewards (O'Doherty, 2004; O'Doherty et al., 2006; Tanaka et al., 2004) and the pharmacological modulation of striatal response to reward prediction error (Pessiglione et al., 2006).

RL is compatible with any model of BG function and dysfunction, as it does not attribute a particular function to BG but rather specify the path of the latter to the function (Schroll and Hamker, 2013). The actor-critic framework is a recent development in RL theory. According to these RL models, the "actor" is a sub-network performing actions in order to maximize the weighted sum of future rewards (Barto, 1995). Another sub-network, the "critic", computes the latter at every time step and learns to predict it based on the actor's policy and the current sensory input (Barto, 1995). The critic is therefore adaptive and performs an iterative process of comparison between its predictions and the actual rewards obtained by the acting agent (Barto, 1995). The adaptive critic's weights are updated using the temporal difference error between two adjacent predictions, i.e. a temporal difference learning rule (Sutton, 1988).

Among the models using this framework, some postulate that the actor is implemented by the dorsal striatum and the critic is attributed to the ventral striatum, while others assume that these are fulfilled by the striatal matrix and striosomal compartments respectively (Brown et al., 1999; Contreras-Vidal and Schultz, 1999; Gillies and Arbuthnott, 2000; Houk et al., 1995; Joel et al., 2002; Seger, 2008; Suri and Schultz, 1998, 1999; Suri et al., 2001). Some of these address issues related to timing is omitted rewards, MSNs states, LTP in corticostriatal transmission, DA response to novelty, generalization and discrimination of appetitive and aversive stimuli (Joel et al., 2002).

Contrasting with conventional models that use monosynaptic Hebbian learning, another RL model formalized heterosynaptic Hebbian learning and allowed for neuromodulation of synaptic plasticity to evolve neuronal learning rules of a neural network model of decision-making in foraging bumble-bees using evolutionary computation techniques (Joel et al., 2002; Niv et al., 2002). While neuromodulation of synaptic plasticity states that the activity of a neuron can modify connections between other neurons heterosynaptic, Hebbian learning rules allow for synaptic plasticity even when only the pre-, only the post-, or none of the synaptic component has been active, both of which having been shown in neural tissue (Joel et al., 2002). Some other RL models of BG consider that PD is due to random learning (Parush et al., 2011) or deficient information integration (Ashby et al., 2007), explaining impairments in set-shifting and value reversal tasks (Hikosaka et al., 2014). Most of the implementations of the actor-critic framework at the neuronal level are based

on assumptions that are inconsistent with neuroanatomical knowledge regarding their underlying neural substrates (Joel et al., 2002).

The prefrontal cortex and basal ganglia (PBWM) model, alternatively designated as the Basal Ganglia Go/NoGo (BG-GNG) model, is a distinctive computational account that puts an emphasis on the cognitive domain and the role of BG in working memory gating and maintenance (Frank et al., 2001; Hazy et al., 2007; Maia and Frank, 2011; O'Reilly and Frank, 2006; O'Reilly et al., 2007). This model is based on grounds like those of the "box and arrow" model and attributes to the BG the process of updating working memory representations maintained by the PFC. According to this model, DAergic signals implement a Primary Value and Learned Value (PVLV) Pavlovian learning algorithm that modulates BG function to learn selectively updating working memory representations when needed. In the PBWM model, the indirect – or "no-go" – pathway, associated with D_2 receptors, mediates learning from positive and negative outcome via DA bursts and dips respectively and produces LTD and LTP respectively. On the contrary, the direct – or "go" – pathway, associated with D_1 receptors, promotes learning from positive and negative outcome via DA bursts and dips respectively and induces LTP and LTD respectively, the latter effect being caused indirectly via the effect on D_2. Increase and decrease in tonic DA produces "go" and "no-go" biases respectively through both direct and indirect pathways.

Cumulating empirical evidence validated the predictions of this model (Cavanagh et al., 2011; D'Ardenne et al., 2012; Frank, 2004; Frank et al., 2007; Moustafa et al., 2013, 2014; Shohamy et al., 2008). Here, DA depletion results in an amplified "no-go" bias via hyperexcitability of the indirect pathway, which induces increased resistance to distractors and deficits in working memory updating. On one hand, DA replacement therapy reverse this bias towards an exaggerated "go" bias (Frank, 2004). On the other hand, as predicted by the key role played by the STN within this computational model, STN DBS leads to impulsivity during high-conflict choices (Cavanagh et al., 2011; Frank et al., 2007). Based on the assumptions of the PBWM model, the basal ganglia acetylcholine-based entropy (BABE) model tries to account for the role of striatal cholinergic interneurons and to explain some dynamics aspects of decision-making as well as skill acquisition such as the generation of exploratory actions (Stocco, 2012). Another computational model attempts to reconcile cognitive action planning with habitual and goal-directed control (Daw et al., 2005) in the form of a trade-off between automatically executed and attention demanding cognitive actions (Norman and Shallice, 1986).

The reinforcement-driven dimensionality reduction (RDDR) model aims at unifying hypo- and hyperkinetic movement disorders and postulates that movement disorders, including PD, dystonia, GTS and chorea as seen in HD, LIDs and hemiballism, as well as behavioural disorders such as OCD and ADHD, are characterized by a loss of specificity (LOS) in neuronal activity at the BG level (Bar-Gad and Bergman, 2001; Bar-Gad et al., 2000, 2003a;

Bergman and Deuschl, 2002; Bergman et al., 1998a, 1998b; Bronfeld and Bar-Gad, 2011). This hypothesis states that in these neurological conditions, multiple behavioural events are equally encoded at the neuronal level. Regarding the debate between hypotheses on information funnelling and parallel processing, the LOS hypothesis might be translated as an increased funnelling of information – or a loss of functional segregation – across cortico-BG-thalamic loops, i.e. an inability of keeping parallel channels independent in movement disorders. The identity of functional territories affected by LOS and the extent of the latter might underlie these different disorders. In normal conditions, the BG, notably the striatum, are thought to perform a dimensionality reduction of the massive cortical input, similarly to principal component analysis (PCA). Decorrelation, or desynchronisation, of activity from multiple cortical sources is considered as necessary, given the remarkable reduction in the number of processing units (i.e. neurons) throughout cortico-BG-thalamic loops, especially in cortico-striatal and cortico-pallidal projections (Bar-Gad et al., 2003a).

Although the whole cerebral cortex projects to BG, it has been estimated that cortical afferents do not project on neighbouring striatal neurons, each of the latter receiving inputs from at most 0.01% of the corticostriatal projections neurons, and that in the case of convergence, corticostriatal input is likely coming from adjacent cortical neurons (Bar-Gad et al., 2003a; Kincaid et al., 1998; Zheng and Wilson, 2002). An additional funnelling of information operates from striatum to pallidum (Oorschot, 1996). The RDDR model is therefore based on the funnelling structure of BG and the lack of electrophysiological evidence for mutual inhibition between striatal neurons despite extensive lateral connectivity between MSNs. In the RDDR model, the weights of the dimensionality reduction performed by the BG are modulated by DA input. Therefore, the dimensionality of cortical signals should not be reduced based solely on statistical properties of the input but also and mostly regarding their behavioural significance, i.e. the novelty, salience and predictive ability of the input patterns. Stronger reinforcement signals result in more discriminative information extraction and better reconstruction of the input signals, while novel inputs induce correlated activity between output neurons, which produces transient changes in lateral inhibitory synapses and feed-forward connections that lead to efficient active decorrelation and compression of information.

A subtle and key difference between RDDR and action selection models lies therefore in the transient nature of lateral connectivity within BG nuclei. Correlation between pallidal neurons, which is initially weak, was increased when a primate learned associations between cues and key presses (Bar-Gad et al., 2000, 2003b). This experimental validation cannot be explained by the sparsity of BG connectivity – it rather represents a proof-of-concept of the assumption of the PCA-like role of the BG.

The method used to calculate correlation between neuronal activity can greatly influence the resulting estimate of response similarity between neuronal pairs (Cohen and Kohn, 2011; Nevet et al., 2007). Because the number of events and the magnitude of the event-

related rate modulations can influence correlation estimates, a lack of correlation does not necessarily imply a lack of LOS (Leblois et al., 2007; Levy et al., 2002). Conversely, correlated neuronal activity can be elicited in the absence of LOS by global brain activation states or population wide oscillatory activity patterns (Nini et al., 1995; Urbain et al., 2000). Various neural mechanisms might underlie LOS. Intra-nuclei mechanisms such as lateral connections between MSNs or striatal interneurons, as well as inter-nuclei mechanisms such as DA innervation and STN input, may implement neuronal specificity (Bronfeld and Bar-Gad, 2011). Both DAergic and cholinergic neurotransmission might play a role in dimensionality reduction in the BG (Bergman et al., 1998a; Morris et al., 2003, 2004).

While a combination of multiple mechanisms might be in play, the sources of LOS remain to be elucidated. LOS might explain multiple facets of PD symptoms, such as tremor, bradykinesia and rigidity (Bar-Gad and Bergman, 2001; Bar-Gad et al., 2003a; Bergman and Deuschl, 2002; Bergman et al., 1998a; Bronfeld and Bar-Gad, 2011; Helmich et al., 2012). In this view, a persistent state of negative reinforcement, inefficient dimensionality reduction, and abnormally synchronized BG activity characterize PD. There are indeed several reports of synchronized oscillatory BG activity in PD (Belluscio et al., 2013; Ellens and Leventhal, 2013; Levy et al., 2000; Nambu and Tachibana, 2014), after DA depletion (Dejean et al., 2008, 2012; Jaidar et al., 2010). This oscillatory neuronal activity was found within and between BG nuclei (Moran et al., 2012) and typically affects beta frequency bands (Brown, 2007; Stein and Bar-Gad, 2013). Evidence also suggests that DA substitution does not fully abolish synchronous activity (Heimer et al., 2006).

Although somatotopy is still preserved to a certain extent in the parkinsonian state, at least in the GPi and STN (Baker et al., 2010; Rodriguez-Oroz et al., 2001; Theodosopoulos et al., 2003), several studies also showed a larger relative number of pallidal neurons exhibiting movement-related activity (Baker et al., 2010; Erez et al., 2011; Filion et al., 1988; Williams et al., 2005), as well as a substantial proportion of neurons modulating their activity in response to more than a single body part (Baker et al., 2010; Boraud et al., 2000; Filion et al., 1988; Levy et al., 2001; Taha et al., 1996a). Although not explicitly predicted by the RDDR model, one study found increased synchronous activity in M1 (Goldberg et al., 2002). The RDDR model is therefore supported by multiple experimental observations made in non-human primates and in patients undergoing surgery using intracranial recordings (Bronfeld and Bar-Gad, 2011). Moreover, LOS has been confirmed in humans with dystonia (Delmaire et al., 2005; Nelson et al., 2009; Quartarone et al., 2008; Tamburin et al., 2002), and indirectly in patients with GTS (Ganos et al., 2015; Yael et al., 2015). Furthermore, its relevance to the study of PD pathophysiology is attested by studies using MPTP in primates, which found evidences of LOS in the GPi (Leblois et al., 2006) and BG-recipient thalamus (Pessiglione et al., 2005). Although the RDDR model builds on motor function and dysfunction, it may also apply to associative and limbic functions, both which being differentially affected along PD progression and according to symptomatic treatments

(Cools, 2006; Tremblay et al., 2015). Although a recent fMRI study interpreted cortical activity changes in PD as supporting the LOS hypothesis, it provided only weak evidence for minor changes in the BG (Disbrow et al., 2013). In summary, in PD patients the relationship between LOS, disease progression and their modulation by DA substitution remain under-investigated and largely unknown.

1.3. Brain imaging

In humans, the striatal loss of DA innervation is particularly evident when investigated with PET and SPECT imaging (Brooks and Pavese, 2011; Stoessl, 2011a). PET imaging is more expensive, but usually provides imaging at higher resolution as compared to the latter (Weingarten et al., 2015). These non-invasive methods quantify the density of presynaptic terminals within the striatum or striatal DA receptors and are commonly used to differentiate PD from other neurological diseases without loss of DA neurons such as ET, vascular parkinsonism, psychogenic movement disorder, dystonic tremor, normal pressure hydrocephalus, dopa-responsive dystonia and AD (Kalia and Lang, 2015).

Nowadays, MRI, PET and SPECT are part of the medical procedure that assist differential diagnosis in PD (Brooks, 2010). PET and SPECT imaging measures include activity of aromatic aminoacid decarboxylase with ^{18}F-dopa PET, availability of presynaptic DA transporters with ^{123}I-2β-carbomethoxy-3β-(4-iodophenyl)tropane (^{123}I-CIT) or ^{123}I-2β-carbomethoxy-3β-(4-iodophenyl)-N-(3-fluoropropyl)nortropane (^{123}I-FP-CIT) SPECT and amount of vesicular monoamine transporter (VMAT2) with ^{11}C-dihydrotetrabenazine (^{11}C-DTBZ) or ^{18}F-dihydrotetrabenazine (^{18}F-DTBZ) PET, as well as less common radio ligands such as ^{11}C-PK11195 (Algarni and Stoessl, 2016; Brooks and Pavese, 2011; Pavese and Brooks, 2009; Politis, 2014; Weingarten et al., 2015). Asymmetric loss of putaminal fluoro-dopa or DA transporter, typically following a rostro-caudal gradient, further confirms PD diagnosis (Obeso et al., 2010; Schapira, 2006). The posterior-to-anterior gradient is preserved but the initial side-to-side asymmetry later vanishes with disease progression (Politis, 2014). Additionally, DA imaging techniques revealed that loss of DA innervation is faster early in disease course.

The discovery of patients diagnosed with early PD but presenting scans without evidence of DAergic deficit (SWEDD), questioned the validity of these imaging markers. However, DA imaging approaches fail to distinguish PD from atypical forms of parkinsonism such as PSP, MSA, CBD and dementia with LB (Kalia and Lang, 2015). On the other hand, metabolic PET and diffusion MRI can differentiate relatively well between PD, MSA and PSP (Brooks, 2010; Politis, 2014; Stoessl et al., 2014). PET imaging can also be used to measure regional cerebral blood flow (CBF). Apart from the main findings highlighted in section 1.1.5, PD is associated with a linearly increased glucose metabolism in the subthalamic nucleus, pallidum, pons and motor cortex, and decreased metabolism in prefrontal and parietal

areas. However, metabolic PET has an attenuated ability to track preclinical PD compared with DAergic PET, the latter preceding clinical diagnosis by about 5 years (Politis, 2014; Savica et al., 2010).

$H_2{}^{15}O$-PET studies showed a decreased activity of the rostral SMA and right dorsolateral prefrontal cortex (DLPFC) in non-medicated ("OFF") PD patients moving their hands without external instructions regarding the type of movement and the onset of the latter (van Eimeren and Siebner, 2006). To induce a selective release of endogenous DA in the motor cortico-BG-thalamic loop, focal high-frequency transcranial magnetic stimulation (TMS) was applied on M1. ^{11}C-raclopride-binding potential in the posterior putamen was reduced in healthy control (HC) subjects, suggesting an increase in endogenous DA release caused by repetitive stimulation of cortico-striatal glutamatergic inputs from M1. Conversely, the same procedure applied in patients with unilateral PD produced a similar putaminal DA release but of smaller magnitude. Similar to STN lesions, chronic STN stimulation in PD seems to attenuate metabolic increase in pallidum, thalamus, pons and cerebellum that co-vary with metabolic decrease in lateral premotor and parieto-occipital associative areas. A ^{11}C-raclopride PET study showed that DA release increase after administration of oral levodopa was large and returned to baseline within 4 hours in patients with motor fluctuations, whereas it was smaller and more sustained in patients who maintained a stable therapeutic response. PD patients experiencing LIDs, as well as longer disease duration, were shown to be associated with increased DA release (Stoessl, 2011b).

It is worth noting that DBS effects are detectable using PET, EEG or fMRI (Perlmutter and Mink, 2006). Mapping of ^{18}F-Dopa PET before and after STN DBS did not reveal any difference in nigrostriatal denervation but SPECT imaging showed rCBF increase in rostral SMA, lateral premotor cortex (PMC) and DLPFC (van Eimeren and Siebner, 2006). Other PET studies found several neurotransmitter changes in PD associated with various non-motor symptoms (Stoessl, 2009). Although PET showed an increase in striatal ^{18}F-dopa uptake associated with intra-putaminal infusion of recombinant human GDNF, it did not result in clinical improvements in PD. Striatal transplantation of human fetal DA neurons hold great promises as ^{18}F-dopa PET studies revealed that cells survived and stored DA but double blind controlled trials showed that these changes were not associated with improvements at the clinical level (Brooks and Pavese, 2011). Carriers of *parkin* mutation without any clinical manifestation showed reduced presynaptic DA uptake in the posterior putamen, suggesting a latent nigrostriatal deficit (van Eimeren and Siebner, 2006). In line with the idea that PD is a multifactorial disease, it has generally been argued that the combination of multiple imaging methods provides great benefits in terms of specificity and sensitivity (Weingarten et al., 2015).

Other imaging methods assisting PD diagnosis include notably transcranial B-mode sonography to detect SN hyper-echogenicity due to iron overload, cardiac imaging to reveal

cardiac denervation, ^{123}I-metaiodobenzylguanidine (MIBG) scintigraphy for the detection of reduced cardiac postganglionic sympathetic innervation, arterial spin labelling techniques using perfusion MRI to detect reduced CBF in cortex or BG, magnetic resonance spectroscopy (MRS) to detect changes in DA, GABA, glutamate and energy metabolism, as well as various markers in event-related potentials (ERPs) – such as the Bereitschaftspotential, the contingent negative variation, the lateralized readiness potential, alpha and beta frequency bands – derived from electroencephalography (EEG) and magnetoencephalography (MEG) (Auer, 2009; Chahine and Stern, 2011; De Virgilio et al., 2016; Georgiev et al., 2016; Pavese and Brooks, 2009; Politis, 2014; Pyatigorskaya et al., 2013; Sharma et al., 2013; Sian-Hülsmann et al., 2011; Weingarten et al., 2015). These imaging methods will not be discussed further. In the following sections a brief overview of MRI methods and their use in the study of PD is given. MRI has many advantages: contrarily to intracranial EEG, it is non-invasive; unlike PET or SPECT imaging that complicates routine use and intensive patient's follow-up due to radioactive compounds usage, it allows for longitudinal design studies; MRI potentially provides whole brain coverage at high spatial resolution, despite limited temporal resolution in comparison to surface EEG or MEG.

1.3.1. Functional MRI of the brain

MRI measures how radio frequency electromagnetic waves affect energy states of dipoles within a magnetic field. Hydrogen nuclei in water are the main source of signal in the case of brain MRI (Logothetis, 2008; Logothetis and Wandell, 2004; Logothetis et al., 2001). Functional MRI (fMRI) is widely available and does not require the injection of a radiotracer. This technique indirectly measures dynamic changes in neural activity by detecting the deoxygenated haemoglobin, which is paramagnetic. It interacts with water molecules surrounding blood vessels, leading to a change in the proton signal (Niethammer et al., 2012). fMRI signals acquired using traditional acquisition schemes are not quantitative. The observed blood-oxygen-level dependent (BOLD) effect is the result of neurovascular coupling, whereby CBF overcompensates for oxygen decrease. The BOLD effect is thought to reflect primarily neuronal activity through changes involving a complex interaction between cerebral blood volume (CBV), cerebral metabolic rate of oxygen consumption ($CMRO_2$) and CBF (Mullinger et al., 2014). Furthermore, neuro-vascular coupling might be affected by astrocytes, pericytes, ageing and pathological states (Hillman, 2014).

While increased fMRI signal following stimulation – i.e. a positive BOLD – might be relatively safely considered as neuronal activity increase, a different neurovascular coupling mechanism might underlie decreased fMRI signal, i.e. a negative BOLD (Mullinger et al., 2014). The BOLD effect is often considered as reflecting peri-synaptic activity in the form of local field potentials rather than spiking rate of individual neurons but the exact

underlying neuronal phenomenon might vary from a brain region to another (Ekstrom, 2010). The common modelling scheme for fMRI data relies on the linear transform model (Heeger and Ress, 2002). The assumption here is that the fMRI signal is proportional to a measure of local neural activity, although averaged over a spatial extent of several millimetres and over a period of few seconds. Although these assumptions might be invalid in some circumstances, they hold for some recording sites and using certain experimental protocols.

Recently, a growing interest has emerged into experimental protocols that do not impose a particular task to perform to subjects lying in the MRI scanner. Typical instructions in resting-state fMRI (rsfMRI) studies consist of requesting the subject to close the eyes and to not think about anything in particular while staying awake. Subsequent analyses of such data classically involve correlation or connectivity analyses, which are usually termed "functional" or "intrinsic" connectivity. Because such protocols do not involve an experimental or psychological manipulation like in task-based fMRI, and depending on the way data analysis is conducted, there is a substantial risk of violation of the construct validity, i.e. of looking at a vascular rather than psychological effect (Webb et al., 2013). Task-based fMRI also allows for investigating relationships between brain regions in terms of brain activity. In the latter case, these connectivity analyses are often referred to as "effective" functional connectivity analysis (2004).

Besides connectivity, common schemes applied to analyse fMRI data consists of applying general linear modelling (GLM) after data filtering and spatial registration pre-processing steps. GLM is essentially a multiple linear regression and is frequently performed independently at every voxel ("volume element") to produce statistical parametric maps (Friston et al., 1994). As mentioned above, depending on the acquisition protocol, fMRI data acquisition can be fast and produce brain images of varying spatial resolution. The magnetic field strength of the MRI scanner also plays an important role in this context (Duyn, 2012; Francis and Panchuelo, 2014; Harel, 2012; Olman and Yacoub, 2011). Recently, several advances were made to optimize fMRI acquisition (Ben-Eliezer et al., 2012; Feinberg and Setsompop, 2013; Hyde et al., 2001; Jesmanowicz et al., 1998; Lin et al., 2012; Lutti et al., 2012; Posse, 2012; Posse et al., 2012; Triantafyllou et al., 2005, 2011) and test complex scientific questions using powerful methods (Davis and Poldrack, 2013). Lately, remarkable achievements in terms of spatial precision were accomplished with fMRI, such as the investigation of computational heterogeneity within the mesencephalic DA system (D'Ardenne et al., 2013) or the mapping of orientation dominance columns in the visual cortex (Cheng, 2012). Nevertheless, BG remain particularly challenging areas for fMRI as these small nuclei are located far away from channels of the MRI head coil and are associated with a complex functional topography and high iron content that reduces signal-to-noise ratio, especially in the pallidum (Drayer et al., 1986; Dušek et al., 2013).

fMRI has been notably used to compare PD patients to HC subjects, but also to compare different groups of patients based on the presence or absence of motor or non-motor symptoms, to investigate neural mechanisms underlying PD-related deficits in various tasks, as well as to study the effect of various treatments (Christopher and Strafella, 2013; Lenka et al., 2015; Monchi and Stoessl, 2012; Ray and Strafella, 2012; Ryterska et al., 2013; Snijders et al., 2016; Weingarten et al., 2015). fMRI studies mostly focused on cognition in PD (Marino et al., 2012). Besides rsfMRI results which are not considered here, the main findings using fMRI are that PD patients, due to abnormal pallidal outflow, show impaired activation of the DLPFC and SMA – which can be restored after apomorphine administration – during motor imagery and execution, increased activation in M1 and lateral premotor cortex bilaterally, over-activation of inferolateral parietal and premotor areas during sequential finger activation – probably due to the facilitation of movement initiation by external cues (van Eimeren and Siebner, 2006; Nandhagopal et al., 2008). These results are consistent with findings using PET.

Overall, studies revealed that attention might be responsible for a considerable source of variation in fMRI results and interpreted most of the activity changes in the cerebral cortex as a consequence of a compensatory mechanism following altered output in cortico-BG-thalamic loops. Besides a study showing that effective connectivity between motor regions in PD is not strikingly affected by DA administration (Rowe et al., 2010), fMRI findings using effective connectivity globally showed increased connectivity between PFC, pre-SMA, cingulate motor cortex and cerebellum in PD, as well as decreased coupling between putamen and M1 – which is conversely increased after levodopa intake in PD who later develop LIDs (Gao and Wu, 2016). Furthermore, it was reported that attention to action did not enhance connectivity between PFC, lateral premotor cortex and SMA in PD. Rather than reviewing more in detail results from fMRI studies in PD, a visual summary of a meta-analysis based on activity changes coordinates in space is presented with focus on BG structures (**Figure 5**).

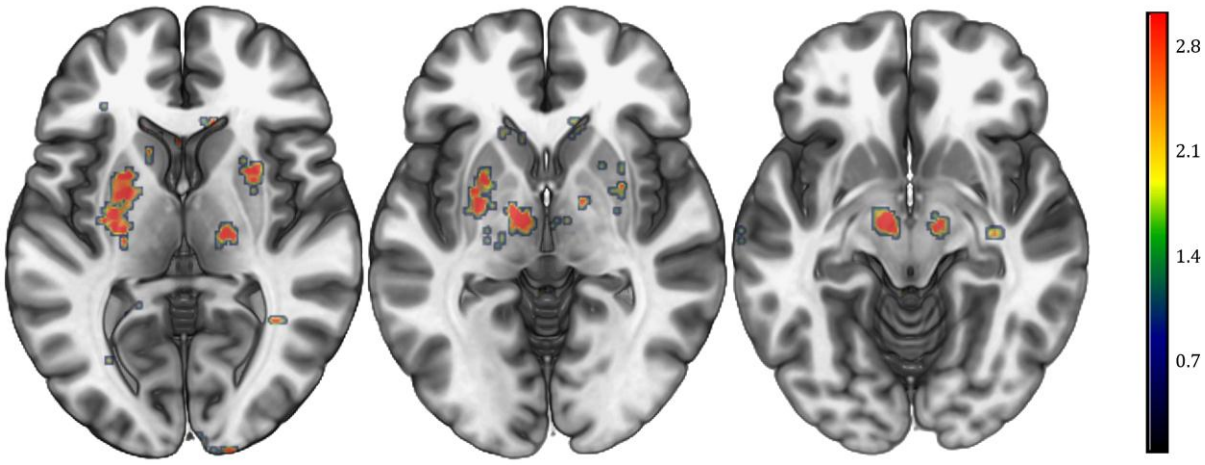

Figure 5: Results of a meta-analysis on functional imaging studies including the term "Parkinson's disease", using reverse inference (http://neurosynth.org; Yarkoni et al., 2011). The colour bar indicates z-scores. Statistical significance is set to $p < 0.01$, corrected for multiple comparisons using false discovery rate. Statistical maps were rendered on a canonical T1-weighted image.

The question of functional topography, especially for motor function in the cortex, has been debated through several fMRI studies. The very existence of an iconic homunculus (Penfield and Rasmussen, 1950) generated many studies aiming at demonstrating segregated representations of different body parts. Some studies, explicitly testing the degree of segregation, used metrics such as Euclidean distances between activation maxima or centres of gravity to quantify between-limb (Alkadhi et al., 2002a, 2002b; Lotze et al., 2000), within-limb (Cunningham et al., 2013; Kapreli et al., 2007; Kleinschmidt et al., 1997; Plow et al., 2010; Strother et al., 2012) and finger somatotopy (Beisteiner et al., 2001; Dechent and Frahm, 2003; Indovina and Sanes, 2001). Studies investigating somatotopy representations of orofacial articulators used similar approaches (Grabski et al., 2012). Centers of gravity were sometimes weighted by the strength of the BOLD signal at each coordinate (Hlustik et al., 2001). One study developed a similar metric termed "selectivity index" to reveal finger somatotopy (Olman et al., 2012). Findings from these studies support the idea of segregated representations of body parts in motor cortical areas despite substantial overlap, especially between different limbs, whereas finger somatotopy is more debated.

A small number of fMRI studies investigated motor somatotopy in the BG and thalamus and yielded contradictory findings regarding the amount of overlap between representations (Gerardin et al., 2003; Maillard et al., 2000; Oguri et al., 2013; Scholz et al., 2000; Staempfli et al., 2008). A flexible framework has been proposed to study what is referred to as "representational similarity analysis" (RSA). This approach extends the usage of distance metrics to any kind of dissimilarity measure such as linear correlation or Manhattan distance and suggests to perform notably clustering or multidimensional scaling methods

to summarize results (Kriegeskorte, 2008; Kriegeskorte and Kievit, 2013; Nili et al., 2014). The pitfall of geographic approaches and RSA is that they do not take into account for the presence of noise in the fMRI signal. More specifically, noise in fMRI is known to vary according to the region of interest (ROI) and the BG, brainstem and cerebellum are particularly susceptible to be associated with noisy fMRI time courses (Brooks et al., 2013; Liu, 2016; van der Zwaag et al., 2015). In some circumstances, comparing indices of dissimilarity across brain regions or group of subjects is invalid because the distance metric does not only reflect the distance between patterns of brain activity but also inherent noise in the measurement.

Recently, an extension of RSA, termed "pattern component model" (PCM), has been developed to overcome this limitation (Diedrichsen et al., 2011). The latter method provides robust estimates of similarity between brain activity patterns and has shown promising results when applied to digit somatotopy (Diedrichsen et al., 2013; Ejaz et al., 2015). However, spatial hypotheses can be tested differently. An alternative framework is based on Bayesian model comparison and reverses the classical scheme aiming at predicting the fMRI signal based on experimental factors: instead, signals from multiple voxels is combined with the objective to predict experimental variables, hence the term "multivariate Bayes" (MVB) (Friston et al., 2008). This method allows for testing how information is represented in the brain and to typically test explicitly whether a given set of brain signals predict better the behavioural outcome as compared to another.

1.3.2. Diffusion MRI

A growing interest recently emerged for diffusion MRI in PD. Diffusion MRI, or diffusion-weighted imaging (DWI), is close to fMRI from the MRI physics point of view and captures the translational displacement of water molecules (Bammer, 2003; Le Bihan, 2012; Le Bihan et al., 2001). The basic principle by which DWI allows the reconstruction of structural connectivity in the human brain relies on the behaviour of water molecules: in the CSF, the latter move freely according to Brownian motion, whereas when trapped in axon bundles, they move in a restricted fashion, following the directions of axonal tracts (Johansen-Berg and Rushworth, 2009). By sampling water diffusion in many directions, an accurate reconstruction of white matter tracts is possible. Advanced diffusion acquisition protocols manipulate additionally other factors such as the *b*-value in order to resolve complex situations such as crossing or "kissing" fibres, as well as to later apply more complex biophysical models (Frank, 2001, 2002; Nagy et al., 2013; Tournier et al., 2013; Tuch et al., 2002; Zhang et al., 2012). Tractography is the process of modelling – using one among several tracking algorithms available (Fillard et al., 2011; Staempfli et al., 2006; Tournier et al., 2007, 2008) – connections between two locations in the brain. DWI allows also computing different parameters of diffusivity based on the tensor model, which essentially extract eigenvalues from the tensor consisting of intensities of diffusion in each

direction (Le Bihan et al., 2001; Soares et al., 2013; Tournier et al., 2011). Common diffusion tensor imaging (DTI) parameters include fractional anisotropy (FA), mean diffusivity (MD), radial diffusivity (RD) and the apparent diffusion coefficient (ADC). Information provided by DWI has shown great efficacy to parcellate thalamic nuclei (Draganski et al., 2008; Klein et al., 2010; Lambert et al., 2016). Besides the inability of inferring directionality of connections from diffusion MRI data, the latter have to be carefully interpreted (Jones and Basser, 2004; Jones and Cercignani, 2010; Jones et al., 2013).

DTI studies in PD revealed decreased FA and MD in the SN and other cortical, subcortical, brainstem and cerebellar regions (Duncan et al., 2013; Schwarz et al., 2013; Tessitore et al., 2016; Weingarten et al., 2015). Reduction of FA was greater in the caudal than rostral SN. Although diffusion MRI findings are occasionally divergent in PD (Weingarten et al., 2015), the same study reported a 100% sensitivity and specificity in distinguishing PD from HC subjects (Wu et al., 2011). Correlations between the latter measures and symptoms severity generally suggest that increased FA and MD are normally associated with better clinical function – with few exceptions though. Indeed, PD was associated with increased MD compared to HC subjects in the corona radiata, internal capsule, cerebral peduncle, cingulum, uncinate fasiculus, crus fornix stria terminalis, corpus callosum, external capsule, superior longitudinal fasiculus, posterior thalamic radiation, superior cerebellar peduncle and tracts near the precuneus and supramarginal gyrus. It is worth mentioning that the cortico-striatal, cortico-spinal, cortico-pontine and cortico-bulbar tracts are crossing at the level of the corona radiata. Furthermore, the cingulum, uncinate fasciulus and external capsule are pathways of cholinergic projections from the nucleus basalis of Meynert (Weingarten et al., 2015). The presence of symptoms such as depression in PD has shown to be associated with reduced FA in the frontal cortex (Chagas et al., 2013). DTI might also detect early subcortical white matter tract degeneration (Duncan et al., 2013; Sharma et al., 2013). In addition, ADC, notably putaminal diffusivity, seems to differentiate PD from MSA and PSP (Mahlknecht et al., 2010; Politis, 2014). Reduced probability of connections has been also reported in PD (Pyatigorskaya et al., 2013). Furthermore, diffusion MRI is helpful in differentiating PD from atypical parkinsonism and other neurodegenerative diseases (De Virgilio et al., 2016; Goveas et al., 2015; Kalia and Lang, 2015; Meijer et al., 2013; Sharma et al., 2013).

1.3.3. Quantitative MRI

In this sub-section, findings regarding grey and white matter volume as estimated by voxel-based morphometry, as well as cortical thickness, are briefly mentioned, while MRI techniques including relaxometry, susceptibility weighted imaging and multi-parameter mapping are particularly emphasized. In contrast to sections 1.3.1 and 1.3.2, the detailed

description of imaging sequences would be particularly lengthy and is beyond the scope of this work. Brain atrophy and various morphological changes associated with PD such as cortical thickness have been reported in cortical, BG and brainstem regions, consistent with pathological findings (Stoessl et al., 2014; Weingarten et al., 2015). Obvious atrophy in SN is visible but, taken alone, does not help differentiating early stage PD neither from HC subjects, nor from other forms of neurodegeneration (Politis, 2014). Atrophy in other brain regions such as the cerebral peduncles is found in PSP. VBM results show grey matter volume (GMV) increases in posterior putamen correlating with reduction in putaminal ^{18}F-DA uptake (van Eimeren and Siebner, 2006). Striatal hypertrophy is thought to reflect a compensatory mechanism promoting motor function in the absence of DAergic dysfunction. T2 hypo-intensities can differentiate PD from MSA, and VBM allows for distinguishing PD from PSP, PD and HC based on atrophy patterns in subcortical motor networks (Hotter et al., 2009; Mahlknecht et al., 2010; Politis, 2014). Reports of decreased GMV in PD with depression are controversial and some studies found instead white matter loss in anterior cingulate, frontal and orbitofrontal regions (Kostic and Filippi, 2011). Dementia and FOG in PD are associated with extensive cortical atrophy in multiple regions, which may also be present in PD with mild cognitive impairment (MCI) (Duncan et al., 2013; Ibarretxe-Bilbao et al., 2009, 2011; Kostic et al., 2012; Sharma et al., 2013). Genetic mutations affecting *parkin*, *PINK1* and *ATP13A2* were associated with GMV changes in the BG (Godau et al., 2012).

Recent advances in structural MRI include ultra-high field strength imaging at 7 Tesla, new MRI sequences such as diffusion tensor imaging, susceptibility-weighted imaging (SWI) and T2*-weighted magnitude imaging (T2*WI), as well as image reconstruction methods like susceptibility-weighted phase imaging (SWPI) and quantitative susceptibility mapping (QSM) (Lehéricy et al., 2014; Liu et al., 2014; Reichenbach et al., 2015). The SN appears hyperintense in proton density-weighted (PDw) images and neuromelanin T1-weighted spin-echo images (NMw) and hypointense in two-dimensional T2*WI and three-dimensional T1-weighted MP2RAGE (3DT1w) (Lehéricy et al., 2012, 2014). Other MRI techniques such as fast spin echo acquisitions have great potential for BG and SN imaging. Magnetic field strength is particularly important in this context to improve signal-to-noise ratio (Schuff, 2009). While these new imaging techniques may greatly improve DBS surgery (Hickey and Stacy, 2016; Rowland et al., 2016), they also have generally confirmed pathological findings.

Increased susceptibility in the SN, consistent with iron accumulation, alterations in adiabatic R1 ρ mapping in brainstem, as well as decreased SN magnetization transfer (MT) values and diminished smoothness in SN borders using T2*WI has been demonstrated (Tuite et al., 2013; Weingarten et al., 2015). Relaxation along a fictitious field (RAFF) has also shown great potential in separating the SN from other nuclei (Tuite et al., 2013). Reduced MT ratio, as well as reduced T2/T2* and increased R2/R2* derived from

relaxometry, were shown in PD (Pyatigorskaya et al., 2013). Moreover, imaging techniques sensitive to neuromelanin changes has shown decreased SN volumes and locus cœruleus signals. Other studies using multispectral structural MRI – including multi-echo T1-weighted, multi-echo proton density, T2-weighted and T2-weighted fluid-attenuated inversion recovery (FLAIR) sequences) – suggested that degeneration of SNc precedes that of cholinergic basal forebrain (Sharma et al., 2013). While nigral iron elevation has been shown to correlate positively with the severity of motor symptoms but not disease duration, iron content in the STN correlates with the latter (Sian-Hülsmann et al., 2011). Moreover, MRI field-dependent relaxation rate (R2) (FDRI) in the SN is shown to increase in early-onset PD and decrease in late-onset PD, suggesting that ferritin iron, known to increase R2, can differentiate between different forms of parkinsonian syndromes. R2* in SN and caudal putamen has been recently shown to correlate with PD progression over several years (Ulla et al., 2013). Iron levels in the putamen seem to correlate also positively with disease duration as shown by partially refocused interleaved multiple echo (PRIME) magnetic resonance sequence. This finding contradicts previous results showing iron content reduction only in the GPe and GPi in PD. While many brain metals such as iron, copper, zinc, manganese, selenium, magnesium, molybdenum, calcium and potassium have interesting potential to evaluate therapies for neurodegenerative diseases (Gh Popescu and Nichol, 2010), careful consideration of iron deposition imaging sensitivity and specificity is required before interpreting such results derived from MRI (Haacke et al., 2005). Nevertheless, most of the semi-quantitative MRI methods have completed and reflected results from biochemical analyses of post-mortem tissue (Sian-Hülsmann et al., 2011).

More generally, MT as assessed using multi-parameter mapping (MPM) showed more accuracy in delineating BG structures, revealing age-related changes and differentiating between motor, limbic and associating circuits in terms of tissue properties (Accolla et al., 2014; Draganski et al., 2011; Helms et al., 2009). These parameters, which include the longitudinal relaxation rate (R1), the effective transverse relaxation rate (R2*) and effective proton density (PD*) in addition to MT, are robustly linked to specific tissue properties, are feasible in clinical settings even at high-resolution imaging (Weiskopf et al., 2013) and can overcome limitations of standard structural MRI techniques. Indeed, the lack of specificity of T1-weighted imaging, as well as commonly derived measures of cortical thickness and GMV, does not solely depend on genuine neurobiological phenomena such as brain atrophy or neurogenesis (Lorio et al., 2016).

1.4. Research questions and hypotheses

In this work, I try to answer pertinent questions on the pathophysiology of PD using state-of-the-art non-invasive imaging methods. Given recent experimental evidences coming from primate and rat studies supporting the RDDR model, the main goal of our research was to validate the LOS hypothesis in PD. Furthermore, I investigated whether DA

substitution would attenuate the LOS in PD. PD is mainly defined as a movement disorder despite a broad range of non-motor symptoms, therefore motor somatotopy was chosen as a working example. In what follows, we refer to "functional segregation" as a proxy for assessing the LOS.

However, reports of motor somatotopy in the BG are conflicting, a preliminary study was thus performed to objectively evaluate the influence of fMRI spatial resolution on the effective overlap between representations of different body parts. To maximize the separation between activation patterns at the representational level, subjects were instructed to move different limbs. Although finger movements would have been easy to control and record during fMRI acquisition, the overlap between digit representations would have probably been too important at baseline to find any difference in PD patients as finger somatotopy is already debated at M1 level. Subjects were requested to perform repeated movements of hands, feet and lower facial musculature within block-design experiments, which are known to maximize activation detection efficiency (Henson, 2011). Different fMRI protocols were tested, each being optimized for a given isotropic voxel size. PCM was then performed to find whether the effective overlap between motor somatotopy representations, in various brain regions throughout the motor cortico-BG-thalamic loop, would be influenced by the scheme for fMRI acquisition, and if so, to which extent. This produced similarity – or correlation – estimates, which were transformed into a metric that we termed "Index of Specificity" (*IoS*), with low values indicating high functional segregation.

For the main study, I recruited PD patients and tested HC subjects with an optimized experimental paradigm. Monitoring movements of PD patients was crucial to make valid inferences at the representational level. Thus, we anticipate potential criticisms arguing that the loss of functional segregation in PD would be induced by motor performance bias, such as PD patients performing more often simultaneous movements of different body parts. A custom device was designed and built to measure to monitor task performance of HC subjects and PD patients and account for potential differences in movement features. Additionally, movements of lower facial musculature were not requested due to practical reasons, the custom device being capable of monitoring only movements of hands and feet. The duration of the fMRI experiment was also slightly increased to augment the number of trials, thereby maximizing statistical power. PD patients were tested twice, ON and OFF medication, to examine the effect off DA therapy on functional segregation. To test additional hypotheses outlined below, this experiment comprised acquisition of DWI data. Similarly to the preliminary study, MPM provided MT maps, which, in combination with advanced spatial registration algorithms, aimed at better delineating BG structures and improving spatial registration of MRI data across subjects. The main questions were as follows:

- Is PD associated with a loss of functional segregation?
- If so, does DA therapy restore functional segregation back to normal?
- What is the relationship between LOS and disease severity?

Given the massive connections shared between striatum and insula, the increased susceptibility of the latter to α-synuclein aggregation, its implication in non-motor symptoms in PD as well as results from meta-analyses suggesting a shift of insular activity in PD, we used another multivariate framework, MVB, which can also test for a loss of functional segregation, to test the hypothesis that PD is also associated with functional segregation in the insula. This resulted from our definition of the loss of segregation, which can be conceptualised in two different but complementary ways. According to the definition we used in the present work, "segregation" relates to spatial independence of neuronal signals associated to different behavioural events. In the extreme case, it refers to a one-to-one structure-function mapping (Friston and Price, 2003, 2011; Pessoa, 2014; Price and Friston, 2002). Conversely, loss of segregation can be defined either as: a) a given brain structure participating to multiple functions, like exemplified in Bronfeld and colleagues (2011); b) multiple brain structures involved in the same function, termed by Friston and Price as "degeneracy". While previous studies suggest a spatial shift of insular activity from the anterior to the posterior part relating to non-motor manifestations in PD, we aimed at testing whether this phenomenon is also present in a simple motor execution task.

Additionally, our objective was to test whether the LOS hypothesis applies, at a more general level, to the segregation between limbic, associative and motor cortico-BG-thalamic loops, as well as examining whether LOS extends to structural in addition to functional topography. To answer this question, we used DWI data acquired in the same study protocol and investigate the loss of segregation at the connectivity level, hence termed "structural segregation" in this context, while using the same metric – *IoS*, as derived from PCM – as for functional segregation. Because PD is associated with several non-motor symptoms in addition to motor symptoms, an additional goal was to test whether the loss of structural segregation in cortico-BG-thalamic connections would vary as a function of the profile of clinical symptoms in each PD patient.

To recapitulate, research questions for this work were as follows:

- What is the optimal fMRI spatial resolution to separate motor somatotopy patterns in the BG? This question was the purpose of Study 1.
- Is PD associated with a loss of functional segregation at the BG level? If so, does DA replacement therapy restores functional segregation back to normal? These questions were the matter of Study 2.

- Is PD further associated with a loss of functional segregation in the insula? We attempted to answer to this question in Study 3.
- Does the LOS presumably found for motor function extends to other functional territories as assessed by structural connectivity? Does this effect depend on the clinical symptomatic profile of PD patients? These topics were investigated in Study 4.

2. Experimental work

2.1. Optimal mapping of motor somatotopy in healthy subjects

2.1.1. Study 1

In this experiment, we evaluate the benefits of high-resolution fMRI to study motor somatotopy. In contrast to previous studies focusing on activation detection power, we investigate the trade-off between spatial resolution and SNR by quantifying the effective overlap between representations of different body parts as a measure of spatial precision. This allowed us to estimate the advantages of high-resolution fMRI beyond the considerations about the expected size of the activation cluster and make an informed decision on the optimal fMRI protocol for motor somatotopy mapping in deep brain nuclei and cortical areas.

Functional magnetic resonance imaging of motor somatotopy in cortical and subcortical brain regions – the "free lunch" dilemma between high spatial resolution and enhanced signal-to-noise ratio

Renaud Marquis[1], Sandrine Muller[1], Sara Lorio[1], Borja Rodriguez-Herreros[1], Anne Ruef[1], Lester Melie-Garcia[1], Ferath Kherif[1], Antoine Lutti[1], Bogdan Draganski[1,2]

[1] *LREN – Department of Clinical Neurosciences - CHUV, University of Lausanne, Lausanne Switzerland*

[2] *Max Planck Institute for Human Cognitive and Brain Sciences, Leipzig, Germany*

Running title: *Motor somatotopy in basal ganglia*

Abstract: 229

Text body: 2648

References: 52

Tables: 0

Figures: 2

Supplementary material: 5 figures, 21 tables in 3 Excel workbooks

Keywords: functional magnetic resonance imaging; segregation; image resolution; BOLD sensitivity

Corresponding author:
Bogdan Draganski
LREN - Département des Neurosciences Cliniques
CHUV, Université de Lausanne
Mont Paisible 16
1011 Lausanne
Switzerland
email: bogdan.draganski@chuv.ch
phone: +41-21-314 9638

Abstract

Although there is a growing motivation to increase the topological precision of functional magnetic resonance imaging (fMRI) to represent functional sensorimotor bran areas, the particular tissue properties of subcortical brain regions, notably in terms of iron content, pose significant challenges in terms of activation detection power. Because functional representations of small size might benefit from high-resolution fMRI, we test empirically the impact of fMRIs spatial resolution on the ability to segregate between body part representations in cortex and basal ganglia. Our block-design paradigm consisted of visually cued movements of facial musculature, upper and lower limbs. The motor task was repeated in a pseudo-randomized order using 2D/3D echo-planar imaging (EPI) acquisitions at 1.5mm, 2mm and 3mm spatial resolution. For statistical analysis of the degree of segregation between the body parts' spatial representations we used a pattern component model (PCM) to extract pattern similarity estimates. In contrast to cortical motor areas, the degree of effective similarity between spatial representations in subcortical areas was strongly impacted by the image resolution. The 1.5mm 3D EPI and 3mm 2D EPI protocol led to enhanced segregation between motor representations compared to the 2mm 3D EPI protocol. We recommend that future functional imaging studies with emphasis on motor mapping of subcortical brain structures take in account the particular importance of image resolution and encoding scheme when aiming at robustness and topological precision of the obtained results.

Introduction

The optimisation of functional MRI (fMRI) protocols for the study of sensorimotor function is a recurring issue (Hlustik et al., 2001; Kapreli et al., 2007; Kleinschmidt et al., 1997; Meier et al., 2008; Olman et al., 2012). The inherent inter-individual variability of sensorimotor representations is one of the main factors that hampers the straightforward comparison of applied imaging parameters and analytical strategies (Alkadhi et al., 2002; Beisteiner et al., 2001; Picard and Strick, 1996). Other factors influencing the degree of segregation of motor representations depend on the co-occurrence of limb joint movements that lead to multiple activation foci (Luft et al., 2002) and the differential organisation of functional representations across brain regions. It was generally found that BOLD activity patterns elicited during movement of different body parts were relatively segregated in the primary motor cortex (M1) despite substantial overlap (Cunningham et al., 2013; Kapreli et al., 2007; Meier et al., 2008; Zeharia et al., 2012), while the same representations in the supplementary motor area (SMA) were less separated (Indovina and Sanes, 2001; Strother et al., 2012). In the basal ganglia (BG) and thalamus, the literature shows either negligible (Lehéricy et al., 1998; Staempfli et al., 2008a) or substantial (Gerardin et al., 2003; Maillard et al., 2000) overlap between representation. We underline the fact that these studies used fMRI protocols with unequal spatial resolution parameters. Up to date, there are no reported fMRI findings focusing on deep brain nuclei and tackling the question about the impact of image resolution on the ability to spatially discriminate motor somatotopy patterns (Gerardin et al., 2003; Maillard et al., 2000; Oguri et al., 2013; Scholz et al., 2000; Staempfli et al., 2008b). This might be explained by the decay of the MRI signal that reduces BOLD sensitivity in these areas and complicates the mapping of fine-grained motor somatotopy (Pfefferbaum et al., 2010; Sullivan et al., 2009).

To quantify segregation between blood-oxygen-level dependent (BOLD) activity patterns, common metrics are the Euclidean distance between centers of gravity or activation maxima (Besle et al., 2013a; Delmaire et al., 2005; Hashimoto et al., 2013), Jaccard or Dice coefficients (Bennett and Miller, 2010; Bracci et al., 2012; Cunningham et al., 2013; Gorgolewski et al., 2010; Gupta et al., 2014; Maitra, 2010; Pajula et al., 2012; Plow et al., 2010) and the selectivity index (Olman et al., 2012). Most of these metrics share the issue of being strongly affected by noise, corrupting thereby the comparison of estimates across brain regions or groups of subjects (Diedrichsen et al., 2011).

The main aim of our study is to investigate the impact of fMRI spatial resolution on the ability to differentiate between representations of body parts in cortical and subcortical brain areas. Specifically, we compare fMRI protocols at 1.5mm, 2mm and 3mm isotropic spatial resolution in a

visually cued motor paradigm. We hypothesise that higher fMRI resolution will improve the ability to segregate between functional representations of different body parts, especially in deep brain nuclei, which are associated with fine-grained topographical organisation. For quantification of spatial precision we use a well-established analytical strategy measuring the degree of similarity between representations while accounting for differential noise level across brain regions (Diedrichsen et al., 2011).

Methods

Participants

From the recruited 16 right-handed healthy volunteers we discarded one individual due to insufficient data quality (9 female, mean age: 36.6 years, SEM: 4.47 years). The study was approved by the local ethics committee and participants gave their written informed consent.

Experimental paradigm

All volunteers performed the same motor execution task consisting of: 1) unilateral foot movement - flexion and extension of the right or left foot with the legs resting in flexed position on a platform, 2) unilateral hand movement – opening and closing of the hand with the arm kept in a resting position, or 3) unilateral lower face movement, in three separate sessions corresponding to the three different spatial resolution fMRI protocols. Each of the 3 experimental sessions comprised 18 blocks of movement repetitions during 16 seconds. Blocks of motor activity were interspersed with blocks of rest with the same duration. Before each block, the designated body part was shown on the screen followed by a countdown of 3 seconds. Subjects were instructed to move at a pace of 1Hz indicated by an icon of the corresponding body part displayed at that rate during the active blocks. The rest condition was marked by a fixation cross at the centre of the screen and subjects were asked to fixate it. Motor activity blocks were in pseudo-randomized order to prevent bias induced by potential effects of learning, performance and attention. This experiment was realised using Cogent 2000 developed by the Cogent 2000 team at the FIL and the ICN and Cogent Graphics developed by John Romaya at the LON at the Wellcome Department of Imaging Neuroscience. Movement execution was practiced before MRI scanning.

MRI acquisition

MRI data was acquired on a Siemens Prisma 3T scanner with a 64-channel head coil. The 3 mm isotropic resolution fMRI data was acquired using a 2D EPI sequence and the 1.5 and 2 mm

isotropic voxel size data were acquired using a 3D EPI encoding scheme because it provides enhanced BOLD sensitivity at high resolution (Lutti et al., 2012). The acquisition parameters were as follows: 1.5 x 1.5 x 1.5 mm^3: TE = 63 ms, slice TR = 63 ms, 64 slices, flip angle = 15°; 2 x 2 x 2 mm^3: TE = 66 ms, slice TR = 52 ms, 52 slices, flip angle = 15°; 3 x 3 x 3 mm^3: TE = 66 ms, slice TR = 66 ms, 30 slices, flip angle = 90°. The order of the 3 EPI sequences was pseudo-randomized across subjects. The structural MRI data consisted of quantitative images (Weiskopf et al., 2013) or T1-weighted MPRAGE images (TR = 2000 ms; TI = 920 ms; α = 9°; BW = 250 Hz / pixel; readout in inferior-superior direction; FoV = 256 x 232 mm; 176 slices) at 1 mm resolution.

MRI data pre-processing

All statistical analyses and data pre-processing were performed using the freely available Statistical Parametric Mapping software (SPM12; Wellcome Trust Centre for Neuroimaging, http://www.fil.ion.ucl.ac.uk/spm/) running under Matlab 7.13 (The MathWorks, Inc., Natick, Massachusetts, United States). EPI images were realigned to the subject's average image across runs, corrected for spatial distortions using the SPM fieldmap toolbox (Hutton, 2002). The parameters of registration to standardized MNI space were calculated on the anatomical image and the default settings of the "unified segmentation" framework followed by the diffeomorphic registration algorithm DARTEL (Ashburner and Friston, 2005; Ashburner, 2007). The spatial registration parameters were then applied to the functional time-series co-registered to the corresponding individual's anatomical scan and up-sampled to a uniform 1.5mm isotropic resolution. Prior to statistical analysis, we applied a spatial smoothing with a Gaussian kernel of 6 mm full-width-at-half-maximum.

Subject-level fMRI modelling

The statistical analysis at subject-specific level was performed using the General Linear Model (GLM) after convolving the onsets of the active blocks with a canonical hemodynamic response function (Friston et al., 1994, 1995; Worsley and Friston, 1995). We estimated six differential contrasts for each body side and body part separately while using the resting blocks as baseline. Preparation periods and realignment parameters estimated by SPM were included as covariates.

Group-level mass-univariate analysis

We used three identical flexible factorial designs for the group-level analyses corresponding to the three different EPI protocols and modelling the results from the six differential contrasts as

independent levels. The differential contrasts at the group level tested the positive correlation between movement and BOLD signal changes.

Pattern component modelling

Levels of segregation between functional representations of different body parts were estimated using the pattern component modelling (PCM) approach (Diedrichsen et al., 2011). The analysis required voxel-specific regression coefficients, which were extracted from subject-level GLMs in each of the following regions-of-interest (ROIs): M1, SMA, putamen, pallidum and thalamus (ventro-lateral and ventral postero-lateral nucleus). The PCM allowed producing unbiased estimates of correlation between multivariate voxel pattern decomposed into different components. The obtained coefficients of representational similarity (or correlation) were calculated in two ways: a) between movement representations across resolutions; b) between resolutions across movement representations. Only contralateral representations were considered, such that for each ROI, PCM was performed with a 3 x 3 factorial design (MOVEMENT x RESOLUTION) and without any constraint imposed on the variance-covariance matrix. The correlation coefficients were transformed using the Fisher r-to-z' transform (Sanabria-Diaz et al, 2013) and the absolute value was taken as an Index of Similarity (IoS). In other terms the IoS is the absolute value of the inverse hyperbolic tangent of the correlation coefficient r between representations:

$$IoS = |tanh^{-1}(r)|$$

Low values of IoS indicate high segregation between representations, whereas high values of IoS indicate high similarity between representations, i.e. lack of functional segregation between representations. These indices were subsequently converted to Z-statistics to allow for statistical comparisons (Sanabria-Diaz et al, 2013) using p-values corrected for multiple comparisons using false discovery rate (Benjamini & Hochberg, 1995). We performed comparisons of IoS Z-scores between resolutions for all pairs of movements and across resolutions for all types of movements. All p-values reported for these comparisons are corrected for multiple comparisons using false discovery rate (FDR).

Detection power analyses

Although activation detection power has been shown to decrease strongly with increased resolution elsewhere (Lutti et al., 2012; Triantafyllou et al., 2005), we provide as sanity tests

average t-scores per ROI within the 5% most significant voxels (Supplementary figure 3) and estimates of temporal signal-to-noise ratio (tSNR) at the voxel level (Supplementary figure 4).

Results

Mass-univariate analyses

The group level analysis demonstrated the expected somatotopy patterns in cortical and subcortical areas without major differences between different protocols (Figure 1; Supplementary figure 2). We report activations in primary motor cortical areas, thalamus, putamen and pallidum (whole brain results as supplementary material).

Indices of similarity

There were no significant differences between EPI protocols in cortical ROIs when comparing the IoS Z-scores across pairs of movements for each resolution and ROIs (Figure 2). We observed differences in subcortical ROIs where 3 mm provided lower IoS values compared to 1.5 mm in the left pallidum ($p = 0.01$) and right thalamus ($p = 0.001$). IoS values were significantly lower for 1.5 mm as compared to 2 mm EPI in the left putamen ($p = 0.02$) and right thalamus ($p < 0.001$). We showed that IoS values were lower for 3 mm compared to 2 mm EPI in the left putamen ($p = 0.01$), left pallidum ($p = 0.01$) and the right thalamus ($p < 0.001$). All z-scores of motor representations between EPI protocols were significant ($p < 0.05$, FDR-corrected), except for 3 mm EPI against other protocols in the thalamus, showing that motor representations were robustly mapped (Supplementary figure 1).

Discussion

In our study we provide empirical evidence for the importance of imaging protocol's spatial resolution settings when focusing on subcortical brain regions. Image resolution was shown to have marked effects on the measured segregation between functional representations of different body parts.

The prerequisite for our comparative analysis of fMRI parameter settings was the demonstration of a robust somatotopy pattern in cortical and subcortical regions. The obtained somatotopy map including primary motor cortex, SMA, putamen, pallidum and thalamic motor nuclei are anatomically plausible and in agreement with previous findings (Grafton et al., 1991; Lotze et al., 2000; Meier et al., 2008). We then used an established data-driven analytical approach (Diedrichsen et al, 2011) to obtain an index of segregation between functional representations of

different body parts. Our first observation confirmed that motor representations in cortical regions - M1 and SMA, show a higher degree of segregation when compared with subcortical structures and corroborate previous reports (Chainay et al., 2004; Cunningham et al., 2013; Indovina and Sanes, 2001).

Following this, we focused on estimating the impact of image resolution on segregation of functional representation in the deep brain nuclei. Our findings clearly demonstrate that the differentiation between cortical somatotopy patterns does not benefit from an increase of fMRI spatial resolution, however the opposite was true for the subcortical structures. The simplistic view that the higher spatial resolution will yield better segregation was confirmed when comparing 1.5 mm with 2 mm 3D EPI. However, we also observed that 3 mm 2D EPI provided better differentiation than 2mm 3D EPI and occasionally outperformed the 1.5 mm 3D EPI. One could speculate that the observed effects are due to the cumulated effects of image resolution and encoding scheme, with 3D EPI artificially increasing the effective overlap between representations in deep brain nuclei. Previous findings showing greater activation spread for 3D as compared to 2D EPI at identical resolution might support this hypothesis (Hu and Glover, 2007). Nevertheless, it is impossible to dissociate the respective contributions of image resolution and encoding scheme in our study. To validate this interpretation, we recommend thorough evaluation of functional imaging protocols with different encoding schemes and image resolution.

Unlike some of the metrics aiming at measuring functional segregation, the method used here is independent of an arbitrary threshold for statistical significance (Gorgolewski et al., 2010; Stevens et al., 2013) to enable the comparison of representational similarity across brain regions with differential noise distribution (Diedrichsen et al, 2011). There are however several limitations of our study that should be mentioned. One critical point that has to be addressed is the possibility that low IoS values could be the result of reduced BOLD signal. This interpretation is contradictory with several observations. 3 mm EPI systematically produced low IoS estimates while being associated with a very strong BOLD sensitivity (Supplementary figure 3 and Supplementary figure 4). In addition, comparable IoS values were obtained for all EPI protocols in cortical areas, where differences in BOLD sensitivity across image resolutions are expected (Triantafyllou et al., 2005) and were observed in our study (Supplementary figure 4). Thus, there is no systematic relationship between IoS values and BOLD sensitivity. Moreover, motor activity patterns were robustly mapped in cortical as well as subcortical regions and most of these patterns were consistent across EPI protocols (Supplementary figure 1). The only exception is the motor thalamus, where motor

mapping appeared to be consistent only across high-resolution protocols, i.e. between 1.5 mm and 2 mm. Furthermore, PCM reliably furthermore estimates similarity values between representations even when 75% of the voxels in the ROI are uninformative (Diedrichsen et al, 2011). This gives us the confidence that even a significant lack of overlap of activity between protocols will not change IoS values drastically.

We also investigated the interaction between spatial resolution and applied smoothing kernel to demonstrate that even when different spatial smoothing strategies are used we obtain similar results (Supplementary figure 5). The correspondences between results obtained using unsmoothed data, uniformly smoothed data, and data smoothed using a spatial kernel proportional to the sampling resolution strongly support the statement that the effect being examined in our study relates closely to fMRI resolution and not spatial smoothing. Nevertheless, the fact that the observed effects were not always present bilaterally in subcortical ROIs remains to be elucidated.

We show that spatial resolution of fMRI acquisition affects the degree of separation of motor somatotopy patterns and that this effect was varying across different brain regions. Deep brain nuclei, containing small-scale motor somatotopy, were affected by the effect of spatial resolution. Additional factors can modulate the observed similarity between functional representations. Previous studies have shown that the experimental design (Besle et al., 2013b), the way neuroimaging data are preprocessed (Geissler et al., 2005) and mass univariate inferences are conducted (Dechent and Frahm, 2003) can affect the effective overlap between BOLD activity patterns. In our study, these factors were kept constant.

Conclusion

We estimated the impact of fMRI's spatial resolution on the ability to segregate different BOLD activity patterns at 3T in cortical and subcortical areas. In contrast to cortical areas, motor somatotopy patterns in deep brain nuclei were more separable at very high and very low spatial resolution. Future studies might generalize our results to functional imaging of other brain functions, in other brain areas, at other field strengths, or using other imaging protocols and spatial resolutions.

References

Alkadhi, H., Crelier, G.R., Boendermaker, S.H., Golay, X., Hepp-Reymond, M.-C., and Kollias, S.S. (2002). Reproducibility of primary motor cortex somatotopy under controlled conditions. AJNR Am. J. Neuroradiol. *23*, 1524–1532.

Ashburner, J. (2007). A fast diffeomorphic image registration algorithm. NeuroImage *38*, 95–113.

Ashburner, J., and Friston, K.J. (2005). Unified segmentation. NeuroImage *26*, 839–851.

Beisteiner, R., Windischberger, C., Lanzenberger, R., Edward, V., Cunnington, R., Erdler, M., Gartus, A., Streibl, B., Moser, E., and Deecke, L. (2001). Finger Somatotopy in Human Motor Cortex. NeuroImage *13*, 1016–1026.

Bennett, C.M., and Miller, M.B. (2010). How reliable are the results from functional magnetic resonance imaging? Ann. N. Y. Acad. Sci. *1191*, 133–155.

Besle, J., Sánchez-Panchuelo, R.-M., Bowtell, R., Francis, S., and Schluppeck, D. (2013a). Event-related fMRI at 7T reveals overlapping cortical representations for adjacent fingertips in S1 of individual subjects. Hum. Brain Mapp. *35*, 2027–2043.

Besle, J., Sanchez-Panchuelo, R.M., Bowtell, R., Francis, S., and Schluppeck, D. (2013b). Single-subject fMRI mapping at 7 T of the representation of fingertips in S1: a comparison of event-related and phase-encoding designs. J. Neurophysiol. *109*, 2293–2305.

Bracci, S., Cavina-Pratesi, C., Ietswaart, M., Caramazza, A., and Peelen, M.V. (2012). Closely overlapping responses to tools and hands in left lateral occipitotemporal cortex. J. Neurophysiol. *107*, 1443–1456.

Chainay, H., Krainik, A., Tanguy, M.-L., Gerardin, E., Le Bihan, D., and Lehericy, S. (2004). Foot, face and hand representation in the human supplementary motor area. NeuroReport *15*, 765–769.

Cunningham, D.A., Machado, A., Yue, G.H., Carey, J.R., and Plow, E.B. (2013). Functional somatotopy revealed across multiple cortical regions using a model of complex motor task. Brain Res. *1531*, 25–36.

Dechent, P., and Frahm, J. (2003). Functional somatotopy of finger representations in human primary motor cortex. Hum. Brain Mapp. *18*, 272–283.

Delmaire, C., Krainik, A., Tezenas du Montcel, S., Gerardin, E., Meunier, S., Mangin, J.F., Sangla, S., Garnero, L., Vidailhet, M., and Lehericy, S. (2005). Disorganized somatotopy in the putamen of patients with focal hand dystonia. Neurology *64*, 1391–1396.

Diedrichsen, J., Ridgway, G.R., Friston, K.J., and Wiestler, T. (2011). Comparing the similarity and spatial structure of neural representations: A pattern-component model. NeuroImage *55*, 1665–1678.

Fonov, V., Evans, A.C., Botteron, K., Almli, C.R., Mckinstry, R.C., Collins, D.L., and Group, the B.D.C. (2011). Unbiased average age-appropriate atlases for pediatric studies. NeuroImage *54*, 313–327.

Fonov, V.S., Evans, A.C., McKinstry, R.C., Almli, C.R., and Collins, D.L. (2009). Unbiased nonlinear average age-appropriate brain templates from birth to adulthood. NeuroImage *47*, *Supplement 1*, S102-.

Friston, K.J., Holmes, A.P., Worsley, K.J., Poline, J.P., Frith, C.D., and Frackowiak, R.S. (1994). Statistical parametric maps in functional imaging: a general linear approach. Hum. Brain Mapp. *2*, 189–210.

Friston, K.J., Holmes, A.P., Poline, J.B., Grasby, P.J., Williams, S.C., Frackowiak, R.S., and Turner, R. (1995). Analysis of fMRI time-series revisited. NeuroImage *2*, 45–53.

Geissler, A., Lanzenberger, R., Barth, M., Tahamtan, A.R., Milakara, D., Gartus, A., and Beisteiner, R. (2005). Influence of fMRI smoothing procedures on replicability of fine scale motor localization. NeuroImage *24*, 323–331.

Gerardin, E., Lehericy, S., Pochon, J.-B., Tézenas du Montcel, S., Mangin, J.-F., Poupon, F., Agid, Y., Le Bihan, D., and Marsault, C. (2003). Foot, hand, face and eye representation in the human striatum. Cereb. Cortex *13*, 162–169.

Gorgolewski, K.J., Storkey, A.J., Bastin, M.E., Whittle, I., and Pernet, C. (2010). Single subject fMRI test–retest reliability metrics and confounding factors. NeuroImage *69*, 1–13.

Grafton, S.T., Woods, R.P., Mazziotta, J.C., and Phelps, M.E. (1991). Somatotopic mapping of the primary motor cortex in humans: activation studies with cerebral blood flow and positron emission tomography. J. Neurophysiol. *66*, 735–743.

Gupta, L., Besseling, R.M.H., Overvliet, G.M., Hofman, P.A.M., de Louw, A., Vaessen, M.J., Aldenkamp, A.P., Ulman, S., Jansen, J.F.A., and Backes, W.H. (2014). Spatial heterogeneity analysis of brain activation in fMRI. YNICL *5*, 266–276.

Hashimoto, T., Ueno, K., Ogawa, A., Asamizuya, T., Suzuki, C., Cheng, K., Tanaka, M., Taoka, M., Iwamura, Y., Suwa, G., et al. (2013). Hand before foot? Cortical somatotopy suggests manual dexterity is primitive and evolved independently of bipedalism. Philos. Trans. R. Soc. B Biol. Sci. *368*, 20120417–20120417.

Hlustik, P., Solodkin, A., Gullapalli, R.P., Noll, D.C., and Small, S.L. (2001). Somatotopy in human primary motor and somatosensory hand representations revisited. Cereb. Cortex N. Y. N 1991 *11*, 312–321.

Hu, Y., and Glover, G.H. (2007). Three-dimensional spiral technique for high-resolution functional MRI. Magn. Reson. Med. *58*, 947–951.

Hutton, C. (2002). Image Distortion Correction in fMRI: A Quantitative Evaluation. NeuroImage *16*, 217–240.

Indovina, I., and Sanes, J.N. (2001). On Somatotopic Representation Centers for Finger Movements in Human Primary Motor Cortex and Supplementary Motor Area. NeuroImage *13*, 1027–1034.

Kapreli, E., Athanasopoulos, S., Papathanasiou, M., Van Hecke, P., Kelekis, D., Peeters, R., Strimpakos, N., and Sunaert, S. (2007). Lower Limb Sensorimotor Network: Issues of Somatotopy and Overlap. CORTEX *43*, 219–232.

Kleinschmidt, A., Nitschke, M.F., and Frahm, J. (1997). Somatotopy in the human motor cortex hand area. A high-resolution functional MRI study. Eur. J. Neurosci. *9*, 2178–2186.

Lehéricy, S., Van de Moortele, P.F., Lobel, E., Paradis, A.L., Vidailhet, M., Frouin, V., Neveu, P., Agid, Y., Marsault, C., and Le Bihan, D. (1998). Somatotopical organization of striatal activation during finger and toe movement: a 3-T functional magnetic resonance imaging study. Ann. Neurol. *44*, 398–404.

Lotze, M., Erb, M., Flor, H., Huelsmann, E., Godde, B., and Grodd, W. (2000). fMRI Evaluation of Somatotopic Representation in Human Primary Motor Cortex. NeuroImage *11*, 473–481.

Luft, A.R., Smith, G.V., Forrester, L., Whitall, J., Macko, R.F., Hauser, T.-K., Goldberg, A.P., and Hanley, D.F. (2002). Comparing brain activation associated with isolated upper and lower limb movement across corresponding joints. Hum. Brain Mapp. *17*, 131–140.

Lutti, A., Thomas, D.L., Hutton, C., and Weiskopf, N. (2012). High-resolution functional MRI at 3 T: 3D/2D echo-planar imaging with optimized physiological noise correction. Magn. Reson. Med. *69*, 1657–1664.

Maillard, L., Ishii, K., Bushara, K., Waldvogel, D., Schulman, A.E., and Hallett, M. (2000). Mapping the basal ganglia: fMRI evidence for somatotopic representation of face, hand, and foot. Neurology *55*, 377–383.

Maitra, R. (2010). A re-defined and generalized percent-overlap-of-activation measure for studies of fMRI reproducibility and its use in identifying outlier activation maps. NeuroImage *50*, 124–135.

Meier, J.D., Aflalo, T.N., Kastner, S., and Graziano, M.S.A. (2008). Complex Organization of Human Primary Motor Cortex: A High-Resolution fMRI Study. J. Neurophysiol. *100*, 1800–1812.

Oguri, T., Sawamoto, N., Tabu, H., Urayama, S., Matsuhashi, M., Matsukawa, N., Ojika, K., and Fukuyama, H. (2013). Overlapping connections within the motor cortico-basal ganglia circuit: fMRI-tractography analysis. NeuroImage *78*, 353–362.

Olman, C.A., Pickett, K.A., Schallmo, M.-P., and Kimberley, T.J. (2012). Selective BOLD responses to individual finger movement measured with fMRI at 3T. Hum. Brain Mapp. *33*, 1594–1606.

Pajula, J., Kauppi, J.-P., and Tohka, J. (2012). Inter-Subject Correlation in fMRI: Method Validation against Stimulus-Model Based Analysis. PLoS ONE *8*, e41196.

Pfefferbaum, A., Adalsteinsson, E., Rohlfing, T., and Sullivan, E.V. (2010). Diffusion tensor imaging of deep gray matter brain structures: Effects of age and iron concentration. Neurobiol. Aging *31*, 482–493.

Picard, N., and Strick, P.L. (1996). Motor areas of the medial wall: a review of their location and functional activation. Cereb. Cortex N. Y. N 1991 *6*, 342–353.

Plow, E.B., Arora, P., Pline, M.A., Binenstock, M.T., and Carey, J.R. (2010). Within-limb somatotopy in primary motor cortex - revealed using fMRI. CORTEX *46*, 310–321.

Scholz, V.H., Flaherty, A.W., Kraft, E., Keltner, J.R., Kwong, K.K., Chen, Y.I., Rosen, B.R., and Jenkins, B.G. (2000). Laterality, somatotopy and reproducibility of the basal ganglia and motor cortex during motor tasks. Brain Res. *879*, 204–215.

Staempfli, P., Reischauer, C., Jaermann, T., Valavanis, A., Kollias, S., and Boesiger, P. (2008a). Combining fMRI and DTI: A framework for exploring the limits of fMRI-guided DTI fiber tracking and for verifying DTI-based fiber tractography results. NeuroImage *39*, 119–126.

Staempfli, P., Reischauer, C., Jaermann, T., Valavanis, A., Kollias, S., and Boesiger, P. (2008b). Combining fMRI and DTI: A framework for exploring the limits of fMRI-guided DTI fiber tracking and for verifying DTI-based fiber tractography results. NeuroImage *39*, 119–126.

Stevens, M.T.R., D'Arcy, R.C.N., Stroink, G., Clarke, D.B., and Beyea, S.D. (2013). Thresholds in fMRI studies: Reliable for single subjects? J. Neurosci. Methods *219*, 312–323.

Strother, L., Medendorp, W.P., Coros, A.M., and Vilis, T. (2012). Double representation of the wrist and elbow in human motor cortex. Eur. J. Neurosci. *36*, 3291–3298.

Sullivan, E.V., Adalsteinsson, E., Rohlfing, T., and Pfefferbaum, A. (2009). Relevance of Iron Deposition in Deep Gray Matter Brain Structures to Cognitive and Motor Performance in Healthy Elderly Men and Women: Exploratory Findings. Brain Imaging Behav. *3*, 167–175.

Triantafyllou, C., Hoge, R.D., Krueger, G., Wiggins, C.J., Potthast, A., Wiggins, G.C., and Wald, L.L. (2005). Comparison of physiological noise at 1.5 T, 3 T and 7 T and optimization of fMRI acquisition parameters. NeuroImage *26*, 243–250.

Weiskopf, N., Suckling, J., Williams, G., Correia, M.M., Inkster, B., Tait, R., Ooi, C., Bullmore, E.T., and Lutti, A. (2013). Quantitative multi-parameter mapping of R1, PD(*), MT, and R2(*) at 3T: a multi-center validation. Front. Neurosci. *7*, 95.

Worsley, K.J., and Friston, K.J. (1995). Analysis of fMRI time-series revisited–again. NeuroImage *2*, 173–181.

Zeharia, N., Hertz, U., Flash, T., and Amedi, A. (2012). Negative blood oxygenation level dependent homunculus and somatotopic information in primary motor cortex and supplementary motor area. Proc. Natl. Acad. Sci. U. S. A. *109*, 18565–18570.

Figures

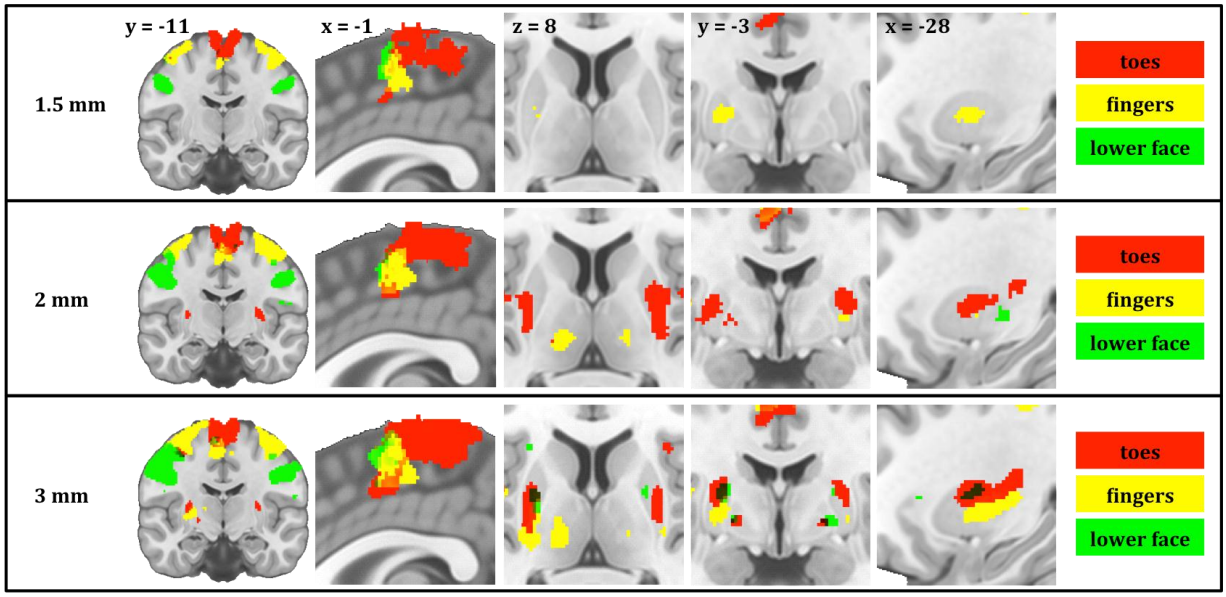

Figure 1: Motor somatotopy patterns across resolutions and brain regions. Group results obtained using the flexible factorial design showing the binarized statistical parametric maps (t values) thresholded at $\alpha = 0.05$ (corrected for multiple comparisons, family-wise error rate) for each resolution and overlaid on a skull-stripped canonical anatomical image (Fonov et al., 2011, 2009). Left and right hemibody movements are merged (red : toes ; yellow : fingers ; green : lower face). The statistical threshold used ($p < 0.05$, FWE-corrected) is the same on all renderings.

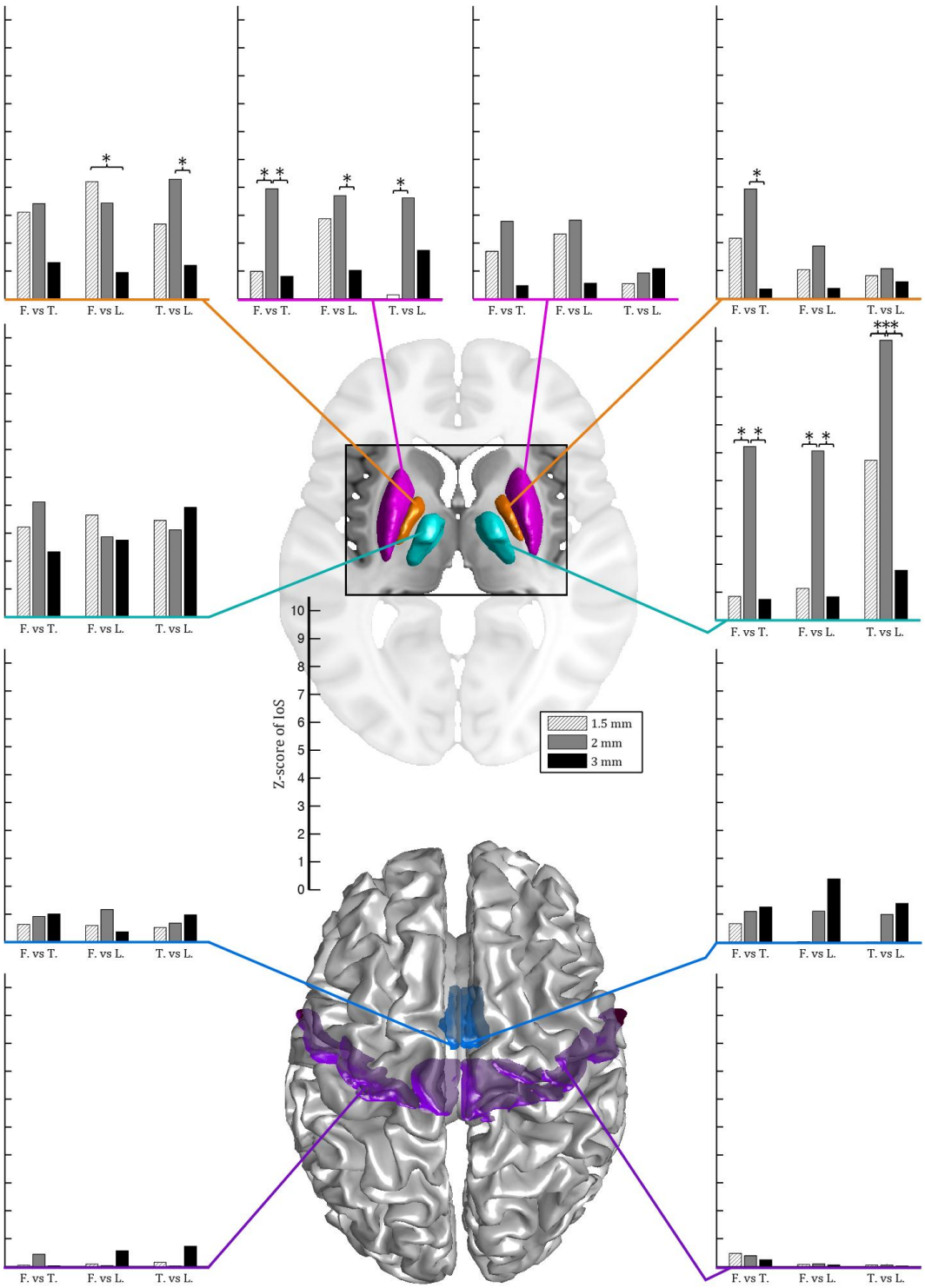

2088

2089 **Figure 2**: Z-scores of IoS for Fingers against Toes, Fingers against Lower face and Toes against
2090 Lower face per resolution and ROI. Bar plots on the left are for left ROIs, bar plots on the right are
2091 for right ROIs. Surface renderings of the putamen (magenta), pallidum (orange), motor nuclei of the

thalamus (cyan), SMA (mid-tone blue) and M1 (violet) are shown on a canonical anatomical image (Fonov et al., 2011, 2009) and on SPM12 cortical surface rendering (20484 vertices). The scale is identical for all bar plots and is shown on the middle left of the figure. Legend for the different EPI protocols (1.5 mm (hatched light grey); 2 mm (mid-tone grey); 3 mm (black)) is shown on the middle right of the figure. Stars indicate significantly different Z-scores ($p < 0.05$, FDR-corrected).

Supplementary figures and tables

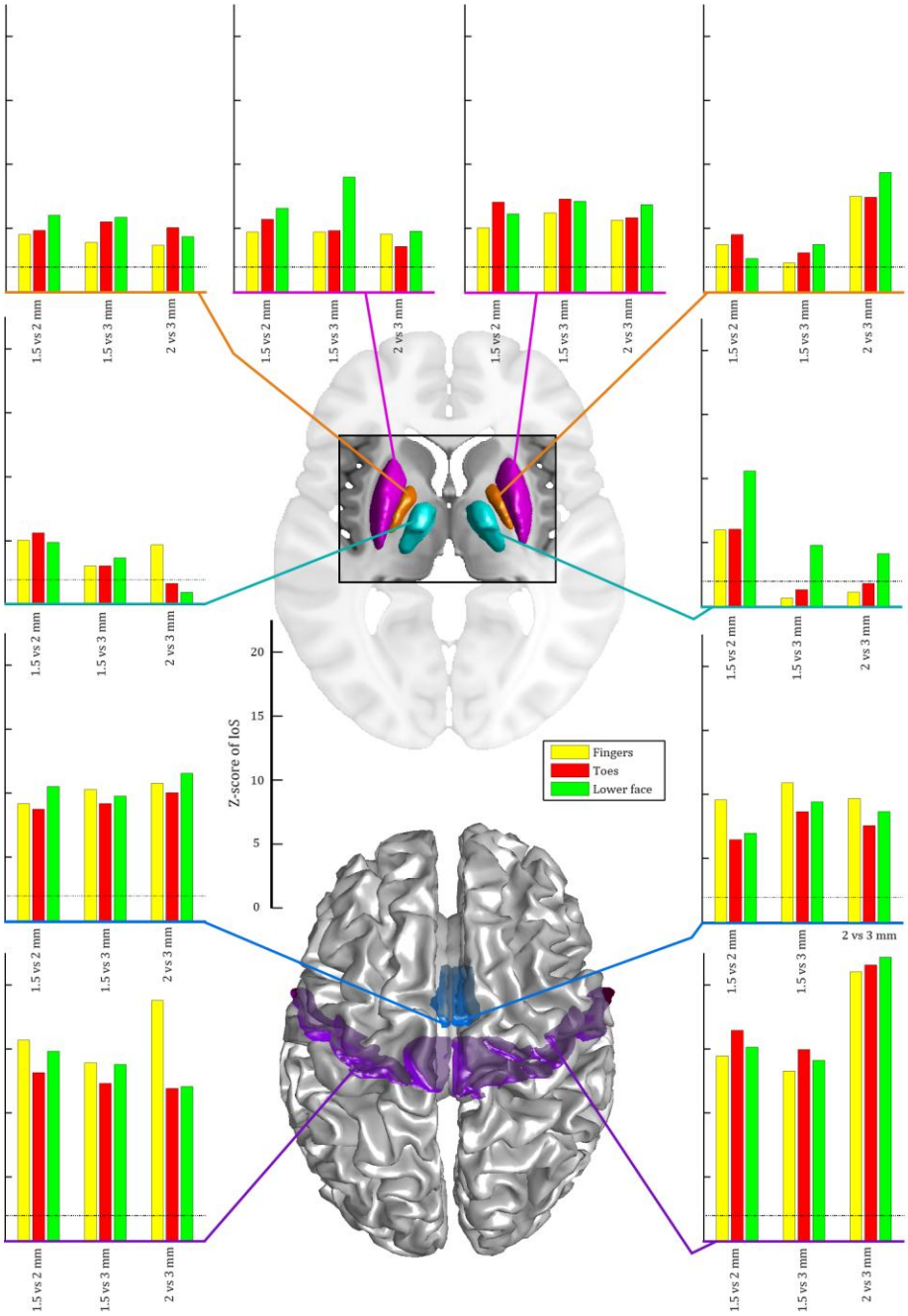

Supplementary figure 1: Z-scores of IoS for 1.5 mm against 2 mm, 1.5 mm against 3 mm and 2 mm against 3 mm per type of movement (fingers, toes, lower face) and ROI. Bar plots on the left are for left ROIs, bar plots on the right are for right ROIs. Again, only contralateral activity is shown. Surface renderings of the putamen (magenta), pallidum (orange), motor nuclei of the thalamus

(cyan), SMA (mid-tone blue) and M1 (violet) are shown on a canonical anatomical image (Fonov et al., 2011, 2009) and on SPM12 cortical surface rendering (20484 vertices). The scale is identical for all bar plots and is shown on the middle left of the figure. Legend for the different EPI protocols (1.5 mm (hatched light grey); 2 mm (mid-tone grey); 3 mm (black)) is shown on the middle right of the figure. Dotted lines indicate significance of correlation ($p < 0.05$ uncorrected for multiple comparisons, bilateral test). All Z-scores significant at uncorrected $p < 0.05$ level survived FDR-correction.

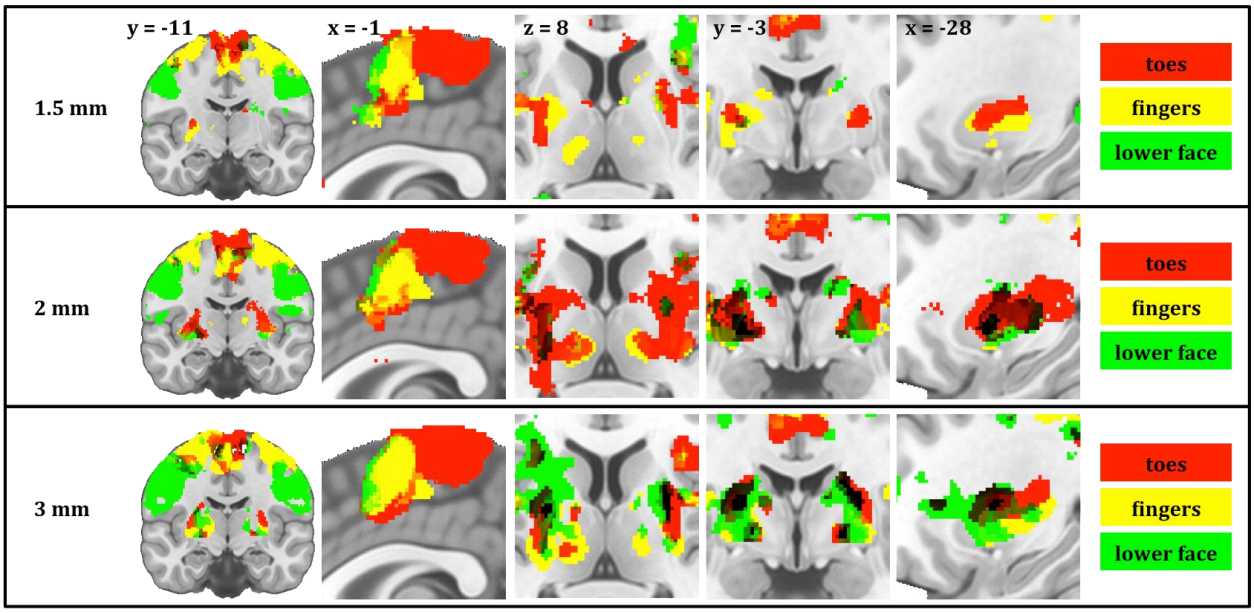

Supplementary figure 2: Motor somatotopy patterns across resolutions and brain regions. Group results obtained using the flexible factorial designs showing the binarized statistical parametric maps (t values) thresholded at $\alpha = 0.001$ (uncorrected for multiple comparisons, minimal cluster extent of 10 voxels) for each resolution and overlaid on a skull-stripped canonical anatomical image (Fonov et al., 2011, 2009). Left and right hemibody movements are merged (red : toes ; yellow : fingers ; green : lower face). The statistical threshold used ($p < 0.001$) is the same on all renderings.

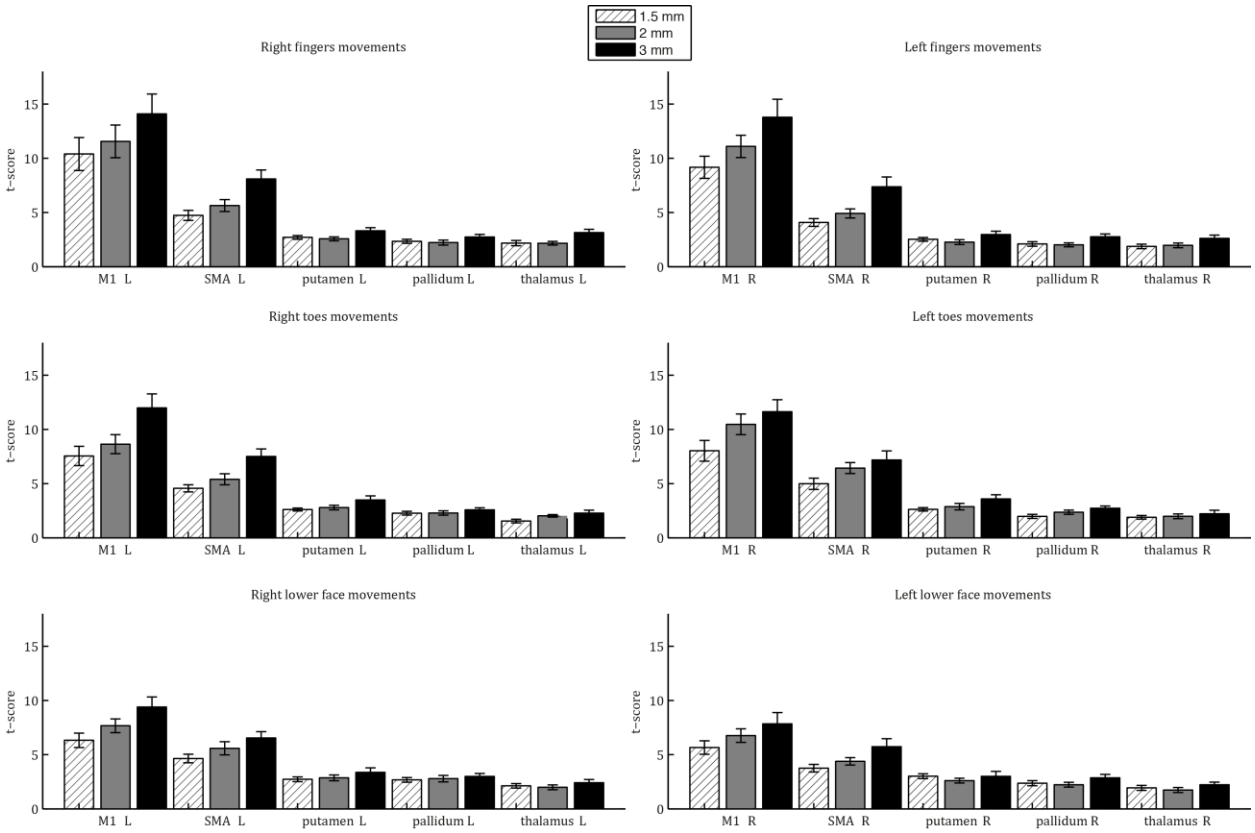

Supplementary figure 3: average t-score for all movements in each ROI as a function of EPI protocol. The average t-score was calculated for each subject (error bars indicate standard error of the mean) in the 5% most significant voxels within the ROI.

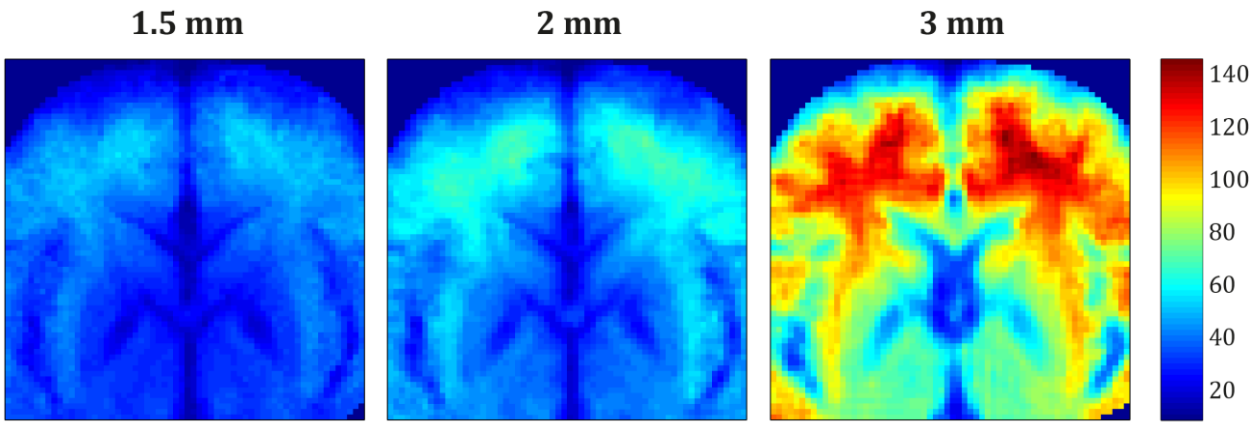

Supplementary figure 4: voxel-wise temporal signal-to-noise ratio (tSNR) maps (averaged across all subjects) computed by dividing the average signal intensity across time points by the standard deviation of the residuals from the GLM fit. As expected, 3 mm EPI provides greater tSNR as compared to 2 mm EPI, the latter providing bigger tSNR than 1.5 mm EPI.

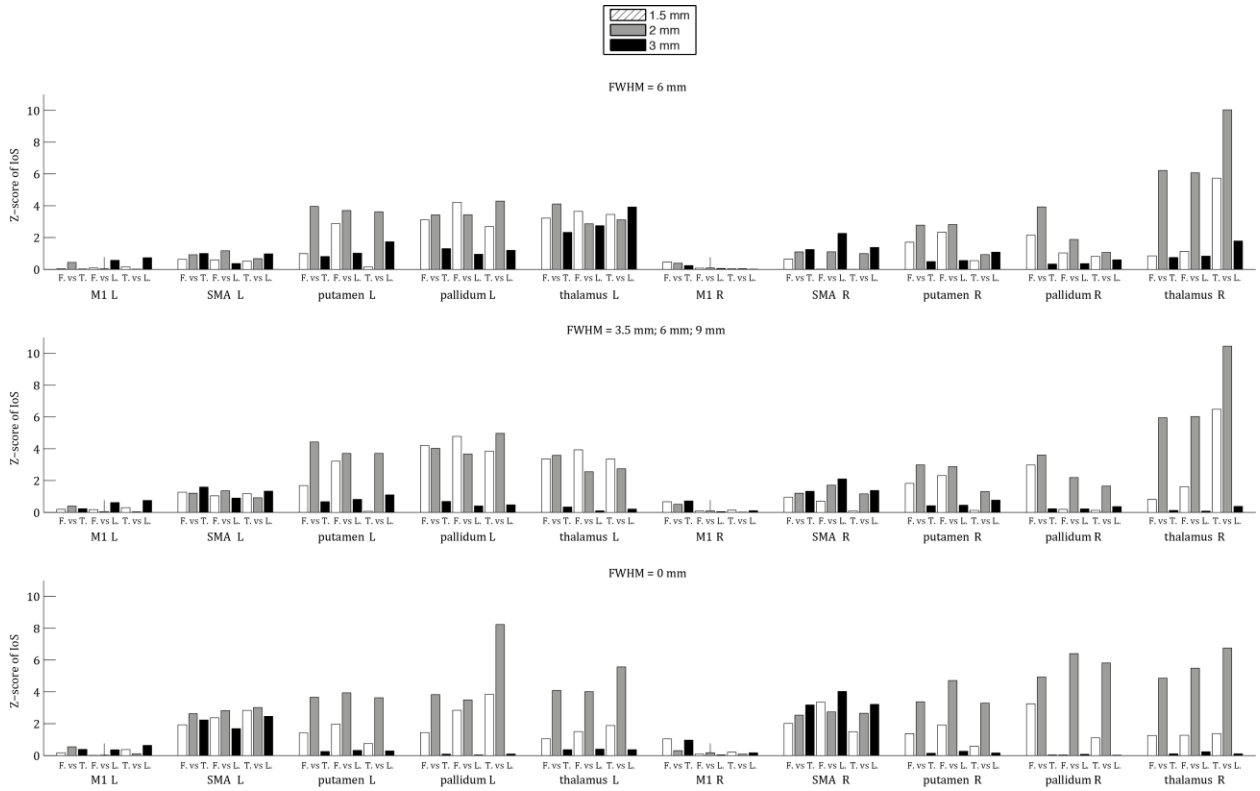

Supplementary figure 5: shows the effect of different spatial smoothing strategies on PCM results. Z-scores of IoS across all ROIs as a function of EPI protocol and pairs of movement representations compared, using: a 6 mm FWHM Gaussian kernel (top); a Gaussian kernel whose FWHM is proportional to the resolution of the EPI protocol (4.5, 6 and 9 mm for 1.5, 2 and 3 mm EPI respectively) (middle); no spatial smoothing. PCM results are very similar regardless of the spatial smoothing strategy used, except that: a) proportional smoothing kernel and absence of smoothing seem to produce more bilateral differences between EPI protocols in the basal ganglia; b) without spatial smoothing, representational similarity in the SMA resembles more the one found in deep brain nuclei, except for 3 mm EPI.

2.2. Functional segregation in Parkinson's disease

2.2.1. Study 2

This study tests and validates the LOS hypothesis in PD using motor somatotopy as a working example. It shows that PD is associated with a loss of functional segregation in the striatum, SN and thalamus but not in the cortex. DA substitution is shown to restore only partially functional segregation. Estimates of functional segregation allow predicting the severity of motor symptoms and cortico-striatal connectivity. This study provides the first evidence in favour of the LOS hypothesis in PD at the functional level.

Somatotopy shaken up: segregation and integration of information in Parkinson's disease

Renaud Marquis[1], Sara Lorio[1,2], Deepa Pothalil[3,4], Rémi Castella[1], Elisabeth Roggenhofer[1,5], Maya Jastrzębowska[1,6], Lester Melie-Garcia[1], François Vingerhoets[4], Christian WIDER[4], Antoine Lutti[1], Ferath Kherif[1], Bogdan Draganski[1,7]

[1] *Laboratory of Research in Neuroimaging (LREN) – Department of Clinical Neuroscience, Lausanne University Hospital (CHUV), University of Lausanne (UNIL), Lausanne, Switzerland*

[2] *Institute of Child Health (ICH), University College London (UCL), London, United Kingdom*

[3] *Department of Neurology, Clinique Saint Jean, Brussels, Belgium*

[4] *Department of Neurology, Lausanne University Hospital (CHUV), Lausanne, Switzerland*

[5] *Department of Neurology, Geneva University Hospital (HUG), Geneva, Switzerland*

[6] *Laboratory of Psychophysics, Brain Mind Institute, École Polytechnique Fédérale de Lausanne (EPFL), Lausanne, Switzerland*

[7] *Max-Planck-Institute for Human Cognitive and Brain Sciences, Leipzig, Germany*

Running title: Loss of functional segregation in Parkinson's disease

Title: Somatotopy shaken up: segregation and integration of information in cortico-subcortical circuits of Parkinson's disease

Abstract: 214

Text body: 3688

References: 59

Tables: 6

Figures: 2

Supplementary material: supplementary methods and results, 7 tables, 6 figures, 23 tables in 2 separate Excel workbooks

Keywords: Parkinson's disease; functional magnetic resonance imaging; segregation; dopamine

Corresponding author:
Bogdan Draganski
LREN - Département des Neurosciences Cliniques
CHUV, Université de Lausanne
Mont Paisible 16
1011 Lausanne
Switzerland
email: bogdan.draganski@chuv.ch
phone: +41-21-314 9638

Abstract

There is much controversy about the root causes and consequences of basal ganglia dysfunction aiming to unify hypokinetic and hyperkinetic movement disorders into a unique generative model. Recent empirical evidence suggests that movement disorders are associated with loss of neuronal specificity in basal ganglia that results in abnormal functional representation of body parts in the brain. Main aim of our study is to test the hypothesis of motor somatotopy changes in Parkinson's disease (PD) using functional magnetic resonance imaging (fMRI) and behavioural testing while modulating patients' dopaminergic state. Using a data-driven metric of spatial segregation between functional representations of upper and lower limbs we observed greater overlap between motor representations within putamen, thalamus and substantia nigra in PD patients OFF medication compared with healthy controls. Dopaminergic treatment in the very same patients restored the level of segregation in thalamus back to normal, but only partially in the basal ganglia. We show that the proposed index of similarity predicts both the degree of bradykinesia and the magnitude of effective cortico-striatal connectivity in PD patients when OFF dopamine. Our study provides evidence supporting the recent theoretical framework suggesting loss of segregation in movement disorders, which we validate empirically demonstrating the strong link between the proposed index of similarity and the motor symptoms severity in PD patients.

Introduction

Despite an impressive number of theoretical approaches attempting to explain the pathophysiology of movement disorders, up to date there is no unique concept that unifies hypo- and hyperkinetic movement disorders into a single generative model (Albin et al., 1989; DeLong, 1990; Mink, 1996). Common models do not explain abnormal basal ganglia (BG) activity patterns and lead to predictions that are contradictory with experimental findings (Bronfeld and Bar-Gad, 2011; Nambu, 2008; Nelson and Kreitzer, 2014; Obeso et al., 2008). Furthermore, the effectiveness of available therapeutic options is puzzling in such frameworks (Hickey and Stacy, 2016; Kalia and Lang, 2015). Recent studies using animal models brought empirical evidence about loss of neuronal specificity (LOS) in BG as governing pathophysiological mechanism in movement disorders (Bar-Gad and Bergman, 2001; Bronfeld and Bar-Gad, 2011). Under this hypothesis, the loss of the ability of BG to decorrelate cortical inputs results in abnormal motor behaviour, such as motor tics in Tourette syndrome, tremor and bradykinesia in PD, and choreic movements in Huntington's disease. Dimensionality reduction might be subserved by inter-nuclei mechanisms such as subthalamic input or dopaminergic innervation, as well as intra-nuclei processing implemented by lateral connections between striatal neurons or cholinergic interneurons (Bar-Gad et al., 2003a, 2003a; Bergman et al., 1998; Morris et al., 2004). However, investigations on the topic are hampered by the complex structural and functional organisation of BG showing not only co-existence of segregated and integrated motor, associative and limbic representations (Alexander et al., 1986; Draganski et al., 2008), but also a consistent somatotopy pattern throughout the entire cortico-BG circuitry (Obeso et al., 2008). Studies in non-human primates demonstrate LOS in the GPi (Leblois et al., 2006) and BG-recipient – but not cerebellar – thalamus (Pessiglione et al., 2005) associated with parkinsonism. In the latter study, activity and receptive fields of thalamic neurons were shown to increase even in the asymptomatic state. In addition, the LOS hypothesis in PD is supported by a larger proportion of neurons responding to more than a single body part (Baker et al., 2010; Boraud et al., 2000; Filion et al., 1988; Levy et al., 2001; Taha et al., 1996) and a higher relative number of active pallidal neurons during movements (Baker et al., 2010; Erez et al., 2011; Filion et al., 1988; Williams et al., 2005).

Previous functional imaging studies in humans supported the notion of abnormal BG function in movement disorders demonstrating abnormal motor somatotopy in subcortical areas of patients with dystonia (Delmaire et al., 2005; Nelson et al., 2009; Quartarone et al., 2008; Tamburin et al., 2002). Nevertheless, there is currently no evidence confirming that other movement disorders, such as Parkinson's disease (PD), lead to a disruption of motor somatotopy patterns in the BG. This may be partly explained by the fact that the BG are challenging areas for fMRI because they contain substantial iron content, which reduces the signal-to-noise ratio, and are distant from MRI head coil channels (Drayer et al., 1986; Dušek et al., 2013).

Many data-driven methods for investigation of differential functional representations have a susceptibility to be biased by noise in the measurements (Diedrichsen et al., 2011). This methodological issue parallels the one hindering accurate estimation of correlation between neuronal pairs in electrophysiological recordings (Bar-Gad et al., 2003b). Pattern component modelling (PCM) incorporates a noise term that accounts for noise influence in the signal measured

(Diedrichsen et al., 2011). This method has shown to be very successful in restoring the true similarity between statistical maps even at high noise level (Diedrichsen et al., 2011) and has been extensively validated (Diedrichsen et al., 2013a, 2013b; Ejaz et al., 2015).

We use high-resolution fMRI to investigate motor somatotopy in cortical and subcortical brain areas to test the hypothesis of abnormal functional segregation in Parkinson's disease. Under the assumption that DA modulates the degree of information segregation at the BG level we further hypothesized that functional segregation in the BG would be at least partially recovered under DA therapy. For analysis of the whole-brain fMRI data we use established mass-univariate statistics framework additionally to data-driven multi-variate pattern recognition tools. Given the importance of behavioural changes, we carefully monitored motor performance of PD patients and health controls aiming at correlational analysis and prediction of motor symptom's severity undergoing modulation by DA.

Methods

Participants

Among the recruited 32 PD patients and 21 healthy controls (HC) we excluded 1 HC with low-quality MRI data due to motion artefacts. From the 32 PD patients 13 dropped out after the first scan, 1 was not included in the final analysis due to suspicion of underlying disorder other than PD, another 4 – due to lack of compliance in task performance. The final analysis consisted of 14 PD patients (6 female; age = 58.75 ± 1.89 standard error, SEM) and 20 HCs (10 female; age = 61.79 ± 2.11 SEM). Although there was no significant age difference between groups (2-tailed 2-samples t-test, $t(32) = 1.0593$; $p = 0.2974$) all subsequent analyses were controlled for the linear effects of age. The Edinburgh inventory (Oldfield, 1971) indicated that all PD patients except 1 were right-handed. 17 HC subjects were right-handed and 3 - left-handed. The average handedness scores were 55.88 ± 12.52 SEM for HCs and 79.79 ± 14.29 SEM for PD patients. There was no significant handedness difference between groups (2-tailed 2-samples t-test, $t(32) = 1.2479$, $p = 0.2211$). The local Ethics committee approved the study and all volunteers gave written informed consent prior to participation.

The neurological assessment comprising UPDRS parts III and IV was performed by 3 board-certified neurologists. Accordingly, 11 PD patients were predominantly affected on the left body side and 3 – on the right, consistently with their lateralized bradykinesia sub-score (Buck et al., 2011). The MRI data of patients with predominantly right-sided symptoms were flipped along the x-axis for all subsequent analyses besides the whole-brain analyses focusing on lateralisation of movement-related activity. All obtained results are therefore presented relative to the most affected body side except for the whole-brain mass-univariate group analyses.

To study the DA-related effects we used a cross-over design where 6 patients were scanned first OFF DA medication and 8 – ON. When tested OFF medication, patients were requested to stop medication the day before. The time interval between the two scanning sessions was kept constant (number of days (mean ± SEM): 64.5 ± 12.95). There was no significant difference between patients

first scanned off ($PD_{first\ OFF}$) and patients first scanned on ($PD_{first\ ON}$) in terms of time interval between the two scanning sessions (number of days (mean ± SEM): $PD_{first\ OFF}$ = 60 ± 23.07; $PD_{first\ ON}$ = 67.86 ± 16.02); $t(12) = 0.2900$; $p = 0.7767$). UPDRS III scores were significantly greater in patients off medication (PD OFF) as compared to patients on medication (PD ON) (1-tailed paired t-test: $t(13) = 3.4545$; $p = 0.0021$).

Experimental paradigm

Participants performed every 2 seconds visual cue- paced unilateral flexion/extension of hand and foot within blocks of 8 movements. The 20 blocks of motor activity were separated by rest periods with 16 seconds duration where participants were asked to fixate a cross at the centre of the screen. We indicated on the screen the start of each active movement block by a countdown of 3 seconds. The pseudo-randomized order of tested body parts was balanced within and across participants and movements were practiced prior to scanning.

To avoid potential performance biases, we continuously monitored the behavioural performance during fMRI acquisition using an in-house developed MR-compatible pneumatic device. The hand movements consisted of squeezing a rubber ball connected to air pressure sensors; for the feet we used a similar system installed underneath foot pedals. The air pressure sensors transduced pressure into electrical signal via CED MICRO3 1401 data acquisition unit (Cambridge Electronic Design Limited, UK) at 500 Hz sampling rate and the resulting output was sent to Signal 6 software (Cambridge Electronic Design Limited, UK). We used a peak detection algorithm identified to detect automatically motor responses using event-related moving averages with dynamic threshold (after Elgendi et al. (2013), see Supplementary methods). After classification of motor responses in cued and non-cued movements we excluded from further analysis participants missing more than 50% of trials or performing more than 50 non-cued movements. This resulted in exclusion of 4 PD patients: 2 patients missed on average 65% and 73.13% of trials in one experimental session while 2 other performed an average of 89.75 and 72.5 non-cued movements in one experimental session.

Under the supposition that the applied muscle force level correlates with neural activity (Keisker et al., 2009), all subsequent analyses were controlled for the linear effects of force measured within-subject locked to individual's peak and averaged across trials. Given that velocity of movement is causally linked to the very nature of PD (Hallett and Khoshbin, 1980), we did not control for the effects of movement velocity in our statistical analyses (distributions of peak force and velocity across subjects and per group are shown in Supplementary figure 2).

MRI data acquisition and processing

We used a Siemens Prisma 3T scanner with 64-channel head coil to acquire fMRI data using 3D multi-shot EPI at 2 mm isotropic voxel size (60 slices; slice TR 52 ms; volume TR 3.328 ms; slice oversampling: 6.7%). For brain anatomy imaging we used multi-echo 3D FLASH acquisitions with 1.5 mm voxel size (matrix size: 160 x 150 x 120; FoV 256 x 240 x 176 mm) to quantitatively map longitudinal relaxation rate, effective proton density, magnetization transfer and effective transverse relaxation rate. We applied parallel imaging along the phase-encoding direction with 8 equidistant TEs (Lorio et al. 2016); the repetition time (TR) and flip angle (α) were TR/α = 24.5

ms/6° (for PD-weighted); TR/ α = 24.5 ms/21° (for T1-weighted). For correction of the effects of RF transmit inhomogeneities we used the acquired radio frequency (RF) transmit field map, and a static magnetic field map - for geometric distortion and off-resonance effects.

All steps of MRI data processing and analysis were performed in the framework of SPM12 (Wellcome Trust Center for Neuroimaging, www.fil.ion.ucl.ac.uk/spm) running under Matlab 7.13 (The MathWorks, Inc., Natick, Massachusetts, United States). The fMRI data was realigned to the session mean, corrected for receive coil inhomogeneities and EPI distortion, and co-registered to the brain anatomy data. The calculated individuals' head motion parameters led to the exclusion of 1 HC with more than 5mm of head movement along a principal axis during the motor task (Van Dijk et al., 2012). For further stringent control of the effects of excessive head movements we carried out additional analyses (see Supplementary material). We used the diffeomorphic spatial registration algorithm DARTEL to achieve optimal anatomical precision within the study cohort (Ashburner, 2007). The resulting spatial registration parameters were applied to the functional data for transformation into standardised Montreal Neurological Institute (MNI) space. Before statistical analysis we applied spatial smoothing using a Gaussian kernel of 3mm full-width-at-half-maximum.

Whole-brain mass-univariate fMRI analyses

Within-subject analysis: All cued and non-cued movements as detected by the peak detection algorithm were included as separate events in the fMRI design matrix, the preparation periods were modelled as epochs of 3 seconds, and the estimated realignment parameters were included as additional regressors. For the pattern component modelling at the subject-level we created a separate subject-level analysis that included only the realignment parameters as regressors, thus removing the confounding linear effects from the time series and leaving only variance related to the motor somatotopy paradigm.

Group-level analysis: To verify the anatomical plausibility of the obtained motor somatotopy patterns we included the contrasts for positive effect of each cued movement with age and peak force as covariates in a flexible factorial design across all study participants. Additionally, effects of age and peak force were tested and are available as supplementary materials. We report statistically significant results surviving the threshold of $p<.05$ after family-wise error (FWE) correction for multiple comparisons. Results below $p<.001$, uncorrected for multiple comparisons are reported as trends.

ROI-based multivariate fMRI analyses

For our region-of-interest (ROI) approach we selected nodes of the motor circuitry including the primary motor cortex (M1), supplementary motor area (SMA), putamen, pallidum, subthalamic nucleus (STN), thalamus and the substantia nigra (SN). The ROI definition was based on the Harvard-Oxford atlas (fsl.fmrib.ox.ac.uk/fsl/fslwiki/Atlases), the ATAG atlas (Keuken et al., 2014) and Morel's atlas of the thalamus (Krauth et al., 2010; Niemann et al., 2000). The presence of brain activity during the motor somatotopy task in all these ROIs was verified using whole-brain univariate analyses (Supplementary table 1).

We measured the representational similarity between brain activity patterns using the established PCM strategy (Diedrichsen et al., 2011). The multivariate analysis was performed at the subject level on the residuals of the GLM including only the realignment parameters. All cued, non-cued movements and preparation epochs were modelled using the same parameters as for subject-level fMRI modelling except head motion parameters. There was no shared variance component added as constraint. We estimated the variance and covariance between ipsilateral representations of hand and foot in the ROI contralateral to the corresponding body part. The variance-covariance matrices were transformed to correlation matrices.

Aiming to obtain a metric of segregation between motor representations, the magnitudes of the correlation coefficients from the PCM were transformed using the Fisher *r*-to-*z'* transform (Sanabria-Diaz et al. 2013). The resulting metric - Index of Similarity (IoS) represents the inverse hyperbolic tangent of the magnitude of the correlation coefficient *r* between representations:

$$IoS = |tanh^{-1}(r)|$$

High segregation between representations results in low IoS values, whereas high similarity between representations (i.e. lack of functional segregation between representations) produces high values of IoS.

Additionally, we extracted volume-of-interest data represented by the 1st eigenvariate of the fMRI time course from putamen and M1. The extraction was based on the results of a F-test across all cued movements adjusting the data for the effects of interests. We calculated normalized mutual information (NMI) between cortex and putamen time courses dividing the mutual information by the geometric mean entropies (Strehl and Ghosh, 2002).

Given the non-normal distribution of IoS values (see Supplementary figure 5), we applied bilateral Wilcoxon sum of ranks and signed rank tests across groups for each ROI after having removed the linear effects of age and peak force. Statistical significance threshold was set to $p < 0.05$, uncorrected for multiple comparisons.

The relationship between IoS and bradykinesia sub-score in PD patients OFF was assessed using multiple regression models with age and peak force as covariate in ROIs yielding significant group differences. Spearman's rank correlation coefficients were calculated between IoS values and bradykinesia, which was adjusted for linear effects of age and peak force. The same procedure was used to test the prediction of UPDRS III score and tremor sub-score. All multiple linear regression models used the IoS in the SN contralateral to the most affected body side in PD patients as predictor, and lateralized versions of the UPDRS III scores, bradykinesia and tremor sub-scores.

We tested multiple regression models in PD OFF using IoS in ROIs with significant group effect as predictor, NMI estimates between M1 and the putamen in the hemisphere contralateral to the most affected body side as dependent variable, and age and peak force as covariates. We report non-linear correlation coefficient between IoS and NMI estimates adjusted for linear effects of age and peak force.

Results

Clinical and behavioural performance

The UPDRS III, UPDRS IV scores, Hoehn & Yahr stage and Levodopa Equivalent Dose represented the expected differentiation between patients ON and OFF medication (Table 1). The observed side predominance of symptom distribution in PD patients was confirmed by the absolute difference in bradykinesia sub-score between body sides (mean = 2.39; SEM = 0.53). Accordingly, there was a differential performance between cohorts and body parts tested (Table 2).

Whole-brain results

We observed robust motor somatotopy pattern extending over M1, SMA, putamen, GPe, GPi, the thalamus, the STN and the SN (Table 3; Supplementary figure 4). Reliable motor activity patterns were also found in the insula, parietal operculum, and cerebellum. The F-contrast performed to test for differences across cohorts did not show any significant results. There was a significant interaction between cohort and movement within the motor cortex contralateral to the most affected side in PD (see Supplementary material). Age and peak force were associated with unique spatial patterns of motor activity (Supplementary figure 4).

Region-of-interest results

The PCM performed on the residuals of the simple GLM converged for all subjects and for all ROIs.

Effects of disease and DA: The non-parametric tests demonstrated higher IoS scores in PD OFF as compared to HC in the putamen ($W = 280$, $Z = -2.43$, $p = 0.015$), thalamus ($W = 288$, $Z = -2.15$, $p = 0.031$) and SN ($W = 293$, $Z = -1.98$, $p = 0.048$), in the hemisphere contralateral to the most affected body side as compared to HC (i.e. in the right hemisphere for 11 out of 14 patients). The effects of PD ON patients were mostly in-between HC and PD OFF (Figure 1). We did not find any differences in the hemisphere ipsilateral to the most affected side in PD patients ($p > 0.05$). There was an effect of DA medication status in the thalamus contralateral to the most affected body side, where PD patients ON had lower IoS scores as compared to PD OFF ($W = 17$, $p = 0.025$).

Prediction of symptoms severity: The results of the multiple linear regression model showed a significant regression equation (Table 4, Table 6 and Supplementary figure 6). There was a positive correlation between IoS in the SN contralateral to the predominantly affected body side and the bradykinesia sub-score (Table 4). High values of IoS in the SN were associated with high values of lateralized bradykinesia sub-score in PD OFF (Figure 2). The nonlinear correlation coefficient also demonstrated a positive relationship ($\rho = 0.60$, $p = 0.023$). Results of the equivalent multiple linear regression model for lateralized UPDRS III scores showed a significant model fit and a significant effect of IoS score in SN on UPDRS III (Supplementary table 3). Tremor was not predicted by IoS in the SN (Supplementary table 2). All multiple linear regression models using IoS in putamen or thalamus in PD OFF did not show any significant results.

Prediction of cortico-striatal connectivity: The regression equations and the effects of IoS were not significant in multiple linear regression models on M1–putamen NMI using IoS in the SN (β = -

0.004, t(4,10) = -0.69, p = 0.5, see Table 6) and thalamus (β = 0.003, t(4,10) = 1.12, p = 0.29, see Table 6). Conversely, the corresponding regression equation of the model using IoS in putamen as predictor was significant (Table 6). IoS in the putamen was negatively correlated with M1–putamen NMI estimates (Table 5). Additionally, Spearman's correlation coefficient between putaminal IoS and NMI values – adjusted for age and peak force effects – was significant (ρ = -0.66; p = 0.01). In PD OFF, high values of IoS in the putamen were associated with low values of M1–putamen NMI (Figure 2, see also Supplementary figure 6).

Discussion

In our study we provide unique evidence supporting the notion of dopamine related loss of functional segregation in Parkinson's disease. The impact of disease and dopaminergic modulation was most evident in the SN and putamen contralateral to the predominantly affected body side. Furthermore, PD patients ON medication lying most frequently in between PD OFF and HC, the motor thalamus was the only region where dopaminergic therapy was restoring functional segregation back to normal. While the predominant thalamic target for PD is the Vim, other thalamic nuclei have been considered for deep brain stimulation (DBS) (Kovanlikaya et al., 2014; Perlmutter and Mink, 2006; Rivlin-Etzion et al., 2006), such as the VPL for chronic pain (Bittar et al., 2005; Kovanlikaya et al., 2014) or the VLa for dystonia (Mure et al., 2014). Notwithstanding the density of thalamic connections that might cause Vim DBS to influence adjacent nuclei (Perlmutter and Mink, 2006) and although the main source of thalamo-striatal projections are though to lie in the centromedian-parafascicular complex (Smith et al., 2009), the Vim has also been shown to project to the striatum (Perlmutter and Mink, 2006) and there are growing evidences suggesting a pivotal role of thalamo-striatal connections in cortico-BG circuitry as a node subserving integration (Haber and Calzavara, 2009).

We then showed that functional segregation in the SN is linked to the severity of motor symptoms in PD OFF, but more specifically to bradykinesia. The latter is the cardinal symptom mostly correlated with loss of striatal dopamine (Pahwa and Lyons, 2003). Although dissociating bradykinesia from rigidity, akinesia and hypokinesia is not trivial, each motor symptoms may be viewed as resulting from different profiles of loss of specificity (Bronfeld and Bar-Gad, 2011).

Finally, we demonstrated that in PD OFF putaminal loss of functional segregation predicted a loss of connectivity between M1 and the putamen. We interpret this finding as suggesting that loss of functional segregation in the putamen – potentially induced by the lack of functional segregation in the SN – causes a disconnection between M1 and putamen, inducing a faulty putaminal processing of cortical information.

In our study, differences in functional segregation in the pallidum and STN were not observed. This could be due to technical limitations or to the fact that we grouped patients according to the body side most affected by bradykinesia, not tremor. Knowing that tremor is relatively independent from other motor symptoms in PD (Helmich et al., 2012), future studies might investigate the links between tremor severity and the loss of functional segregation.

Although we controlled for task performance using an automated algorithm for motor responses detection and included individual force level as a covariate in all analyses, more precise monitoring could potentially be achieved through EMG recordings (Dirkx et al., 2016). Though head motion parameters were included in the fMRI design and couldn't account for IoS differences (see Head motion as a confounding factor in the Supplementary results section), more sophisticated methods are available for removal of head motion artifacts (Power et al., 2014). It has also to be noted that the PCM is shown to be relatively robust to the size of the smoothing kernel used for spatial smoothing of fMRI images (Diedrichsen et al., 2011), hence advocating for the generalizability of our findings.

We strongly recommend future studies to validate these findings using larger sample sizes, investigate the evolution of functional segregation in PD using longitudinal study designs, and explore the consequences of these findings to develop new therapeutic solutions.

Acknowledgements

We would like to thank all participants for their contribution to the study and to E. Dupuis for her essential help with MRI data acquisition. BD is supported by the Swiss National Science Foundation (NCCR Synapsy, project grant Nr 32003B_159780), Foundation Parkinson Switzerland and Foundation Synapsis. The research leading to these results has received funding from the European Union Seventh Framework Programme (FP7/2015-2018) under grant agreement no. 604102 (Human Brain Project). LREN is very grateful to the Roger De Spoelberch and Partridge Foundations for their generous financial support.

References

Albin, R.L., Young, A.B., and Penney, J.B. (1989). The functional anatomy of basal ganglia disorders. Trends Neurosci. *12*, 366–375.

Alexander, G.E., DeLong, M.R., and Strick, P.L. (1986). Parallel organization of functionally segregated circuits linking basal ganglia and cortex. Annu. Rev. Neurosci. *9*, 357–381.

Ashburner, J. (2007). A fast diffeomorphic image registration algorithm. NeuroImage *38*, 95–113.

Baker, K.B., Lee, J.Y.K., Mavinkurve, G., Russo, G.S., Walter, B., DeLong, M.R., Bakay, R.A.E., and Vitek, J.L. (2010). Somatotopic organization in the internal segment of the globus pallidus in Parkinson's disease. Exp. Neurol. *222*, 219–225.

Bar-Gad, I., and Bergman, H. (2001). Stepping out of the box: information processing in the neural networks of the basal ganglia. Curr. Opin. Neurobiol. *11*, 689–695.

Bar-Gad, I., Morris, G., and Bergman, H. (2003a). Information processing, dimensionality reduction and reinforcement learning in the basal ganglia. Prog. Neurobiol. *71*, 439–473.

Bar-Gad, I., Heimer, G., Ritov, Y., and Bergman, H. (2003b). Functional correlations between neighboring neurons in the primate globus pallidus are weak or nonexistent. J. Neurosci. *23*, 4012–4016.

Bergman, H., Feingold, A., Nini, A., Raz, A., Slovin, H., Abeles, M., and Vaadia, E. (1998). Physiological aspects of information processing in the basal ganglia of normal and parkinsonian primates. Trends Neurosci. *21*, 32–38.

Bittar, R.G., Burn, S.C., Bain, P.G., Owen, S.L., Joint, C., Shlugman, D., and Aziz, T.Z. (2005). Deep brain stimulation for movement disorders and pain. J. Clin. Neurosci. *12*, 457–463.

Boraud, T., Bézard, E., Bouliac, B., and Gross, C.E. (2000). Ratio of inhibited-to-activated pallidal neurons decreases dramatically during passive limb movement in the MPTP-treated monkey. J. Neurophysiol. *83*, 1760–1763.

Bronfeld, M., and Bar-Gad, I. (2011). Loss of specificity in Basal Ganglia related movement disorders. Front. Syst. Neurosci. *5*, 38.

Buck, P.O., Wilson, R.E., Seeberger, L.C., Conner, J.B., and Castelli-Haley, J. (2011). Examination of the UPDRS bradykinesia subscale: equivalence, reliability and validity. J. Park. Dis. *1*, 253–258.

Delmaire, C., Krainik, A., Tezenas du Montcel, S., Gerardin, E., Meunier, S., Mangin, J.F., Sangla, S., Garnero, L., Vidailhet, M., and Lehéricy, S. (2005). Disorganized somatotopy in the putamen of patients with focal hand dystonia. Neurology *64*, 1391–1396.

DeLong, M.R. (1990). Primate models of movement disorders of basal ganglia origin. Trends Neurosci.

Diedrichsen, J., Ridgway, G.R., Friston, K.J., and Wiestler, T. (2011). Comparing the similarity and spatial structure of neural representations: A pattern-component model. NeuroImage *55*, 1665–1678.

Diedrichsen, J., Wiestler, T., and Ejaz, N. (2013a). A multivariate method to determine the dimensionality of neural representation from population activity. NeuroImage *76*, 225–235.

Diedrichsen, J., Wiestler, T., and Krakauer, J.W. (2013b). Two Distinct Ipsilateral Cortical Representations for Individuated Finger Movements. Cereb. Cortex *23*, 1362–1377.

Dirkx, M.F., den Ouden, H., Aarts, E., Timmer, M., Bloem, B.R., Toni, I., and Helmich, R.C. (2016). The Cerebral Network of Parkinson's Tremor: An Effective Connectivity fMRI Study. J. Neurosci. *36*, 5362–5372.

Draganski, B., Kherif, F., Kloppel, S., Cook, P.A., Alexander, D.C., Parker, G.J.M., Deichmann, R., Ashburner, J., and Frackowiak, R.S.J. (2008). Evidence for Segregated and Integrative Connectivity Patterns in the Human Basal Ganglia. J. Neurosci. *28*, 7143–7152.

Drayer, B., Burger, P., Darwin, R., Riederer, S., Herfkens, R., and Johnson, G.A. (1986). MRI of brain iron. AJR Am. J. Roentgenol. *147*, 103–110.

Dušek, P., Dezortova, M., and Wuerfel, J. (2013). Imaging of iron. Int. Rev. Neurobiol. *110*, 195–239.

Ejaz, N., Hamada, M., and Diedrichsen, J. (2015). Hand use predicts the structure of representations in sensorimotor cortex. Nat. Publ. Group.

Elgendi, M., Norton, I., Brearley, M., Abbott, D., and Schuurmans, D. (2013). Systolic Peak Detection in Acceleration Photoplethysmograms Measured from Emergency Responders in Tropical Conditions. PLoS ONE *8*, e76585.

Erez, Y., Tischler, H., Belelovsky, K., and Bar-Gad, I. (2011). Dispersed Activity during Passive Movement in the Globus Pallidus of the 1-Methyl-4-Phenyl-1,2,3,6-Tetrahydropyridine (MPTP)-Treated Primate. PLoS ONE *6*, e16293.

Filion, M., Tremblay, L., and Bédard, P.J. (1988). Abnormal influences of passive limb movement on the activity of globus pallidus neurons in parkinsonian monkeys. Brain Res. *444*, 165–176.

Haber, S.N., and Calzavara, R. (2009). The cortico-basal ganglia integrative network: The role of the thalamus. Brain Res. Bull. *78*, 69–74.

Hallett, M., and Khoshbin, S. (1980). A physiological mechanism of bradykinesia. Brain *103*, 301–314.

Helmich, R.C., Hallett, M., Deuschl, G., Toni, I., and Bloem, B.R. (2012). Cerebral causes and consequences of parkinsonian resting tremor: a tale of two circuits? Brain *135*, 3206–3226.

Hickey, P., and Stacy, M. (2016). Deep Brain Stimulation: A Paradigm Shifting Approach to Treat Parkinson's Disease. Front. Neurosci. *10*, 76.

Kalia, L.V., and Lang, A.E. (2015). Parkinson's disease. The Lancet *386*, 896–912.

Keisker, B., Hepp-Reymond, M.-C., Blickenstorfer, A., Meyer, M., and Kollias, S.S. (2009). Differential force scaling of fine-graded power grip force in the sensorimotor network. Hum. Brain Mapp. *30*, 2453–2465.

Keuken, M.C., Bazin, P.L., Crown, L., Hootsmans, J., Laufer, A., Müller-Axt, C., Sier, R., van der Putten, E.J., Schäfer, A., Turner, R., et al. (2014). Quantifying inter-individual anatomical variability in the subcortex using 7T structural MRI. NeuroImage *94*, 40–46.

Kovanlikaya, I., Heier, L., and Kaplitt, M. (2014). Treatment of Chronic Pain: Diffusion Tensor Imaging Identification of the Ventroposterolateral Nucleus Confirmed with Successful Deep Brain Stimulation. Stereotact. Funct. Neurosurg. *92*, 365–371.

Krauth, A., Blanc, R., Poveda, A., Jeanmonod, D., Morel, A., and Székely, G. (2010). A mean three-dimensional atlas of the human thalamus: Generation from multiple histological data. NeuroImage *49*, 2053–2062.

Leblois, A., Meissner, W., Bezard, E., Bioulac, B., Gross, C.E., and Boraud, T. (2006). Temporal and spatial alterations in GPi neuronal encoding might contribute to slow down movement in Parkinsonian monkeys. Eur. J. Neurosci. *24*, 1201–1208.

Levy, R., Dostrovsky, J.O., Lang, A.E., Sime, E., Hutchison, W.D., and Lozano, A.M. (2001). Effects of apomorphine on subthalamic nucleus and globus pallidus internus neurons in patients with Parkinson's disease. J. Neurophysiol. *86*, 249–260.

Lorio, S., Kherif, F., Ruef, A., Melie-Garcia, L., Frackowiak, R., Ashburner, J., Helms, G., Lutti, A., and Draganski, B. (2016). Neurobiological origin of spurious brain morphological changes: A quantitative MRI study. Hum. Brain Mapp. *37*, 1801–1815.

Mink, J.W. (1996). The basal ganglia: focused selection and inhibition of competing motor programs. Prog. Neurobiol. *50*, 381–425.

Morris, G., Arkadir, D., Nevet, A., Vaadia, E., and Bergman, H. (2004). Coincident but distinct messages of midbrain dopamine and striatal tonically active neurons. Neuron *43*, 133–143.

Mure, H., Morigaki, R., Koizumi, H., Okita, S., Kawarai, T., Miyamoto, R., Kaji, R., Nagahiro, S., and Goto, S. (2014). Deep Brain Stimulation of the Thalamic Ventral Lateral Anterior Nucleus for DYT6 Dystonia. Stereotact. Funct. Neurosurg. *92*, 393–396.

Nambu, A. (2008). Seven problems on the basal ganglia. Curr. Opin. Neurobiol. *18*, 595–604.

Nelson, A.B., and Kreitzer, A.C. (2014). Reassessing Models of Basal Ganglia Function and Dysfunction. Annu. Rev. Neurosci. *37*, 117–135.

Nelson, A.J., Blake, D.T., and Chen, R. (2009). Digit-specific aberrations in the primary somatosensory cortex in Writer's cramp. Ann. Neurol. *66*, 146–154.

Niemann, K., Mennicken, V.R., Jeanmonod, D., and Morel, A. (2000). The Morel Stereotactic Atlas of the Human Thalamus: Atlas-to-MR Registration of Internally Consistent Canonical Model. NeuroImage *12*, 601–616.

Obeso, J.A., Rodríguez-Oroz, M.C., Benitez-Temino, B., Blesa, F.J., Guridi, J., Marin, C., and Rodriguez, M. (2008). Functional organization of the basal ganglia: Therapeutic implications for Parkinson's disease. Mov. Disord. *23*, S548–S559.

Oldfield, R.C. (1971). The assessment and analysis of handedness: the Edinburgh inventory. Neuropsychologia *9*, 97–113.

Pahwa, R., and Lyons, K.E. (2003). Handbook of Parkinson's Disease, Third Edition (Kansas City, Kansas, USA: CRC Press).

Perlmutter, J.S., and Mink, J.W. (2006). Deep brain stimulation. Annu. Rev. Neurosci. *29*, 229–257.

Pessiglione, M., Guehl, D., Rolland, A.-S., Francois, C., Hirsch, E.C., Féger, J., and Tremblay, L. (2005). Thalamic neuronal activity in dopamine-depleted primates: evidence for a loss of functional segregation within basal ganglia circuits. J. Neurosci. *25*, 1523–1531.

Power, J.D., Mitra, A., Laumann, T.O., Snyder, A.Z., Schlaggar, B.L., and Petersen, S.E. (2014). Methods to detect, characterize, and remove motion artifact in resting state fMRI. NeuroImage *84*, 320–341.

Quartarone, A., Morgante, F., Sant'Angelo, A., Rizzo, V., Bagnato, S., Terranova, C., Siebner, H.R., Berardelli, A., and Girlanda, P. (2008). Abnormal plasticity of sensorimotor circuits extends beyond the affected body part in focal dystonia. J. Neurol. Neurosurg. Psychiatry *79*, 985–990.

Rivlin-Etzion, M., Marmor, O., Heimer, G., Raz, A., Nini, A., and Bergman, H. (2006). Basal ganglia oscillations and pathophysiology of movement disorders. Curr. Opin. Neurobiol. *16*, 629–637.

Sanabria-Diaz, G., Martínez-Montes, E., Melie-Garcia, L., and Alzheimer's Disease Neuroimaging Initiative (2013). Glucose metabolism during resting state reveals abnormal brain networks organization in the Alzheimer's disease and mild cognitive impairment. PLoS ONE *8*, e68860.

Smith, Y., Raju, D., Nanda, B., Pare, J.-F., Galván, A., and Wichmann, T. (2009). The thalamostriatal systems: Anatomical and functional organization in normal and parkinsonian states. Brain Res. Bull. *78*, 60–68.

Strehl, A., and Ghosh, J. (2002). Cluster ensembles - a knowledge reuse framework for combining multiple partitions. J. Mach. Learn. Res.

Taha, J.M., Favre, J., Baumann, T.K., and Burchiel, K.J. (1996). Characteristics and somatotopic organization of kinesthetic cells in the globus pallidus of patients with Parkinson's disease. J. Neurosurg. *85*, 1005–1012.

Tamburin, S., Manganotti, P., Marzi, C.A., Fiaschi, A., and Zanette, G. (2002). Abnormal somatotopic arrangement of sensorimotor interactions in dystonic patients. Brain *125*, 2719–2730.

Van Dijk, K.R.A., Sabuncu, M.R., and Buckner, R.L. (2012). The influence of head motion on intrinsic functional connectivity MRI. NeuroImage *59*, 431–438.

Williams, Z.M., Neimat, J.S., Cosgrove, G.R., and Eskandar, E.N. (2005). Timing and direction selectivity of subthalamic and pallidal neurons in patients with Parkinson disease. Exp. Brain Res. *162*, 407–416.

2649 **Tables**

2650

			PD OFF	PD ON
UPDRS III	**Total**		19.00 ± 2.12	13.57 ± 2.08
	Upper limbs	**Right**	3.64 ± 0.79	2.14 ± 0.64
		Left	6.29 ± 1.08	4.93 ± 0.98
	Lower limbs	**Right**	0.79 ± 0.40	0.43 ± 0.23
		Left	1.86 ± 0.35	1.57 ± 0.43
Bradykinesia	**Total**		8.93 ± 1.14	6.07 ± 0.95
	Upper limbs	**Right**	3.71 ± 0.59	2.07 ± 0.39
		Left	5.07 ± 0.71	3.93 ± 0.71
	Lower limbs	**Right**	1.57 ± 0.23	1.21 ± 0.21
		Left	2.21 ± 0.28	1.86 ± 0.28
Tremor	**Total**		2.71 ± 0.54	2.43 ± 0.72
	Upper limbs	**Right**	0.36 ± 0.17	0.36 ± 0.20
		Left	1.14 ± 0.35	0.93 ± 0.32
	Lower limbs	**Right**	0.21 ± 0.16	0.14 ± 0.14
		Left	0.29 ± 0.13	0.43 ± 0.20
UPDRS IV			1.14 ± 0.44	
Hoehn & Yahr stadium			1.64 ± 0.16	
Levodopa Equivalent Dose			684.86 ± 95.73	

2651

2652 **Table 1** : average and standard error of UPDRS III, bradykinesia sub-score, tremor sub-score
2653 separately for PD patients ON and OFF. Average and standard error of UPDRS IV, Hoehn and Yahr
2654 stadium, and Levodopa Equivalent Dose were measured once for all PD patients and are also
2655 reported.

2656

		All	HC	PD ON	PD OFF
Percentage of cued movements	**mean ± SEM**	88.72 ± 0.81	88.91 ± 1.19	87.28 ± 1.82	89.91 ± 1.26
	minimum	66.25	75.63	66.25	78.75
	maximum	96.25	95.63	95.00	96.25
Number of uncued movements	**mean ± SEM**	10.58 ± 1.35	6.09 ± 0.65	11.40 ± 1.94	16.20 ± 3.65
	minimum	2.50	2.50	3.50	3.25
	maximum	41.50	13.75	28.75	41.50

Table 2 : percentage of cued movements and number of uncued movements summarised with the average, standard error (SEM), minimum and maximum, across all groups of subjects and separately for each group.

Region			*F*	x [mm]	y [mm]	z [mm]
M1	right hemisphere	hand area	69.71	38	-25	56
		foot area	61.78	11	-31	70
	left hemisphere	hand area	69.11	-38	-25	54
		foot area	64.27	-9	-33	68
SMA			44.47	0	1	56
putamen	right hemisphere		30.94	-31	-9	5
	left hemisphere		38.87	-30	-7	7
GPe	right hemisphere		21.32	22	-4	3
	left hemisphere		23.41	-24	-4	3
GPi	right hemisphere		13.46	22	-9	-2
	left hemisphere		17.62	-17	-6	-4
thalamus	right hemisphere		16.81	13	-14	7
	left hemisphere		26.63	-14	-17	9
STN			12.74	-8	-15	-11
SN			12.19	12	-14	-7

Table 3 : whole-brain univariate results for the flexible factorial design including HC subjects summarised with the F-statistic and MNI coordinates of cluster maxima within each ROI selected. Complete tables of all significant clusters (at $p < 0.001$, $k \geq 10$) are available as separate supplementary material in "group_results_mass_univariate_full_fact.xls" and "group_results_mass_univariate_HC_flexible_fact.xls".

	Coefficient (β)	Standard error	t	p
Intercept	4.112	1.14	3.606	0.005
SN IoS	0.237	0.084	2.82	0.018
Age	0.69	0.52	1.328	0.214
Peak force	-0.923	0.521	1.771	0.107

Table 4 : Results table for the multiple linear regression model in PD OFF with the regression equation *Bradykinesia ~ Intercept + IoS_{SN} + Age + PeakForce*.

	Coefficient (β)	Standard error	t	p
Intercept	0.32	0.048	6.746	< 0.001
Putamen IoS	-0.009	0.003	-2.904	0.016
Age	0.036	0.018	1.986	0.075
Force	-0.033	0.018	1.792	0.104

Table 5 : Results table for the multiple linear regression model in PD OFF with the regression equation $NMI_{M1-putamen} \sim Intercept + IoS_{putamen} + Age + PeakForce$.

Model	R^2	R^2 adjusted	RMSE	*F*	*p*
$Bradykinesia \sim Intercept + IoS_{SN} + Age + PeakForce$	0.55	0.41	1.87	4.07	0.04
$UPDRSIII \sim Intercept + IoS_{SN} + Age + PeakForce$	0.55	0.41	3	4.06	0.04
$NMI_{M1-putamen} \sim Intercept + IoS_{SN} + Age + PeakForce$	0.31	0.103	0.09	1.5	0.28
$NMI_{M1-putamen} \sim Intercept + IoS_{thalamus} + Age + PeakForce$	0.36	0.16	0.08	1.85	0.29
$NMI_{M1-putamen} \sim Intercept + IoS_{putamen} + Age + PeakForce$	0.61	0.49	0.07	5.16	0.02

Table 6: Model fitting results for all multiple linear regression models performed in PD OFF to predict symptom severity and cortico-striatal connectivity estimates.

Figures

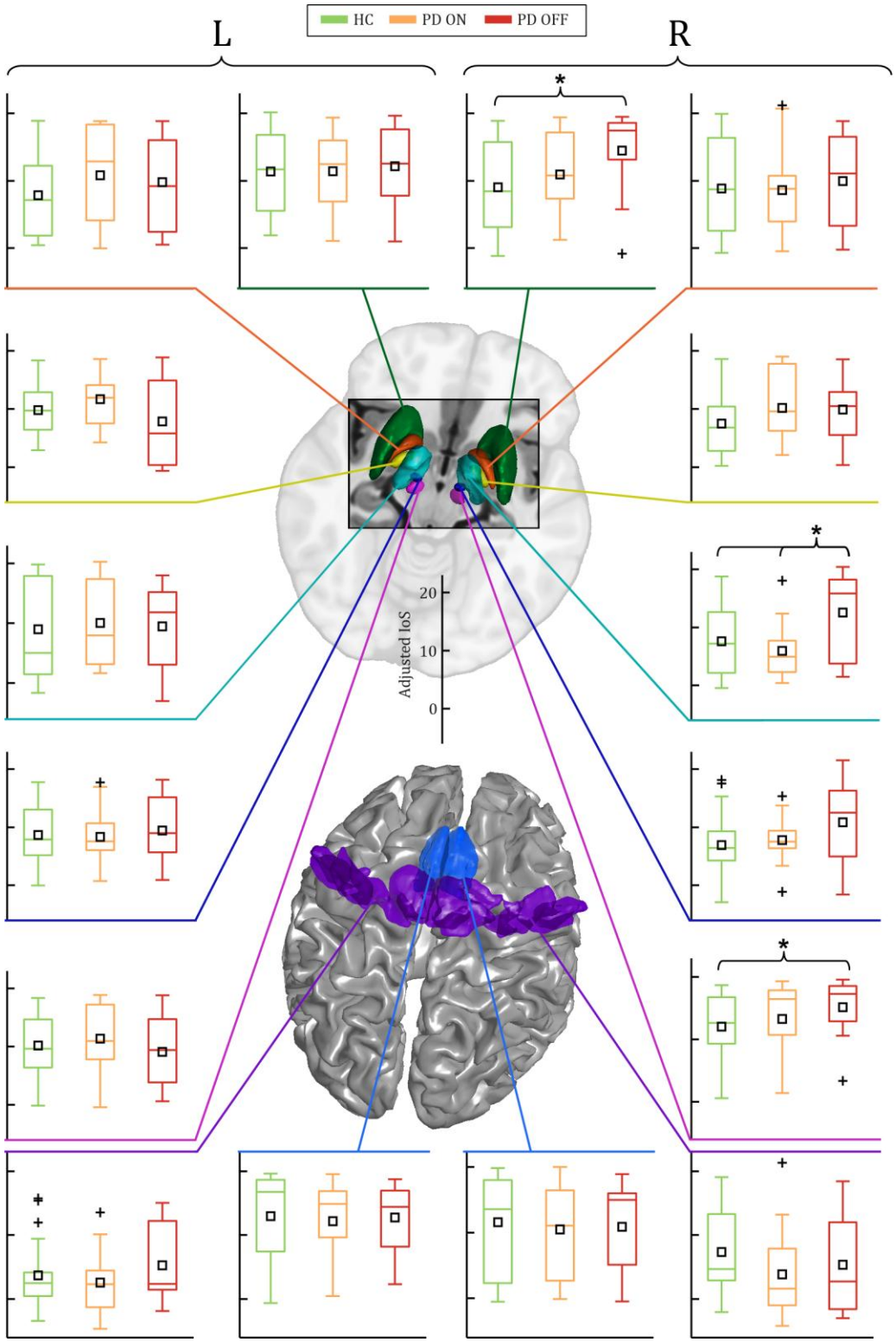

Figure 1 : boxplots of IoS estimates per group for each ROI. Subcortical (top) and cortical (bottom) ROI masks used are rendered using custom Matlab code, following neurological convention. Left

boxplots represent IoS estimates in left ROIs and reversely for the right, although left and right ROIs were flipped in 3 PD patients affected mostly on the left body side. Dark green: putamen; dark orange: GPe; light yellow: GPi; light blue: thalamus (VL and VPL nuclei); dark blue: STN; magenta: SN; mid-tone blue: SMA; violet: M1. Black squares in box plots represent the average. Significance ($p < 0.05$) is marked with an asterisk.

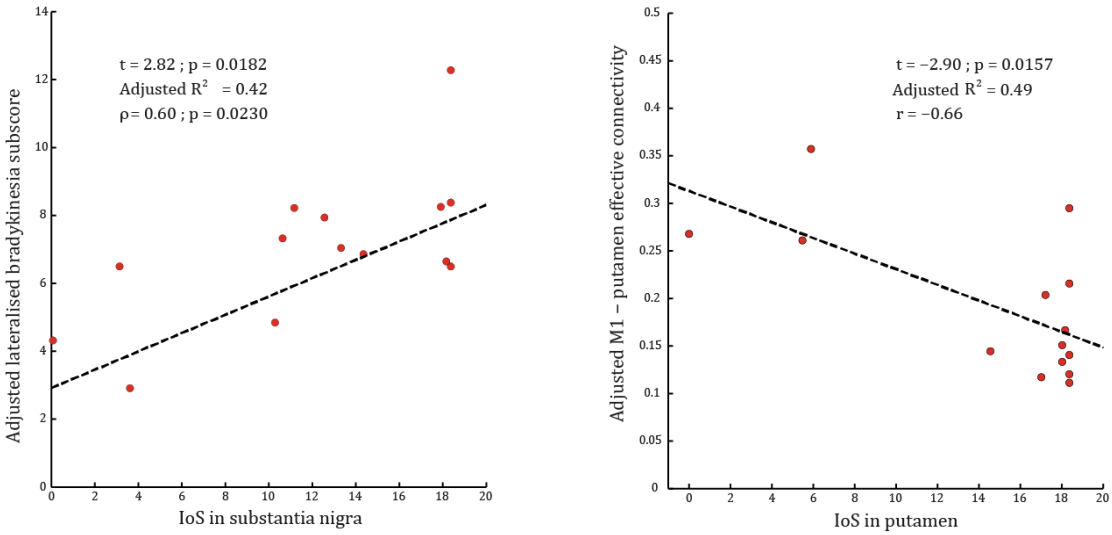

Figure 2 : scatter plots summarising results of the multiple linear regression models. Left part shows lateralized bradykinesia sub-score in PD OFF, adjusted for effects of age and force, as a function of IoS in the SN contralateral to the most affected body side. Right part depicts adjusted cortico-striatal connectivity as measured by M1–putamen NMI (adjusted for effects of age and force), as a function of IoS in the putamen contralateral to the most affected hemibody in PD patients OFF medication. In all scatter plots, the black dotted line represents the regression line.

Supplementary material

Supplementary methods

Kinematic analyses

Motor response peaks were detected using a modified version of the algorithm proposed by Elgendi and colleagues (2013). We provide here details about the procedure employed. For our purpose, the outcome of the peak detection was optimized by setting parameters to the following values: W_1 = 700; W_2 = 3500; β = 0.35. The following cut-off frequencies were used for the Butterworth band-pass filter: low-pass = 0.1 Hz, high-pass = 30 Hz. The formula for parameters THR_1 and THR_2 were modified such that:

$$THR_1 = \gamma \cdot MA_{beat}[n] + \alpha$$

Where γ = 0.45. And:

$$THR_2 = \frac{W_1}{4}$$

These parameter values were adjusted manually to maximize detection accuracy according to a visual inspection of every dataset done by the experimenter. An example of motor responses detected in three subjects is shown in Supplementary figure 1. Peri-response peak time histograms (PRTH) were extracted from task performance recordings by averaging over time windows comprised 1000 ms before to 1000 ms after each motor response captured by the peak detection algorithm. These responses were filtered using a Butterworth bandpass filter (highpass cutoff = 15 Hz ; lowpass cutoff = 0 Hz). Because units of motor responses were arbitrarily defined by the experimental setup – i.e the gain applied to each channel was adjusted to provide an approximately similar response for all body parts –, maximal and minimal values were estimated among all recordings for each channel and all PRTH were scaled to convert units in percentage of air pressure. From the latter force PRTH, response velocity (velocity PRTH) was estimated as the absolute value of the derivative across time points. Right and left body part channels were flipped for the 3 PD patients mostly affected on the right body side, and linear effects of age were removed at the baseline level (i.e taking into account the average across time points for each PRTH). Removing age effects at each time point separately was not performed to prevent distortion of the response shape. T-tests between groups were then performed at each time point for force and velocity PRTHs. A p-value threshold was set to $p < 0.001$ and a minimal time extent for each difference was set to 50 ms (50 samples).

Supplementary results

Kinematic analyses

Two-samples t-tests on force level showed a significant difference between PD OFF and HC on the right (least affected) hand between -84 and 342 ms (relative to response peak), while paired t-tests showed significant differences between PD OFF and PD ON on the least affected hand between -30 and 484 ms (Supplementary figure 3). The velocity of motor responses was significantly different between PD OFF and PD ON on the most affected hand between -368 and -278 ms (Supplementary figure 3). Additionally, correlation analyses were conducted at each time point of the PRTH for response velocity of PD OFF and the corresponding bradykinesia sub-score for each body part. Spearman's rank correlation coefficients were used and the same p-value and minimal time extent thresholds were applied. We found significant negative correlations between response velocity and bradykinesia sub-score at for the least affected hand in between -286 and -196 ms (Supplementary figure 3). During this period, Spearman's coefficient was bounded between -0.6798 and -0.7454 (on average, ρ = -0.7060 with a standard deviation of 0.0189). The fact that group differences were observed on the most affected body side is not surprising, but observing significant correlation between velocity and bradykinesia only on the least affected body side is relatively puzzling. This could however be explained by the fact that the least affected body side is the one which yielded the highest variation in terms of bradykinesia severity, as shown in Supplementary table 4.

Control analyses

<u>Handedness as a confounding factor</u>

The subtle difference in IoS estimates between the two hemispheres might be caused by handedness. Furthermore, the IoS in each ROI could potentially be affected by handedness in a different way. As shown in Supplementary table 5, this is apparently not the case, as none of the Pearson's linear correlation coefficients between handedness and IoS estimates were found significant in any ROI considered (neither before nor after flipping ROIs for the 3 patients affected mostly on the left).

<u>Head motion as a confounding factor</u>

Although head motion during scanning would most likely affect spatial frequencies of functional images, IoS estimates might have been biased by a spurious combination of head motion and spatial smoothing. However, in this specific case we expect a global effect across all ROIs. We calculated head motion metrics as defined in Van Dijk et al (2012) and estimated Pearson's linear correlation coefficient between each metric and the average IoS across ROIs. No significant correlation between IoS and head motion metrics was found as shown in Supplementary table 6.

To further rule out the possibility that head motion might have biased results regarding functional imaging, we tested whether any head motion metric was significantly different between groups using two-samples and paired t-tests and although subjects moved substantially during the motor task, only trends towards significant differences between groups were observed as shown in Supplementary table 7.

Prediction of symptoms severity with putaminal and thalamic IoS

As noted above, none of the results for multiple linear regressions using IoS in the putamen or thalamus were significant contrarily to the ones obtained using IoS in the SN. Age and gender were also used as covariates. For IoS in the putamen (contralateral to the most affected body side), results were as follows: a) for lateralized bradykinesia subcore, $F(4,10) = 0.8$, $p = 0.522$, $R^2 = 0.194$, adjusted $R^2 = -0.0484$, $RMSE = 2.51$, $\beta = 0.014581$, $t(4,10) = 0.14686$, $p = 0.88616$; b) for lateralized UPDRS III score, $F(4,10) = 1.25$, $p = 0.342$, $R^2 = 0.273$, adjusted $R^2 = 0.0552$, $RMSE = 3.81$, $\beta = 0.015577$, $t(4,10) = 0.10341$, $p = 0.91968$; c) for lateralized tremor sub-score, $F(4,10) = 0.703$, $p = 0.571$, $R^2 = 0.174$, adjusted $R^2 = -0.0735$, $RMSE = 1.43$, $\beta = 0.012666$, $t(4,10) = 0.22332$, $p = 0.82778$. Regression results for IoS in the thalamus (contralateral to the most affected body side) were as follows: a) for lateralized bradykinesia subcore, $F(4,10) = 0.798$, $p = 0.523$, $R^2 = 0.193$, adjusted $R^2 = -0.049$, $RMSE = 2.51$, $\beta = -0.014401$, $t(4,10) = -0.12627$, $p = 0.90202$; b) for lateralized UPDRS III score, $F(4,10) = 1.83$, $p = 0.206$, $R^2 = 0.354$, adjusted $R^2 = 0.16$, $RMSE = 3.59$, $\beta = 0.18332$, $t(4,10) = 1.1242$, $p = 0.28718$; c) for lateralized tremor sub-score, $F(4,10) = 1.39$, $p = 0.303$, $R^2 = 0.294$, adjusted $R^2 = 0.0817$, $RMSE = 1.33$, $\beta = 0.079644$, $t(4,10) = 1.3222$, $p = 0.21555$.

Supplementary tables

ROI	Number of voxels	Volume [mm³]
M1 L	3647	15843.37
M1 R	3975	17268.27
putamen L	1595	6929.03
putamen R	1512	6568.46
SMA L	1237	5373.80
SMA R	1506	6542.39
thalamus L	464	2015.72
thalamus R	475	2063.50
GPe L	210	912.29
GPe R	193	838.43
GPi L	62	269.34
GPi R	67	291.06
SN L	50	217.21
SN R	57	247.62
STN L	21	91.23
STN R	22	95.57

Supplementary table 1 : number of voxels and volume in mm^3 for all ROIs selected for the PCM.

	Coefficient (β)	Standard error	*t*	*p*
Intercept	1.091	0.846	1.289	0.226
SN IoS	0.051	0.063	0.821	0.431
Age	0.312	0.386	0.81	0.437
Peak force	-0.501	0.387	-1.3	0.225

Supplementary table 2 : Results table for the multiple linear regression model in PD OFF with the regression equation *tremor ~ Intercept + IoS_{SN} + Age + PeakForce.*

	Coefficient (β)	Standard error	t	p
Intercept	5.585	1.824	3.063	0.012
SN IoS	0.334	0.135	2.477	0.033
Age	0.932	0.8313	1.121	0.289
Peak force	-1.968	0.834	2.361	0.04

Supplementary table 3 : Results table for the multiple linear regression model in PD OFF with the regression equation *UPDRSIII ~ Intercept + IoS_{SN} + Age + PeakForce.*

		Coefficient of variation (σ / μ)	Average
Upper limbs	Least affected	**0.662**	2.929
	Most affected	0.366	**5.857**
Lower limbs	Least affected	0.596	1.429
	Most affected	0.394	2.357

Supplementary table 4 : shows the dispersion and severity of bradykinesia sub-scores per body part (most affected vs. least affected) in PD OFF. The least affected hand is associated with the highest coefficient of variation of bradykinesia in the studied sample of patients. This may explain why correlation analyses between velocity PRTH and bradykinesia sub-scores revealed significant relationships only for the least affected hand. On the contrary, results for velocity PRTH revealed by group comparisons may be driven by the intensity of bradykinesia, the average of the latter being higher on the most affected hand.

	r	*p*
Left M1 (BA4)	-0.19	0.197
Left SMA	0.13	0.397
Left putamen	-0.01	0.941
Left thalamus	0.13	0.383
Left GPe	0.002	0.989
Left GPi	-0.12	0.432
Left STN	0.04	0.766
Left substantia nigra	-0.05	0.714
Right M1 (BA4)	-0.16	0.287
Right SMA	0.12	0.417
Right putamen	0.05	0.716
Right thalamus	-0.04	0.804
Right GPe	-0.07	0.651
RIght GPi	0.09	0.547
Right STN	-0.1	0.503
Right substantia nigra	-0.1	0.483

Supplementary table 5 : Pearson's *r* between handedness and (unflipped) IoS with associated *p*-values.

	r	*p*
Mean motion	-0.183	0.211
Maximum motion	-0.105	0.479
Number of motions	0.029	0.844
Rotations	0.003	0.984

Supplementary table 6 : Pearson's *r* between average IoS and head motion metrics and associated *p*-values

	HC (mean ± std)	PD ON (mean ± std)	PD OFF (mean ± std)	HC vs PD ON (*p*)	HC vs PD OFF (*p*)	PD ON vs PD OFF (*p*)
Mean head motion	0.95 ± 0.41	1.45 ± 1.16	1.19 ± 0.79	0.128	0.147	0.896
Maximum head motion	1.78 ± 0.75	2.42 ± 1.59	2.39 ± 1.59	0.401	0.539	0.713
Number of head motions	189.25 ± 41.09	200.71 ± 34.83	197 ± 26.2	0.05001	0.268	0.455
Head rotations	0.01 ± 0.01	0.01 ± 0.01	0.01 ± 0.01	0.086	0.253	0.069

Supplementary table 7 : mean and standard deviation (std) for each head motion metric for each group and t-tests results (*p*-value) for the comparisons of head motion metrics between groups.

Supplementary figures

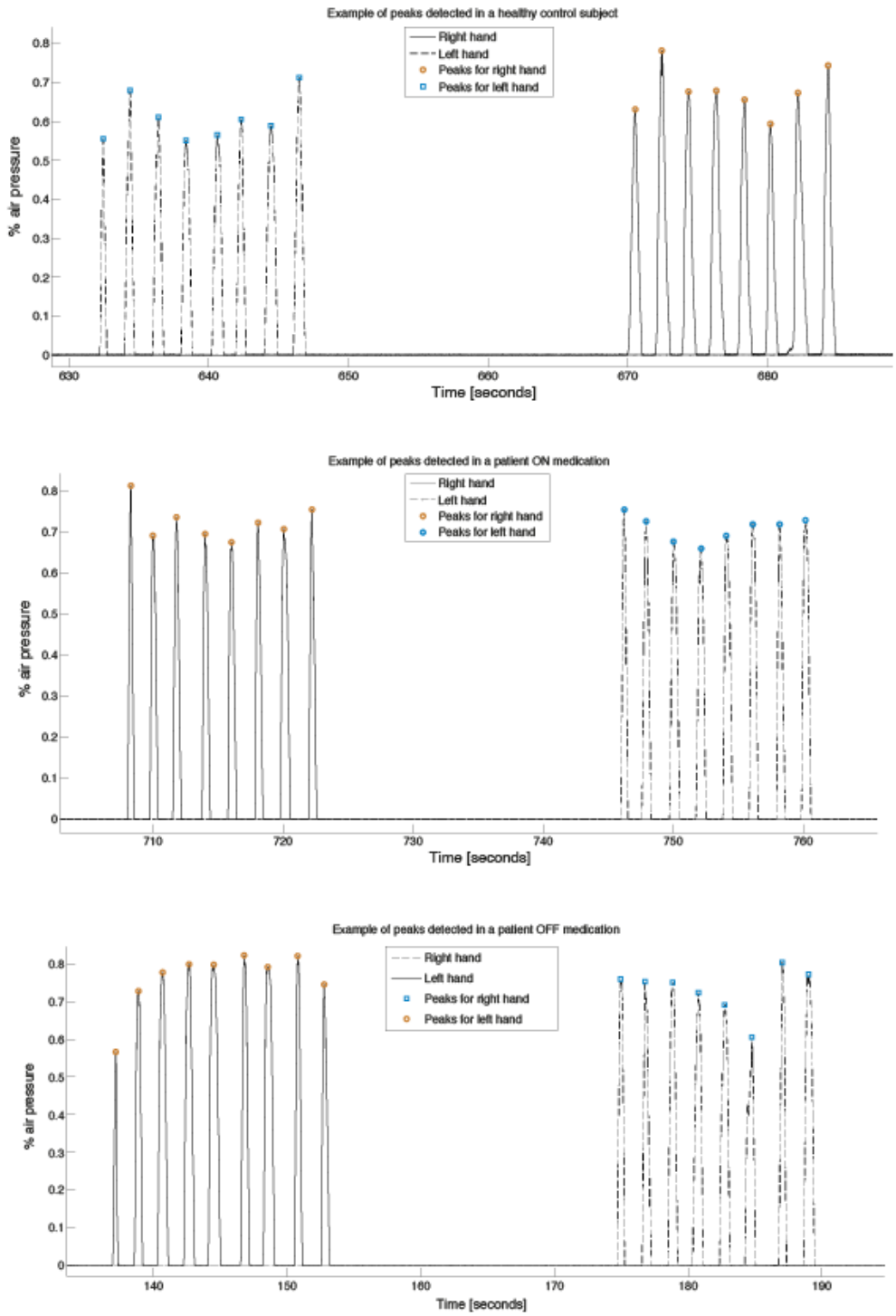

Supplementary figure 1: examples of motor performance recordings of the right and left hands in 3 subjects (top: HC subject; middle: PD patient ON; bottom: PD patient OFF), with motor responses

detected by the algorithm using event-related moving averages with dynamic threshold. Figure legend is embedded in each graph.

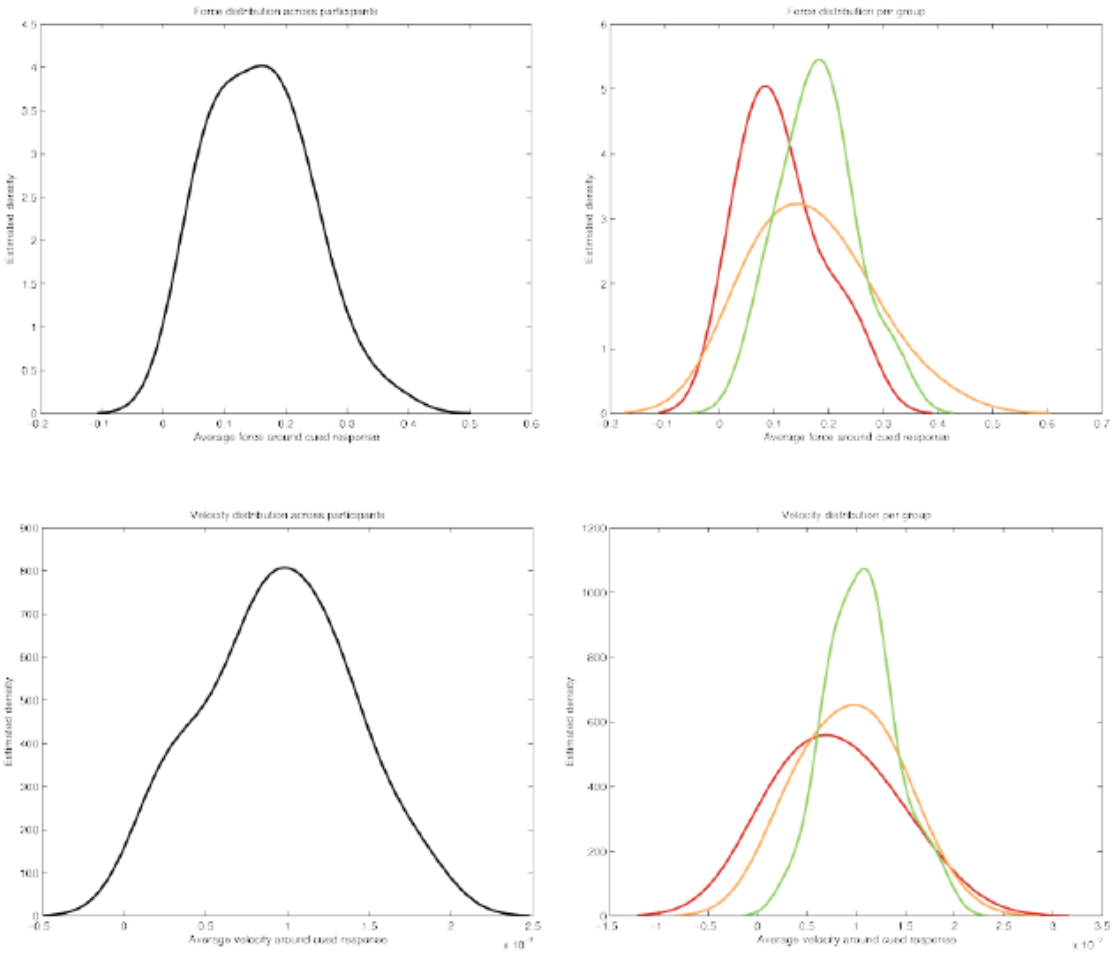

Supplementary figure 2: smoothed histograms (made using Matlab function `ksdensity` with default parameters) of the distribution of peak force (top graphs) and peak velocity (bottom graphs), averaged across body parts, across all subjects (left graphs, black) and per group of subjects (right graphs; light green: HC; light orange: PD ON; dark red: PD OFF). There is trend suggesting that HC subjects elicit motor responses with the highest force and velocity and PD patients OFF the lowest, PD patients ON lying in between the two.

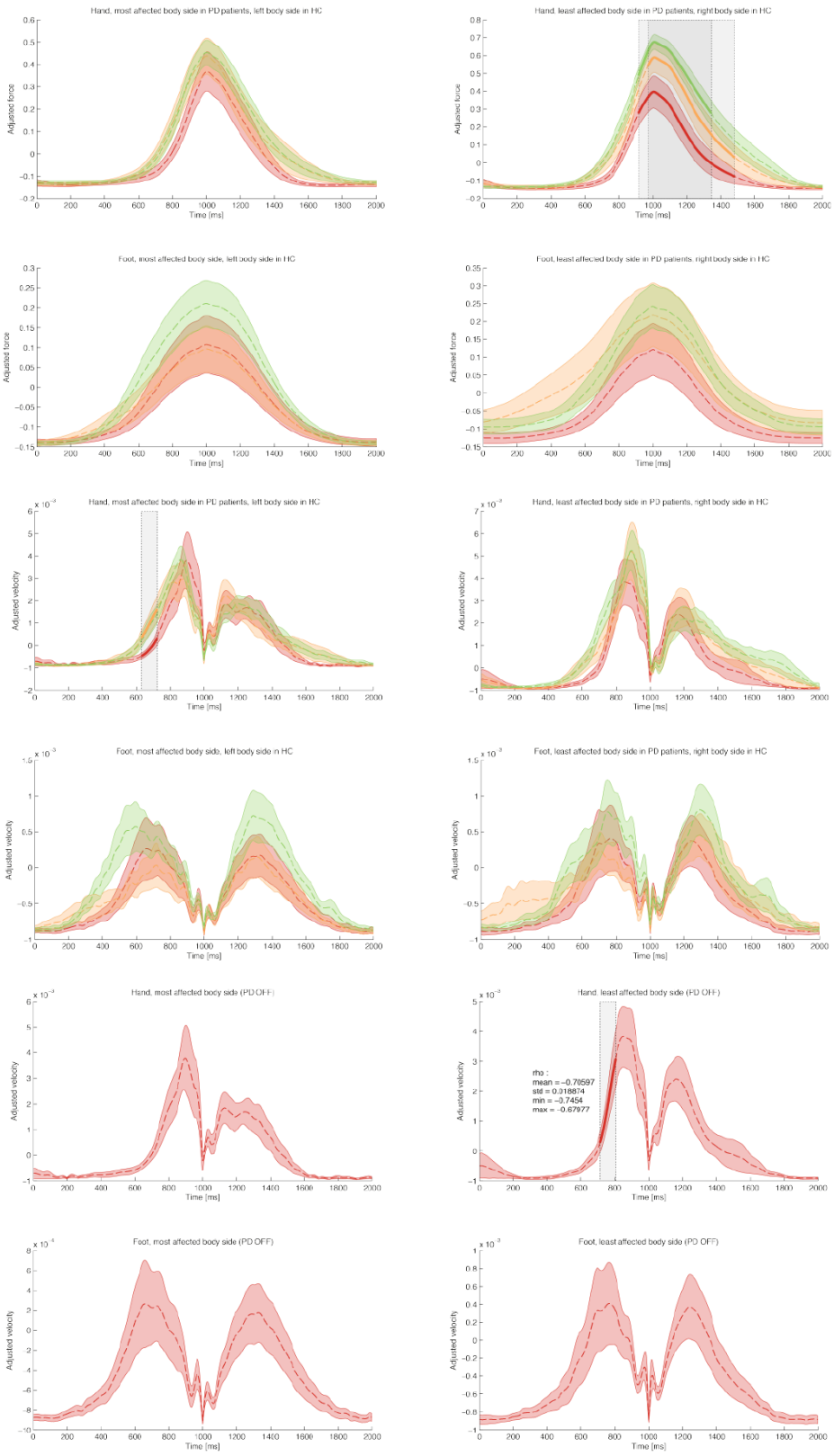

Supplementary figure 3: Results of the kinematic analyses between groups over the PRTH for each limb. Light green: HC; light orange: PD ON; dark red: PD OFF. Top 4 graphs: force differences;

middle 4 graphs: velocity differences; bottom 4 graphs: correlation with severity of bradykinesia in PD OFF. Dashed lines represent the average force or velocity per group accordingly, and shaded patches with the corresponding colour represent the standard error around the mean. Shaded grey rectangles highlight the periods in time yielding prolonged significant results – i.e. all time points within the grey rectangles show a significant difference between groups or a significant correlation with symptoms, accordingly. To help visualizing the results, strokes of curves characterizing the average time course of groups concerned with the significant differences are made thicker. Statistical threshold was set to $p < 0.01$ with a minimal time extent of 25 time points (50 milliseconds). Regarding correlation analyses (4 graphs on the bottom), the correlation coefficient within the time period yielding significance was always negative. The average (mean), minimal (min) and maximal (max) value of Spearman's ρ, as well as its standard deviation (std), is shown in the appropriate graph.

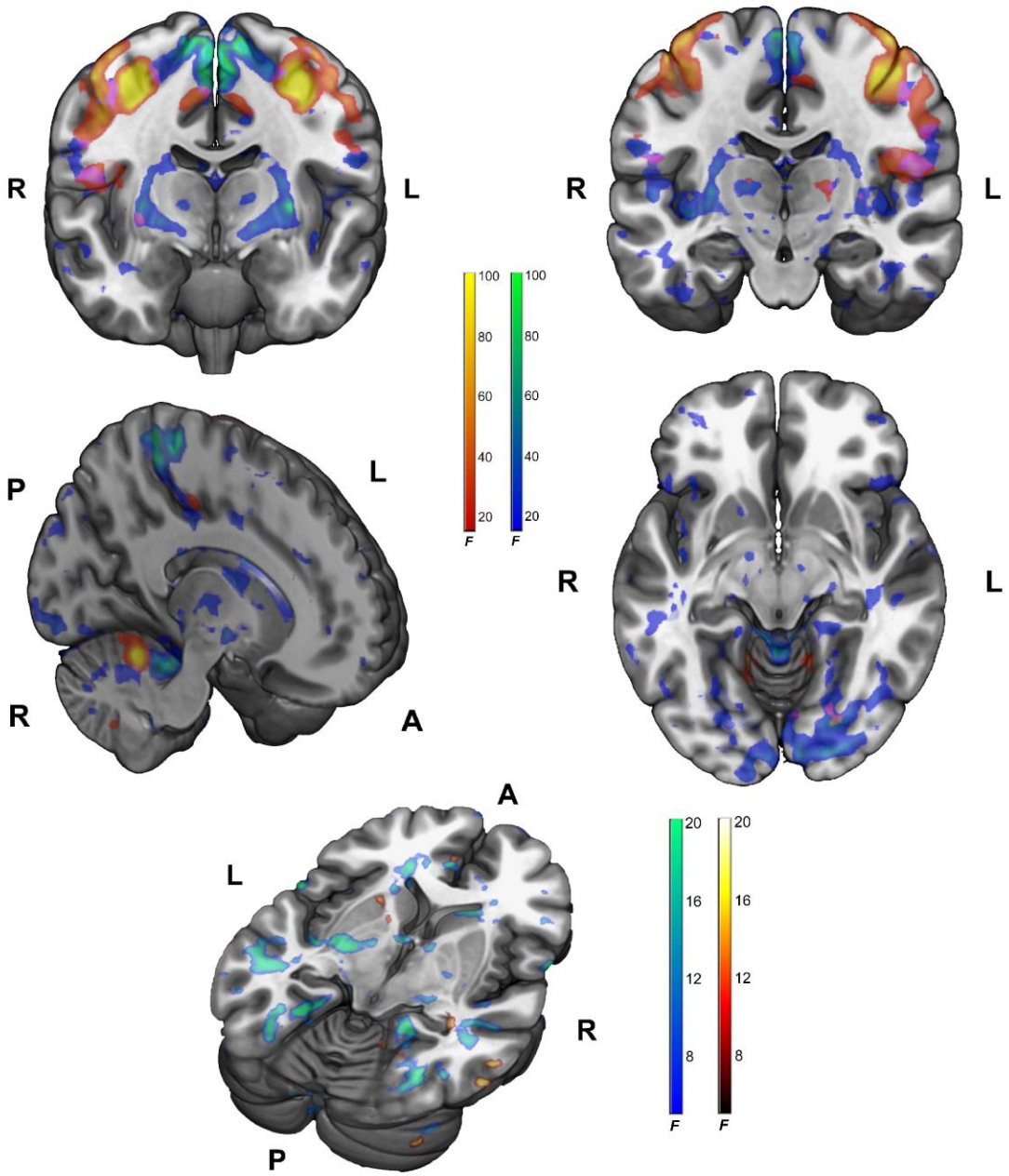

Supplementary figure 4: group results of whole-brain analyses in HC subjects, rendered on a canonical T1-weighted image (mni152_2009_256.nii.gz) clipped in three dimensions using MRIcroGL (Mac OS X version 1.150909). Upper scale legend in the centre applies to all renderings except the one in the bottom centre: the red-to-yellow scale represents the *F*-statistic for hand movements while the blue-to-green is the equivalent for feet movements. Bottom centre rendering reveals regions where the brain response during the motor somatotopy task correlates with age (blue-to-light green ("winter") scale) or force (black-to-white ("hot") scale). Bottom right scale legend indicates the corresponding *F*-statistic as before. Statistical maps are overlaid in an additive

manner, i.e. magenta depicts regions where hand and foot representations overlap at the group level. For display purposes, statistical threshold was set to $p < 0.001$ with a minimal cluster extent of 10 voxels.

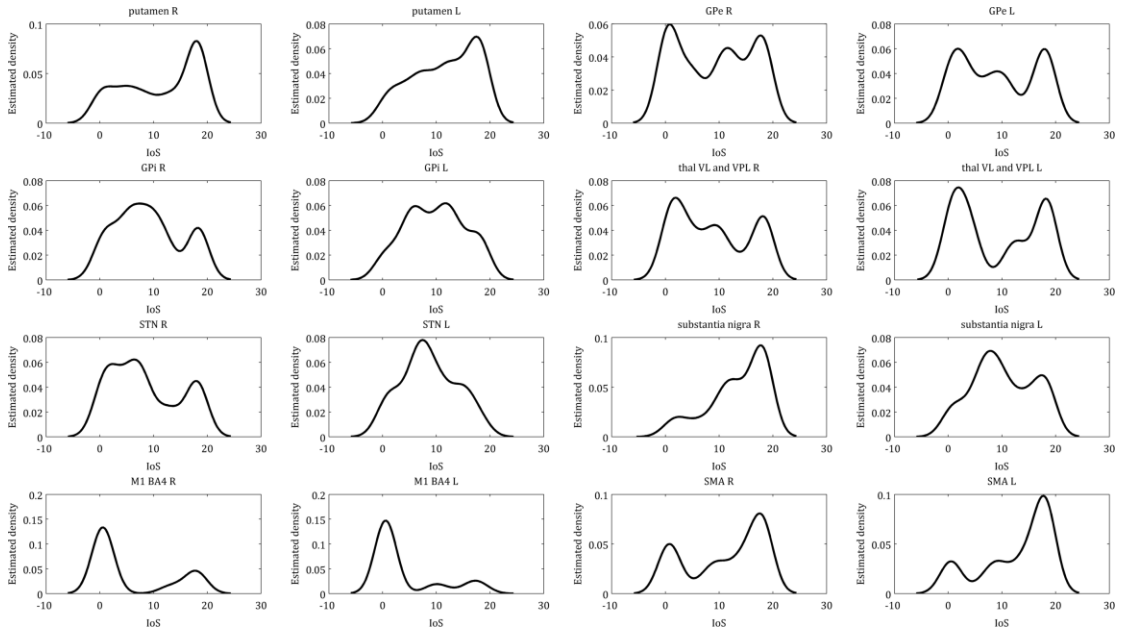

Supplementary figure 5: Smoothed histograms (made using Matlab function `ksdensity` with a bandwith of 2 samples) showing the distribution of IoS scores per ROI across all subjects. One can see that even after the *r*-to-*z'* Fisher transform, many distributions are skewed and potentially multimodal, henceforth justifying the use of non-parametric tests. This arises – at least partially – from the fact that we use the absolute value of *z'*.

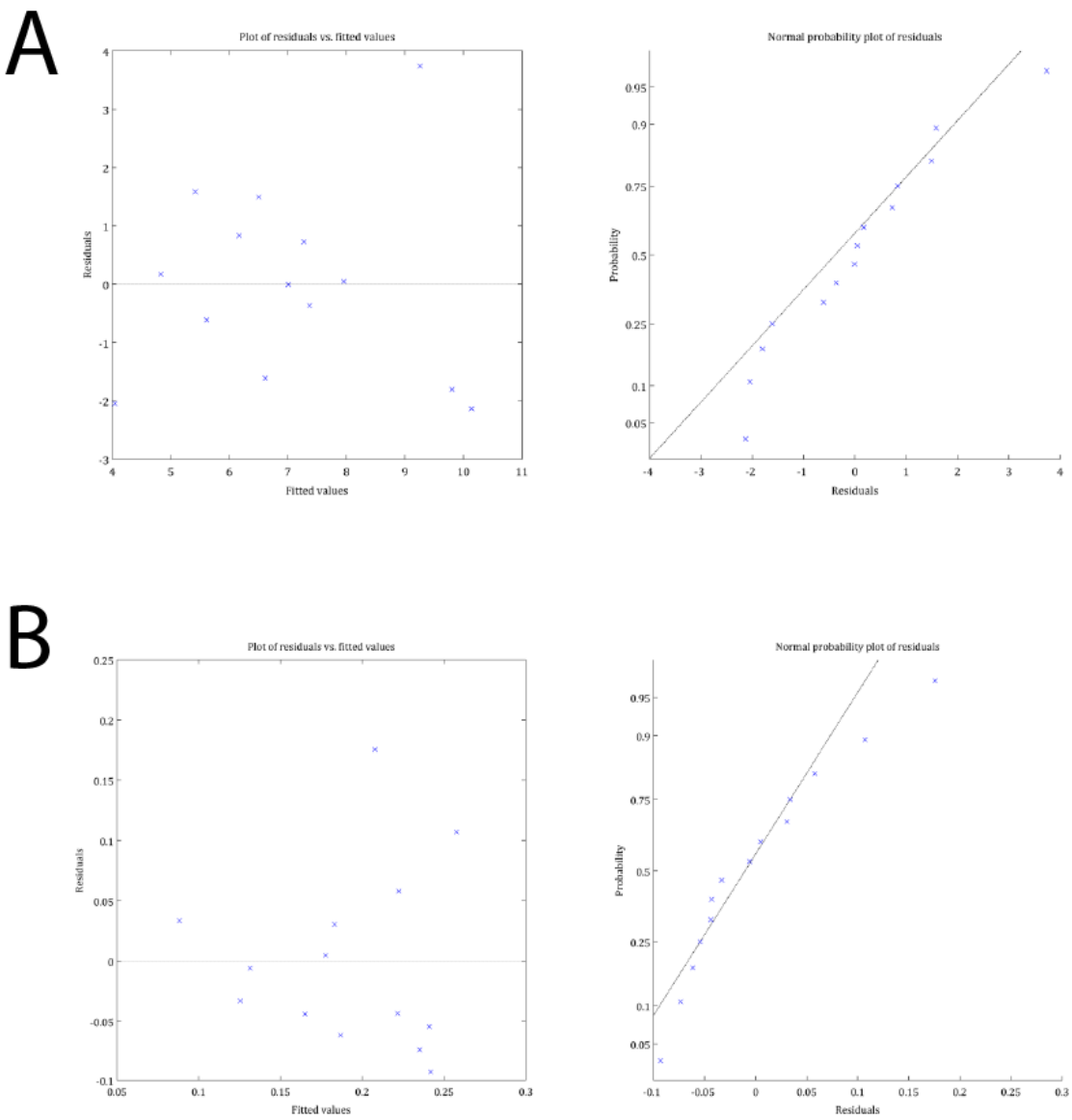

Supplementary figure 6: plots of residuals against fitted values (left graphs) and normality plots of residuals (right graphs) for the multiple linear regression models performed on bradykinesia sub-score as a function of IoS in SN (A) and M1–putamen estimates as a function of IoS in putamen (B).

2.2.2. Study 3

In this work, we show that PD is associated with a loss of functional segregation not only at the BG level but also in the insula, a hub region densely connected to the striatum and with high susceptibility to degeneration. This study confirms the idea that PD induces a shift of insular activity from anterior to posterior regions, even in the context of a simple motor task. Here, DA substitution does not affect functional segregation estimates. This work highlights the insula as playing a key role in PD.

Antero-posterior shift of insular cortex activity during motor somatotopy task in Parkinson's disease patients

Renaud Marquis*[1], Sandrine Muller*[1], Ferath Kherif[1], Bogdan Draganski[1,2]

[1] *Laboratory of Research in Neuroimaging (LREN) – Department of Clinical Neuroscience, Neuroscience Research Center, Lausanne University Hospital (CHUV), University of Lausanne (UNIL), Lausanne, Switzerland*

[2] *Max Planck Institute for Human Cognitive and Brain Sciences, Leipzig, Germany*

* Authors contributed equally to the work

Running title: PD causes a shift of motor activity in the insula

Title: Antero-posterior shift of insular cortex activity during motor somatotopy task in Parkinson's disease patients

Abstract: 149

Text body: 2808

References: 28

Tables: 1

Figures: 2

Supplementary material: 1 figure, 2 tables in a separate Excel file

Keywords: Parkinson's disease; functional magnetic resonance imaging; multivariate Bayes; insula

Corresponding author:
Bogdan Draganski
LREN - Département des Neurosciences Cliniques
CHUV, Université de Lausanne
Mont Paisible 16
1011 Lausanne
Switzerland
email: bogdan.draganski@chuv.ch
phone: +41-21-314 9638

Abstract

There is mounting evidence about the pivotal role of insula in Parkinson's disease (PD) to suggest a spatial modulation of brain activity in this region. Using Multivariate Bayes (MVB) and Bayesian Model Selection (BMS), functional MRI data were decoded in 11 PD patients tested ON and OFF medication and compared to 20 healthy control (HC) subjects performing the very same externally paced motor task. We show that in both PD OFF and PD ON the posterior and anterior parts of the insula are equally predictive of motor activity, in contrast to HC. Further, this shift towards the posterior part of the insula was observed only while patients were moving limbs on the most affected body side. Together, these results confirm that functional topography of motor activity in the insula may be altered in PD, and suggest that the directionality of this shift could be independent of dopaminergic medication status.

Introduction

Recent studies highlight the potential role of the insula in Parkinson's disease (PD) (Christopher et al., 2014). The insular cortex sends massive projections to the striatum. These are topographically organised, such that the posterior insula projects to the posterior dorsal striatum and the anterior insula projects to the more anterior and ventral portions of the striatum. The insula has been mainly seen as an integrating hub involved in processing emotional, cognitive and visceral information. Furthermore, this region participates to motor behaviour, as insular activity has been reported in simple motor tasks (Criaud et al., 2016; Fink et al., 1997; Kurth et al., 2010) and PD seems to alter connectivity between the insula and the pre-SMA (Chang et al., 2013). The contribution of the insula in PD recently gained more attention and this growing interest is supported by the fact that it is one of the first and most affected cortical regions by alpha-synuclein deposition according to Braak's staging hypothesis (Braak et al., 2006; Christopher et al., 2014). More recently Criaud and colleagues (2016) used activation likelihood estimation (ALE), a coordinate-based quantitative meta-analysis approach, and showed that in PD patients, convergence of activation maxima was differentially located in the insula compared to normal control subjects, especially when considering cognitive and affective symptoms. Furthermore, convergence of activation maxima was observed in ventral anterior portions of the insula in PD on medication, whereas for PD off medication it was more in the dorsal posterior insula. In contrast, activation maxima generally converged in the left mid-insula and right anterior insula for sensorimotor function and were not influenced by disease or medication status. Criaud et al. (2016) acknowledged that ALE, although overcoming typical limitations of neuroimaging studies such as small sample size or heterogeneity of patient population, does not allow looking at brain activations per se. The goal of our research was to test for the very presence of a spatial shift of brain activity in the insula in PD. Although Parkinson's disease is associated with a range of non-motor symptoms (Burn, 2002; Christopher et al., 2014; Goldman and Litvan, 2011; Kaji and Hirata, 2011; Lieberman, 2006; Voon et al., 2011), it is primarily a movement disorders, therefore our objective was to examine insular cortex activity during a simple motor task and determine whether PD would produce a shift of the brain response in space within this region. In this study, we acquired functional MRI data while normal control subjects and PD patients, tested on and off dopaminergic medication, performed movements of upper and lower limbs on each body side. We then applied the multivariate Bayesian decoding scheme proposed by Friston and colleagues (MVB, 2008) that allows the mapping of brain activity patterns to a psychological variable. The advantage of MVB, in combination with Bayesian model comparison (Rigoux et al., 2014; Stephan et al., 2009), is that it provides an appropriate procedure to explicitly test spatial hypotheses by comparing model evidences, e.g. infer the most plausible model characterizing the way information is distributed in a brain region (FitzGerald et al., 2012) or compare the contribution of different brain structure elements in the production of a cognitive process or motor command (Morcom and Friston, 2012; Park et al., 2015). By separating the insula into an anterior and posterior portions using atlas-based priors and comparing the model evidences for each insular subregion, we hypothesized, following Criaud et al. (2016), that PD would be associated with a shift of motor activity in the posterior part of the insula, henceforth increasing the ability to predict movements from the posterior insula. Based on results of Criaud and colleagues (2016), we also predicted that dopaminergic medication would shift insular activity back to the anterior insula.

Methods

Participants

Participants in the study comprised 19 PD patients tested on and off dopaminergic medication, as well as 21 healthy control (HC) subjects. One HC subject presented severe head motion while scanning and was excluded. Neurologists suspected essential tremor in one patient, leading to the exclusion of the case. Neurological assessment comprising UPDRS III and IV and performed by 3 neurologists indicated that 5 patients were predominantly affected on the right body side. The latter cases were not included in the analyses, because flipping data for these patients would have required assuming that the model evidences decoding movements of right and left limbs have the same target to predict, which is not the case. The lack of compliance in performing the motor task led to further exclusion of 2 patients. There remained 11 PD patients (6 men, 5 women; age = 61.19 ± 2.62 standard error, or SEM) and 20 HC subjects (10 men, 10 women; age = 58.75 ± 1.89 SEM) of comparable age ranges (2-tailed 2-samples t-test, $t(29) = 0.76$; $p = 0.4534$). The Edinburgh inventory (Oldfield, 1971) indicated comparable handedness scores ($L.Q._{PD}$ = 74.27 ± 18 SEM; $L.Q._{HC}$ = 55.88 ± 12.52 SEM; 2-tailed 2-samples t-test, $t(29) = 0.8554$, $p = 0.3993$), with 17 right-handed and 3 left-handed HC subjects, together with 10 right-handed and 1 left-handed PD patients. All participants gave written informed consent and the local ethics committee approved the study.

Study design

5 patients were scanned first off medication and 6 – on medication. Patients tested off medication were asked to stop dopaminergic therapy the day before at noon, while they were asked to continue it as normal when tested on medication. The two scanning sessions were separated by 68.8 ± 16.1 SEM days on average, a time interval which was similar in patients tested first off and patients first tested on medication ($PD_{first\ OFF}$ = 63.8 ± 27.87 SEM days; $PD_{first\ ON}$ = 73 ± 20.6 SEM days; 2-tailed 2-sample t-tests, $t(9) = 0.2712$; $p = 0.7924$). UPDRS III scores increased when patients were off medication as compared to on medication (PD OFF = 19.91 ± 2.39 SEM; PD ON = 15.36 ± 2.35 SEM; 1-tailed paired t-test: $t(10) = 2.7310$; $p = 0.0106$).

Experimental paradigm

Unilateral grasping movements on the right and left hands and flexion/extension of the right and left ankle feet were performed during each block, consisting of 8 movements of the same body part. Flickering visual symbol depicting the body part to move appeared every 2 seconds to pace movements externally. Blocks were repeated 5 times for each body part, intermixed with equally numbered rest periods of the same duration, during which a fixation cross was displayed. A preparation phase informed the subject before each block about the next task to perform, together with a countdown lasting 3 seconds. Blocks of movements were ordered in a pseudo-random and balanced fashion. Subjects practiced movements before scanning and were requested to fixate the centre of the screen.

Behavioural performance monitoring

We used a custom MR-compatible pneumatic device to monitor behavioural performance during fMRI acquisition. While performing grasping movements, subjects held in each hand rubber balls connected to air pressure sensors via plastic tubes. To capture feet movements, a similar system was installed underneath foot pedals. Pressure sensors transduced air pressure into electrical signal, whose gain was amplified and which was sent to Signal 6 software via a CED MICRO3 1401 (Cambridge Electronic Design Limited) data acquisition unit. The latter digitalized the waveforms at 500 Hz sampling rate. Motor responses were detected using event-related moving averages with dynamic threshold adapted from Elgendi et al. (2013). Peak detection on the datasets was optimized by setting the algorithm parameters as follows: W_1 = 700; W_2 = 3500; β = 0.35. The Butterworth band-pass filter used low- and high-pass cut-off at 0.1 and 30 Hz respectively. The formulas giving parameters THR_1 and THR_2 were adapted such that $THR_1 = \gamma \cdot MA_{beat}[n] + \alpha$, where γ = 0.45, and $THR_2 = \frac{W_1}{4}$. Detected peaks divided motor responses into cued and uncued movements.

Imaging protocol

We acquired MR images on a Siemens Prisma 3T scanner with a 64-channel head coil, using a 3D multishot EPI sequence at 2 mm isotropic voxel size (number of volumes: 239; 60 slices; slice TR = 52 ms; volume TR = 3.328 ms; slice oversampling: 6.7%) for functional images. We used multiparameter mapping (MPM) protocol at 1.5 mm voxel size (FoV 256 x 240 x 176 mm; matrix size: 160 x 150 x 120) for anatomical imaging, obtaining the longitudinal relaxation rate, effective proton density, magnetization transfer and effective transverse relaxation rate using multiecho 3D FLASH sequences. We chose suitable flip angle (α) and repetition time (TR) for mostly proton density-weighted (PDw) and T1-weighted contrast (PDw: TR/α = 24.5 ms/6°; T1w: TR/α = 24.5 ms/21°). As in the study of Lorio and colleagues (2016), we used parallel imaging along the phase-encoding direction and 8 equidistant echo time to acquire multiple gradient echoes. To correct quantitative maps for the effects of RF transmit inhomogeneities, a radio frequency transmit field map was acquired and corrected for geometric distortion and off-resonance effects using a static magnetic field map.

Image preprocessing

Data processing and analysis was performed using SPM12 (Wellcome Trust Center for Neuroimaging, http://www.fil.ion.ucl.ac.uk/spm/) and Matlab 7.13 (The MathWorks, Inc., Natick, Massachusetts, United States). Functional images were realigned to the mean, corrected for EPI distortion and receive coil inhomogeneities, and coregistered to the anatomical image. We built a study-specific template using DARTEL (Ashburner, 2007), warped functional images to MNI space with the resulting flow fields and applied spatial smoothing using a Gaussian kernel with full width at half maximum of 3mm. One healthy control subject was excluded from subsequent analyses because of an average head motion during functional imaging (Van Dijk et al., 2012) above 5mm.

Within-subject whole-brain univariate fMRI analyses

The design matrix for fMRI modelling comprised motor responses peak for cued and uncued movements as identified by the peak detection algorithm. We modelled preparation periods as

epochs of 3 seconds and included realignment parameters as covariates. Contrasts for positive effects of each cued movement (right and left hand and foot) were tested. Furthermore, we tested the effects of moving right and left limbs in 2 separate F-contrasts.

Group-level whole-brain univariate fMRI analysis

We performed a random effects analysis with contrasts for the positive effects of each cued movement at the group level to verify the presence of motor activity in the insula across all groups of subjects.

Regions of interest

Regions of interest (ROIs) for the left and right anterior and posterior insula were defined using the atlas provided by Neuromorphometrics, Inc. (http://neuromorphometrics.com/) under academic subscription and originating from the OASIS project (http://www.oasis-brains.org/).

Canonical Variate Analysis

To confirm the existence of a multivariate mapping between the voxels and the movements to predict, we performed canonical variate analysis (CVA) for each body part movement within each ROI (Friston et al., 1995).

Multivariate Bayesian decoding

We applied multivariate Bayes (MVB) (Friston et al., 2008) at the subject-level to predict the movements of right and left limbs in separate analyses. The model log-evidences were assessed for 4 candidate models – one for each ROI within the insula. Given the complex topography of brain functions in the insula, sparse spatial priors over voxels were used in each ROI, such that each activity pattern is composed of subsets of individual voxel without neither assuming that the latter should be neighbouring nor that the patterns should follow a smooth Gaussian response. The same design matrix was used for each MVB analyses aiming at predicting the movement of right and left limbs. Therefore, for each decoding analysis, the movements of body parts other than the predicted targets, as well as preparation periods and realignment parameters constituted the space of confounding variables that were accounted for.

Bayesian Model Selection

First, we combined the anterior and posterior portions of the insula to obtain two families of models: the contralateral family of models predicted the movements of right and left limbs using the left – respectively right – insula, and vice versa for the ipsilateral family of models. Family-level inference based on model space partitioning (spm_compare_families.m) was performed to compare these two families of models using fixed and random effects Bayesian model comparison at the group level (Penny et al., 2010; Stephan et al., 2010). Secondly, as the elected family of models was the contralateral one, we performed random effects Bayesian model selection (BMS, spm_BMS.m) at the group level (Rigoux et al., 2014) between the contralateral anterior and posterior parts of the insula in predicting right and left limbs movements in each group of subjects. Group Bayes Factors (Stephan et al., 2009), computed as the sum of log-evidences across subjects, were also reported.

Results

Whole-brain univariate analyses

Reliable patterns of motor-related brain activity were found in the insula. Clusters of active voxels surviving FWE-correction were present in all ROIs as shown by an F-test on all movements across all groups (Figure 1, detailed results table is available as supplementary material).

CVA

We observed significant mappings in each ROI for the movement of each body part across all groups ($p < 0.001$, except for predicting right hand movements using the right posterior insula for which $p = 0.00333$).

MVB

Across all subjects and ROIs, 99.4 – respectively 100% – of the negative free energy approximation to the model log-evidences produced by MVB for predicting movements of right – respectively left – limbs had a Bayes Factor above 20, denoting strong evidence in favour of the alternative hypothesis against the null model. There was only one model predicting movements of right limbs for which the Bayes Factor against the null model was equal to 7.4102.

BMS: comparison of contralateral and ipsilateral families of models

Fixed effects BMS revealed that contralateral families of model were strongly more predictive than ipsilateral ones. Posterior probabilities were equal to 1 and 0 for contralateral – respectively ipsilateral – families of models for right as well as left limbs movements. Random effects BMS endorsed these results with identical posterior probabilities except for right limbs movements, for which exceedance probabilities were 0.98 and 0.02 for contralateral and ipsilateral families of models respectively (Supplementary figure 1).

BMS: comparison of anterior and posterior models

Group Bayes Factors indicated a bigger discrepancy between anterior and posterior insula models in HC as compared to PD patients (Table 1). Random effects BMS confirmed this observation, electing the anterior insula as the most predictive model in HC, but not in PD patients. More specifically, the anterior insula was the winning model in all analyses except for predicting the movement of left limbs in PD patients, both ON and OFF medication (Figure 2).

Discussion

Using MVB and BMS, we first showed that the contralateral insula better predicts the movements of upper and lower limbs as compared to the ipsilateral inula. We then demonstrated that the elected model to predict externally cued movements in normal control subjects was the anterior insula. Because Neuromorphometrics atlas divides the insula into a posterior and anterior region, the sensorimotor part of this region – i.e. the mid-insula – lies primarily in the anterior ROIs (Criaud et al., 2016; Fink et al., 1997; Kurth et al., 2010). This might explain why the latter ROIs were more predictive than the posterior ROIs. In contrast to HC subjects, we showed that in PD patients the

anterior and posterior insular cortex are equally contributing in the execution of movements. Our results suggest a shift of motor activity in the insula to the posterior part, similarly to the results of Criaud and colleagues (2016) who reported a comparable shift of insular activity associated with cognitive and affective symptoms. The latter study did not report differential loci for the convergence of activation maxima related to sensorimotor function. Assuming that the definition of insula subregions we used separated the anterior and posterior portions in a sufficiently accurate fashion, the reason we found different results for PD patients and normal controls might lie in the outstanding sensitivity of MVB (Friston et al., 2008). Nevertheless, in contradiction with ALE results, dopaminergic medication was not found to reverse the location of brain activity back to the anterior insula, neither bringing it back to the mid-insula, nor bringing it further anteriorly. This could suggest that contrary to cognitive and limbic function, insular activity patterns related to sensorimotor function are not affected by dopaminergic medication. Our results suggest therefore that the posterior insula may be involved in a mechanism of compensation in PD, mirroring the caudorostral gradient of progressive nigrostriatal denervation (Cools, 2006; Vaillancourt et al., 2013). Interestingly, dopaminergic medication seems to neither reverse nor cancel this process in the insular cortex. Altogether, our study provides evidence for a loss of functional segregation in the insular cortex in PD: the antero-posterior gradient of response selectivity in the insula, seen in normal controls, seems to be lost in PD; such that both the anterior and posterior insula are involved in the movement of distal body parts. Given the importance of the insula as an integrating hub massively connected to the striatum and other cortical regions, future investigations might use multivariate methods and examine in detail whether the loss of segregation caused by PD in the insula can be detected in other fMRI tasks – extending to other brain functions such as attentions or reward –, if it occurs also in patients mostly affected on the right body side – or affected bilaterally –, and whether other neurological disorders are also associated with a loss of functional segregation.

References

Braak, H., Bohl, J.R., Müller, C.M., Rüb, U., de Vos, R.A.I., and Del Tredici, K. (2006). Stanley Fahn Lecture 2005: The staging procedure for the inclusion body pathology associated with sporadic Parkinson's disease reconsidered. Mov. Disord. *21*, 2042–2051.

Burn, D.J. (2002). Depression in Parkinson's disease. Eur. J. Neurol. Off. J. Eur. Fed. Neurol. Soc. *9 Suppl 3*, 44–54.

Chang, L.J., Yarkoni, T., Khaw, M.W., and Sanfey, A.G. (2013). Decoding the Role of the Insula in Human Cognition: Functional Parcellation and Large-Scale Reverse Inference. Cereb. Cortex *23*, 739–749.

Christopher, L., Koshimori, Y., Lang, A.E., Criaud, M., and Strafella, A.P. (2014). Uncovering the role of the insula in non-motor symptoms of Parkinson's disease. Brain *137*, 2143–2154.

Cools, R. (2006). Dopaminergic modulation of cognitive function-implications for L-DOPA treatment in Parkinson's disease. Neurosci. Biobehav. Rev. *30*, 1–23.

Criaud, M., Christopher, L., Boulinguez, P., Ballanger, B., Lang, A.E., Cho, S.S., Houle, S., and Strafella, A.P. (2016). Contribution of insula in Parkinson's disease: A quantitative meta-analysis study. Hum. Brain Mapp. *37*, 1375–1392.

Elgendi, M., Norton, I., Brearley, M., Abbott, D., and Schuurmans, D. (2013). Systolic Peak Detection in Acceleration Photoplethysmograms Measured from Emergency Responders in Tropical Conditions. PLoS ONE *8*, e76585.

Fink, G.R., Frackowiak, R.S., Pietrzyk, U., and Passingham, R.E. (1997). Multiple nonprimary motor areas in the human cortex. J. Neurophysiol. *77*, 2164–2174.

FitzGerald, T.H.B., Friston, K.J., and Dolan, R.J. (2012). Action-Specific Value Signals in Reward-Related Regions of the Human Brain. J. Neurosci. *32*, 16417–16423.

Fonov, V., Evans, A.C., Botteron, K., Almli, C.R., Mckinstry, R.C., Collins, D.L., and the Brain Development Cooperative Group (2011). Unbiased average age-appropriate atlases for pediatric studies. NeuroImage *54*, 313–327.

Fonov, V.S., Evans, A.C., McKinstry, R.C., Almli, C.R., and Collins, D.L. (2009). Unbiased nonlinear average age-appropriate brain templates from birth to adulthood. NeuroImage *47*, *Supplement 1*, S102-.

Friston, K., Chu, C., Mourão-Miranda, J., Hulme, O., Rees, G., Penny, W., and Ashburner, J. (2008). Bayesian decoding of brain images. NeuroImage *39*, 181–205.

Friston, K.J., Frith, C.D., Frackowiak, R.S., and Turner, R. (1995). Characterizing dynamic brain responses with fMRI: a multivariate approach. NeuroImage *2*, 166–172.

Goldman, J.G., and Litvan, I. (2011). Mild cognitive impairment in Parkinson's disease. Minerva Med. *102*, 441.

Kaji, Y., and Hirata, K. (2011). Apathy and Anhedonia in Parkinson's Disease. ISRN Neurol. *2011*, 1–9.

Kurth, F., Zilles, K., Fox, P.T., Laird, A.R., and Eickhoff, S.B. (2010). A link between the systems: functional differentiation and integration within the human insula revealed by meta-analysis. Brain Struct. Funct. *214*, 519–534.

Lieberman, A. (2006). Depression in Parkinson's disease - a review. Acta Neurol. Scand. *113*, 1–8.

Lorio, S., Kherif, F., Ruef, A., Melie-Garcia, L., Frackowiak, R., Ashburner, J., Helms, G., Lutti, A., and Draganski, B. (2016). Neurobiological origin of spurious brain morphological changes: A quantitative MRI study. Hum. Brain Mapp. *37*, 1801–1815.

Morcom, A.M., and Friston, K.J. (2012). Decoding episodic memory in ageing: A Bayesian analysis of activity patterns predicting memory. NeuroImage *59*, 1772–1782.

Oldfield, R.C. (1971). The assessment and analysis of handedness: the Edinburgh inventory. Neuropsychologia *9*, 97–113.

Park, C., Chang, W.H., Lee, M., Kwon, G.H., Kim, L., Kim, S.T., and Kim, Y.-H. (2015). Which motor cortical region best predicts imagined movement? NeuroImage *113*, 101–110.

Penny, W.D., Stephan, K.E., Daunizeau, J., Rosa, M.J., Friston, K.J., Schofield, T.M., and Leff, A.P. (2010). Comparing Families of Dynamic Causal Models. PLoS Comput. Biol. *6*, e1000709.

Rigoux, L., Stephan, K.E., Friston, K.J., and Daunizeau, J. (2014). Bayesian model selection for group studies - Revisited. NeuroImage *84*, 971–985.

Stephan, K.E., Penny, W.D., Daunizeau, J., Moran, R.J., and Friston, K.J. (2009). Bayesian model selection for group studies. NeuroImage *46*, 1004–1017.

Stephan, K.E., Penny, W.D., Moran, R.J., den Ouden, H.E.M., Daunizeau, J., and Friston, K.J. (2010). Ten simple rules for dynamic causal modeling. NeuroImage *49*, 3099–3109.

Vaillancourt, D.E., Schonfeld, D., Kwak, Y., Bohnen, N.I., and Seidler, R. (2013). Dopamine overdose hypothesis: Evidence and clinical implications. Mov. Disord. *28*, 1920–1929.

Van Dijk, K.R.A., Sabuncu, M.R., and Buckner, R.L. (2012). The influence of head motion on intrinsic functional connectivity MRI. NeuroImage *59*, 431–438.

Voon, V., Mehta, A.R., and Hallett, M. (2011). Impulse control disorders in Parkinson's disease. Curr. Opin. Neurol. *24*, 324–330.

3224 **Tables**

3225

	Limbs	ROI	HC	PD ON	PD OFF
Summed log-evidences	**Right**	**AIns L**	1742.185	699.811	718.318
		PIns L	1140.434	481.939	509.186
	Left	**AIns R**	1876.741	658.539	726.991
		PIns R	1324.545	543.841	569.339
Exceedance probabilities	**Right**	**AIns L**	0.999	0.984	0.994
		PIns L	0.001	0.016	0.006
	Left	**AIns R**	1.000	0.784	0.759
		PIns R	0.000	0.216	0.241
Protected exceedance probabilities	**Right**	**AIns L**	0.973	0.872	0.929
		PIns L	0.027	0.128	0.071
	Left	**AIns R**	0.998	0.591	0.579
		PIns R	0.002	0.409	0.421
Bayesian omnibus risk	**Right**	**Ins L**	0.052	0.231	0.132
	Left	**Ins R**	0.004	0.679	0.696

3226 **Table 1** : summary of BMS comparing anterior and posterior insula models for each group of
3227 subjects and for movements of each body side. AIns L: left anterior insula; AIns R: right anterior
3228 insula; PIns L: left posterior insula; PIns R: right posterior insula.

3229

Figures

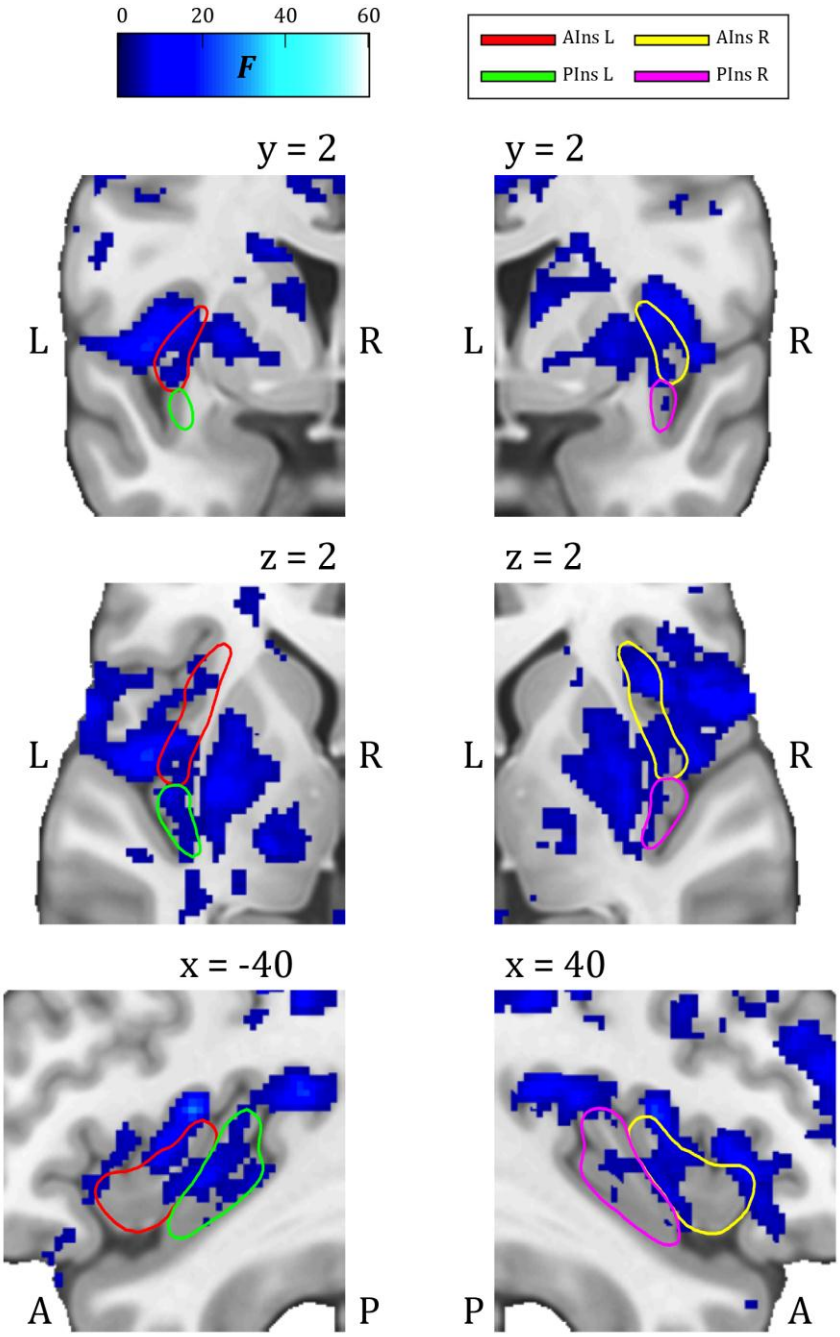

Figure 1 : whole-brain univariate group results overlaid on a skull-stripped canonical image (Fonov et al., 2011, 2009), showing clusters of voxels significantly active ($p < 0.001$, minimal cluster extent of 10 voxels) during limbs movement across all groups of subjects. Insular cortex subregions

are delineated in different colors: red = left anterior insula; yellow = right anterior insula; green = left posterior insula; magenta = right posterior insula. L = left ; R = right ; A = anterior ; P = posterior.

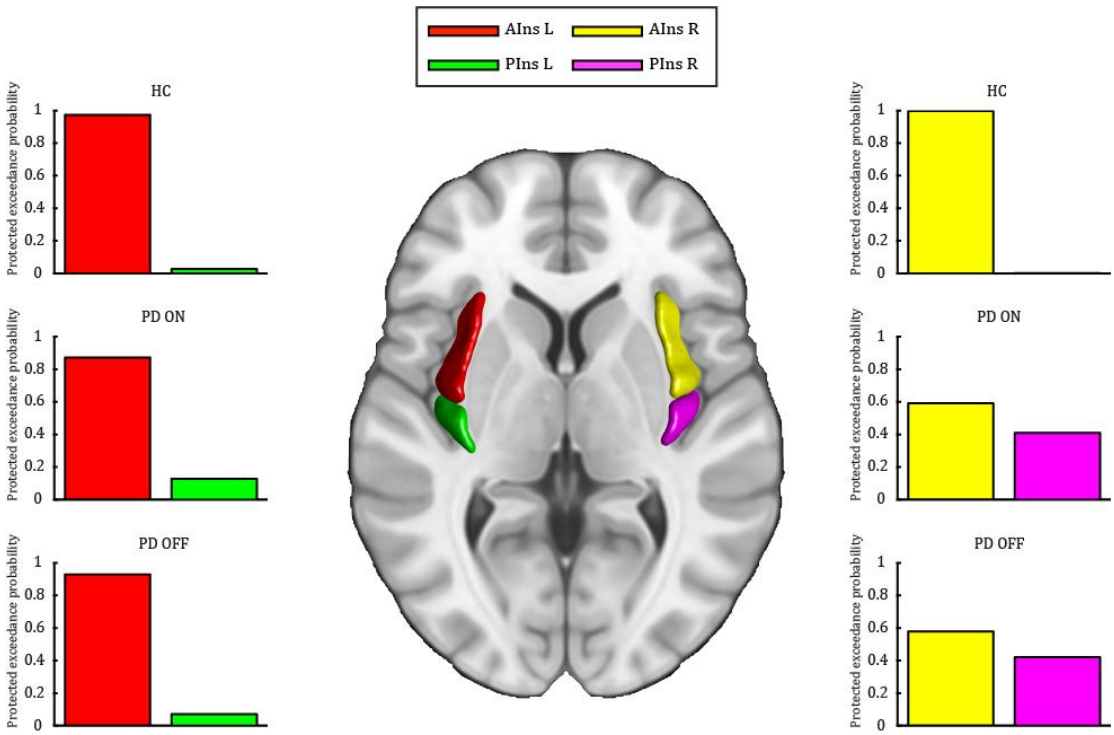

Figure 2 : BMS results comparing anterior and posterior portions of the contralateral insula for each group. ROIs are rendered (centre) on a skull-stripped canonical image (Fonov et al., 2011, 2009) following neurological convention. Protected exceedance probabilities are represented with bar plots right and left from the center for left and right limb movements respectively. Colour of bar plots corresponds to ROI colour. AIns L: left anterior insula; AIns R: right anterior insula; PIns L: left posterior insula; PIns R: right posterior insula.

Supplementary figures

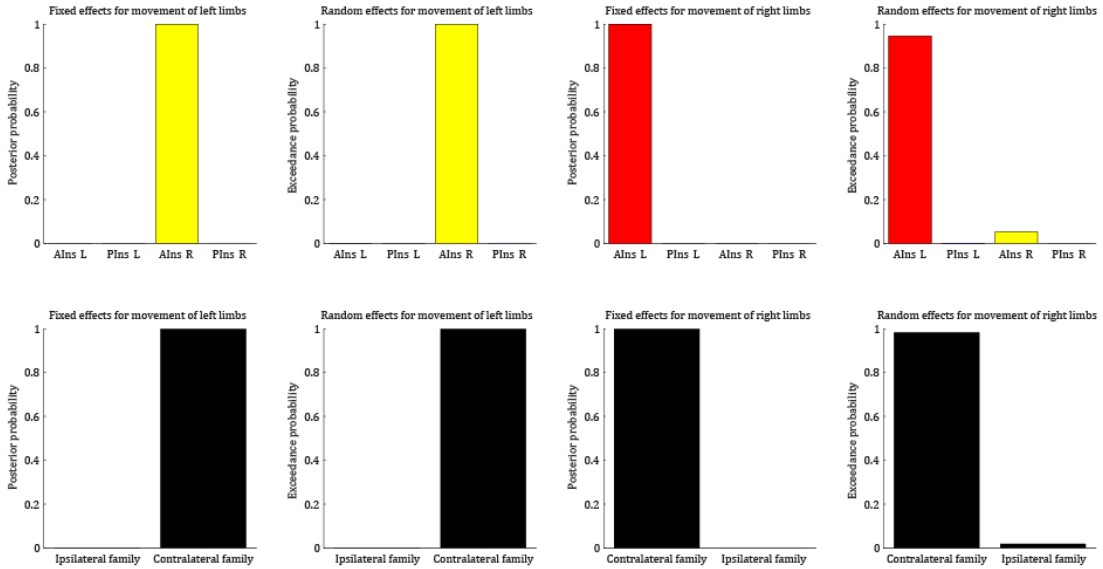

Supplementary figure 1 : fixed and random effects BMS results comparing contralateral and ipsilateral families of models. Bar plots on the top represent each model's posterior probabilities and exceedance probabilities. Bottom graphs show the elected family for left and right limbs movements. Color code is the same as in Figure 2. AIns L: left anterior insula; AIns R: right anterior insula; PIns L: left posterior insula; PIns R: right posterior insula.

2.3. Structural segregation in Parkinson's disease

2.3.1. Study 4

In this study, we test the LOS hypothesis in PD at the structural connectivity level. This experiment shows that limbic, associative and sensorimotor circuits are rewired across cortico-striatal and thalamo-cortical level in PD. In addition, different clinical symptoms profiles in patients are associated with distinct changes in structural connectivity patterns. This work provides the first evidence supporting the LOS hypothesis in PD at the structural level.

Parkinson's disease rewires cortico-striatal and thalamo-cortical connectivity

Renaud Marquis*[1], David A. Slater*[1], Ferath Kherif[1], Bogdan Draganski[1,2]

[1] *Laboratory of Research in Neuroimaging (LREN) – Department of Clinical Neuroscience, Neuroscience Research Center, Lausanne University Hospital (CHUV), University of Lausanne (UNIL), Lausanne, Switzerland*

[2] *Max Planck Institute for Human Cognitive and Brain Sciences, Leipzig, Germany*

* Authors contributed equally to the work

Running title: PD rewires cortico-subcortical connectivity

Title: Parkinson's disease rewires cortico-striatal and thalamo-cortical connectivity

Abstract: 125

Text body: 4378

References: 71

Tables: 1

Figures: 6

Supplementary material: 9 figures, 5 tables in a separate Excel file

Keywords: Parkinson's disease; diffusion-weighted imaging; tractography; segregation; cognition; motivation; sensorimotor

Corresponding author:
Bogdan Draganski
LREN - Département des Neurosciences Cliniques
CHUV, Université de Lausanne
Mont Paisible 16
1011 Lausanne
Switzerland
email: bogdan.draganski@chuv.ch
phone: +41-21-314 9638

Abstract

Given the steadily growing number of studies demonstrating that diffusion tractography can reveal the topography of cortico-basal ganglia connectivity patterns in vivo in humans we aim to test the loss of specificity hypothesis in movement disorders at the structural level. We propose here that Parkinson's disease (PD) is associated with remapping of cortico-striatal and thalamo-cortical connectivity between limbic, associative and sensorimotor territories. Using constrained spherical deconvolution, we compare covariance components of connectivity patterns in 19 healthy control subjects and 19 PD patients, and show how the spatial distribution of these connections relate to clinical symptoms. Our results demonstrate that PD affects structural segregation in the striatum and thalamus, and that different profiles of clinical manifestations are linked to specific patterns of rewiring in cortico-subcortical loops.

Introduction

Parkinson's disease (PD), the second most common neurodegenerative disease, is caused by the loss of dopaminergic neurons in the substantia nigra pars compacta (SNc). Its cardinal symptoms are slowness and poverty of movements, muscle rigidity, postural instability and rest tremor. However PD features also a range of non-motor symptoms including apathy (Kaji and Hirata, 2011), depression (Burn, 2002; Lieberman, 2006), anxiety (Marsh, 2000), cognitive impairment (Goldman and Litvan, 2011), impulse control disorders (Sharma et al., 2013; Voon et al., 2009, 2011), hyposmia (Sharma et al., 2013), sleep disorders (Sharma et al., 2013), dementia (Munhoz et al., 2015), psychosis (Munhoz et al., 2015), pain, gastrointestinal and autonomic disturbances (Sethi, 2002). Based on these various manifestations, some studies suggested different subtypes of PD (Marras and Chaudhuri, 2016; Moustafa and Poletti, 2013).

Dopaminergic cells in the SNc project to the striatum, the main input station of the basal ganglia. The functional architecture of the latter notably involves limbic, associative and motor circuits (Jahanshahi et al., 2015). Dopamine, together with striatal interneurons, modulate the structure and function of striatal circuitry through different mechanisms of synaptic plasticity (Calabresi et al., 2007; Lim et al., 2014; Morikawa and Paladini, 2011; Obeso et al., 2008; Surmeier et al., 2010). Within cortico-basal ganglia circuits, segregation (Alexander et al., 1986; Redgrave et al., 2010) and integration (Haber, 2003; Haber et al., 2000) of information seem to coexist (Draganski et al., 2008).

Recent evidences suggest that PD and other movement disorders are associated with a loss of neuronal specificity in the basal ganglia (Bar-Gad and Bergman, 2001; Bar-Gad et al., 2000, 2003; Bronfeld and Bar-Gad, 2011). Studies in non-human primates showed a loss of functional segregation following MPTP intoxication (Pessiglione et al., 2005), and recent studies in humans report that dopamine depletion in PD could lead to a remapping of cortico-striatal circuitry (Helmich et al., 2010). More recently, abnormal patterns of structural connectivity have been observed in Gilles de la Tourette syndrome (Worbe et al., 2015). While the value of diffusion-weighted imaging (DWI) in detecting alterations of white matter integrity in PD (Tessitore et al., 2016) and in differentiating PD from atypical parkinsonism (Meijer et al., 2013) has been acknowledged, there is currently no study addressing the question of segregation of structural connectivity in PD.

The goal of our research was therefore to test whether PD was associated with a loss of segregation in structural connectivity patterns within cortico-subcortical circuits. We hypothesized that PD affects the segregation of cortico-striatal and thalamo-cortical circuits into limbic, associative and motor functions. First, we used spherical deconvolution – an advanced diffusion tractography technique that has shown more sensitivity than DTI-based tractography detecting fibre pathways in the motor system (Farquharson et al., 2013) –, built an Index of Similarity to quantify structural segregation between connectivity patterns, and compared PD patients to healthy volunteers. Secondly, because motor symptoms in PD are initially unilateral, we estimated structural segregation with patients divided into right- and left-affected. Thirdly, we aimed at finding whether different profiles of clinical symptoms could be linked to different patterns of structural segregation.

Methods

Participants

32 patients and 27 healthy control (HC) subjects participated in the study after giving written informed consent. 3 patients were excluded because of diagnostic criterion (suspicion of essential tremor, multiple system atrophy and Alzheimer's disease) and one because of incomplete neuropsychological tests. Of the remaining 55 datasets, 10 were excluded because of bad image quality, head motion artefacts, gross tissue misclassifications in cortical targets for the tractography, or failures of spatial registration algorithms. There remained 19 patients passing data quality visual check done by R.M. and D.S. Among the remaining 26 HC subjects, the 19 oldest volunteers were selected to obtain balanced groups with comparable age ranges (age PD: 64.47 ± 1.74 standard error, or SEM; age HC: 62.89 ± 1.56 SEM; 2-tailed 2-sample t-test, $t(36) = 0.6748$, $p = 0.57709$).

Clinical measures

Neurological assessment comprised Unified Parkinson's Disease Rating Scale (UPDRS) parts III and IV. Three neurologists additionally scored the patients' Hoehn and Yahr stage and assigned 11 patients as predominantly affected on the left body side and 8 – on the right, consistently with their lateralized bradykinesia subscore (Buck et al., 2011). Age ranges were similar across patients affected on each side (age PD L: 62.27 ± 1.87; age PD R: 67.5 ± 1.36) and with healthy volunteers ($p > 0.05$ for all pairwise-comparisons using 2-tailed 2-sample t-tests). Neuropsychological assessment was carried out by the experimenter and included the Montreal Cognitive Assessment (MoCA; Nasreddine et al., 2005), the self-assessment part of the Apathy Inventory (Robert et al., 2002) and the Hospital Anxiety and Depression scale (HADS; Zigmond and Snaith, 1983). MoCA scores were binarised with a cut-off at < 26 to maximise the distinction between patients with and without mild cognitive impairment (Dalrymple-Alford et al., 2010).

MRI acquisition

We collected MRI data on a 3T Prisma MRI scanner (Siemens Medical Solutions, Erlangen, Germany). The diffusion-weighted images (DWI) were acquired using a 2D echo-planar imaging sequence with the following parameters: TR/TE = 7420/69ms, parallel GRAPPA acceleration factor = 2, FOV = 192 x 212 mm^2, matrix size = 96 x 106, 70 axial slices, 2 mm isotropic voxel dimension, 118 diffusion sensitization directions (15 at b = 650 s/mm^2, 30 at b = 1000 s/mm^2 and 60 at b = 2000 s/mm^2) and 13 b=0 images interleaved throughout the acquisition. Diffusion directions were isotropically distributed for each b-value shell using an electrostatic repulsion algorithm (Jones et al., 1999). We acquired multiparameter maps (MPM) at 1.5 mm voxel size using multiecho 3D FLASH acquisitions to get quantitative mapping of the magnetization transfer, effective proton density, longitudinal and effective transverse relaxation rate (FoV: 256 x 240 x 176 mm; matrix size: 160 x 150 x 120mm). Predominantly T1-weighted and proton density-weighted (PDw) contrasts were obtained by choosing appropriate repetition time (TR) and flip angle (α) (T1w:

TR/α = 24.5 ms/21°; PDw: TR/α = 24.5 ms/6°) as in Lorio and colleagues (2016). We acquired multiple gradient echoes using 8 equidistant echo times and parallel imaging along the phase-encoding direction. Quantitative maps were corrected for radio frequency (RF) transmit inhomogeneities using a RF transmit field (B1) map, whose geometric distortions and off-resonance effects were removed by acquiring a static magnetic field (B0) map (Lutti et al., 2010, 2012).

MPM preprocessing

Each participant's MT image was processed using the FreeSurfer version 5.3.0 software package pipeline (http://surfer.nmr.mgh.harvard.edu/). The standard pipeline reconstructs an individual's cortical and white matter surfaces from the participant's structural image data. The following steps comprise the surface preprocessing pipeline: correction of image intensity variations due to MR inhomogeneities (Dale et al., 1999); skull stripping (Ségonne et al., 2004); cortical grey and white matter segmentation (Dale et al., 1999); separation of the brain hemispheres and subcortical structures (Dale et al., 1999; Fischl et al., 2002, 2004); and finally a set of grey/white matter interface and pial surfaces for both brain hemispheres (Dale et al., 1999). After surface reconstruction the individual participant's surfaces were used to estimate the transformation which achieved maximal correspondence between the sucal and gyral patterns of the individual and those of an average brain (Fischl et al., 1999a, 1999b). This information was later used to bring a gyri based cortical parcellation (Desikan et al., 2006) into each individual's native image space.

DWI preprocessing

DWIs were corrected for eddy currents and subject motion using the FSL EDDY tool (Andersson and Sotiropoulos, 2016) and the gradient directions were appropriately rotated to correct for subject movement (Leemans and Jones, 2009). The B0 maps acquired as part of the structural imaging session were used to correct for EPI susceptibility distortions with the SPM field mapping toolbox (Hutton, 2002). The DWI images were then rigid body aligned to the MT image with the aid of the mean *b*=0 image using SPM12 (http://www.fil.ion.ucl.ac.uk/spm/software/spm12).

Tractography

All processing procedures described within this section were performed using the MRTrix3 software package (www.mrtrix.org; Tournier et al., 2012). The constrained spherical deconvolution (CSD; Tournier et al., 2004, 2007) FODs were calculated using a multi-shell, multi-tissue CSD (MSMT-CSD) algorithm which has been shown to reduce the presence of spurious fODF peaks in voxels containing GM and/or CSF partial volumes (Jeurissen et al., 2014). The spherical harmonic degrees used for the WM multi-shell fibre response functions were l_{max} = [0, 2, 6, 10] for each *b*-value shell respectively. GM and CSF response functions were assumed to be isotropic with l_{max} = 0 for each shell. All tractography streamline reconstructions were made using the probabilistic 2nd-order Integration over Fibre Orientation Distributions (iFOD2) algorithm (Tournier et al., 2010) in conjunction with the ACT framework (Smith et al., 2012). The following parameters were used for streamline tracking of each study participant: step size 1 mm, maximum curvature per step 45°,

length 5-250 mm, FOD amplitude threshold 0.1. Subcortical seed regions comprised the caudate, putamen and thalamus, based on the Harvard-Oxford atlas provided with FSL. To keep the caudate and putamen as separate ROIs, voxels in the nucleus accumbens were not considered. For each subcortical seed, tractography was run with a seeding density of 51'653 streamlines per voxel. Streamlines were projected unidirectionally and accepted if they reached an ipsilateral cortical mask, defining all cortical areas of the corresponding hemisphere as potential targets. We selected a set of cortical targets, identified using Desikan-Killiany atlas (Desikan et al., 2006), and grouped them into sensorimotor (paracentral, postcentral and precentral gyrus), associative (caudal and rostral middle frontal gyrus) and limbic areas (caudal anterio cingulate gyrus, lateral and medial orbitofrontal gyrus), similarly to Draganski, Kherif and colleagues (2008). The superior frontal gyrus was not considered as a target because it comprised the supplementary motor area, making it difficult to attribute the region to the sensorimotor or associative group. Only the subset of fibres terminating in these cortical locations was included in further analysis. Because subsequent needed the data to be in the same anatomical space, SPM routines used the flow fields estimated by DARTEL to warp images indicating the number of tracts connected to each group of cortical areas into MNI space using nearest neighbour interpolation. For display purposes, an additional tractography was generated in one participant with 100 tracks per voxel by using the exact same processing constraints.

Structural segregation

We defined structural segregation as the presence of topographically organized connectivity patterns to the different groups of cortical targets. More specifically, let v be the total number of voxels in a seed ROI r, and let i and j be two sets of voxels in r such that $i \cap j = \emptyset$ and $i \cup j = U$ where U is the set comprising all v voxels in r. If according to the tractography results, two sets of voxels i and j in r are connected specifically to different cortical areas, i.e. target t_1 (e.g. limbic) and respectively target t_2 (e.g. associative), patterns of connectivity for t_1 and t_2 in r are segregated. This ideal case of segregation can be extended to three targets, such that three different sets of voxels i, j and k are specifically connected to t_1 (e.g. limbic), t_2 (e.g. associative) and t_3 (e.g. sensorimotor) respectively (Figure 1A). Again, sets of voxels i, j and k would be mutually exclusive, such that $i \cap j = \emptyset, i \cap k = \emptyset, j \cap k = \emptyset$ and $i \cup j \cup k = U$. If one set of voxels, e.g. j, is not only connected to target t_2 but also to t_3, and to a lesser extent to t_1, then connectivity patterns are less segregated (Figure 1B). One can then imagine a situation in which patterns are even less segregated, e.g. the set of voxels j is equally connected to all targets, and other sets of voxels are also connected to multiple targets (Figure 1C). Consequently, when connectivity patterns are segregated, voxel-wise correlation between the number of connections for each target should be low, whereas it should be high when patterns are overlapping.

Pattern component modelling

To quantify structural segregation as defined above, we used the pattern component model (PCM; Diedrichsen et al., 2011). Some notable advantages of this method are its robustness to noise and that it does not require that all voxels in the ROI contain an informative signal (Diedrichsen et al., 2011). We therefore used the PCM in each seed region to assess the similarity between representations of limbic, associative and sensorimotor connections. This method extends

representational similarity analysis (RSA; Kriegeskorte, 2008; Nili et al., 2014) by estimating the variance and covariance associated with pattern components and accounting for possible noise in the signal. Using the PCM, if for example two patterns are similar in their distribution over voxels but the signals are noisier in one brain region as compared to another, the coefficients of correlation – i.e. similarity – between the two patterns will remain similar (Diedrichsen et al., 2011). This method has been previously applied on regression coefficients estimated from functional MRI data, but there is essentially no reason to restrict its use to brain activity data. Images containing the number of connections to the different cortical targets at each voxel, once normalised to a standardised space, can be treated as brain activity maps if the aim is to measure the similarity between patterns distributed over voxels. With brain activity data, the regression coefficient at each voxel indicates the relationship with each psychological variable that is manipulated in the experimental paradigm, while with tractography results, each voxel denotes the number of successful connections to each group of cortical targets. Although specifying shared variance between patterns can be useful under some circumstances, no constraint on the variance-covariance matrix was imposed in the PCM analyses we performed. Three two-factors (TARGET x GROUP) PCM were performed to estimate the similarity between groups of cortical targets for each group of subjects. The first divided subjects in two groups: PD patients and HC subjects. The second further split patients into left- (PD L, n = 11) and right-affected (PD R, n = 8) (see Clinical measures). The last separated patients according to their profile of clinical symptoms (see Clustering of patients based on clinical symptoms).

Index of Similarity

Correlation coefficients between connectivity patterns obtained using PCM were transformed using the Fisher r-to-z' transform as described in Sanabria-Diaz and colleagues (2013). In order to measure segregation between patterns, we defined the Index of Similarity as follows:

$$IoS = |tanh^{-1}(r)|$$

Such that highly segregated patterns produce low *IoS* values, and overlapping patterns corresponds to high *IoS* values. We subsequently converted *IoS* values to *Z*-statistics (Sanabria-Diaz et al., 2013) and compared, across groups, each *Z*-score of *IoS* between pairs of cortical targets, adjusting *p*-values for multiple comparisons using Bonferroni correction.

Clustering of patients based on clinical symptoms

We applied principal component analysis (PCA) on standardized clinical scores including Hoehn and Yahr stage, apathy, depression, anxiety and binarized MoCA. Because 8 patients were tested off and 11 on dopaminergic medication, we did not use UPDRS scores to generate subgroups of patients but rather used the Hoehn and Yahr stage, which is independent from dopaminergic medication status. Concerning other clinical measures, dopaminergic treatment is often considered to be of little effect on non-motor symptoms (Goldman and Litvan, 2011). Based on Joliffe's criterion (Jolliffe, 2002), three components were retained because they explained together more than 80% of the variance. *K*-means clustering was applied on these 3-dimensional PCA scores and repeated 100 times with different starting centroids to avoid local minimum problem. Based on

silhouette analysis and within-cluster sums of points-to-centroid distances (WCD; Saitta et al., 2007), and in order to obtain subgroups of comparable size with specific clinical symptoms, patients were divided into three subgroups: patients with motivational or mood disorders-predominant symptoms (PD MDp, n = 3), patients with mild cognitive impairment-predominant symptoms (PD MCIp, n = 7), and patients with motor-predominant symptoms (PD Mp, n = 9). Age ranges were similar across all subgroups of patients (PD MDp: 58.33 ± 1.18; PD MCIp: 65.71 ± 2.36; PD Mp: 65.56 ± 1.19) and with healthy volunteers ($p > 0.05$ for all pairwise-comparisons using 2-tailed 2-sample t-tests).

Univariate voxel-based analyses of connection density

Additionally, to verify that topography of connections were consistent across subjects, images of the number of tracts for each group of cortical targets were modelled three times using voxel-based approach as a function of two factors: group of cortical targets (TARGET) and group of subjects (GROUP). The three factorial designs differed in the number of levels in the GROUP factor: two levels (PD, HC) in the first analysis, three levels (HC, PD L, PD R) in the second analysis, and four levels (HC, PD MDp, PD MCIp, PD Mp) in the third analysis. In each group of subjects, T-contrasts were performed for each level of the TARGET factor against the other two. Moreover, in order to assess possible differences in terms of number of tracts across groups of subjects, F-contrasts testing the main effect of GROUP and the interaction effect between GROUP and TARGET were performed. Statistical threshold for the univariate voxel-based analyses was set to $p < 0.001$, uncorrected for multiple comparisons, with a minimal cluster extent (k) of 10 voxels.

Results

Topographically organised connectivity in the striatum and thalamus

Tractography revealed anatomically plausible segregated connectivity patterns, with sensorimotor, associative and limbic cortical areas being connected to different portions within each subcortical ROI (Figure 2). The rostroventral caudate and putamen, close to the nucleus accumbens, were mostly connected to limbic cortical areas, whereas the dorsolateral putamen, tail of the caudate and posterolateral portions of the thalamus had connections to sensorimotor areas. The intermediate caudate and putamen, as well as the medial anterior portion of the thalamus seemed to be mostly connected to associative cortical regions. Across all seed ROIs, most of the voxels had between 100 and 1'000 streamlines reaching motor, associative and limbic cortical areas (Figure 2D).

Structural segregation in PD

Results demonstrated higher *IoS* estimates in PD compared to HC between sensorimotor and associative targets in the right caudate ($p = 0.00233$) and between associative and limbic targets in the right putamen ($p < 0.001$). In the left putamen, PD had lower *IoS* between associative and limbic targets ($p < 0.001$) (Figure 3).

Structural segregation as a function of disease laterality

When separating patients into left- and right-affected, both PD groups were associated, as compared to HC, with higher *IoS* estimates between sensorimotor and associative targets in the right caudate ($p = 0.02789$ for PD L against HC, $p < 0.001$ for PD R against HC) and between associative and limbic in the right putamen ($p < 0.001$ for both groups against HC) (Figure 4). However, while PD L showed higher *IoS* between associative and limbic as compared to HC in the left thalamus ($p < 0.001$), PD R showed lower *IoS* between the same targets as compared to HC in the same region ($p = 0.00240$). Therefore PD L had higher *IoS* between associative and limbic targets as compared to PD R ($p < 0.001$) in the left thalamus, whereas PD R had higher *IoS* between sensorimotor and associative targets than PD L in the right caudate ($p = 0.00701$).

Clusters of patients based on clinical symptoms

Anxiety, depression and apathy seem to be related to each other, and Hoehn and Yahr stage had a relatively uniform distribution across patients (Figure 5E). Some MoCA scores clearly suggested a cognitive impairment (Table 1), the minimal score being equal to 21. PCA revealed that principal components explained respectively 37.9%, 23.1%, 19.2%, 13.5% and 6.4% of the variance in clinical scores. Principal component vectors for depression, apathy and anxiety scores were very close together, whereas MoCA scores and Hoehn and Yahr stage were rather two other dissociable dimensions (Figure 5A). Normalized varimax rotation indicated that loadings for the 1st component were indeed high for Anxiety, Depression and Apathy (0.70, 0.65 and 0.27 respectively) and low for MoCA and Hoehn and Yahr stage (0.1 and 0.12 respectively), whereas for the 2nd component loadings were respectively 0.09, -0.03, -0.4, 0.9 (MoCA) and -0.17, and for the 3rd component respectively 0.23, -0.17, -0.5, -0.1 and 0.81 (Hoehn and Yahr stage). The first three components explained together 80.1% of variance (see scree plot in Figure 5B) and were therefore kept for *k*-means clustering. The latter showed an optimal solution with $k = 3$ (Figure 5C) by producing groups of relatively equivalent size, without introducing groups of only one patient, and with relatively high silhouette values (Figure 5D and Supplementary figure 1). Within-cluster sums of point-to-centroid distances linearly decreased as k increased (Supplementary figure 1). Each cluster of patients was then associated with a different profile of clinical symptoms (Figure 5F).

Structural segregation as a function of clinical symptoms

When dividing patients according to their clinical symptoms, PD MDp had extremely high *IoS* estimates bilaterally in the caudate, regardless of the group of cortical targets compared (Figure 6). *IoS* for PD MDp were higher than all other groups for each pair of cortical targets ($p < 0.001$). However PD MDp were associated with lower *IoS* between associative and limbic targets in the right thalamus as compared to HC ($p < 0.001$) and PD MCIp ($p = 0.00845$). In the right putamen, all groups of PD patients had higher *IoS* between associative and limbic targets as compared to HC ($p < 0.001$ for PD MDp, PD MCIp and PD Mp), whereas in the left putamen, IoS values between associative and limbic targets were lower for PD MDp and PD Mp as compared to PD MCIp ($p < 0.001$ and $p = 0.00357$ respectively) and compared to HC ($p < 0.001$). In the left thalamus, PD MCIp had higher *IoS* estimates between associative and limbic targets compared to all other groups ($p < 0.001$ against HC, PD MDp and PD Mp). Furthermore, in HC as compared to PD Mp, *IoS* between sensorimotor and associative targets were higher in the left ($p = 0.03214$) but lower in the right ($p < 0.001$) caudate.

Univariate voxel-based analyses of connection density

Robust topographical patterns were present consistently in each group of subject (Supplementary figure 2 to Supplementary figure 9). In the striatum, the most ventral and anterior portions – close to the nucleus accumbens –, were more connected to limbic cortical areas than any other group of targets, while the most dorsal and posterior portions – comprising notably the dorsolateral putamen and the tail of the caudate –, were more connected to sensorimotor areas compared to any other cortical target. The intermediate portions of the striatum were more connected to associative cortical areas compared to any other group of targets. In the thalamus, medial anterior nuclei were preferentially connected to associative areas, while posterior lateral nuclei were mostly connected to sensorimotor cortical regions. The main effect of GROUP and interaction effect between GROUP and TARGET were not significant ($p < 0.001$, $k \geq 10$), in any model built (detailed results tables available as Supplementary material).

Discussion

Results showed that cortico-striatal and thalamo-cortical connectivity patterns are affected in PD. We demonstrated that PD affects structural segregation between sensorimotor and associative targets in the right caudate, and between associative and limbic targets in the putamen bilaterally. When splitting PD patients into left- and right-affected, whereas both groups of patients had an equivalent loss of structural segregation in the right putamen, the loss of structural segregation was greater in the right caudate for right-affected patients, and left-affected patients had decreased structural segregation between associative and limbic targets in the left thalamus. After having grouped patients based on their clinical symptoms, we observed different changes in structural segregation across groups. Altogether, except for PD with motivational symptoms in the caudate, we mostly observed differences in structural segregation between associative and limbic but almost never between sensorimotor and limbic brain functions. Knowing that cortical areas supporting the latter functions converge to very distant locations at the striatal level – the most dorsal and posterior, and most ventral and anterior portions respectively –, it is possible that these two antipodal connectivity patterns are too segregated at baseline to be strongly affected by PD. Further, while the reasons underlying asymmetric changes in structural segregation associated with PD remain unclear, previous reports suggest a higher prevalence of apathy in right-affected PD patients (Harris et al., 2013). The authors of this study suggest that it might be due to the fact that the right striatum, evidencing less dopamine at baseline even in healthy subjects, might be more vulnerable, and they link their findings with reports of motor symptoms severity being also associated with side of PD onset (Haaxma et al., 2010). It has to be noted that in our sample, the proportion of patients affected on the right was 66.7% in PD with motivational symptoms, 57.1% in PD with cognitive symptoms, and 33.3% in PD with motor symptoms. Consistently with the above percentages and in line with the results of Harris and colleagues (2013), PD with motivational symptoms were similar to PD affected on the right in terms of structural segregation. Interestingly, percentages of side of onset follow the spatial progression of nigrostriatal denervation in PD (Redgrave et al., 2010; Vaillancourt et al., 2013).

Furthermore, changes in structural segregation of connectivity patterns were not mirrored by changes in the density of connections. Indeed, robust and consistent patterns of connectivity were

found in all groups of subjects, with a spatial distribution in line with the known anatomy of subcortical connectivity (Draganski et al., 2008; Lambert et al., 2016; Lehéricy et al., 2004), but no difference between groups in terms of connection density was found. The alternative explanation that PD affects connection density and henceforth biases results in terms of structural segregation is therefore less likely. Our results rather support the idea that cortico-subcortical tracts differentially connect the thalamus and striatum to our group of cortical areas.

Because in our sample 8 PD patients were tested off – respectively 11 on – dopaminergic medication, the assumption on which our study relies is that acute withdrawal of dopaminergic drugs does not strongly affects DWI data. Knowing that even long-term effects of dopaminergic treatment on diffusivity measures remains controversial (Meijer et al., 2013), we think it is reasonable to assume that stopping dopaminergic medication for only 1 day cannot strongly alter structural connectivity, and that it cannot therefore constitute a bias in the reported tractography results.

In our study, clustering of patients was done based on results from cognitive tests and mood questionnaires, as well as on the progression of motor disability. The categories we used do not perfectly match the different subtypes of PD (Marras and Chaudhuri, 2016; Moustafa and Poletti, 2013) but rather links some of the proposed categories to the brain functions supported by the cortical areas considered for tractography. While the choice of cortical targets was mostly driven by the goal to simplify basal ganglia functional architecture based on previous findings (Jahanshahi et al., 2015; Obeso et al., 2000, 2008), other clinical measures might help disentangling effects of multiple factors on structural segregation, such as the predominance of akinesia or tremor, the presence of postural instabilities, dyskinesia, hallucinations, or impulse control disorders. Future studies might collect data in more various groups of PD patients, increase sample size for each profile of clinical symptoms, and investigate further structural segregation between other groups of cortical areas at the basal ganglia level.

References

Alexander, G.E., DeLong, M.R., and Strick, P.L. (1986). Parallel organization of functionally segregated circuits linking basal ganglia and cortex. Annu. Rev. Neurosci. *9*, 357–381.

Andersson, J.L.R., and Sotiropoulos, S.N. (2016). An integrated approach to correction for off-resonance effects and subject movement in diffusion MR imaging. NeuroImage *125*, 1063–1078.

Bar-Gad, I., and Bergman, H. (2001). Stepping out of the box: information processing in the neural networks of the basal ganglia. Curr. Opin. Neurobiol. *11*, 689–695.

Bar-Gad, I., Havazelet-Heimer, G., Goldberg, J.A., Ruppin, E., and Bergman, H. (2000). Reinforcement-driven dimensionality reduction -a model for information processing in the basal ganglia. J. Basic Clin. Physiol. Pharmacol. *11*, 305–320.

Bar-Gad, I., Morris, G., and Bergman, H. (2003). Information processing, dimensionality reduction and reinforcement learning in the basal ganglia. Prog. Neurobiol. *71*, 439–473.

Bronfeld, M., and Bar-Gad, I. (2011). Loss of specificity in Basal Ganglia related movement disorders. Front. Syst. Neurosci. *5*, 38.

Buck, P.O., Wilson, R.E., Seeberger, L.C., Conner, J.B., and Castelli-Haley, J. (2011). Examination of the UPDRS bradykinesia subscale: equivalence, reliability and validity. J. Park. Dis. *1*, 253–258.

Burn, D.J. (2002). Depression in Parkinson's disease. Eur. J. Neurol. Off. J. Eur. Fed. Neurol. Soc. *9 Suppl 3*, 44–54.

Calabresi, P., Picconi, B., Tozzi, A., and Di Filippo, M. (2007). Dopamine-mediated regulation of corticostriatal synaptic plasticity. Trends Neurosci. *30*, 211–219.

Dale, A.M., Fischl, B., and Sereno, M.I. (1999). Cortical surface-based analysis. I. Segmentation and surface reconstruction. NeuroImage *9*, 179–194.

Dalrymple-Alford, J.C., MacAskill, M.R., Nakas, C.T., Livingston, L., Graham, C., Crucian, G.P., Melzer, T.R., Kirwan, J., Keenan, R., Wells, S., et al. (2010). The MoCA: well-suited screen for cognitive impairment in Parkinson disease. Neurology *75*, 1717–1725.

Desikan, R.S., Ségonne, F., Fischl, B., Quinn, B.T., Dickerson, B.C., Blacker, D., Buckner, R.L., Dale, A.M., Maguire, R.P., Hyman, B.T., et al. (2006). An automated labeling system for subdividing the human cerebral cortex on MRI scans into gyral based regions of interest. NeuroImage *31*, 968–980.

Diedrichsen, J., Ridgway, G.R., Friston, K.J., and Wiestler, T. (2011). Comparing the similarity and spatial structure of neural representations: A pattern-component model. NeuroImage *55*, 1665–1678.

Draganski, B., Kherif, F., Kloppel, S., Cook, P.A., Alexander, D.C., Parker, G.J.M., Deichmann, R., Ashburner, J., and Frackowiak, R.S.J. (2008). Evidence for Segregated and Integrative Connectivity Patterns in the Human Basal Ganglia. J. Neurosci. *28*, 7143–7152.

Farquharson, S., Tournier, J.-D., Calamante, F., Fabinyi, G., Schneider-Kolsky, M., Jackson, G.D., and Connelly, A. (2013). White matter fiber tractography: why we need to move beyond DTI. J. Neurosurg. *118*, 1367–1377.

Fischl, B., Sereno, M.I., and Dale, A.M. (1999a). Cortical Surface-Based Analysis: II: Inflation, Flattening, and a Surface-Based Coordinate System. NeuroImage *9*, 195–207.

Fischl, B., Sereno, M.I., Tootell, R.B.H., and Dale, A. M. (1999b). High-resolution inter-subject averaging and a surface-based coordinate system. Hum. Brain Mapp. *8*, 272–284.

Fischl, B., Salat, D.H., Busa, E., Albert, M., Dieterich, M., Haselgrove, C., van der Kouwe, A., Killiany, R., Kennedy, D., Klaveness, S., et al. (2002). Whole Brain Segmentation: Automated Labeling of Neuroanatomical Structures in the Human Brain. Neuron 33, 341–355.

Fischl, B., Salat, D.H., Van Der Kouwe, A.J.W., Makris, N., Ségonne, F., Quinn, B.T., and Dale, A.M. (2004). Sequence-independent segmentation of magnetic resonance images. NeuroImage *23*, 69–84.

Goldman, J.G., and Litvan, I. (2011). Mild cognitive impairment in Parkinson's disease. Minerva Med. *102*, 441.

Haaxma, C.A., Helmich, R.C.G., Borm, G.F., Kappelle, A.C., Horstink, M.W.I.M., and Bloem, B.R. (2010). Side of symptom onset affects motor dysfunction in Parkinson's disease. NSC *170*, 1282–1285.

Haber, S.N. (2003). The primate basal ganglia: parallel and integrative networks. J. Chem. Neuroanat. *26*, 317–330.

Haber, S.N., Fudge, J.L., and McFarland, N.R. (2000). Striatonigrostriatal pathways in primates form an ascending spiral from the shell to the dorsolateral striatum. J. Neurosci. *20*, 2369–2382.

Harris, E., McNamara, P., and Durso, R. (2013). Apathy in Patients With Parkinson Disease as a Function of Side of Onset. J. Geriatr. Psychiatry Neurol. *26*, 95–104.

Helmich, R.C., Derikx, L.C., Bakker, M., Scheeringa, R., Bloem, B.R., and Toni, I. (2010). Spatial Remapping of Cortico-striatal Connectivity in Parkinson's Disease. Cereb. Cortex *20*, 1175–1186.

Hutton, C. (2002). Image Distortion Correction in fMRI: A Quantitative Evaluation. NeuroImage *16*, 217–240.

Jahanshahi, M., Obeso, I., Rothwell, J.C., and Obeso, J.A. (2015). A fronto–striato–subthalamic–pallidal network for goal-directed and habitual inhibition. Nat. Publ. Group *16*, 719–732.

Jeurissen, B., Tournier, J.-D., Dhollander, T., Connelly, A., and Sijbers, J. (2014). Multi-tissue constrained spherical deconvolution for improved analysis of multi-shell diffusion MRI data. NeuroImage *103*, 411–426.

Jolliffe, I.T. (2002). Principal Component Analysis (Springer).

Jones, D.K., Horsfield, M. A, and Simmons, A. (1999). Optimal strategies for measuring diffusion in anisotropic systems by magnetic resonance imaging. Magn. Reson. Med. Off. J. Soc. Magn. Reson. Med. Soc. Magn. Reson. Med. *42*, 515–525.

Kaji, Y., and Hirata, K. (2011). Apathy and Anhedonia in Parkinson's Disease. ISRN Neurol. *2011*, 1–9.

Kriegeskorte, N. (2008). Representational similarity analysis – connecting the branches of systems neuroscience. Front. Syst. Neurosci. *2*, 4.

Lambert, C., Simon, H., Colman, J., and Barrick, T.R. (2016). Defining Thalamic Nuclei and Topographic Connectivity Gradients in vivo. NeuroImage 1–40.

Leemans, A., and Jones, D.K. (2009). The B-matrix must be rotated when correcting for subject motion in DTI data. Magn. Reson. Med. *61*, 1336–1349.

Lehéricy, S., Ducros, M., Van de Moortele, P.-F., Francois, C., Thivard, L., Poupon, C., Swindale, N., Ugurbil, K., and Kim, D.-S. (2004). Diffusion tensor fiber tracking shows distinct corticostriatal circuits in humans. Ann. Neurol. *55*, 522–529.

Lieberman, A. (2006). Depression in Parkinson's disease - a review. Acta Neurol. Scand. *113*, 1–8.

Lim, S.A.O., Kang, U.J., and McGehee, D.S. (2014). Striatal cholinergic interneuron regulation and circuit effects. Front. Synaptic Neurosci. *6*, 22.

Lorio, S., Kherif, F., Ruef, A., Melie-Garcia, L., Frackowiak, R., Ashburner, J., Helms, G., Lutti, A., and Draganski, B. (2016). Neurobiological origin of spurious brain morphological changes: A quantitative MRI study. Hum. Brain Mapp. *37*, 1801–1815.

Lutti, A., Hutton, C., Finsterbusch, J., Helms, G., and Weiskopf, N. (2010). Optimization and validation of methods for mapping of the radiofrequency transmit field at 3T. Magn. Reson. Med. *64*, 229–238.

Lutti, A., Stadler, J., Josephs, O., Windischberger, C., Speck, O., Bernarding, J., Hutton, C., and Weiskopf, N. (2012). Robust and Fast Whole Brain Mapping of the RF Transmit Field B1 at 7T. PLoS ONE *7*, e32379.

Marras, C., and Chaudhuri, K.R. (2016). Nonmotor features of Parkinson's disease subtypes. Mov. Disord. *31*, 1095–1102.

Marsh, L. (2000). Anxiety disorders in Parkinson's disease. Int. Rev. Psychiatry *12*, 307–318.

Meijer, F.J.A., Bloem, B.R., Mahlknecht, P., Seppi, K., and Goraj, B. (2013). Update on diffusion MRI in Parkinson's disease and atypical parkinsonism. J. Neurol. Sci. 1–9.

Morikawa, H., and Paladini, C.A. (2011). Dynamic regulation of midbrain dopamine neuron activity: intrinsic, synaptic, and plasticity mechanisms. NEUROSCIENCE *198*, 95–111.

Moustafa, A.A., and Poletti, M. (2013). Neural and behavioral substrates of subtypes of Parkinson's disease. Front. Syst. Neurosci. *7*, 117.

Munhoz, R.P., Moro, A., Silveira-Moriyama, L., and Teive, H.A. (2015). Non-motor signs in Parkinson's disease: a review. Arq. Neuropsiquiatr. *73*, 454–462.

Nasreddine, Z.S., Phillips, N.A., Bédirian, V., Charbonneau, S., Whitehead, V., Collin, I., Cummings, J.L., and Chertkow, H. (2005). The Montreal Cognitive Assessment, MoCA: a brief screening tool for mild cognitive impairment. J. Am. Geriatr. Soc. *53*, 695–699.

Nili, H., Wingfield, C., Walther, A., Su, L., Marslen-Wilson, W., and Kriegeskorte, N. (2014). A Toolbox for Representational Similarity Analysis. PLoS Comput. Biol. *10*, e1003553.

Obeso, J.A., Rodríguez-Oroz, M.C., Rodríguez, M., Lanciego, J.L., Artieda, J., Gonzalo, N., and Olanow, C.W. (2000). Pathophysiology of the basal ganglia in Parkinson's disease. Trends Neurosci. *23*, S8–19.

Obeso, J.A., Rodríguez-Oroz, M.C., Benitez-Temino, B., Blesa, F.J., Guridi, J., Marin, C., and Rodriguez, M. (2008). Functional organization of the basal ganglia: Therapeutic implications for Parkinson's disease. Mov. Disord. *23*, S548–S559.

Pessiglione, M., Guehl, D., Rolland, A.-S., Francois, C., Hirsch, E.C., Féger, J., and Tremblay, L. (2005). Thalamic neuronal activity in dopamine-depleted primates: evidence for a loss of functional segregation within basal ganglia circuits. J. Neurosci. *25*, 1523–1531.

Redgrave, P., Rodriguez, M., Smith, Y., Rodriguez-Oroz, M.C., Lehéricy, S., Bergman, H., Agid, Y., DeLong, M.R., and Obeso, J.A. (2010). Goal-directed and habitual control in the basal ganglia: implications for Parkinson's disease. Nat. Publ. Group *11*, 760–772.

Robert, P.H., Clairet, S., Benoit, M., Koutaich, J., Bertogliati, C., Tible, O., Caci, H., Borg, M., Brocker, P., and Bedoucha, P. (2002). The Apathy Inventory: assessment of apathy and awareness in Alzheimer's disease, Parkinson's disease and mild cognitive impairment. Int. J. Geriatr. Psychiatry *17*, 1099–1105.

Saitta, S., Raphael, B., and Smith, I.F. (2007). A bounded index for cluster validity. In International Workshop on Machine Learning and Data Mining in Pattern Recognition, (Springer), pp. 174–187.

Sanabria-Diaz, G., Martínez-Montes, E., Melie-Garcia, L., and Alzheimer's Disease Neuroimaging Initiative (2013). Glucose metabolism during resting state reveals abnormal brain networks organization in the Alzheimer's disease and mild cognitive impairment. PLoS ONE *8*, e68860.

Ségonne, F., Dale, A.M., Busa, E., Glessner, M., Salat, D., Hahn, H.K., and Fischl, B. (2004). A hybrid approach to the skull stripping problem in MRI. NeuroImage *22*, 1060–1075.

Sethi, K.D. (2002). Clinical aspects of Parkinson disease. Curr. Opin. Neurol. *15*, 457–460.

Sharma, S., Moon, C.S., Khogali, A., Haidous, A., Chabenne, A., Ojo, C., Jelebinkov, M., Kurdi, Y., and Ebadi, M. (2013). Biomarkers in Parkinson's disease (recent update). Neurochem. Int. *63*, 201–229.

Smith, R.E., Tournier, J.-D., Calamante, F., and Connelly, A. (2012). Anatomically-constrained tractography: improved diffusion MRI streamlines tractography through effective use of anatomical information. NeuroImage *62*, 1924–1938.

Surmeier, D.J., Shen, W., Day, M., Gertler, T., Chan, S., Tian, X., and Plotkin, J.L. (2010). The role of dopamine in modulating the structure and function of striatal circuits. Prog. Brain Res. *183*, 149–167.

Tessitore, A., Giordano, A., Russo, A., and Tedeschi, G. (2016). Structural connectivity in Parkinson's disease. Park. Realt. Disord. *22*, S56–S59.

Tournier, J.-D., Calamante, F., Gadian, D.G., and Connelly, A. (2004). Direct estimation of the fiber orientation density function from diffusion-weighted MRI data using spherical deconvolution. NeuroImage *23*, 1176–1185.

Tournier, J.-D., Calamante, F., and Connelly, A. (2007). Robust determination of the fibre orientation distribution in diffusion MRI: non-negativity constrained super-resolved spherical deconvolution. NeuroImage *35*, 1459–1472.

Tournier, J.-D., Calamante, F., and Connelly, A. (2010). Improved probabilistic streamlines tractography by 2nd order integration over fibre orientation distributions. In Proceedings of the International Society for Magnetic Resonance in Medicine, p. 1670.

Tournier, J.-D., Calamante, F., and Connelly, A. (2012). MRtrix: Diffusion tractography in crossing fiber regions. Int. J. Imaging Syst. Technol. *22*, 53–66.

Vaillancourt, D.E., Schonfeld, D., Kwak, Y., Bohnen, N.I., and Seidler, R. (2013). Dopamine overdose hypothesis: Evidence and clinical implications. Mov. Disord. *28*, 1920–1929.

Voon, V., Fernagut, P.-O., Wickens, J., Baunez, C., Rodriguez, M., Pavon, N., Juncos, J.L., Obeso, J.A., and Bezard, E. (2009). Chronic dopaminergic stimulation in Parkinson's disease: from dyskinesias to impulse control disorders. Lancet Neurol. *8*, 1140–1149.

Voon, V., Mehta, A.R., and Hallett, M. (2011). Impulse control disorders in Parkinson's disease. Curr. Opin. Neurol. *24*, 324–330.

Worbe, Y., Marrakchi-Kacem, L., Lecomte, S., Valabregue, R., Poupon, F., Guevara, P., Tucholka, A., Mangin, J.F., Vidailhet, M., Lehéricy, S., et al. (2015). Altered structural connectivity of cortico-striato-pallido-thalamic networks in Gilles de la Tourette syndrome. Brain *138*, 472–482.

Yeatman, J.D., Dougherty, R.F., Myall, N.J., Wandell, B.A., and Feldman, H.M. (2012). Tract Profiles of White Matter Properties: Automating Fiber-Tract Quantification. PLoS ONE *7*, e49790.

Zigmond, A.S., and Snaith, R.P. (1983). The Hospital Anxiety and Depression Scale. Acta Psychiatr. Scand. *67*, 361–370.

Tables

	Average	Standard deviation	Minimum	Maximum
Hoehn and Yahr stage	1.68	0.58	1	2.5
Anxiety	6.11	2.94	0	13
Depression	2.68	2.43	0	9
Apathy	1.99	4.50	0	16.52
MOCA	25.58	2.32	21	29

Table 1: summary of clinical scores in PD patients. Average, standard deviation, minimum and maximum score are given for motor (Hoehn and Yahr stage), motivational (anxiety, depression, apathy) and executive (MOCA) symptoms.

Figures

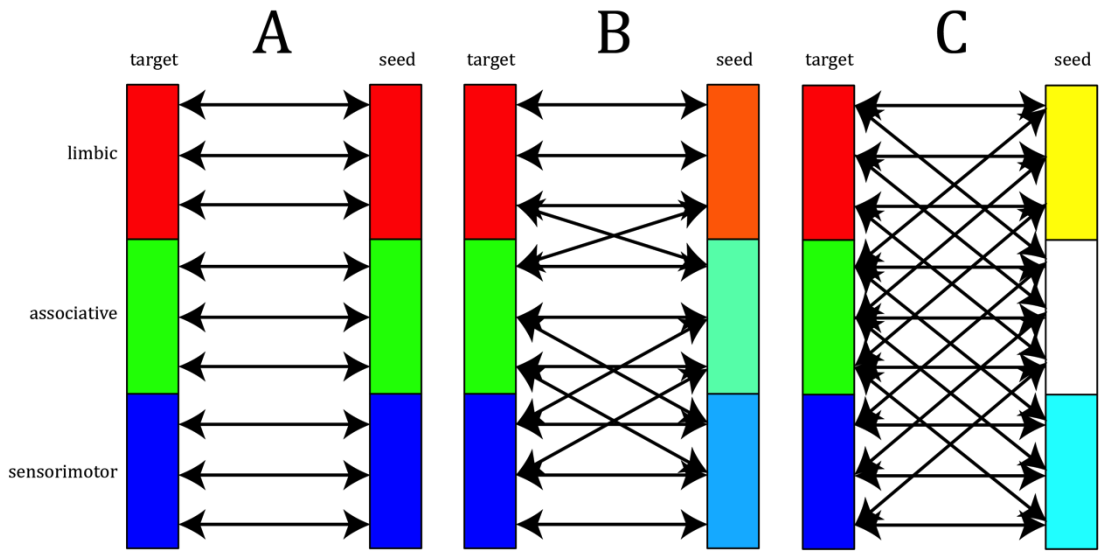

Figure 1: theoretical examples of various levels of structural segregation. For each panel, the colour of segments for bars representing the seed ROI in the subcortex illustrate the mixing of connections in a red-green-blue scheme fashion. By definition, segments of bars representing the target ROI in the cortex are always pure colours. A) Fibres connecting the seed and target follow a one-to-one mapping, a case of extremely high segregation. B) Relative segregation between connectivity patterns, the light green segment is less segregated than the light blue segment, which is itself less segregated than the dark orange segment. C) Particularly low segregation between connectivity patterns. The white segment is a case of total absence of segregation, whereas the yellow and cyan segments are situations in between cases presented in B) and the white segment in C).

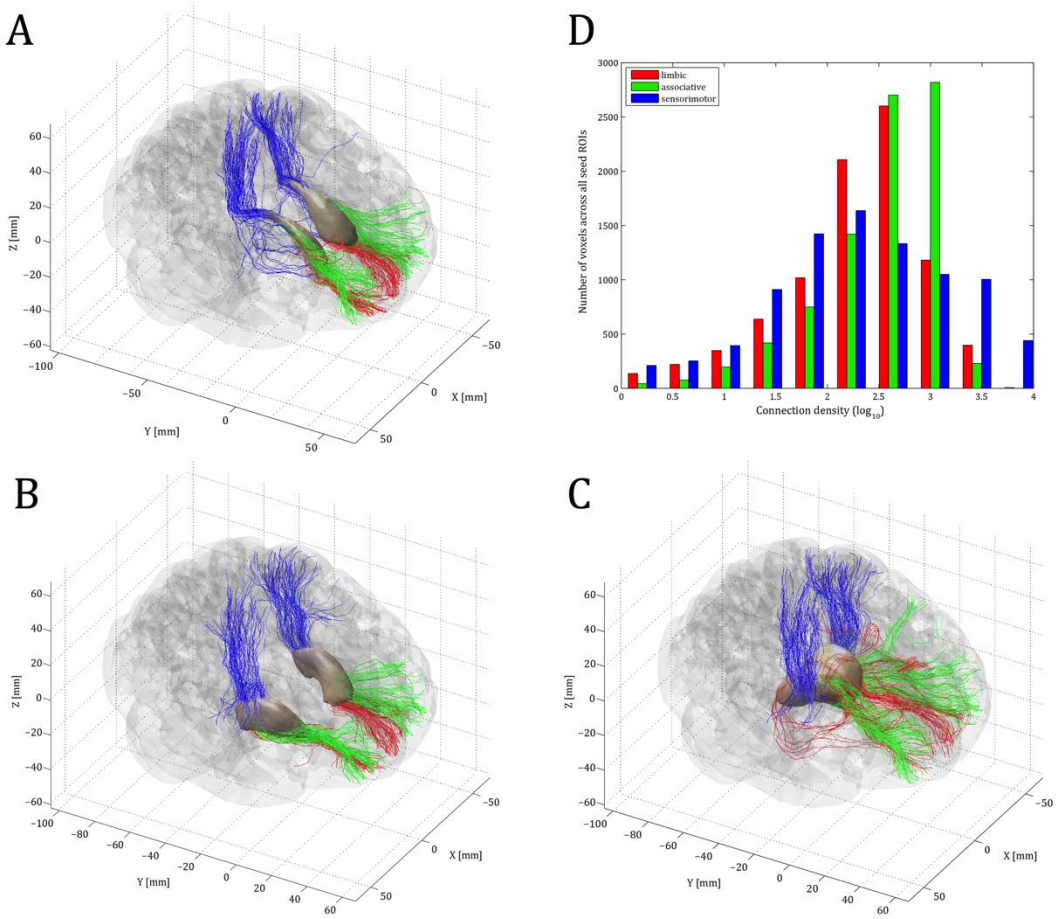

Figure 2 : cortico-striatal and thalamo-cortical tracts to sensorimotor (blue), associative (green) and limbic (red) cortical targets in the caudate (A), putamen (B) and thalamus (C) for a representative healthy control subject. Tracts were generated using the exact same procedure as the main tractography but only with 100 streamlines per voxel. Tracts were then cleaned using AFQ (Yeatman et al., 2012), keeping only fibres with maximum 4 standard deviations above the mean tract length and maximum ± 4 standard deviations of distance from the average tract core. Panel D) shows the average connection density across all seed ROIs for limbic, associative and sensorimotor cortical targets.

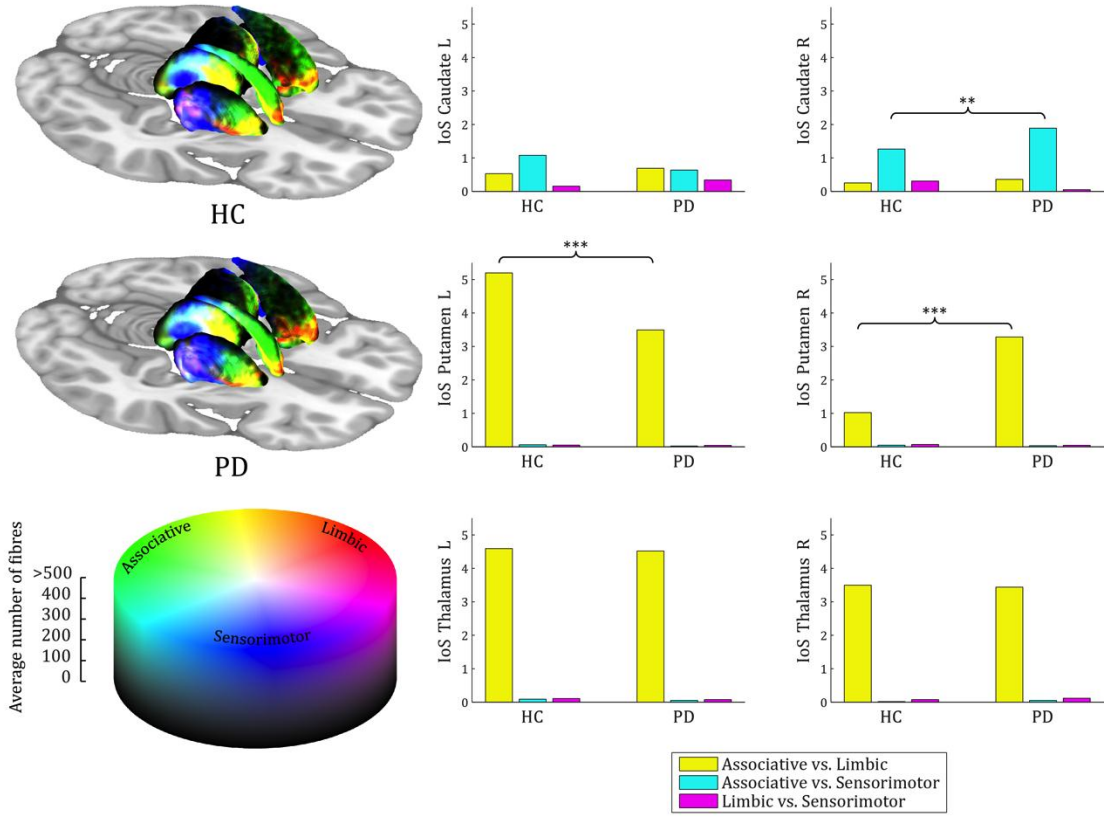

Figure 3 : structural segregation in PD and HC. 3-dimensional renderings of average number of fibres per voxel for each cortical target in all seed ROI are shown on the upper left. Colour codes the number of connections to limbic (red), associative (green) and sensorimotor (blue) cortical targets in an additive fashion. The colour scale cylinder on the lower left represents the number of fibres coded by each colour in the upper renderings: black = 0 fibres to all targets, blue = 0 fibres to all targets but more than 500 to sensorimotor cortical areas, green = 0 fibres to all targets but more than 500 to associative areas, red = 0 fibres to all targets but more than 500 to limbic areas, cyan = more than 500 fibres to all targets but 0 to limbic areas, yellow = more than 500 fibres to all targets but 0 to sensorimotor areas, magenta = more than 500 fibres to all targets but 0 to associative areas, white = more than 500 fibres to all targets. IoS estimates per pair of cortical targets and for each group and seed ROI are shown on the right, following the same red-green-blue colour scheme. Significance stars indicate Bonferroni-corrected p-values: $p < 0.05$ (*), $p < 0.01$ (**) and $p < 0.001$ (***).

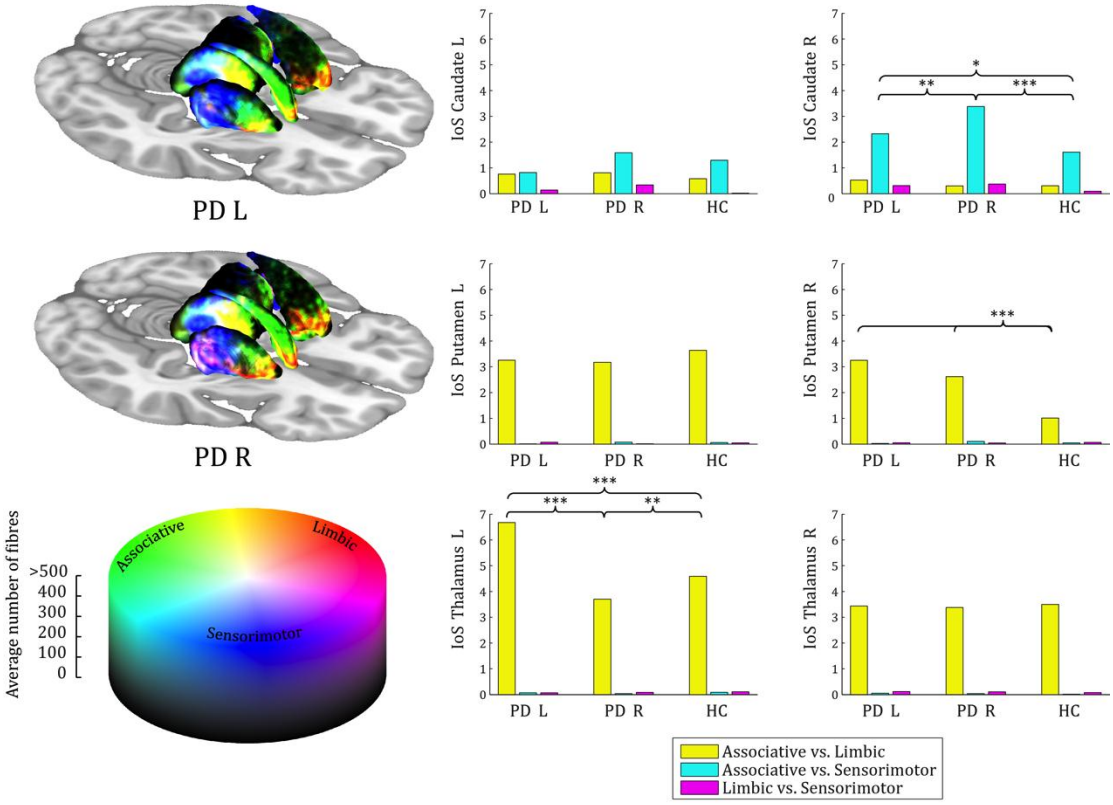

Figure 4 : structural segregation in left-affected and right-affected PD patients. Legends for colour scheme and significance stars are identical to Figure 2.

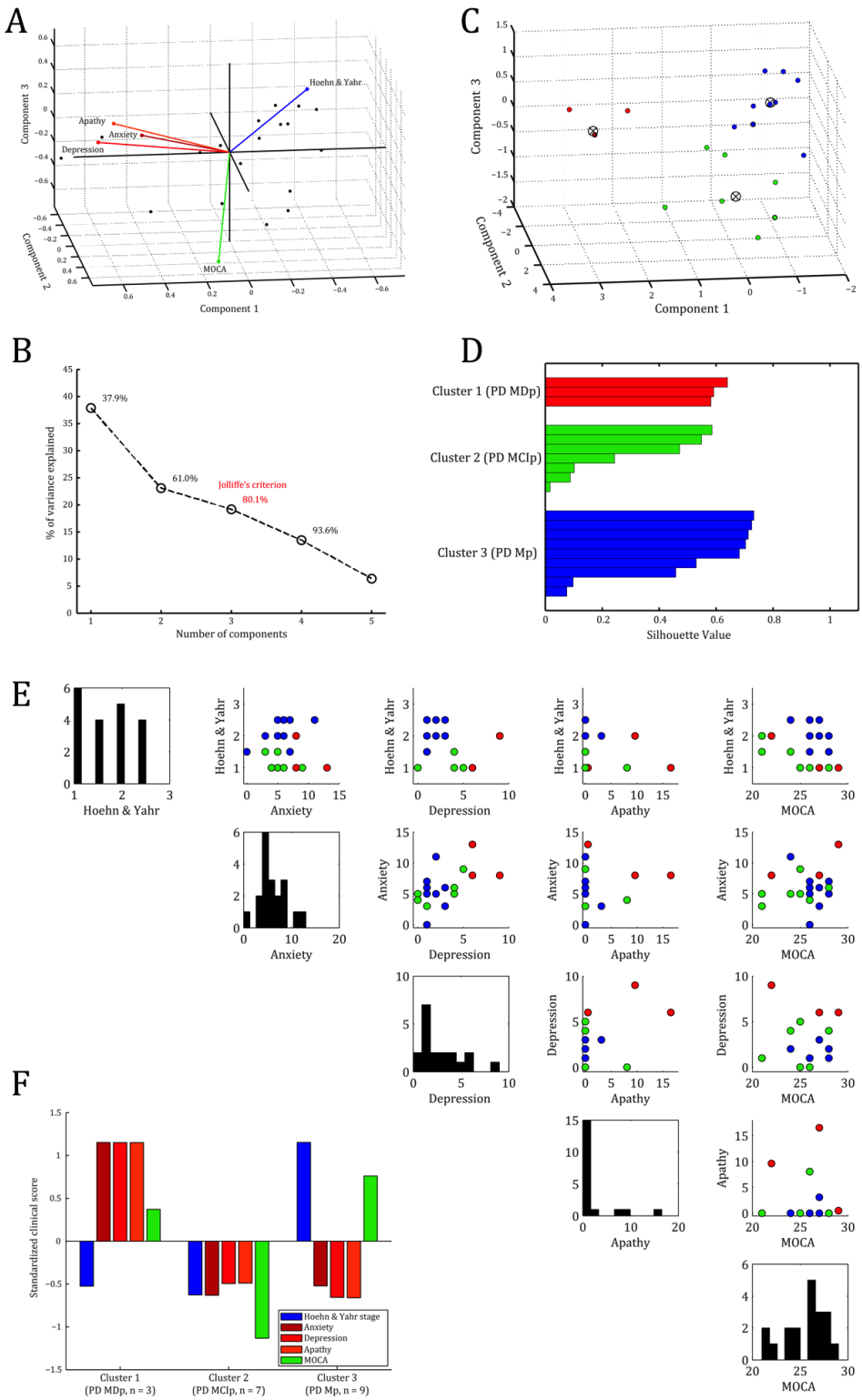

Figure 5 : A) PCA results displaying the projection of PD patients in components space, together with principal component vectors for Hoehn and Yahr stage (blue), anxiety score (dark red),

depression score (red), apathy score (dark orange) and MOCA score (green). B) Scree plot showing the cumulative percentage of variance explained as a function of number of components. Jolliffe's criterion is marked in red. C) Results of *k*-means clustering with 3 components and 3 groups. Principal component scores of individuals are filled with red for MD-predominant, green for MCI-predominant and blue for M-predominant PD patients. Centroids are marked with black crosses outlined with black circles. D) Silhouette plots for *k*-means clustering with 3 groups. Color legend as in panel C). E) Distribution of clinical scores and relationships between them, showed by histograms and scatter plots. Color legend as in panel C). F) Averaged standardized clinical score per cluster of PD patients. Note that low MOCA score is an indicator of possible cognitive impairment, whereas high values in other clinical scores suggests impairment in the corresponding brain function. Color legend is identical to panel A).

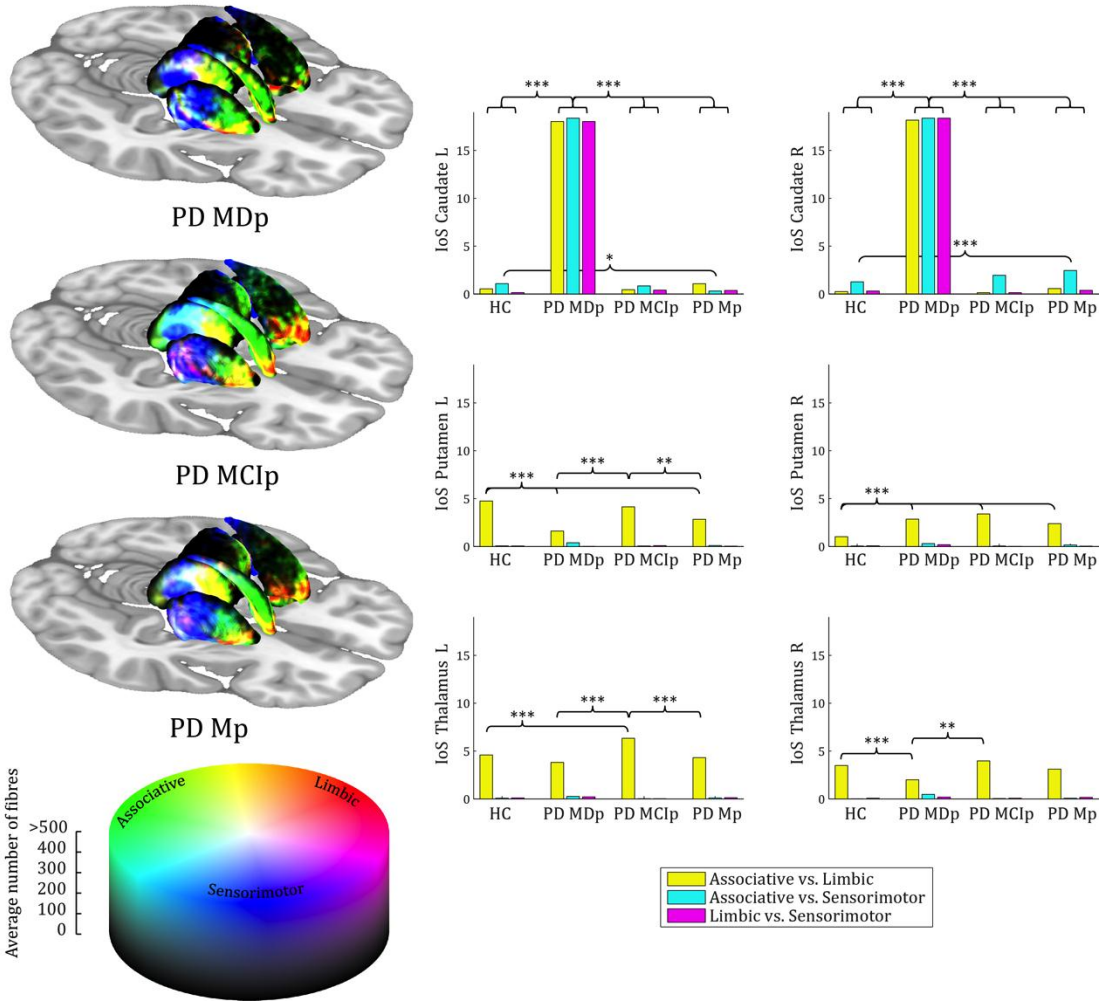

Figure 6 : structural segregation in MD-, MCI- and M-predominant PD patients. Legends for colour scheme and significance stars are identical to Figure 2.

Supplementary figures

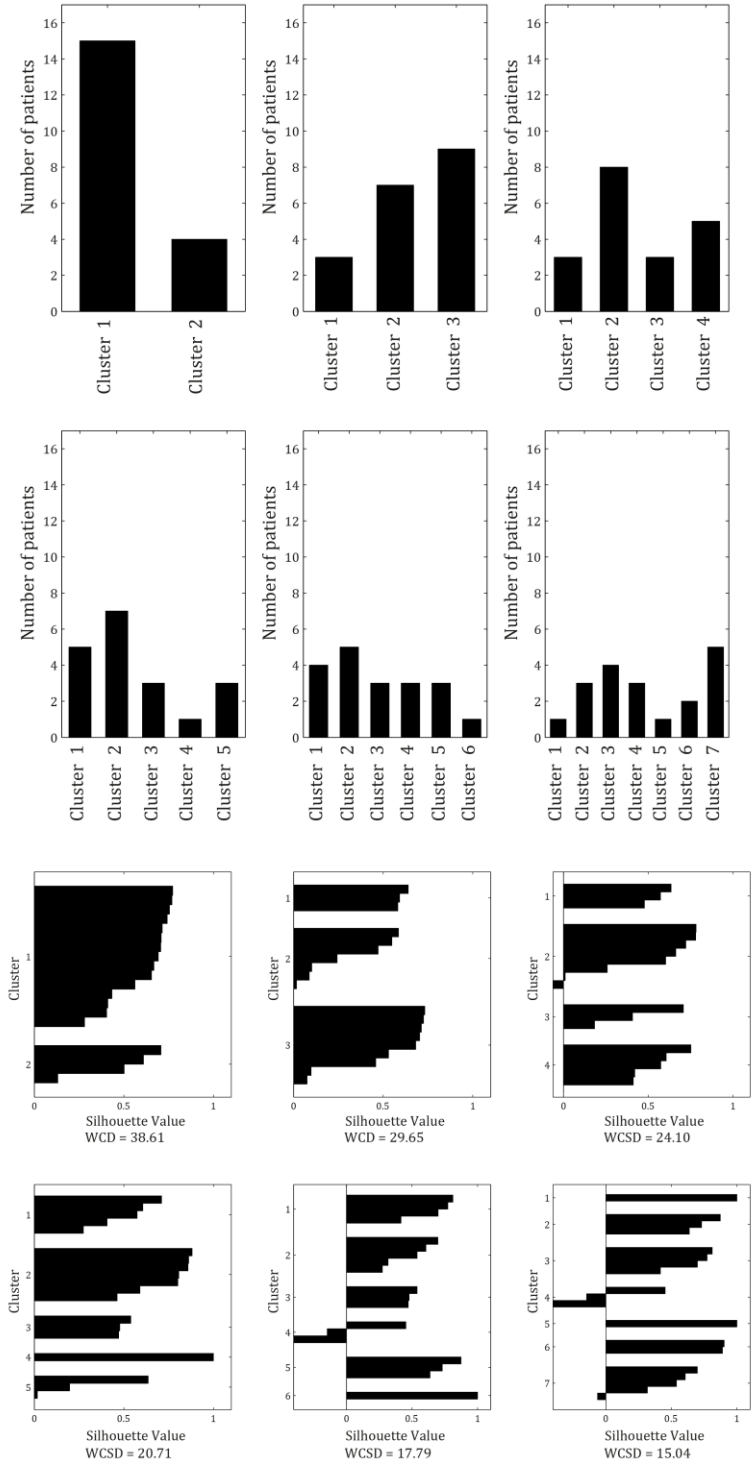

Supplementary figure 1 : *k*-means clustering solutions for one up to seven clusters. Starting from five clusters, groups of one subject are generated (upper graphs). When k = 2, group size is

particularly imbalanced, and when k = 4 and above – except for k = 5 –, negative silhouette values are observed, indicating a particularly bad assignment for those individuals. Altogether, these results suggest that setting parameter k to 3 provides a reasonable solution balancing group size and avoiding clusters with only one individual.

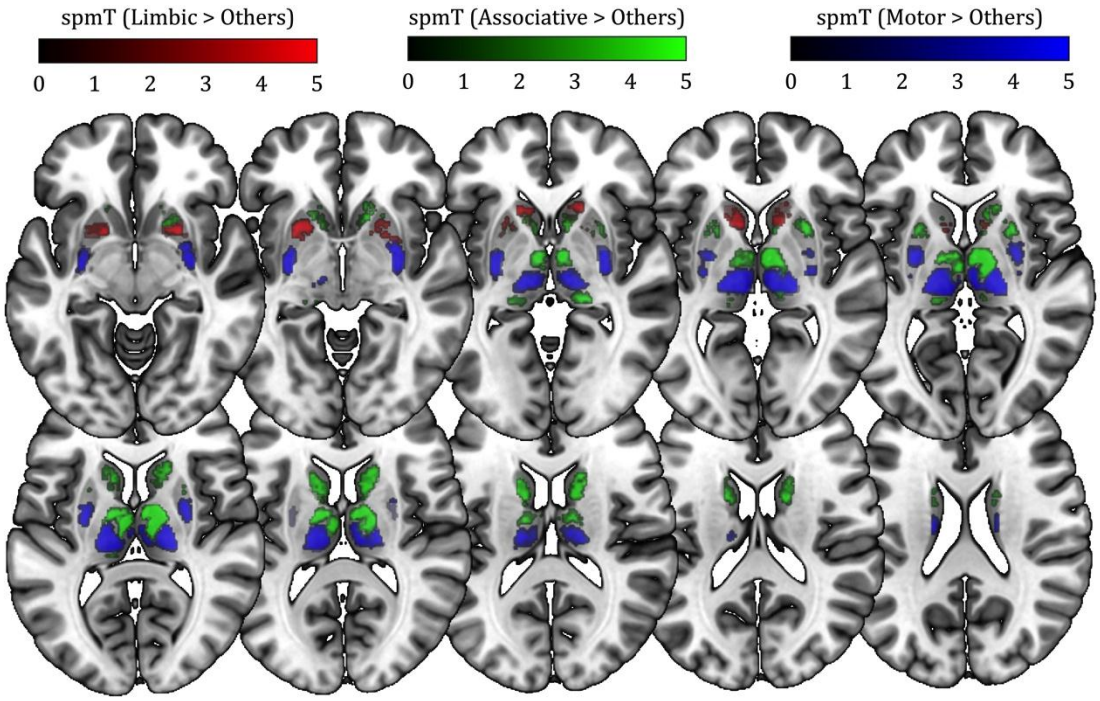

Supplementary figure 2 : T-contrasts testing the effect of each brain function against the two others across all subjects, applying mass-univariate voxel-based analysis on the number of tracts images. Robust topographical patterns are observed, which survive a statistical threshold of $p < 0.001$ with a minimal cluster extent of 10 voxels. Note how spatial distributions of patterns are similar to previous reports on subcortical connectivity (Draganski et al., 2008), with the most ventral and anterior part of the striatum being connected mostly to limbic cortical areas (rostral and ventral striatum, close to the nucleus accumbens), the most dorsal and posterior part to sensorimotor areas (tail of the caudate, dorsolateral putamen), and the intermediate part of the to associative areas. Note also the anterior-medial to posterior-lateral gradient from associative to sensorimotor areas. Statistical maps are rendered using MRIcroGL (Mac OS X version 1.150909) on a canonical T1-weighted image (mni152_2009_256.nii.gz).

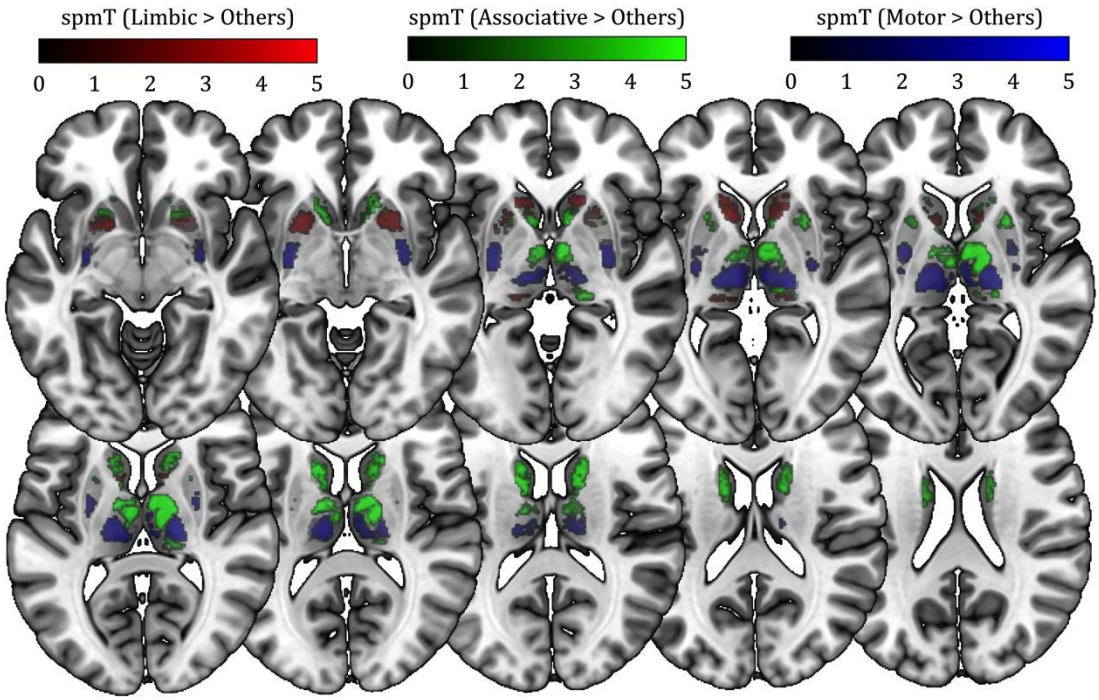

Supplementary figure 3 : T-contrasts testing the effect of each brain function against the two others in HC subjects, the rest of figure legend being identical to Supplementary figure 2. Note the similarity with Supplementary figure 2.

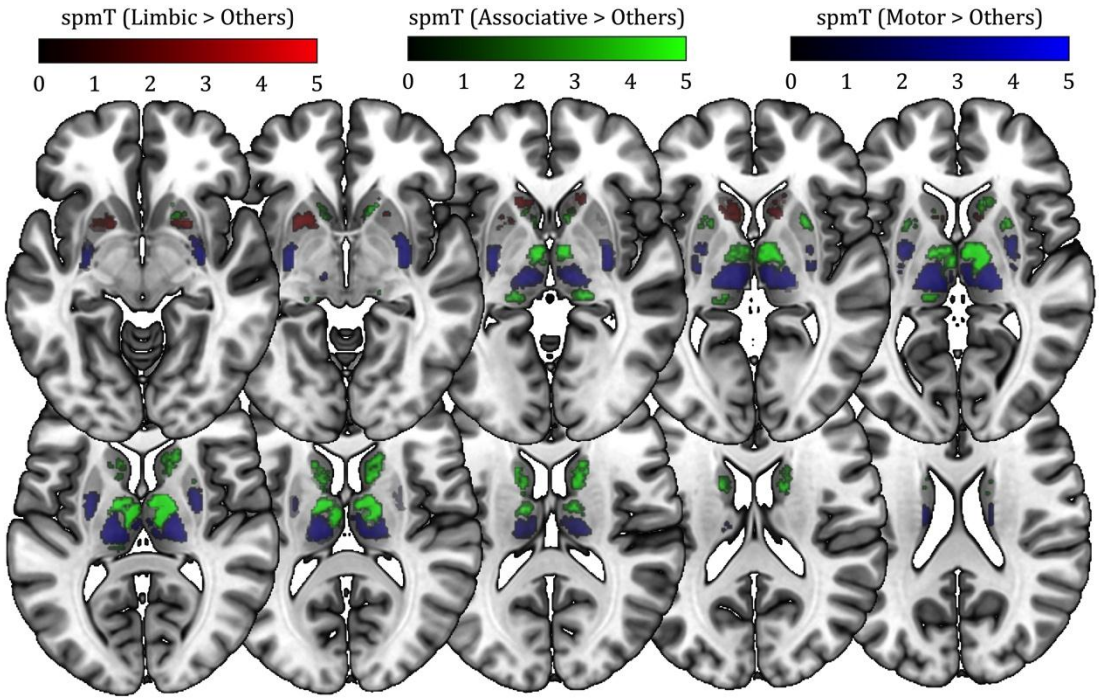

Supplementary figure 4 : T-contrasts testing the effect of each brain function against the two others across all PD patients, the rest of figure legend being identical to Supplementary figure 2. Note the similarity with Supplementary figure 2.

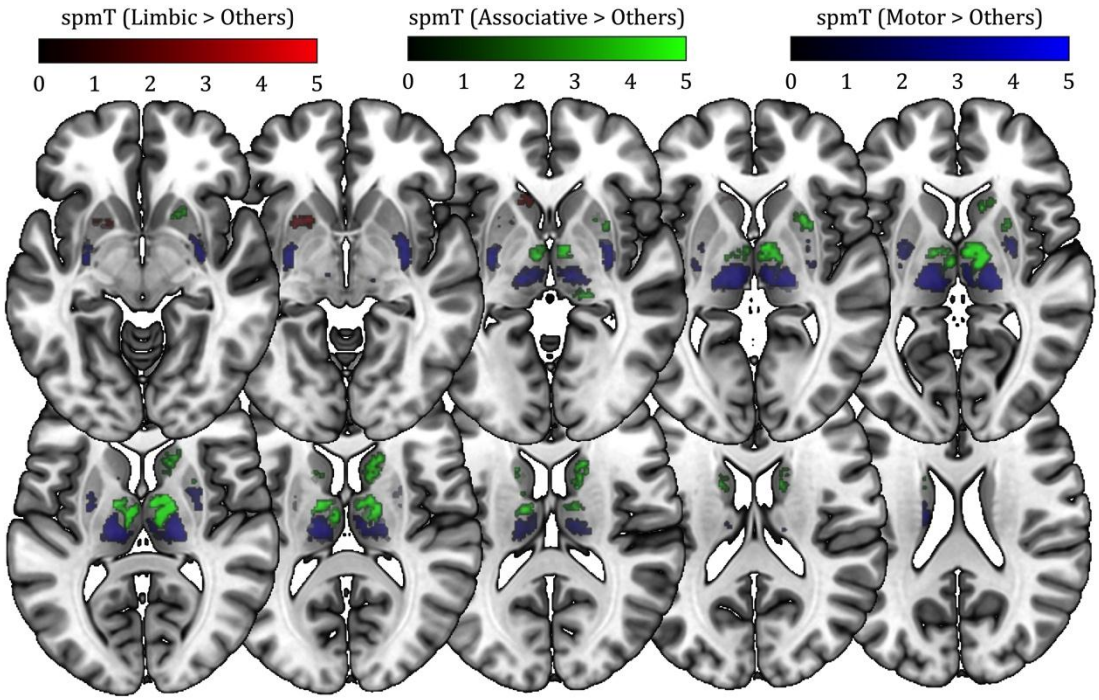

Supplementary figure 5 : T-contrasts testing the effect of each brain function against the two others in PD patients mostly affected on the left body side, the rest of figure legend being identical to Supplementary figure 2. Note the relative similarity with Supplementary figure 2.

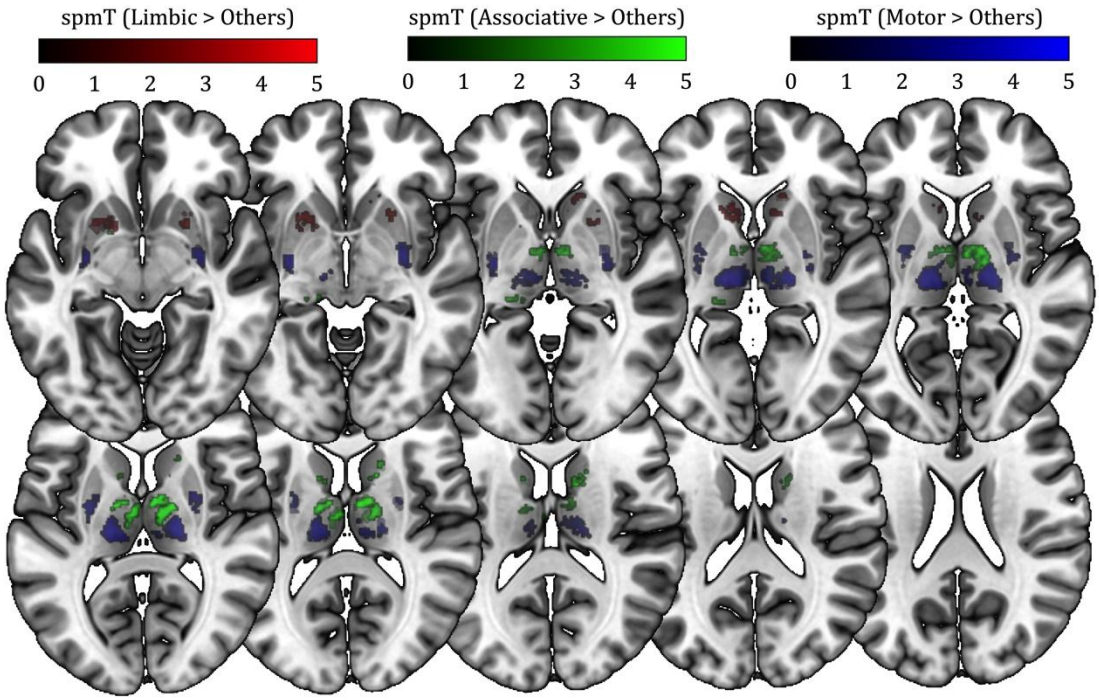

Supplementary figure 6 : T-contrasts testing the effect of each brain function against the two others in PD patients mostly affected on the right body side, the rest of figure legend being identical to Supplementary figure 2. Note the relative similarity with Supplementary figure 2.

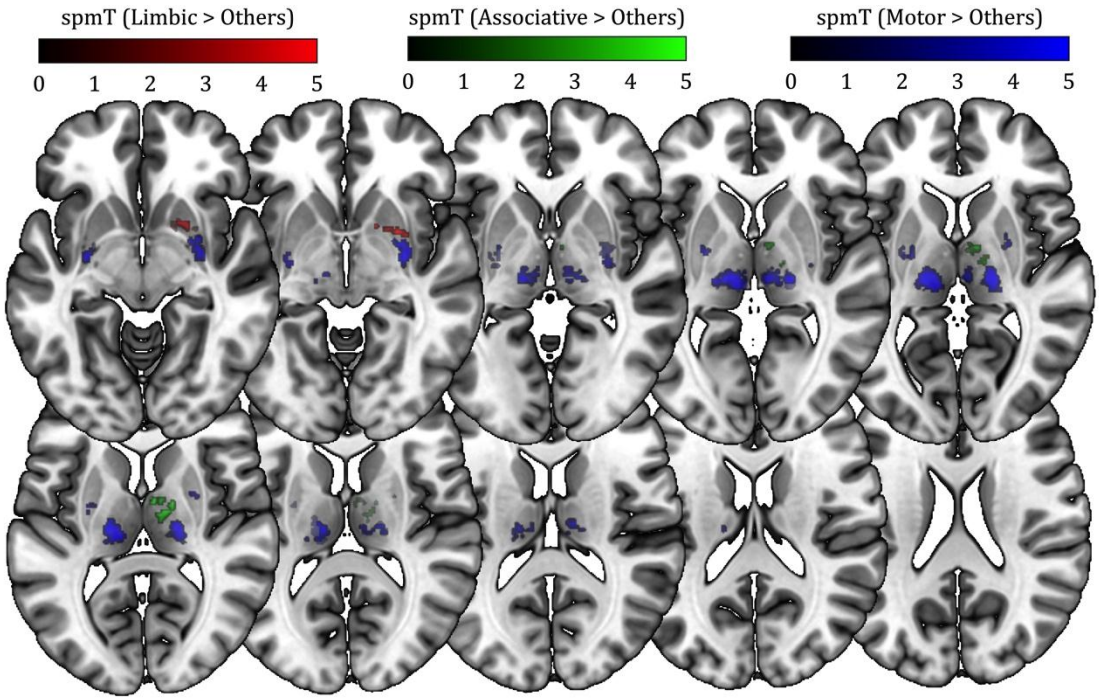

Supplementary figure 7 : T-contrasts testing the effect of each brain function against the two others in PD patients with predominantly motivational symptoms, the rest of figure legend being identical to Supplementary figure 2. Note the relative similarity with Supplementary figure 2 despite low sample size.

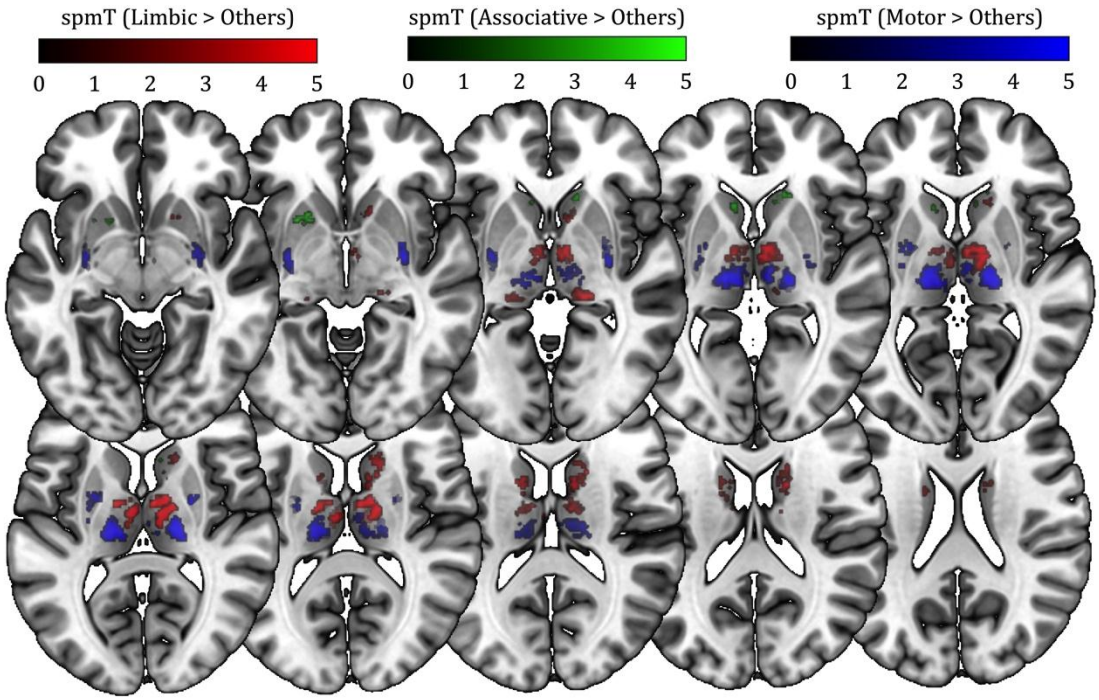

Supplementary figure 8 : T-contrasts testing the effect of each brain function against the two others in PD patients with predominantly cognitive symptoms, the rest of figure legend being identical to Supplementary figure 2. Although these maps were less similar to patterns observed in Supplementary figure 2, with possibly slightly fewer connections to associative areas, no difference between PD MCIp and other groups was observed ($p < 0.001$, $k \geq 10$).

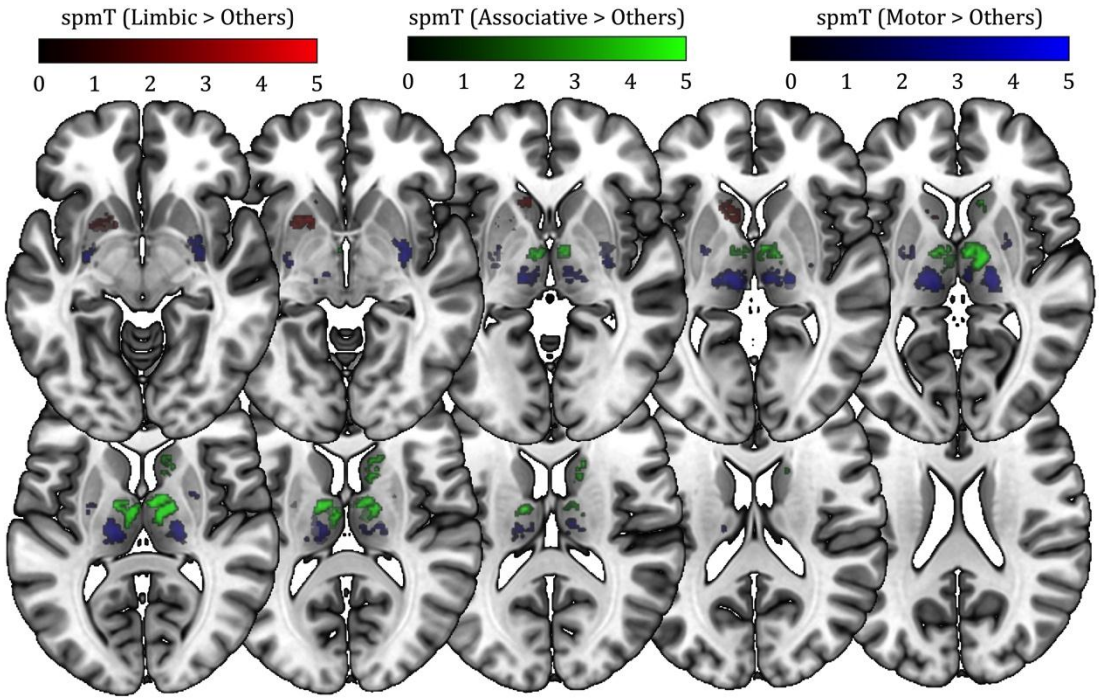

Supplementary figure 9 : T-contrasts testing the effect of each brain function against the two others in PD patients with predominantly motor symptoms, the rest of figure legend being identical to Supplementary figure 2. Although there may be a slight trend towards fewer fibres connected to sensorimotor cortical areas in the dorsolateral putamen, spatial distribution of patterns resembles maps shown in Supplementary figure 2 and no difference between PD Mp and other groups was observed ($p < 0.001$, $k \geq 10$ voxels).

3. General discussion

3.1. Interpretations and limitations

With my studies using non-invasive MRI, I tackled methodological challenges of basal ganglia imaging and provided empirical evidence at the brain structure and function level supporting the LOS hypothesis in PD.

Results of Study 1 showed an inverted U-shaped curve of *IoS* values in the BG, suggesting that higher fMRI spatial resolution improves spatial accuracy in these regions but that 3D EPI protocols artificially increases the effective overlap between somatotopy representations. Further studies are needed to better understand the source of this effect.

There are some limitations regarding results in Study 1. The way images are acquired in 3D and 2D EPI protocols may be problematic for choosing a kernel size for spatial smoothing during fMRI data pre-processing because the number of effective independent samples is not strictly the same (Kirilina et al., 2016). This issue remains unresolved at present and would require further thinking and methodological developments.

In Study 2, we demonstrate a loss of functional segregation in PD patients with and without DA substitution. Despite reports of LOS in the GPi, there are reports suggesting that PD does not alter motor somatotopy in the pallidum (Taha et al., 1996b) and STN (Rodriguez-Oroz et al., 2001). In line with these findings and with a previous study showing that MPTP do not increase synchronous activity in the pallidum (Mitelman et al., 2011), our results did not show evidence of LOS in the GPi, GPe and STN. In contrast, converging evidence implicates the motor thalamus in PD and suggests that it might be affected by a loss of functional segregation (Bosch-Bouju et al., 2013). Given the importance of age in PD and the similarity between neurobiological processes underlying PD and ageing, controlling for age effects was crucial. Recent studies further showed that ageing is accompanied by functional reorganisation (Morcom and Friston, 2012).

IoS is a potential biomarker of PD that may provide additional information on disease severity and responsiveness to DA therapy. *IoS* was found to differ between HC subjects and PD patients, appeared to be sensitive to DA and symptoms laterality, and further correlated with symptoms severity. Despite the crucial role of the SN in PD, differences in terms of IoS observed in the latter brain structure necessitate some important remarks. The SNr is known to contain highly overlapping motor somatotopy patterns (Kaneda et al., 2002; Nambu, 2011), while the SNc is associated with only weak evidence of topographical organization (Nambu, 2011; Rommelfanger, 2010). We found that segregation of motor representations in the SN of PD patients OFF was reduced compared to HC. The degree of loss of functional segregation was positively correlated with motor symptoms severity.

This additional evidence strengthens the notion of a loss of functional segregation in PD, particularly when in "OFF". A possible explanation is that the source of the observed differences lies in the SNr rather than the SNc. Even with greater spatial precision for the definition of the ROIs, distinguishing the SNr from the SNc is particularly challenging using fMRI and one could not rule out the possibility of signals from the two regions contaminating each other.

Our results did not show a significant relationship between functional segregation and tremor scores in PD. Tremor is a sporadic symptom in PD, as it is not present in 25% of patients. It does not respond to DA therapy and its progression is not comparable to that of other motor symptoms. The coherence between BG oscillations and tremor has been shown to be inconsistent (Helmich et al., 2012). Given the singularity of rest tremor in PD, its subtle effects might be more difficult to capture with the coarse spatial resolution of fMRI compared to electrophysiological studies. One could further speculate that tremor in PD results from an interaction between LOS at different BG levels. To demonstrate such a relationship, larger sample size might be necessary. Relationships between LOS and rigidity were not tested, as the effects of the latter are difficult to dissociate from bradykinesia. Further studies are required to identify the contributions of LOS to each motor symptom in PD. In addition, we showed a negative relationship between cortico-striatal connectivity and IoS values, confirming that efficient reconstruction of input patterns when the putamen, which is perhaps associated with the highest information compression ratio in BG circuitry (Bar-Gad et al., 2003a), loses its topographical organization.

One might interpret these findings as supporting the idea that LOS is induced by DA depletion. In the scenario, SNc neurons die, inducing LOS in the SN and putamen through striato-nigro-striatal pathways, and consequently LOS reaches the motor thalamus via thalamo-striatal pathways. Alternatively, DA depletion might induce LOS as a result of synchronous activity by weakening of collaterals between MSN, changing the preferential target of FSIs from MSNs of the direct pathway to MSNs of the indirect pathway, or by increasing ACh due to reduced auto-receptor function in cholinergic interneurons driving NPY-expressing interneurons (Gittis and Kreitzer, 2012). LTS interneurons and TH-positive interneurons might also play a role in striatal micro-circuitry dysfunction and induce LOS after DA depletion. How does the LOS further propagate to the motor thalamus? Given that direct thalamo-striatal connections are not bidirectional, impaired dimensionality reduction should in principle be transferred via the pallidum, presumably inducing thereby abnormal IoS values in the latter region. Several explanations may be considered. Abnormal IoS values in the SN are driven by LOS in the SNr, henceforth LOS propagates from the putamen to the thalamus via the direct pathway. This is surely a speculative explanation, given the underlying assumption of differential impact of LOS on the SNr but not on the GPi, particularly in the context of the performed motor task. Alternatively,

compensatory mechanisms operate at the level of the pallidum, which mask the LOS in BG output. Given the high level of integration in the GPi, it is equally probable that we reached the limits of the applied methods and that higher spatial resolution or increased number of subjects would be needed to detect the presumed effect of LOS at the pallidal level.

Another speculation is that the impaired dimensionality reduction in the striatum might be caused indirectly by cholinergic interneurons inducing plastic changes at the cortico-striatal level via DAergic neurotransmission (Surmeier and Graybiel, 2012) or directly by GABAergic interneurons, which coordinate MSN spiking activity (Clarke and Adermark, 2015) or cholinergic interneurons by specifying the polarity of plasticity towards LTD or LTP via activation of MSN muscarinic postsynaptic receptors (Deffains and Bergman, 2015). High levels of LRRK2 are expressed in cholinergic interneurons and the physiology of the latter might be pathologically affected by abnormal kinase activity (Lim et al., 2014). More evidence is brought by a study showing that DA therapy does not restore the full spectrum of normal pallidal activity in MPTP-intoxicated monkeys (Heimer et al., 2006). Assuming that LOS is the central pathophysiological process underlying PD, one might speculate that this neurodegenerative disease is due to striatal interneuron dysfunction rather than DA depletion. The presence of recurrent striato-nigro-striatal connections and the reports of loss of function and integrity in the striatum preceding SN degeneration support this speculation. Apoptotic mechanisms in the SNc might be triggered remotely via striatonigrostriatal pathways. Dysfunction of cholinergic and GABAergic striatal interneurons has been found to play a role not only in PD but also in dystonia, HD, attention deficit hyperactivity disorder (ADHD), AD, GTS, OCD, bipolar disorders, schizophrenia and major depressive disorders (Clarke and Adermark, 2015; Deffains and Bergman, 2015). Indeed, changes in DA and ACh might underlie abnormal plasticity in dystonia (Peterson et al., 2010). Cholinergic signalling might impact the expression of LIDs (Lim et al., 2014). Regarding this potential explanation, it is worth recalling the reduced risk of developing PD in smokers (Fujita et al., 2005; Mary Ann Chapman, 2009; Miwa et al., 2011; Quik et al., 2008). Other neurotransmitters can modulate cholinergic interneurons, including GABA, glutamate, DA – notably from the SNc –, serotonin – from the dorsal raphe –, histamine, noradrenaline – from the locus cœruleus –, adenosine, ATP, nitric oxide, enkephalin – from D_2 MSNs –, substance P and dynorphin – from D_1 MSNs (Lim et al., 2014). Like in the first explanatory scheme, this speculation does not fully resolve the issue of absence of LOS in the pallidum concurrent to LOS in the motor thalamus. LOS in PD might affect multiple sites simultaneously via non-synaptic pathways, albeit α-synuclein deposition in the thalamus in PD is unlikely to underlie differences in IoS values in the VL and VPL nuclei of the thalamus (Halliday, 2009). A possible explanation is that the loss of functional segregation in the striatum is propagated through thalamostriatal projections and originates in the thalamus. Very recently, it was shown that thalamic cholinergic integrity predicted performance

during a sustained attention task, even after controlling for age, disease severity and DAergic innervation (Kim et al., 2017).

Alternatively, the PPN is a common denominator regarding ROIs affected by a loss of functional segregation and was not considered in our analyses. This heterogeneous structure, located in the upper brainstem and characterized by a topographical organization of its connections, concurrently projects to a broad range of BG and thalamic nuclei, including the striatum, SN as well as to the ventrolateral, centro-median, and para-fascicular nuclei of the thalamus (Benarroch, 2008, 2013; Martinez-Gonzalez et al., 2011; Mena-Segovia et al., 2004; Pahapill and Lozano, 2000). The PPN, which has been considered as a target for DBS in PD, also projects to the STN, pallidum, as well as other thalamic nuclei and multiple structures in the brainstem, tectum and forebrain (Martinez-Gonzalez et al., 2011; Nakano, 2000). Although the role of the PPN remains largely unclear, it has a clear contribution in the control of locomotion (Obeso et al., 2008; Snijders et al., 2016). In primates, akinesia follows PPN lesions whereas chemical disinhibition and stimulation of the PPN alleviates the latter symptom (Zrinzo et al., 2008). About 50% of cholinergic neurons are lost in PD patients (Obeso et al., 2008). A very recent study suggests abnormal PPN connectivity in PD patients with sleep disorders and postural and impaired postural control (Gallea et al., 2017). Still, the absence of LOS at the level of M1 remains an open issue. Even if compensatory mechanisms supported by the SMA or cerebellum can be postulated, longitudinal studies are required to validate our findings in bigger cohorts and decipher the potential mechanisms of propagation of LOS in PD.

The use of electromyography (EMG) might provide additional information for data analysis performed in Study 2. Tremor episodes could be extracted from EMG recordings and added as confounding factor or directly tested. Moreover, additional anatomical precision might be reached by dividing the putamen into an anterior and posterior part, as done in previous studies (Helmich et al., 2010). The latter study suggests that controlling for tremor and head motion using derivatives of realignment parameters improves model fitting in fMRI data analysis.

In Study 3 we showed that PD is associated with a loss of functional segregation not only at the BG level but also in a cortical region considered to be a hub in brain networks, the insula. As discussed above, alterations to DAergic, cholinergic or serotoninergic pathways projecting to the insula may underlie loss of functional segregation observed in the insula (Christopher et al., 2014). This region, which integrates information from multiple brain regions, is likely affected by changes in cortico-subcortical loops, as it sends massive and topographically organized projections to the striatum. Study 2 showed that loss of functional segregation is observed in the putamen of PD patients. This could have an impact on the insula. Alternatively, the loss of functional segregation in the insula might be

caused by α-synuclein deposition, though the latter occurs relatively late in terms of disease time course as it would correspond to Braak stage 5 (Christopher et al., 2014). Aberrant cortico-striatal plasticity resulting in a general increase in cortical activity might explain, at least partially, the loss of functional segregation in the insula with PD (Beeler et al., 2012, 2013). The fact that DA therapy did not seem to affect functional segregation in the insula remains to be elucidated.

In Study 4 we showed that LOS possibly also affects structural connectivity patterns and is not limited to motor circuitry. Besides the anatomical plausibility of the obtained parcellation, the location of functional territories in the striatum corroborates a recent functional connectivity study based on a huge sample (Malherbe et al., 2014). Similarly to remarks made for Study 2, plastic changes affecting cortico-striatal connectivity may explain some of our results. Given the role of DA, ACh and GABAergic interneurons in striatal synaptic plasticity, reorganization of striatal structural connectivity might be induced by the mechanisms like the ones causing loss of functional segregation between motor representations of different body parts. Based on the presence of D_1 and D_5 receptors in the thalamus (Missale et al., 1998) and the existence of DAergic afferent projections in the thalamus, notably from the VTA, SNc and hypothalamus (Sanchez-Gonzalez, 2005), speculate a reorganization of thalamo-cortical connectivity is not totally unreasonable. A nonselective DAergic axon lattice makes thalamo-striatal synapses are as much likely to be influenced by DA release as cortico-striatal synapses (Moss and Bolam, 2008). Changes in structural connectivity patterns observed in the thalamus might therefore result from an abnormal transfer of information between the striatum and thalamus triggering synaptic plasticity and reorganization of thalamo-cortico-thalamic pathways (Haber, 2003). Previous findings accumulated evidences that DA neurons in the midbrain integrate sensory, motor and cognitive information from multiple brain regions (Morikawa and Paladini, 2011). As an alternative interpretation, one may speculate that plastic changes in structural connectivity patterns underlie functional changes associated with PD as observed in Study 2 and Study 3. The mechanisms underlying LOS at the structural level in PD remain unclear and would require further investigations. Future work may include the pallidum as a seed ROI for tractography, as the GPe has been suggested to receive also direct input from the cortex (Kita, 2007). Although the tracking of the latter connections is not trivial, a recent work suggests that it may be feasible using constrained spherical (Milardi et al., 2014), yet the role of this direct cortico-pallidal remains to be clarified. There are also several limitations to Study 4. Although results in terms of structural segregation cannot be explained by differences in terms of connection density, we cannot definitely rule out the possibility that alterations of microstructural tissue properties induced a bias in the tracking algorithm. At present, however, a unified model linking MRI-derived metrics and biological tissue properties is still lacking. While additional analyses might refine our interpretations, they would heavily rely on an

indecent number of speculations. General caveats encountered in tractography as mentioned previously also apply to Study 4 (Eickhoff et al., 2015). Impaired detection of sharply curved, very long, closely neighbouring or poorly myelinated fibre bundles may have affected our results despite the robustness of the chosen tracking algorithm.

3.2. Future directions

Future work may focus on segregation between limbic, associative and sensorimotor territories at the functional level using for example tasks combining multiple behavioural functions (Schmidt et al., 2012). Studies could also investigate structural segregation at the motor somatotopy level, as recent studies demonstrated the feasibility of cortico-striatal tracts reconstruction for different body parts (Staempfli et al., 2008). A remaining question relates to elucidating the presence of loss of functional segregation in the thalamus and determining which thalamic nucleus is affected by LOS. With respect to this question, LOS might primarily resides in the pallidal thalamus given previous reports in the anatomical connectivity of thalamic nuclei. In addition, the presence of a loss of functional segregation in the cerebellum might be investigated and possibly show links with tremor. The same atlas of the thalamus that we used in our studies may be used for this purpose. The PD-related rewiring process suggested in Study 4 might be completed by additional analyses of white matter tract integrity at the level of tissue properties. As PD has been associated with an impaired interhemispheric inhibition (Lieu and Subramanian, 2012), further studies could focus on investigating the link between functional segregation and the lack of interhemispheric inhibition. Based on findings of structural changes in PD and the possible mechanisms inducing LOS, relationships between functional segregation and tissue properties might also exist. We are convinced that one of the most pressings needs is to validate the predictive ability of the loss of functional segregation at the prodromal stage and its relationship with symptoms severity and neurodegeneration over the disease course. In this sense, patients with SWEDD or mutations affecting genes such as *VPS35* might be of particular interest. Given the complexity of pathogenic processes proposed to underlie PD, it might also be especially valuable – once the LOS hypothesis confirmed in a more definite manner – to search for the most likely sequence of events from different biomarkers. The latter may include for instance striatal DA innervation as assessed by PET or SPECT imaging, iron deposition as measured by R2* and functional as well as structural segregation estimates.

Segregation has been defined differently according to other views, promoting studies on information topology in PD that complement the work presented here (Balduzzi and Tononi, 2009; Bullmore and Sporns, 2009, 2009; Deco et al., 2015; Edelman and Gally, 2001; Fornito and Bullmore, 2014; Fornito et al., 2015; Green et al., 2006; Hagmann et al., 2008, 2010; Meunier et al., 2010; Oizumi et al., 2014; Rubinov and Sporns, 2010; Sporns,

2012, 2013, 2015, Sporns et al., 2000, 2000, Tononi, 2004, 2008, Tononi et al., 1994, 1998, 1999; Wei et al., 2014; Whitacre, 2010). Future studies on functional segregation might either extend our results to the mapping of different body parts, or investigate it from a perspective that considers for example the relevance of movements in a ethological framework (Aflalo and Graziano, 2006; Graziano and Aflalo, 2007a, 2007b). The limbic and associative loops may embed further granularity, for example concerning representations of different types of rewards or punishments. We believe that studying topography of information in PD at the structural and functional level will help to better understand PD pathophysiology and improve the monitoring of disease progression.

List of figures and tables

References

Abou-Sleiman, P.M., Muqit, M.M.K., and Wood, N.W. (2006). Expanding insights of mitochondrial dysfunction in Parkinson's disease. Nat. Rev. Neurosci. *7*, 207–219.

Accolla, E.A., Dukart, J., Helms, G., Weiskopf, N., Kherif, F., Lutti, A., Chowdhury, R., Hetzer, S., Haynes, J.-D., Kühn, A.A., et al. (2014). Brain tissue properties differentiate between motor and limbic basal ganglia circuits. Hum. Brain Mapp. *35*, 5083–5092.

Afifi, A.K. (1994a). Basal ganglia: functional anatomy and physiology. Part 1. J. Child Neurol. *9*, 249–260.

Afifi, A.K. (1994b). Basal ganglia: functional anatomy and physiology. Part 2. J. Child Neurol. *9*, 352–361.

Aflalo, T.N., and Graziano, M.S.A. (2006). Possible Origins of the Complex Topographic Organization of Motor Cortex: Reduction of a Multidimensional Space onto a Two-Dimensional Array. J. Neurosci. *26*, 6288–6297.

Albin, R.L., Young, A.B., and Penney, J.B. (1989). The functional anatomy of basal ganglia disorders. Trends Neurosci. *12*, 366–375.

Alexander, G.E., and Crutcher, M.D. (1990). Functional architecture of basal ganglia circuits: neural substrates of parallel processing. Trends Neurosci. *13*, 266–271.

Alexander, G.E., DeLong, M.R., and Strick, P.L. (1986). Parallel organization of functionally segregated circuits linking basal ganglia and cortex. Annu. Rev. Neurosci. *9*, 357–381.

Alexander, G.E., Crutcher, M.D., and DeLong, M.R. (1989). Basal ganglia-thalamocortical circuits: parallel substrates for motor, oculomotor," prefrontal" and" limbic" functions. Prog. Brain Res. *85*, 119–146.

Algarni, M.A., and Stoessl, A.J. (2016). The role of biomarkers and imaging in Parkinson's disease. Expert Rev. Neurother. *16*, 187–203.

Alkadhi, H., Crelier, G.R., Boendermaker, S.H., Golay, X., Hepp-Reymond, M.-C., and Kollias, S.S. (2002a). Reproducibility of primary motor cortex somatotopy under controlled conditions. AJNR Am. J. Neuroradiol. *23*, 1524–1532.

Alkadhi, H., Crelier, G.R., Boendermaker, S.H., Hepp-Reymond, M.-C., and Kollias, S.S. (2002b). Somatotopy in the ipsilateral primary motor cortex. NeuroReport *13*, 2065–2070.

Alves, G., Forsaa, E.B., Pedersen, K.F., Dreetz Gjerstad, M., and Larsen, J.P. (2008). Epidemiology of Parkinson's disease. J. Neurol. *255*, 18–32.

Amano, S., Kegelmeyer, D., and Hong, S.L. (2014). Rethinking energy in parkinsonian motor symptoms: a potential role for neural metabolic deficits. Front. Syst. Neurosci. *8*, 242.

Amemori, K.-I., Gibb, L.G., and Graybiel, A.M. (2011). Shifting responsibly: the importance of striatal modularity to reinforcement learning in uncertain environments. Front. Hum. Neurosci. *5*, 47.

Antzoulatos, E.G., and Miller, E.K. (2011). Differences between Neural Activity in Prefrontal Cortex and Striatum during Learning of Novel Abstract Categories. Neuron *71*, 243–249.

Apps, R., and Hawkes, R. (2009). Cerebellar cortical organization: a one-map hypothesis. Nat. Publ. Group *10*, 670–681.

Ashby, F.G., Alfonso-Reese, L.A., Turken, A.U., and Waldron, E.M. (1998). A neuropsychological theory of multiple systems in category learning. Psychol. Rev. *105*, 442–481.

Ashby, F.G., Ennis, J.M., and Spiering, B.J. (2007). A neurobiological theory of automaticity in perceptual categorization. Psychol. Rev. *114*, 632–656.

Ataie, A., Shadifar, M., and Ataee, R. (2016). Polyphenolic Antioxidants and Neuronal Regeneration. Basic Clin. Neurosci. *7*, 81–90.

Auer, D.P. (2009). In vivo imaging markers of neurodegeneration of the substantia nigra. Exp. Gerontol. *44*, 4–9.

Baas, H. (2000). Dyskinesia in Parkinson's disease. Pathophysiology and clinical risk factors. J. Neurol. *247*, IV12–IV16.

Badre, D., and D'Esposito, M. (2009). Is the rostro-caudal axis of the frontal lobe hierarchical? Nat. Publ. Group *10*, 659–669.

Bainbridge, J.L., Page II, R.L., and Ruscin, J.M. (2008). Elucidating the Mechanism of Action and Potential Interactions of MAO-B Inhibitors. Neurol. Clin. *26*, 85–96.

Baker, K.B., Lee, J.Y.K., Mavinkurve, G., Russo, G.S., Walter, B., DeLong, M.R., Bakay, R.A.E., and Vitek, J.L. (2010). Somatotopic organization in the internal segment of the globus pallidus in Parkinson's disease. Exp. Neurol. *222*, 219–225.

Balduzzi, D., and Tononi, G. (2009). Qualia: The Geometry of Integrated Information. PLoS Comput. Biol. *5*, e1000462.

Bammer, R. (2003). Basic principles of diffusion-weighted imaging. Eur. J. Radiol. *45*, 169–184.

Bar-Gad, I., and Bergman, H. (2001). Stepping out of the box: information processing in the neural networks of the basal ganglia. Curr. Opin. Neurobiol. *11*, 689–695.

Bar-Gad, I., Havazelet-Heimer, G., Goldberg, J.A., Ruppin, E., and Bergman, H. (2000). Reinforcement-driven dimensionality reduction -a model for information processing in the basal ganglia. J. Basic Clin. Physiol. Pharmacol. *11*, 305–320.

Bar-Gad, I., Morris, G., and Bergman, H. (2003a). Information processing, dimensionality reduction and reinforcement learning in the basal ganglia. Prog. Neurobiol. *71*, 439–473.

Bar-Gad, I., Heimer, G., Ritov, Y. 'acov, and Bergman, H. (2003b). Functional correlations between neighboring neurons in the primate globus pallidus are weak or nonexistent. J. Neurosci. *23*, 4012–4016.

Bargiotas, P., and Konitsiotis, S. (2013). Levodopa-induced dyskinesias in Parkinson's disease: emerging treatments. Neuropsychiatr. Dis. Treat. *9*, 1605–1617.

Barto, A.G. (1995). Adaptive Critics and the Basal Ganglia. In Models of Information Processing in the Basal Ganglia, J.C. Houk, J. Davis, and D. Beiser, eds. (Cambridge, MA: MIT Press), pp. 215–232.

Bartus, R.T., Weinberg, M.S., and Samulski, R.J. (2013). Parkinson's Disease Gene Therapy: Success by Design Meets Failure by Efficacy. Mol. Ther. *22*, 487–497.

Basso, M.A., and Sommer, M.A. (2011). Exploring the role of the substantia nigra pars reticulata in eye movements. NEUROSCIENCE *198*, 205–212.

Baumgartner, U., Iannetti, G.D., Zambreanu, L., Stoeter, P., Treede, R.D., and Tracey, I. (2010). Multiple Somatotopic Representations of Heat and Mechanical Pain in the Operculo-Insular Cortex: A High-Resolution fMRI Study. J. Neurophysiol. *104*, 2863–2872.

Beal, M.F. (2001). Experimental models of Parkinson's disease. Nat. Rev. Neurosci. *2*, 325–334.

Beck, S., and Hallett, M. (2011). Surround inhibition in the motor system. Exp. Brain Res. *210*, 165–172.

Beeler, J.A., Frank, M.J., McDaid, J., Alexander, E., Turkson, S., Bernandez, M.S., McGehee, D.S., and Zhuang, X. (2012). A Role for Dopamine-Mediated Learning in the Pathophysiology and Treatment of Parkinson's Disease. CellReports *2*, 1747–1761.

Beeler, J.A., Petzinger, G., and Jakowec, M.W. (2013). The Enemy within: Propagation of Aberrant Corticostriatal Learning to Cortical Function in Parkinson's Disease. Front. Neurol. *4*.

Beisteiner, R., Windischberger, C., Lanzenberger, R., Edward, V., Cunnington, R., Erdler, M., Gartus, A., Streibl, B., Moser, E., and Deecke, L. (2001). Finger Somatotopy in Human Motor Cortex. NeuroImage *13*, 1016–1026.

Belin, D., Jonkman, S., Dickinson, A., Robbins, T.W., and Everitt, B.J. (2009). Parallel and interactive learning processes within the basal ganglia: Relevance for the understanding of addiction. Behav. Brain Res. *199*, 89–102.

Belluscio, M.A., Escande, M.V., Keifman, E., Riquelme, L.A., Murer, M.G., and Zold, C.L. (2013). Oscillations in the basal ganglia in Parkinson's disease: Role of the striatum. Biochem. Pharmacol. 1–10.

Benarroch, E.E. (2008). The midline and intralaminar thalamic nuclei: anatomic and functional specificity and implications in neurologic disease. Neurology *71*, 944–949.

Benarroch, E.E. (2009). Brain iron homeostasis and neurodegenerative disease. Neurology *72*, 1436–1440.

Benarroch, E.E. (2013). Pedunculopontine nucleus: Functional organization and clinical implications. Neurology *80*, 1148–1155.

Ben-Eliezer, N., Goerke, U., Ugurbil, K., and Frydman, L. (2012). Functional MRI using super-resolved spatiotemporal encoding. Magn. Reson. Imaging *30*, 1401–1408.

Bergman, H., and Deuschl, G. (2002). Pathophysiology of Parkinson's disease: From clinical neurology to basic neuroscience and back. Mov. Disord. *17*, S28–S40.

Bergman, H., Feingold, A., Nini, A., Raz, A., Slovin, H., Abeles, M., and Vaadia, E. (1998a). Physiological aspects of information processing in the basal ganglia of normal and parkinsonian primates. Trends Neurosci. *21*, 32–38.

Bergman, H., Raz, A., Feingold, A., Nini, A., Nelken, I., Hansel, D., Ben-Pazi, H., and Reches, A. (1998b). Physiology of MPTP tremor. Mov. Disord. Off. J. Mov. Disord. Soc. *13 Suppl 3*, 29–34.

Berke, J.D. (2011). Functional properties of striatal fast-spiking interneurons. Front. Syst. Neurosci. *5*, 45.

Bernard, J.A., and Mittal, V.A. (2014). Cerebellar-motor dysfunction in schizophrenia and psychosis-risk: the importance of regional cerebellar analysis approaches. Front. Psychiatry *5*, 160.

Berns, G.S., and Sejnowski, T.J. (1998). A computational model of how the basal ganglia produce sequences. Cogn. Neurosci. J. Of *10*, 108–121.

di Biase, L., and Fasano, A. (2016). Low-frequency deep brain stimulation for Parkinson's disease: Great expectation or false hope? Mov. Disord. *31*, 962–967.

Bittar, R.G., Burn, S.C., Bain, P.G., Owen, S.L., Joint, C., Shlugman, D., and Aziz, T.Z. (2005). Deep brain stimulation for movement disorders and pain. J. Clin. Neurosci. *12*, 457–463.

Blandini, F., and Armentero, M.-T. (2014). Dopamine receptor agonists for Parkinson's disease. Expert Opin. Investig. Drugs *23*, 387–410.

Bolam, J.P., Smith, Y., Ingham, C.A., von Krosigk, M., and Smith, A.D. (1993). Chapter 5 Convergence of synaptic terminals from the striatum and the globus pallidus onto single

neurones in the substantia nigra and the entopeduncular nucleus. In Chemical Signalling in the Basal Ganglia, G.W. Arbuthnott, and P.C. Emson, eds. (Elsevier), pp. 73–88.

Bonifati, V. (2013). Genetics of Parkinson's disease - state of the art, 2013. Parkinsonism Relat. Disord. *20*, S23–S28.

Boraud, T., Bézard, E., Bouliac, B., and Gross, C.E. (2000). Ratio of inhibited-to-activated pallidal neurons decreases dramatically during passive limb movement in the MPTP-treated monkey. J. Neurophysiol. *83*, 1760–1763.

Bosboom, J.L.W., Stoffers, D., and Wolters, E.C. (2004). Cognitive dysfunction and dementia in Parkinson's disease. J. Neural Transm. Vienna Austria 1996 *111*, 1303–1315.

Bosch-Bouju, C., Hyland, B.I., and Parr-Brownlie, L.C. (2013). Motor thalamus integration of cortical, cerebellar and basal ganglia information: implications for normal and parkinsonian conditions. Front. Comput. Neurosci. *7*, 163.

Bose, A., and Beal, M.F. (2016). Mitochondrial dysfunction in Parkinson's disease. J. Neurochem. *139 Suppl 1*, 216–231.

Bostan, A.C., Dum, R.P., and Strick, P.L. (2013). Cerebellar networks with the cerebral cortex and basal ganglia. Trends Cogn. Sci. 1–14.

Braak, H., Del Tredici, K., Rüb, U., de Vos, R.A.I., Jansen Steur, E.N.H., and Braak, E. (2003a). Staging of brain pathology related to sporadic Parkinson's disease. Neurobiol. Aging *24*, 197–211.

Braak, H., R b, U., Gai, W.P., and Del Tredici, K. (2003b). Idiopathic Parkinson's disease: possible routes by which vulnerable neuronal types may be subject to neuroinvasion by an unknown pathogen. J. Neural Transm. *110*, 517–536.

Braak, H., Ghebremedhin, E., Rüb, U., Bratzke, H., and Del Tredici, K. (2004). Stages in the development of Parkinson's disease-related pathology. Cell Tissue Res. *318*, 121–134.

Bromberg-Martin, E.S., Matsumoto, M., and Hikosaka, O. (2010). Dopamine in Motivational Control: Rewarding, Aversive, and Alerting. Neuron *68*, 815–834.

Bronfeld, M., and Bar-Gad, I. (2011). Loss of specificity in Basal Ganglia related movement disorders. Front. Syst. Neurosci. *5*, 38.

Brooks, D.J. (2010). Imaging Approaches to Parkinson Disease. J. Nucl. Med. *51*, 596–609.

Brooks, D.J., and Pavese, N. (2011). Imaging biomarkers in Parkinson's disease. Prog. Neurobiol. *95*, 614–628.

Brooks, J.C.W., Zambreanu, L., Godinez, A., Craig, A.D.B., and Tracey, I. (2005). Somatotopic organisation of the human insula to painful heat studied with high resolution functional imaging. NeuroImage *27*, 201–209.

Brooks, J.C.W., Faull, O.K., Pattinson, K.T.S., and Jenkinson, M. (2013). Physiological noise in brainstem FMRI. Front. Hum. Neurosci. *7*, 623.

Broussard, J.I., Jenson, D., and Dani, J.A. (2013). Dopaminergic influence over hippocampal synaptic plasticity and function. Clin. Exp. Ldots.

Brown, P. (2007). Abnormal oscillatory synchronisation in the motor system leads to impaired movement. Curr. Opin. Neurobiol. *17*, 656–664.

Brown, J., Bullock, D., and Grossberg, S. (1999). How the basal ganglia use parallel excitatory and inhibitory learning pathways to selectively respond to unexpected rewarding cues. J. Neurosci. Off. J. Soc. Neurosci. *19*, 10502–10511.

Brown, J.W., Bullock, D., and Grossberg, S. (2004). How laminar frontal cortex and basal ganglia circuits interact to control planned and reactive saccades. Neural Netw. *17*, 471–510.

Brundin, P., Ma, J., and Kordower, J.H. (2016). How strong is the evidence that Parkinson's disease is a prion disorder? Curr. Opin. Neurol. *29*, 459–466.

Bullmore, E., and Sporns, O. (2009). Complex brain networks: graph theoretical analysis of structural and functional systems. Nat. Publ. Group *10*, 186–198.

Burke, R.E., Dauer, W.T., and Vonsattel, J.P.G. (2008). A critical evaluation of the Braak staging scheme for Parkinson's disease. Ann. Neurol. *64*, 485–491.

Burn, D.J. (2002a). Beyond the iron mask: Towards better recognition and treatment of depression associated with Parkinson's disease. Mov. Disord. *17*, 445–454.

Burn, D.J. (2002b). Depression in Parkinson's disease. Eur. J. Neurol. Off. J. Eur. Fed. Neurol. Soc. *9 Suppl 3*, 44–54.

Calabresi, P., Centonze, D., Gubellini, P., Pisani, A., and Bernardi, G. (2000). Acetylcholine-mediated modulation of striatal function. Trends Neurosci. *23*, 120–126.

Calabresi, P., Picconi, B., Tozzi, A., and Di Filippo, M. (2007). Dopamine-mediated regulation of corticostriatal synaptic plasticity. Trends Neurosci. *30*, 211–219.

Calabresi, P., Picconi, B., Tozzi, A., Ghiglieri, V., and Di Filippo, M. (2014). Direct and indirect pathways of basal ganglia: a critical reappraisal. Nat. Publ. Group *17*, 1022–1030.

Calabresi, P., Ghiglieri, V., Mazzocchetti, P., Corbelli, I., and Picconi, B. (2015). Levodopa-induced plasticity: a double-edged sword in Parkinson's disease? Philos. Trans. R. Soc. B Biol. Sci. *370*, 20140184.

Calì, T., Ottolini, D., and Brini, M. (2011). Mitochondria, calcium, and endoplasmic reticulum stress in Parkinson's disease. BioFactors *37*, 228–240.

Cavanagh, J.F., Wiecki, T.V., Cohen, M.X., Figueroa, C.M., Samanta, J., Sherman, S.J., and Frank, M.J. (2011). Subthalamic nucleus stimulation reverses mediofrontal influence over decision threshold. Nat. Publ. Group *14*, 1462–1467.

Chagas, M.H.N., Linares, I.M.P., Garcia, G.J., Hallak, J.E.C., Tumas, V., and Crippa, J.A.S. (2013). Neuroimaging of depression in Parkinson's disease: a review. Int. Psychogeriatr. *25*, 1953–1961.

Chahine, L.M., and Stern, M.B. (2011). Diagnostic markers for Parkinson's disease. Curr. Opin. Neurol. *24*, 309–317.

Chahine, L.M., Stern, M.B., and Chen-Plotkin, A. (2013). Blood-based biomarkers for Parkinson's disease. Parkinsonism Relat. Disord. *20*, S99–S103.

Chan, C.S., Surmeier, D.J., and Yung, W. (2006). Striatal Information Signaling and Integration in Globus Pallidus: Timing Matters. Neurosignals *14*, 281–289.

Chaudhuri, K.R., Healy, D.G., Schapira, A.H.V., and National Institute for Clinical Excellence (2006). Non-motor symptoms of Parkinson's disease: diagnosis and management. Lancet Neurol. *5*, 235–245.

Cheng, K. (2012). Revealing human ocular dominance columns using high-resolution functional magnetic resonance imaging. NeuroImage *62*, 1029–1034.

Chevalier, G., and Deniau, J.M. (1990). Disinhibition as a basic process in the expression of striatal functions. Trends Neurosci. *13*, 277–280.

Christopher, L., and Strafella, A.P. (2013). Neuroimaging of brain changes associated with cognitive impairment in Parkinson's disease. J. Neuropsychol. *7*, 225–240.

Christopher, L., Koshimori, Y., Lang, A.E., Criaud, M., and Strafella, A.P. (2014). Uncovering the role of the insula in non-motor symptoms of Parkinson's disease. Brain *137*, 2143–2154.

Chung, C.L., and Mak, M.K.Y. (2016). Effect of Repetitive Transcranial Magnetic Stimulation on Physical Function and Motor Signs in Parkinson's Disease: A Systematic Review and Meta-Analysis. Brain Stimulat. *9*, 475–487.

Clarke, R., and Adermark, L. (2015). Dopaminergic Regulation of Striatal Interneurons in Reward and Addiction: Focus on Alcohol. Neural Plast. 1–11.

Cleary, D.R., Ozpinar, A., Raslan, A.M., and Ko, A.L. (2015). Deep brain stimulation for psychiatric disorders: where we are now. Neurosurg. Focus *38*, E2.

Cohen, M.R., and Kohn, A. (2011). Measuring and interpreting neuronal correlations. Nat. Neurosci. *14*, 811–819.

Conant, D., Bouchard, K.E., and Chang, E.F. (2014). Speech map in the human ventral sensory-motor cortex. Curr. Opin. Neurobiol. *24*, 63–67.

Conn, P.J., Battaglia, G., Marino, M.J., and Nicoletti, F. (2005). Metabotropic glutamate receptors in the basal ganglia motor circuit. Nat. Publ. Group *6*, 787–798.

Contreras-Vidal, J.L., and Schultz, W. (1999). A predictive reinforcement model of dopamine neurons for learning approach behavior. J. Comput. Neurosci. *6*, 191–214.

Cools, R. (2006). Dopaminergic modulation of cognitive function-implications for L-DOPA treatment in Parkinson's disease. Neurosci. Biobehav. Rev. *30*, 1–23.

Corti, O., Hampe, C., Darios, F., Ibanez, P., Ruberg, M., and Brice, A. (2005). Parkinson's disease: from causes to mechanisms. C. R. Biol. *328*, 131–142.

Crittenden, J.R., and Graybiel, A.M. (2011). Basal Ganglia disorders associated with imbalances in the striatal striosome and matrix compartments. Front. Neuroanat. *5*, 59.

Cunningham, D.A., Machado, A., Yue, G.H., Carey, J.R., and Plow, E.B. (2013). Functional somatotopy revealed across multiple cortical regions using a model of complex motor task. Brain Res. *1531*, 25–36.

Cyron, D. (2016). Mental Side Effects of Deep Brain Stimulation (DBS) for Movement Disorders: The Futility of Denial. Front. Integr. Neurosci. *10*, 1722.

Darbin, O., Soares, J., and Wichmann, T. (2006). Nonlinear analysis of discharge patterns in monkey basal ganglia. Brain Res. *1118*, 84–93.

Darbin, O., Dees, D., Martino, A., Adams, E., and Naritoku, D. (2013a). An Entropy-Based Model for Basal Ganglia Dysfunctions in Movement Disorders. BioMed Res. Int. *2013*, 1–5.

Darbin, O., Adams, E., Martino, A., Naritoku, L., Dees, D., and Naritoku, D. (2013b). Non-linear dynamics in parkinsonism. Front. Neurol. *4*, 211.

D'Ardenne, K., Eshel, N., Luka, J., Lenartowicz, A., Nystrom, L.E., and Cohen, J.D. (2012). Role of prefrontal cortex and the midbrain dopamine system in working memory updating. Proc. Natl. Acad. Sci. U. S. A. *109*, 19900–19909.

D'Ardenne, K., Lohrenz, T., Bartley, K.A., and Montague, P.R. (2013). Computational heterogeneity in the human mesencephalic dopamine system. Cogn. Affect. Behav. Neurosci. *13*, 747–756.

Dauer, W., and Przedborski, S. (2003). Parkinson's disease: mechanisms and models. Neuron *39*, 889–909.

Davie, C.A. (2008). A review of Parkinson's disease. Br. Med. Bull. *86*, 109–127.

Davis, T., and Poldrack, R.A. (2013). Measuring neural representations with fMRI: practices and pitfalls. Ann. N. Y. Acad. Sci. *1296*, 108–134.

Daw, N.D., Niv, Y., and Dayan, P. (2005). Uncertainty-based competition between prefrontal and dorsolateral striatal systems for behavioral control. Nat. Neurosci. *8*, 1704–1711.

Dawson, T.M., Ko, H.S., and Dawson, V.L. (2010). Genetic Animal Models of Parkinson's Disease. Neuron *66*, 646–661.

Dayan, P., and Daw, N.D. (2008). Decision theory, reinforcement learning, and the brain. Cogn. Affect. Behav. Neurosci. *8*, 429–453.

De Virgilio, A., Greco, A., Fabbrini, G., Inghilleri, M., Rizzo, M.I., Gallo, A., Conte, M., Rosato, C., Appiani, M.C., and de Vincentiis, M. (2016). Parkinson's disease: Autoimmunity and neuroinflammation. Autoimmun. Rev. *15*, 1005–1011.

Dechent, P., and Frahm, J. (2003). Functional somatotopy of finger representations in human primary motor cortex. Hum. Brain Mapp. *18*, 272–283.

Deco, G., Tononi, G., Boly, M., and Kringelbach, M.L. (2015). Rethinking segregation and integration: contributions of whole-brain modelling. Nat. Publ. Group *16*, 430–439.

Deffains, M., and Bergman, H. (2015). Striatal cholinergic interneurons and cortico-striatal synaptic plasticity in health and disease. Mov. Disord. *30*, 1014–1025.

Dejean, C., Gross, C.E., Bioulac, B., and Boraud, T. (2008). Dynamic Changes in the Cortex-Basal Ganglia Network After Dopamine Depletion in the Rat. J. Neurophysiol. *100*, 385–396.

Dejean, C., Nadjar, A., Le Moine, C., Bioulac, B., Gross, C.E., and Boraud, T. (2012). Evolution of the dynamic properties of the cortex–basal ganglia network after dopaminergic depletion in rats. Neurobiol. Dis. *46*, 402–413.

Del Tredici, K., and Braak, H. (2008). A not entirely benign procedure: progression of Parkinson's disease. Acta Neuropathol. (Berl.) *115*, 379–384.

Delmaire, C., Krainik, A., Tezenas du Montcel, S., Gerardin, E., Meunier, S., Mangin, J.F., Sangla, S., Garnero, L., Vidailhet, M., and Lehéricy, S. (2005). Disorganized somatotopy in the putamen of patients with focal hand dystonia. Neurology *64*, 1391–1396.

DeLong, M.R. (1990). Primate models of movement disorders of basal ganglia origin. Trends Neurosci.

DeLong, M., and Wichmann, T. (2009). Update on models of basal ganglia function and dysfunction. Parkinsonism Relat. Disord. *15*, S237–S240.

Denny-Brown, D., and Yanagisawa, N. (1976). The role of the basal ganglia in the initiation of movement. Res. Publ. - Assoc. Res. Nerv. Ment. Dis. *55*, 115–149.

Deuschl, G., and Bergman, H. (2002). Pathophysiology of nonparkinsonian tremors. Mov. Disord. Off. J. Mov. Disord. Soc. *17 Suppl 3*, S41–8.

Devan, B.D., Hong, N.S., and McDonald, R.J. (2011). Parallel associative processing in the dorsal striatum: Segregation of stimulus-response and cognitive control subregions. Neurobiol. Learn. Mem. *96*, 95–120.

Dias, V., Junn, E., and Mouradian, M.M. (2013). The role of oxidative stress in Parkinson's disease. J. Park. Dis. *3*, 461–491.

Diedrichsen, J., Ridgway, G.R., Friston, K.J., and Wiestler, T. (2011). Comparing the similarity and spatial structure of neural representations: A pattern-component model. NeuroImage *55*, 1665–1678.

Diedrichsen, J., Wiestler, T., and Krakauer, J.W. (2013). Two Distinct Ipsilateral Cortical Representations for Individuated Finger Movements. Cereb. Cortex *23*, 1362–1377.

Disbrow, E.A., Sigvardt, K.A., Franz, E.A., Turner, R.S., Russo, K.A., Hinkley, L.B., Herron, T.J., Ventura, M.I., Zhang, L., and Malhado-Chang, N. (2013). Movement activation and inhibition in Parkinson's disease: a functional imaging study. J. Park. Dis. *3*, 181–192.

Doya, K. (2000). Complementary roles of basal ganglia and cerebellum in learning and motor control. Curr. Opin. Neurobiol.

Doyon, J. (2008). Motor sequence learning and movement disorders. Curr. Opin. Neurol. *21*, 478–483.

Doyon, J., Bellec, P., Amsel, R., Penhune, V., Monchi, O., Carrier, J., Lehéricy, S., and Benali, H. (2009). Contributions of the basal ganglia and functionally related brain structures to motor learning. Behav. Brain Res. *199*, 61–75.

Draganski, B., Kherif, F., Kloppel, S., Cook, P.A., Alexander, D.C., Parker, G.J.M., Deichmann, R., Ashburner, J., and Frackowiak, R.S.J. (2008). Evidence for Segregated and Integrative Connectivity Patterns in the Human Basal Ganglia. J. Neurosci. *28*, 7143–7152.

Draganski, B., Ashburner, J., Hutton, C., Kherif, F., Frackowiak, R.S.J., Helms, G., and Weiskopf, N. (2011). Regional specificity of MRI contrast parameter changes in normal ageing revealed by voxel-based quantification (VBQ). NeuroImage *55*, 1423–1434.

Drayer, B., Burger, P., Darwin, R., Riederer, S., Herfkens, R., and Johnson, G.A. (1986). MRI of brain iron. AJR Am. J. Roentgenol. *147*, 103–110.

Dudman, J.T., and Krakauer, J.W. (2016). The basal ganglia: from motor commands to the control of vigor. Curr. Opin. Neurobiol. *37*, 158–166.

Duncan, G.W., Firbank, M.J., O'Brien, J.T., and Burn, D.J. (2013). Magnetic resonance imaging: A biomarker for cognitive impairment in Parkinson's disease? Mov. Disord. *28*, 425–438.

Dušek, P., Jankovic, J., and Le, W. (2012). Iron dysregulation in movement disorders. Neurobiol. Dis. *46*, 1–18.

Dušek, P., Dezortova, M., and Wuerfel, J. (2013). Imaging of iron. Int. Rev. Neurobiol. *110*, 195–239.

Duyn, J.H. (2012). The future of ultra-high field MRI and fMRI for study of the human brain. NeuroImage *62*, 1241–1248.

Edelman, G.M., and Gally, J.A. (2001). Degeneracy and complexity in biological systems. Proc. Natl. Acad. Sci. U. S. A. *98*, 13763–13768.

Eickhoff, S.B., Thirion, B., Varoquaux, G., and Bzdok, D. (2015). Connectivity-based parcellation: Critique and implications. Hum. Brain Mapp. *36*, 4771–4792.

van Eimeren, T., and Siebner, H.R. (2006). An update on functional neuroimaging of parkinsonism and dystonia. Curr. Opin. Neurol. *19*, 412–419.

Ejaz, N., Hamada, M., and Diedrichsen, J. (2015). Hand use predicts the structure of representations in sensorimotor cortex. Nat. Publ. Group.

Ekstrom, A. (2010). How and when the fMRI BOLD signal relates to underlying neural activity: the danger in dissociation. Brain Res. Rev. *62*, 233–244.

Ellens, D.J., and Leventhal, D.K. (2013). Electrophysiology of basal ganglia and cortex in models of Parkinson disease. J. Park. Dis. *3*, 241–254.

Erez, Y., Tischler, H., Belelovsky, K., and Bar-Gad, I. (2011). Dispersed Activity during Passive Movement in the Globus Pallidus of the 1-Methyl-4-Phenyl-1,2,3,6-Tetrahydropyridine (MPTP)-Treated Primate. PLoS ONE *6*, e16293.

Eriksen, J.L., Wszolek, Z., and Petrucelli, L. (2005). Molecular pathogenesis of Parkinson disease. Arch. Neurol. *62*, 353–357.

Fahn, S., Elton, R.L., and Members of the UPDRS committee (1987). The Unified Parkinson's Disease Rating Scale. In Recent Developments in Parkinson's Disease, S. Fahn, C.D. Marsden, D.B. Calne, and M. Goldstein, eds. (Florham Park, NJ: Macmillan Healthcare Information), pp. 153–163.

Feany, M.B. (2004). New genetic insights into Parkinson's disease. N. Engl. J. Med. *351*, 1937–1940.

Fearnley, J.M., and Lees, A.J. (1991). Ageing and Parkinson's disease: substantia nigra regional selectivity. Brain *114 (Pt 5)*, 2283–2301.

Feinberg, D.A., and Setsompop, K. (2013). Ultra-fast MRI of the human brain with simultaneous multi-slice imaging. J. Magn. Reson. *229*, 90–100.

Feng, L.R., and Maguire-Zeiss, K.A. (2010). Gene Therapy in Parkinson's Disease. CNS Drugs *24*, 177–192.

Fernandez, H.H., and Chen, J.J. (2007). Monoamine Oxidase-B Inhibition in the Treatment of Parkinson's Disease. Pharmacother. J. Ldots.

Filion, M., Tremblay, L., and Bédard, P.J. (1988). Abnormal influences of passive limb movement on the activity of globus pallidus neurons in parkinsonian monkeys. Brain Res. *444*, 165–176.

Fillard, P., Descoteaux, M., Goh, A., Gouttard, S., Jeurissen, B., Malcolm, J., Ramirez-Manzanares, A., Reisert, M., Sakaie, K., Tensaouti, F., et al. (2011). Quantitative evaluation of 10 tractography algorithms on a realistic diffusion MR phantom. NeuroImage *56*, 220–234.

Filograna, R., Beltramini, M., Bubacco, L., and Bisaglia, M. (2016). Anti-Oxidants in Parkinson's Disease Therapy: A Critical Point of View. Curr. Neurpharmacology *14*, 260–271.

Fink, G.R., Frackowiak, R.S., Pietrzyk, U., and Passingham, R.E. (1997). Multiple nonprimary motor areas in the human cortex. J. Neurophysiol. *77*, 2164–2174.

Fornito, A., and Bullmore, E.T. (2014). Connectomics_ A new paradigm for understanding brain disease. Eur. Neuropsychopharmacol. 1–16.

Fornito, A., Zalesky, A., and Breakspear, M. (2015). The connectomics of brain disorders. Nat. Publ. Group *16*, 159–172.

Forno, L.S. (1996). Neuropathology of Parkinson's disease. J. Neuropathol. Exp. Neurol. *55*, 259–272.

Francis, S., and Panchuelo, R.S. (2014). Physiological measurements using ultra-high field fMRI: a review. Physiol. Meas. *35*, R167–R185.

Frank, L.R. (2001). Anisotropy in high angular resolution diffusion-weighted MRI. Magn. Reson. Med. *45*, 935–939.

Frank, L.R. (2002). Characterization of anisotropy in high angular resolution diffusion-weighted MRI. Magn. Reson. Med. *47*, 1083–1099.

Frank, M. (2005). Dynamic dopamine modulation in the basal ganglia: a neurocomputational account of cognitive deficits in medicated and nonmedicated Parkinsonism. Cogn. Neurosci. J. Of *17*, 51–72.

Frank, M.J. (2004). By Carrot or by Stick: Cognitive Reinforcement Learning in Parkinsonism. Science *306*, 1940–1943.

Frank, M.J., Loughry, B., and O'Reilly, R.C. (2001). Interactions between frontal cortex and basal ganglia in working memory: a computational model. Cogn. Affect. Behav. Neurosci. *1*, 137–160.

Frank, M.J., Samanta, J., Moustafa, A.A., and Sherman, S.J. (2007). Hold Your Horses: Impulsivity, Deep Brain Stimulation, and Medication in Parkinsonism. Science *318*, 1309–1312.

Friston, K.J., and Price, C.J. (2003). Degeneracy and redundancy in cognitive anatomy. Trends Cogn. Sci. *7*, 151–152.

Friston, K.J., and Price, C.J. (2011). Modules and brain mapping. Cogn. Neuropsychol. *28*, 241–250.

Friston, K., Chu, C., Mourão-Miranda, J., Hulme, O., Rees, G., Penny, W., and Ashburner, J. (2008). Bayesian decoding of brain images. NeuroImage *39*, 181–205.

Friston, K.J., Holmes, A.P., Worsley, K.J., Poline, J.P., Frith, C.D., and Frackowiak, R.S. (1994). Statistical parametric maps in functional imaging: a general linear approach. Hum. Brain Mapp. *2*, 189–210.

Fudge, J.L., Kunishio, K., Walsh, P., Richard, C., and Haber, S.N. (2002). Amygdaloid projections to ventromedial striatal subterritories in the primate. NEUROSCIENCE *110*, 257–275.

Fujita, M., Ichise, M., Zoghbi, S.S., Liow, J.-S., Ghose, S., Vines, D.C., Sangare, J., Lu, J.-Q., Cropley, V.L., Iida, H., et al. (2005). Widespread decrease of nicotinic acetylcholine receptors in Parkinson's disease. Ann. Neurol. *59*, 174–177.

Gallea, C., Ewenczyk, C., Degos, B., Welter, M.-L., Grabli, D., Leu-Semenescu, S., Valabregue, R., Berroir, P., Yahia-Cherif, L., Bertasi, E., et al. (2017). Pedunculopontine network dysfunction in Parkinson's disease with postural control and sleep disorders. Mov. Disord.

Galvan, A., Devergnas, A., and Wichmann, T. (2015). Alterations in neuronal activity in basal ganglia-thalamocortical circuits in the parkinsonian state. Front. Neuroanat. *9*, 5.

Gandhi, S. (2005). Molecular pathogenesis of Parkinson's disease. Hum. Mol. Genet. *14*, 2749–2755.

Ganos, C., Bongert, J., Asmuss, L., Martino, D., Haggard, P., and Münchau, A. (2015). The somatotopy of tic inhibition: Where and how much? Mov. Disord. *30*, 1184–1189.

Gao, L., and Wu, T. (2016). The study of brain functional connectivity in Parkinson's disease. Transl. Neurodegener. 1–7.

Garbayo, E., Ansorena, E., and Blanco-Prieto, M.J. (2013). Drug development in Parkinson's disease: From emerging molecules to innovative drug delivery systems. Maturitas *76*, 272–278.

Gelb, D.J., Oliver, E., and Gilman, S. (1999). Diagnostic criteria for Parkinson disease. Arch. Neurol. *56*, 33–39.

Georgiev, D., Lange, F., Seer, C., Kopp, B., and Jahanshahi, M. (2016). Movement-related potentials in Parkinson's disease. Clin. Neurophysiol. Off. J. Int. Fed. Clin. Neurophysiol. *127*, 2509–2519.

Gerardin, E., Lehéricy, S., Pochon, J.-B., Tézenas du Montcel, S., Mangin, J.-F., Poupon, F., Agid, Y., Le Bihan, D., and Marsault, C. (2003). Foot, hand, face and eye representation in the human striatum. Cereb. Cortex *13*, 162–169.

Gerfen, C.R., and Surmeier, D.J. (2011). Modulation of Striatal Projection Systems by Dopamine. Annu. Rev. Neurosci. *34*, 441–466.

Gh Popescu, B.F., and Nichol, H. (2010). Mapping Brain Metals to Evaluate Therapies for Neurodegenerative Disease. CNS Neurosci. Ther. *17*, 256–268.

Gillies, A., and Arbuthnott, G. (2000). Computational models of the basal ganglia. Mov. Disord. Off. J. Mov. Disord. Soc. *15*, 762–770.

Gittis, A.H., and Kreitzer, A.C. (2012). Striatal microcircuitry and movement disorders. Trends Neurosci. *35*, 557–564.

Gläscher, J., Daw, N., Dayan, P., and Doherty, J.P.O. (2010). States versus Rewards: Dissociable Neural Prediction Error Signals Underlying Model-Based and Model-Free Reinforcement Learning. Neuron *66*, 585–595.

Godau, J., Hussl, A., Lolekha, P., Stoessl, A.J., and Seppi, K. (2012). Neuroimaging: Current role in detecting pre-motor Parkinson's disease. Mov. Disord. *27*, 634–643.

Goedert, M., Spillantini, M.G., Del Tredici, K., and Braak, H. (2012). 100 years of Lewy pathology. Nat. Rev. Neurol. *9*, 13–24.

Goetz, C.G. (2011). The History of Parkinson's Disease: Early Clinical Descriptions and Neurological Therapies. Cold Spring Harb. Perspect. Med. *1*, a008862–a008862.

Goetz, C.G., Tilley, B.C., Shaftman, S.R., Stebbins, G.T., Fahn, S., Martinez-Martin, P., Poewe, W., Sampaio, C., Stern, M.B., Dodel, R., et al. (2008). Movement Disorder Society-sponsored revision of the Unified Parkinson's Disease Rating Scale (MDS-UPDRS): Scale presentation and clinimetric testing results. Mov. Disord. *23*, 2129–2170.

Golbe, L.I. (1999). Alpha-synuclein and Parkinson's disease. Mov. Disord. *14*, 6–9.

Goldberg, J.A., Boraud, T., Maraton, S., Haber, S.N., Vaadia, E., and Bergman, H. (2002). Enhanced synchrony among primary motor cortex neurons in the 1-methyl-4-phenyl-1,2,3,6-tetrahydropyridine primate model of Parkinson's disease. J. Neurosci. *22*, 4639–4653.

Goldberg, J.H., Farries, M.A., and Fee, M.S. (2013). Basal ganglia output to the thalamus: still a paradox. Trends Neurosci. *36*, 695–705.

Goto, Y., Otani, S., and Grace, A.A. (2007). The Yin and Yang of dopamine release: a new perspective. Neurophysiol. Clin. Neurophysiol. *53*, 583–587.

Goveas, J., O'Dwyer, L., Mascalchi, M., Cosottini, M., Diciotti, S., De Santis, S., Passamonti, L., Tessa, C., Toschi, N., and Giannelli, M. (2015). Diffusion-MRI in neurodegenerative disorders. Magn. Reson. Imaging *33*, 853–876.

Grabski, K., Lamalle, L., Vilain, C., Schwartz, J.-L., Vallée, N., Tropres, I., Baciu, M., Le Bas, J.-F., and Sato, M. (2012). Functional MRI assessment of orofacial articulators: neural correlates of lip, jaw, larynx, and tongue movements. Hum. Brain Mapp. *33*, 2306–2321.

Graybiel, A.M. (1990). Neurotransmitters and neuromodulators in the basal ganglia. Trends Neurosci. *13*, 244–254.

Graybiel, A.M. (1998). The basal ganglia and chunking of action repertoires. Neurobiol. Learn. Mem. *70*, 119–136.

Graybiel, A.M. (2008). Habits, Rituals, and the Evaluative Brain. Annu. Rev. Neurosci. *31*, 359–387.

Graybiel, A.M., Aosaki, T., Flaherty, A.W., and Kimura, M. (1994). The basal ganglia and adaptive motor control. Science *265*, 1826–1831.

Graziano, M.S.A., and Aflalo, T.N. (2007a). Mapping Behavioral Repertoire onto the Cortex. Neuron *56*, 239–251.

Graziano, M.S.A., and Aflalo, T.N. (2007b). Rethinking Cortical Organization: Moving Away from Discrete Areas Arranged in Hierarchies. The Neuroscientist *13*, 138–147.

Green, D.W., Crinion, J., and Price, C.J. (2006). Convergence, degeneracy and control. Lang. Learn. *56*, 99–125.

Grillner, S., and Robertson, B. (2016). The Basal Ganglia Over 500 Million Years. Curr. Biol. *26*, R1088–R1100.

Grill-Spector, K., and Malach, R. (2004). The human visual cortex. Annu. Rev. Neurosci. *27*, 649–677.

Gruber, A.J. (2003). Modulation of Striatal Single Units by Expected Reward: A Spiny Neuron Model Displaying Dopamine-Induced Bistability. J. Neurophysiol. *90*, 1095–1114.

Guillery, R.W., and Sherman, S.M. (2002). The thalamus as a monitor of motor outputs. Philos. Trans. R. Soc. B Biol. Sci. *357*, 1809–1821.

Gurney, K., Prescott, T.J., and REDGRAVE, P. (2001a). A computational model of action selection in the basal ganglia. I. A new functional anatomy. Biol. Cybern. *84*, 401–410.

Gurney, K., Prescott, T.J., and REDGRAVE, P. (2001b). A computational model of action selection in the basal ganglia. II. Analysis and simulation of behaviour. Biol. Cybern. *84*, 411–423.

Guthrie, M., Myers, C.E., and Gluck, M.A. (2009). A neurocomputational model of tonic and phasic dopamine in action selection: a comparison with cognitive deficits in Parkinson's disease. Behav. Brain Res. *200*, 48–59.

Haacke, E.M., Cheng, N.Y.C., House, M.J., Liu, Q., Neelavalli, J., Ogg, R.J., Khan, A., Ayaz, M., Kirsch, W., and Obenaus, A. (2005). Imaging iron stores in the brain using magnetic resonance imaging. Magn. Reson. Imaging *23*, 1–25.

Haber, S.N. (2003). The primate basal ganglia: parallel and integrative networks. J. Chem. Neuroanat. *26*, 317–330.

Haber, S.N. (2016). Corticostriatal circuitry. Dialogues Clin. Neurosci. *18*, 7–21.

Haber, S.N., and Calzavara, R. (2009). The cortico-basal ganglia integrative network: The role of the thalamus. Brain Res. Bull. *78*, 69–74.

Haber, S.N., and Knutson, B. (2009). The Reward Circuit: Linking Primate Anatomy and Human Imaging. Neuropsychopharmacology *35*, 4–26.

Haber, S.N., Fudge, J.L., and McFarland, N.R. (2000). Striatonigrostriatal pathways in primates form an ascending spiral from the shell to the dorsolateral striatum. J. Neurosci. *20*, 2369–2382.

Haegelen, C., Rouaud, T., Darnault, P., and Morandi, X. (2009). The subthalamic nucleus is a key-structure of limbic basal ganglia functions. Med. HYPOTHESES *72*, 421–426.

Haelterman, N.A., Yoon, W.H., Sandoval, H., Jaiswal, M., Shulman, J.M., and Bellen, H.J. (2014). A Mitocentric View of Parkinson's Disease. Annu. Rev. Neurosci. *37*, 137–159.

Hagmann, P., Cammoun, L., Gigandet, X., Meuli, R., Honey, C.J., Wedeen, V.J., and Sporns, O. (2008). Mapping the structural core of human cerebral cortex. PLoS Biol. *6*, e159.

Hagmann, P., Cammoun, L., Gigandet, X., Gerhard, S., Grant, P.E., Wedeen, V., Meuli, R., Thiran, J.-P., Honey, C.J., and Sporns, O. (2010). MR connectomics: Principles and challenges. J. Neurosci. Methods *194*, 34–45.

Halliday, G.M. (2009). Thalamic changes in Parkinson's disease. Park. Realt. Disord. *15*, S152–S155.

Halliday, G.M., Leverenz, J.B., Schneider, J.S., and Adler, C.H. (2014). The neurobiological basis of cognitive impairment in Parkinson's disease. Mov. Disord. *29*, 634–650.

Hardy, J. (2010). Genetic Analysis of Pathways to Parkinson Disease. Neuron *68*, 201–206.

Hare, D.J., and Double, K.L. (2016). Iron and dopamine: a toxic couple. Brain *139*, 1026–1035.

Harel, N. (2012). Ultra high resolution fMRI at ultra-high field. NeuroImage *62*, 1024–1028.

Hauser, R.A. (2009). Levodopa: Past, Present, and Future. Eur. Neurol. *62*, 1–8.

Hawkes, C.H., Del Tredici, K., and Braak, H. (2009). Parkinson's disease: the dual hit theory revisited. Ann. N. Y. Acad. Sci. *1170*, 615–622.

Hazy, T.E., Frank, M.J., and O'Reilly, R.C. (2007). Towards an executive without a homunculus: computational models of the prefrontal cortex/basal ganglia system. Philos. Trans. R. Soc. B Biol. Sci. *362*, 1601–1613.

Heeger, D.J., and Ress, D. (2002). What does fMRI tell us about neuronal activity? Nat. Rev. Neurosci. *3*, 142–151.

Heimer, G., Rivlin-Etzion, M., Bar-Gad, I., Goldberg, J.A., Haber, S.N., and Bergman, H. (2006). Dopamine Replacement Therapy Does Not Restore the Full Spectrum of Normal Pallidal Activity in the 1-Methyl-4-Phenyl-1,2,3,6-Tetra-Hydropyridine Primate Model of Parkinsonism. J. Neurosci. *26*, 8101–8114.

Hélie, S., Paul, E.J., and Ashby, F.G. (2011). Simulating Parkinson's disease patient deficits using a COVIS-based computational model. 207–214.

Helmich, R.C., Derikx, L.C., Bakker, M., Scheeringa, R., Bloem, B.R., and Toni, I. (2010). Spatial Remapping of Cortico-striatal Connectivity in Parkinson's Disease. Cereb. Cortex *20*, 1175–1186.

Helmich, R.C., Hallett, M., Deuschl, G., Toni, I., and Bloem, B.R. (2012). Cerebral causes and consequences of parkinsonian resting tremor: a tale of two circuits? Brain *135*, 3206–3226.

Helms, G., Draganski, B., Frackowiak, R., Ashburner, J., and Weiskopf, N. (2009). Improved segmentation of deep brain grey matter structures using magnetization transfer (MT) parameter maps. NeuroImage *47*, 194–198.

Henderson, L.A., Gandevia, S.C., and Macefield, V.G. (2007). Somatotopic organization of the processing of muscle and cutaneous pain in the left and right insula cortex: A single-trial fMRI study. Pain *128*, 20–30.

Henderson, L.A., Rubin, T.K., and Macefield, V.G. (2010). Within-limb somatotopic representation of acute muscle pain in the human contralateral dorsal posterior insula. Hum. Brain Mapp. *32*, 1592–1601.

Henson, R.N.A. (2011). Efficient experimental design for fMRI. In Statistical Parametric Mapping: The Analysis of Functional Brain Images: The Analysis of Functional Brain Images, (Academic Press), p.

Herrero, M.-T., Barcia, C., and Navarro, J.M. (2002). Functional anatomy of thalamus and basal ganglia. Childs Nerv. Syst. ChNS Off. J. Int. Soc. Pediatr. Neurosurg. *18*, 386–404.

Hickey, P., and Stacy, M. (2016). Deep Brain Stimulation: A Paradigm Shifting Approach to Treat Parkinson's Disease. Front. Neurosci. *10*, 76.

Higuchi, Y., Matsuda, S., and Serizawa, T. (2016). Gamma knife radiosurgery in movement disorders: Indications and limitations. Mov. Disord. *32*, 28–35.

Hikosaka, O., Kim, H.F., Yasuda, M., and Yamamoto, S. (2014). Basal Ganglia circuits for reward value-guided behavior. Annu. Rev. Neurosci. *37*, 289–306.

Hillman, E.M.C. (2014). Coupling Mechanism and Significance of the BOLD Signal: A Status Report. Annu. Rev. Neurosci. *37*, 161–181.

Hjorth, J., Blackwell, K.T., and Hellgren Kotaleski, J. (2009). Gap Junctions between Striatal Fast-Spiking Interneurons Regulate Spiking Activity and Synchronization as a Function of Cortical Activity. J. Neurosci. *29*, 5276–5286.

Hlustik, P., Solodkin, A., Gullapalli, R.P., Noll, D.C., and Small, S.L. (2001). Somatotopy in human primary motor and somatosensory hand representations revisited. Cereb. Cortex N. Y. N 1991 *11*, 312–321.

Hoehn, M.M., and Yahr, M.D. (1967). Parkinsonism: onset, progression and mortality. Neurology *17*, 427–442.

Hollerman, J.R., and Schultz, W. (1998). Dopamine neurons report an error in the temporal prediction of reward during learning. Nat. Neurosci. *1*, 304–309.

Hoover, J.E., and Strick, P.L. (1993). Multiple output channels in the basal ganglia. Science.

Horvitz, J.C., Stewart, T., and Jacobs, B.L. (1997). Burst activity of ventral tegmental dopamine neurons is elicited by sensory stimuli in the awake cat. Brain Res. *759*, 251–258.

Hotter, A., Esterhammer, R., Schocke, M.F.H., and Seppi, K. (2009). Potential of advanced MR imaging techniques in the differential diagnosis of parkinsonism. Mov. Disord. *24*, S711–S720.

Houk, J.C. (2005). Agents of the mind. Biol. Cybern. *92*, 427–437.

Houk, J.C., Adams, J.L., and Barto, A.G. (1995). A model of how the basal ganglia generate and use neural signals that predict reinforcement. In Models of Information Processing in the Basal Ganglia, (Cambridge, MA: MIT Press), pp. 249–274.

Houk, J.C., Bastianen, C., Fansler, D., Fishbach, A., Fraser, D., Reber, P.J., Roy, S.A., and Simo, L.S. (2007). Action selection and refinement in subcortical loops through basal ganglia and cerebellum. Philos. Trans. R. Soc. B Biol. Sci. *362*, 1573–1583.

Hughes, A.J., Daniel, S.E., and Kilford, L. (1992). Accuracy of clinical diagnosis of idiopathic Parkinson's disease: a clinico-pathological study of 100 cases. J. Neurol. Neurosurg. Psychiatry 181–184.

Humphries, M.D., Stewart, R.D., and Gurney, K.N. (2006). A Physiologically Plausible Model of Action Selection and Oscillatory Activity in the Basal Ganglia. J. Neurosci. *26*, 12921–12942.

Hyde, J.S., Biswal, B.B., and Jesmanowicz, A. (2001). High-resolution fMRI using multislice partial k-space GR-EPI with cubic voxels. Magn. Reson. Med. *46*, 114–125.

Ibarretxe-Bilbao, N., Tolosa, E., Junque, C., and Martí, M.J. (2009). MRI and cognitive impairment in Parkinson's disease. Mov. Disord. *24*, S748–S753.

Ibarretxe-Bilbao, N., Junque, C., Marti, M.J., and Tolosa, E. (2011). Brain structural MRI correlates of cognitive dysfunctions in Parkinson's disease. J. Neurol. Sci. *310*, 70–74.

Indovina, I., and Sanes, J.N. (2001). On Somatotopic Representation Centers for Finger Movements in Human Primary Motor Cortex and Supplementary Motor Area. NeuroImage *13*, 1027–1034.

Irwin, D.J., Y, L.V.M., and Trojanowski, J.Q. (2013). Parkinson's disease dementia: convergence of α-synuclein, tau and amyloid-β pathologies. Nat. Publ. Group *14*, 626–636.

Iwamuro, H. (2011). Electrophysiological evidences of organization of cortical motor information in the Basal Ganglia. J. Mov. Disord. *4*, 8–12.

Jagmag, S.A., Tripathi, N., Shukla, S.D., Maiti, S., and Khurana, S. (2016). Evaluation of Models of Parkinson's Disease. Front. Neurosci. *9*, 6428.

Jahanshahi, M., Obeso, I., Rothwell, J.C., and Obeso, J.A. (2015). A fronto–striato–subthalamic–pallidal network for goal-directed and habitual inhibition. Nat. Publ. Group *16*, 719–732.

Jaidar, O., Carrillo-Reid, L., Hernandez, A., Drucker-Colin, R., Bargas, J., and Hernandez-Cruz, A. (2010). Dynamics of the Parkinsonian Striatal Microcircuit: Entrainment into a Dominant Network State. J. Neurosci. *30*, 11326–11336.

Jankovic, J. (2008). Parkinson's disease: clinical features and diagnosis. J. Neurol. Neurosurg. Psychiatry *79*, 368–376.

Jellinger, K.A. (2009). Formation and development of Lewy pathology: a critical update. J. Neurol. *256*, 270–279.

Jellinger, K.A. (2011). Neuropathology of sporadic Parkinson's disease: Evaluation and changes of concepts. Mov. Disord. *27*, 8–30.

Jesmanowicz, A., Bandettini, P.A., and Hyde, J.S. (1998). Single-shot half k-space high-resolution gradient-recalled EPI for fMRI at 3 Tesla. Magn. Reson. Med. *40*, 754–762.

Joel, D., and Weiner, I. (1997). The connections of the primate subthalamic nucleus: indirect pathways and the open-interconnected scheme of basal ganglia-thalamocortical circuitry. Brain Res. Brain Res. Rev. *23*, 62–78.

Joel, D., and Weiner, I. (2000). The connections of the dopaminergic system with the striatum in rats and primates: an analysis with respect to the functional and compartmental organization of the striatum. NEUROSCIENCE *96*, 451–474.

Joel, D., Niv, Y., and Ruppin, E. (2002). Actor-critic models of the basal ganglia: new anatomical and computational perspectives. Neural Netw. Off. J. Int. Neural Netw. Soc. *15*, 535–547.

Johansen-Berg, H., and Rushworth, M.F.S. (2009). Using Diffusion Imaging to Study Human Connectional Anatomy. Annu. Rev. Neurosci. *32*, 75–94.

Jones, D.K., and Basser, P.J. (2004). "Squashing peanuts and smashing pumpkins": how noise distorts diffusion-weighted MR data. Magn. Reson. Med. *52*, 979–993.

Jones, D.K., and Cercignani, M. (2010). Twenty-five pitfalls in the analysis of diffusion MRI data. NMR Biomed. *23*, 803–820.

Jones, D.K., Knösche, T.R., and Turner, R. (2013). White matter integrity, fiber count, and other fallacies: The do's and don'ts of diffusion MRI. NeuroImage *73*, 239–254.

Kaakkola, S. (2010). Problems with the Present Inhibitors and a Relevance of New and Improved COMT Inhibitors in Parkinson's Disease. In Basic Aspects of Catechol-O-Methyltransferase and the Clinical Applications of Its Inhibitors, E. Nissinen, ed. (Academic Press), pp. 207–225.

Kaji, Y., and Hirata, K. (2011). Apathy and Anhedonia in Parkinson's Disease. ISRN Neurol. *2011*, 1–9.

Kalia, L.V., and Lang, A.E. (2015). Parkinson's disease. The Lancet *386*, 896–912.

Kamali Sarvestani, I., Lindahl, M., Hellgren-Kotaleski, J., and Ekeberg, O. (2011). The arbitration-extension hypothesis: a hierarchical interpretation of the functional organization of the Basal Ganglia. Front. Syst. Neurosci. *5*, 13.

Kaneda, K., Nambu, A., Tokuno, H., and Takada, M. (2002). Differential processing patterns of motor information via striatopallidal and striatonigral projections. J. Neurophysiol. *88*, 1420–1432.

Kanold, P.O., Nelken, I., and Polley, D.B. (2014). Local versus global scales of organization in auditory cortex. Trends Neurosci. *37*, 502–510.

Kapreli, E., Athanasopoulos, S., Papathanasiou, M., Van Hecke, P., Kelekis, D., Peeters, R., Strimpakos, N., and Sunaert, S. (2007). Lower Limb Sensorimotor Network: Issues of Somatotopy and Overlap. CORTEX *43*, 219–232.

Kassavetis, P., Sadnicka, A., Saifee, T.A., Belvisi, D., van den Bos, M., Pareés, I., Kojovic, M., Rothwell, J.C., and Edwards, M.J. (2014). Motor "surround inhibition" is not correlated with activity in surround muscles. Eur. J. Neurosci. *40*, 2541–2547.

Ke, Y., and Ming Qian, Z. (2003). Iron misregulation in the brain: a primary cause of neurodegenerative disorders. Lancet Neurol. *2*, 246–253.

Keeler, J.F., Pretsell, D.O., and Robbins, T.W. (2014). Functional implications of dopamine D1 vs. D2 receptors: A "prepare and select" model of the striatal direct vs. indirect pathways. NEUROSCIENCE *282*, 156–175.

Kempster, P.A., O'Sullivan, S.S., Holton, J.L., Revesz, T., and Lees, A.J. (2010). Relationships between age and late progression of Parkinson's disease: a clinico-pathological study. Brain *133*, 1755–1762.

Keuken, M.C., Bazin, P.L., Crown, L., Hootsmans, J., Laufer, A., Müller-Axt, C., Sier, R., van der Putten, E.J., Schäfer, A., Turner, R., et al. (2014). Quantifying inter-individual anatomical variability in the subcortex using 7T structural MRI. NeuroImage *94*, 40–46.

Kim, K., Müller, M.L.T.M., Bohnen, N.I., Sarter, M., and Lustig, C. (2017). Thalamic cholinergic innervation makes a specific bottom-up contribution to signal detection_ Evidence from Parkinson's disease patients with defined cholinergic losses. NeuroImage *149*, 295–304.

Kincaid, A.E., Zheng, T., and Wilson, C.J. (1998). Connectivity and convergence of single corticostriatal axons. J. Neurosci. Off. J. Soc. Neurosci. *18*, 4722–4731.

Kirilina, E., Lutti, A., Poser, B.A., Blankenburg, F., and Weiskopf, N. (2016). The quest for the best: The impact of different EPI sequences on the sensitivity of random effect fMRI group analyses. NeuroImage *126*, 49–59.

Kirsch-Darrow, L., Marsiske, M., Okun, M.S., Bauer, R., and Bowers, D. (2011). Apathy and Depression: Separate Factors in Parkinson's Disease. J. Int. Neuropsychol. Soc. *17*, 1058–1066.

Kita, H. (2007). Globus pallidus external segment. In Gaba and the Basal Ganglia: From Molecules to Systems, E.D.A. James M Tepper, and J.P. Bolam, eds. (Elsevier), pp. 111–133.

Klein, J.C., Rushworth, M.F.S., Behrens, T.E.J., Mackay, C.E., de Crespigny, A.J., D'Arceuil, H., and Johansen-Berg, H. (2010). Topography of connections between human prefrontal

cortex and mediodorsal thalamus studied with diffusion tractography. NeuroImage *51*, 555–564.

Kleinschmidt, A., Nitschke, M.F., and Frahm, J. (1997). Somatotopy in the human motor cortex hand area. A high-resolution functional MRI study. Eur. J. Neurosci. *9*, 2178–2186.

Koller, W.C., and Rueda, M.G. (1998). Mechanism of action of dopaminergic agents in Parkinson's disease. Neurology *50*, S11–4– NaN–8.

Kolomiets, B.P., Deniau, J.M., Mailly, P., Ménétrey, A., Glowinski, J., and Thierry, A.M. (2001). Segregation and convergence of information flow through the cortico-subthalamic pathways. J. Neurosci. *21*, 5764–5772.

Kolomiets, B.P., Deniau, J.M., Glowinski, J., and Thierry, A.M. (2003). Basal ganglia and processing of cortical information: functional interactions between trans-striatal and trans-subthalamic circuits in the substantia nigra pars reticulata. NEUROSCIENCE *117*, 931–938.

Kostic, V.S., and Filippi, M. (2011). Neuroanatomical correlates of depression and apathy in Parkinson's disease: Magnetic resonance imaging studies. J. Neurol. Sci. *310*, 61–63.

Kostic, V.S., Agosta, F., Pievani, M., Stefanova, E., Jecmenica-Lukic, M., Scarale, A., Spica, V., and Filippi, M. (2012). Pattern of brain tissue loss associated with freezing of gait in Parkinson disease. Neurology *78*, 409–416.

Kreitzer, A.C. (2009). Physiology and Pharmacology of Striatal Neurons. Annu. Rev. Neurosci. *32*, 127–147.

Kreitzer, A.C., and Berke, J.D. (2011). Investigating striatal function through cell-type-specific manipulations. NEUROSCIENCE *198*, 19–26.

Kreitzer, A.C., and Malenka, R.C. (2008). Striatal Plasticity and Basal Ganglia Circuit Function. Neuron *60*, 543–554.

Kriegeskorte, N. (2008). Representational similarity analysis – connecting the branches of systems neuroscience. Front. Syst. Neurosci. *2*, 4.

Kriegeskorte, N., and Kievit, R.A. (2013). Representational geometry: integrating cognition, computation, and the brain. Trends Cogn. Sci. *17*, 401–412.

Kurth, F., Zilles, K., Fox, P.T., Laird, A.R., and Eickhoff, S.B. (2010). A link between the systems: functional differentiation and integration within the human insula revealed by meta-analysis. Brain Struct. Funct. *214*, 519–534.

Lambert, C., Zrinzo, L., Nagy, Z., Lutti, A., Hariz, M., Foltynie, T., Draganski, B., Ashburner, J., and Frackowiak, R. (2012). Confirmation of functional zones within the human subthalamic nucleus: Patterns of connectivity and sub-parcellation using diffusion weighted imaging. NeuroImage *60*, 83–94.

Lambert, C., Simon, H., Colman, J., and Barrick, T.R. (2016). Defining Thalamic Nuclei and Topographic Connectivity Gradients in vivo. NeuroImage 1–40.

Lanciego, J.L., Luquin, N., and Obeso, J.A. (2012). Functional Neuroanatomy of the Basal Ganglia. Cold Spring Harb. Perspect. Med. *2*, a009621–a009621.

Lang, A.E., and Lozano, A.M. (1998a). Parkinson's disease. First of two parts. N. Engl. J. Med. *339*, 1044–1053.

Lang, A.E., and Lozano, A.M. (1998b). Parkinson's disease. Second of two parts. N. Engl. J. Med. *339*, 1130–1143.

Langston, J.W., Ballard, P., Tetrud, J.W., and Irwin, I. (1983). Chronic Parkinsonism in humans due to a product of meperidine-analog synthesis. Science *219*, 979–980.

de Lau, L.M., and Breteler, M.M. (2006). Epidemiology of Parkinson's disease. Lancet Neurol. *5*, 525–535.

Le Bihan, D. (2012). Diffusion, confusion and functional MRI. NeuroImage *62*, 1131–1136.

Le Bihan, D., Mangin, J.F., Poupon, C., Clark, C.A., Pappata, S., Molko, N., and Chabriat, H. (2001). Diffusion tensor imaging: concepts and applications. J. Magn. Reson. Imaging *13*, 534–546.

Leblois, A., Meissner, W., Bezard, E., Bioulac, B., Gross, C.E., and Boraud, T. (2006). Temporal and spatial alterations in GPi neuronal encoding might contribute to slow down movement in Parkinsonian monkeys. Eur. J. Neurosci. *24*, 1201–1208.

Leblois, A., Meissner, W., Bioulac, B., Gross, C.E., Hansel, D., and Boraud, T. (2007). Late emergence of synchronized oscillatory activity in the pallidum during progressive parkinsonism. Eur. J. Neurosci. *26*, 1701–1713.

Lees, A.J. (1989). The on-off phenomenon. J. Neurol. Neurosurg. Psychiatry *Suppl*, 29–37.

Lehéricy, S., Sharman, M.A., Santos, C.L.D., Paquin, R., and Gallea, C. (2012). Magnetic resonance imaging of the substantia nigra in Parkinson's disease. Mov. Disord. *27*, 822–830.

Lehéricy, S., Bardinet, E., Poupon, C., Vidailhet, M., and Francois, C. (2014). 7 tesla magnetic resonance imaging: A closer look at substantia nigra anatomy in Parkinson's disease. Mov. Disord. *29*, 1574–1581.

Lei, W. (2004). Evidence for Differential Cortical Input to Direct Pathway versus Indirect Pathway Striatal Projection Neurons in Rats. J. Neurosci. *24*, 8289–8299.

Lenglet, C., Abosch, A., Yacoub, E., De Martino, F., Sapiro, G., and Harel, N. (2012). Comprehensive in vivo Mapping of the Human Basal Ganglia and Thalamic Connectome in Individuals Using 7T MRI. PLoS ONE *7*, e29153.

Lenka, A., Jhunjhunwala, K.R., Saini, J., and Pal, P.K. (2015). Structural and functional neuroimaging in patients with Parkinson's disease and visual hallucinations: A critical review. Park. Realt. Disord. *21*, 683–691.

Levine, A.J., Lewallen, K.A., and Pfaff, S.L. (2012). Spatial organization of cortical and spinal neurons controlling motor behavior. Curr. Opin. Neurobiol. *22*, 812–821.

Levy, R., Hutchison, W.D., Lozano, A.M., and Dostrovsky, J.O. (2000). High-frequency synchronization of neuronal activity in the subthalamic nucleus of parkinsonian patients with limb tremor. J. Neurosci. *20*, 7766–7775.

Levy, R., Dostrovsky, J.O., Lang, A.E., Sime, E., Hutchison, W.D., and Lozano, A.M. (2001). Effects of apomorphine on subthalamic nucleus and globus pallidus internus neurons in patients with Parkinson's disease. J. Neurophysiol. *86*, 249–260.

Levy, R., Hutchison, W.D., Lozano, A.M., and Dostrovsky, J.O. (2002). Synchronized neuronal discharge in the basal ganglia of parkinsonian patients is limited to oscillatory activity. J. Neurosci. *22*, 2855–2861.

LeWitt, P.A., and Fahn, S. (2016). Levodopa therapy for Parkinson disease: A look backward and forward. Neurology *86*, S3–12.

Lieu, C.A., and Subramanian, T. (2012). The interhemispheric connections of the striatum: Implications for Parkinson's disease and drug-induced dyskinesias. Brain Res. Bull. *87*, 1–9.

Lilienfeld, D.E., and Perl, D.P. (1994). Projected neurodegenerative disease mortality among minorities in the United States, 1990-2040. Neuroepidemiology *13*, 179–186.

Lill, C.M. (2016). Genetics of Parkinson's disease. Mol. Cell. Probes *30*, 386–396.

Lim, S.A.O., Kang, U.J., and McGehee, D.S. (2014). Striatal cholinergic interneuron regulation and circuit effects. Front. Synaptic Neurosci. *6*, 22.

Lima, M., Martins, E., Delattre, A., Proença, M., Mori, M., Carabelli, B., and Ferraz, A. (2012). Motor and non-motor features of Parkinson's disease–a review of clinical and experimental studies. CNS Neurol. Disord.-Drug Targets Former. Curr. Drug Targets-CNS Neurol. Disord. *11*, 439–449.

Lin, F.-H., Tsai, K.W.K., Chu, Y.-H., Witzel, T., Nummenmaa, A., Raij, T., Ahveninen, J., Kuo, W.-J., and Belliveau, J.W. (2012). Ultrafast inverse imaging techniques for fMRI. NeuroImage *62*, 699–705.

Lipsman, N., Woodside, B., and Lozano, A.M. (2013). Chapter 22 - Evaluating the potential of deep brain stimulation for treatment-resistant anorexia nervosa. In Brain Stimulation, A.M. Lozano, and M. Hallett, eds. (Elsevier), pp. 271–276.

Liu, T.T. (2016). Noise contributions to the fMRI signal: An overview. NeuroImage *143*, 141–151.

Liu, C., Li, W., Tong, K.A., Yeom, K.W., and Kuzminski, S. (2014). Susceptibility-weighted imaging and quantitative susceptibility mapping in the brain. J. Magn. Reson. Imaging *42*, 23–41.

Logothetis, N.K. (2008). What we can do and what we cannot do with fMRI. Nature *453*, 869–878.

Logothetis, N.K., and Wandell, B.A. (2004). Interpreting the BOLD Signal. Annu. Rev. Physiol. *66*, 735–769.

Logothetis, N.K., Pauls, J., Augath, M., Trinath, T., and Oeltermann, A. (2001). Neurophysiological investigation of the basis of the fMRI signal. Nature *412*, 150–157.

Lorio, S., Kherif, F., Ruef, A., Melie-Garcia, L., Frackowiak, R., Ashburner, J., Helms, G., Lutti, A., and Draganski, B. (2016). Neurobiological origin of spurious brain morphological changes: A quantitative MRI study. Hum. Brain Mapp. *37*, 1801–1815.

Lotharius, J., and Brundin, P. (2002). Pathogenesis of parkinson's disease: dopamine, vesicles and α-synuclein. Nat. Rev. Neurosci. *3*, 932–942.

Lotze, M., Erb, M., Flor, H., Huelsmann, E., Godde, B., and Grodd, W. (2000). fMRI Evaluation of Somatotopic Representation in Human Primary Motor Cortex. NeuroImage *11*, 473–481.

Lozano, A.M., Dostrovsky, J., Chen, R., and Ashby, P. (2002). Deep brain stimulation for Parkinson's disease: disrupting the disruption. Lancet Neurol. *1*, 225–231.

Lutti, A., Thomas, D.L., Hutton, C., and Weiskopf, N. (2012). High-resolution functional MRI at 3 T: 3D/2D echo-planar imaging with optimized physiological noise correction. Magn. Reson. Med. *69*, 1657–1664.

Macpherson, T., Morita, M., and Hikida, T. (2014). Striatal direct and indirect pathways control decision-making behavior. Front. Psychol. *5*, 1301.

Magalingam, K.B., Radhakrishnan, A.K., and Haleagrahara, N. (2015). Protective Mechanisms of Flavonoids in Parkinson's Disease. Oxid. Med. Cell. Longev. *2015*, 1–14.

Magrinelli, F., Picelli, A., Tocco, P., Federico, A., Roncari, L., Smania, N., Zanette, G., and Tamburin, S. (2016). Pathophysiology of Motor Dysfunction in Parkinson's Disease as the Rationale for Drug Treatment and Rehabilitation. Park. Dis. 1–18.

Mahlknecht, P., Hotter, A., Hussl, A., Esterhammer, R., Schocke, M., and Seppi, K. (2010). Significance of MRI in Diagnosis and Differential Diagnosis of Parkinson's Disease. Neurodegener. Dis. *7*, 300–318.

Maia, T.V., and Frank, M.J. (2011). From reinforcement learning models to psychiatric and neurological disorders. Nat. Neurosci. *14*, 154–162.

Maillard, L., Ishii, K., Bushara, K., Waldvogel, D., Schulman, A.E., and Hallett, M. (2000). Mapping the basal ganglia: fMRI evidence for somatotopic representation of face, hand, and foot. Neurology *55*, 377–383.

Malherbe, C., Messe, A., Bardinet, E., Pélégrini-Issac, M., Perlbarg, V., Marrelec, G., Worbe, Y., Yelnik, J., Lehéricy, S., and Benali, H. (2014). Combining Spatial Independent Component Analysis with Regression to Identify the Subcortical Components of Resting-State fMRI Functional Networks. Brain Connect. *4*, 181–192.

Mandir, A.S., and Vaughan, C. (2000). Pathophysiology of Parkinson's disease. Int. Rev. Psychiatry *12*, 270–280.

Mannella, F., Gurney, K., and Baldassarre, G. (2013). The nucleus accumbens as a nexus between values and goals in goal-directed behavior: a review and a new hypothesis. Front. Behav. Neurosci. *7*, 135.

Manni, E., and Petrosini, L. (2004). A century of cerebellar somatotopy: a debated representation. Nat. Rev. Neurosci. *5*, 241–249.

Marino, S., Ciurleo, R., Di Lorenzo, G., Barresi, M., De Salvo, S., Giacoppo, S., Bramanti, A., Lanzafame, P., and Bramanti, P. (2012). Magnetic resonance imaging markers for early diagnosis of Parkinson's disease. Neural Regen. Res. *7*, 611–619.

Marras, C., and Chaudhuri, K.R. (2016). Nonmotor features of Parkinson's disease subtypes. Mov. Disord. *31*, 1095–1102.

Marsden, C.D. (1982). The mysterious motor function of the basal ganglia: The Robert Wartenberg Lecture. Neurology *32*, 514.

Marsden, C.D., and Obeso, J.A. (1994). The functions of the basal ganglia and the paradox of stereotaxic surgery in Parkinson's disease. Brain *117*, 877–879.

Martí, M.J., and Tolosa, E. (2013). Parkinson disease: New guidelines for diagnosis of Parkinson disease. Nat. Publ. Group *9*, 190–191.

Martinez-Gonzalez, C., Bolam, J.P., and Mena-Segovia, J. (2011). Topographical organization of the pedunculopontine nucleus. Front. Neuroanat. *5*, 22.

Martinu, K., and Monchi, O. (2013). Cortico-basal ganglia and cortico-cerebellar circuits in Parkinson's disease: Pathophysiology or compensation? Behav. Neurosci. *127*, 222–236.

Mary Ann Chapman (2009). Does smoking reduce the risk of Parkinson's disease through stimulation of the ubiquitin–proteasome system? Med. HYPOTHESES *73*, 887–891.

Matsumoto, N., Hanakawa, T., Maki, S., Graybiel, A.M., and Kimura, M. (1999). Nigrostriatal dopamine system in learning to perform sequential motor tasks in a predictive manner. J. Ldots 978–998.

Mazzoni, P., Hristova, A., and Krakauer, J.W. (2007). Why Don't We Move Faster? Parkinson's Disease, Movement Vigor, and Implicit Motivation. J. Neurosci. *27*, 7105–7116.

Mazzoni, P., Shabbott, B., and Cortes, J.C. (2012). Motor Control Abnormalities in Parkinson's Disease. Cold Spring Harb. Perspect. Med. *2*, a009282–a009282.

McGhee, D.J., Royle, P.L., Thompson, P.A., Wright, D.E., Zajicek, J.P., and Counsell, C.E. (2013). A systematic review of biomarkers for disease progression in Parkinson's disease. BMC Neurol. *13*, 1–13.

McHaffie, J., Stanford, T., Stein, B., Coizet, V., and Redgrave, P. (2005). Subcortical loops through the basal ganglia. Trends Neurosci. *28*, 401–407.

van der Meer, M.A., and Redish, A.D. (2011). Ventral striatum: a critical look at models of learning and evaluation. Curr. Opin. Neurobiol. *21*, 387–392.

Meijer, F.J.A., Bloem, B.R., Mahlknecht, P., Seppi, K., and Goraj, B. (2013). Update on diffusion MRI in Parkinson's disease and atypical parkinsonism. J. Neurol. Sci. 1–9.

Mena-Segovia, J., Bolam, J.P., and Magill, P.J. (2004). Pedunculopontine nucleus and basal ganglia: distant relatives or part of the same family? Trends Neurosci. *27*, 585–588.

Mena-Segovia, J., Winn, P., and Bolam, J.P. (2008). Cholinergic modulation of midbrain dopaminergic systems. Brain Res. Rev. *58*, 265–271.

Meunier, D., Lambiotte, R., and Bullmore, E.T. (2010). Modular and Hierarchically Modular Organization of Brain Networks. Front. Neurosci. *4*.

Middleton, F.A., and Strick, P.L. (2000). Basal ganglia and cerebellar loops: motor and cognitive circuits. Brain Res. Brain Res. Rev. *31*, 236–250.

Milardi, D., Gaeta, M., Marino, S., Arrigo, A., Vaccarino, G., Mormina, E., Rizzo, G., Milazzo, C., Finocchio, G., Baglieri, A., et al. (2014). Basal ganglia network by constrained spherical deconvolution: A possible cortico-pallidal pathway? Mov. Disord. n/a–n/a.

Miller, D.B., and O'Callaghan, J.P. (2015). Biomarkers of Parkinson's disease: Present and future. Metabolism *64*, S40–S46.

Mink, J.W. (1996). The basal ganglia: focused selection and inhibition of competing motor programs. Prog. Neurobiol. *50*, 381–425.

Mink, J.W. (2003). The Basal Ganglia and involuntary movements: impaired inhibition of competing motor patterns. Arch. Neurol. *60*, 1365–1368.

Missale, C., Nash, S.R., Robinson, S.W., Jaber, M., and Caron, M.G. (1998). Dopamine receptors: from structure to function. Physiol. Rev. *78*, 189–225.

Mitelman, R., Rosin, B., Zadka, H., Slovik, M., Heimer, G., Ritov, Y. 'akov, Bergman, H., and Elias, S. (2011). Neighboring Pallidal Neurons Do Not Exhibit more Synchronous Oscillations than Remote Ones in the MPTP Primate Model of Parkinson's Disease. Front. Syst. Neurosci. *5*, 54.

Miwa, J.M., Freedman, R., and Lester, H.A. (2011). Neural Systems Governed by Nicotinic Acetylcholine Receptors: Emerging Hypotheses. Neuron *70*, 20–33.

Mizuno, Y., Hattori, N., Kubo, S. i, Sato, S., Nishioka, K., Hatano, T., Tomiyama, H., Funayama, M., Machida, Y., and Mochizuki, H. (2008). Progress in the pathogenesis and genetics of Parkinson's disease. Philos. Trans. R. Soc. B Biol. Sci. *363*, 2215–2227.

Mochizuki, H. (2009). Parkin gene therapy. Park. Realt. Disord. *15*, S43–S45.

Mochizuki, H., and Yasuda, T. (2012). Iron accumulation in Parkinson's disease. J. Neural Transm. *119*, 1511–1514.

Molochnikov, I., and Cohen, D. (2014). Hemispheric differences in the mesostriatal dopaminergic system. Front. Syst. Neurosci. *8*, 110.

Monchi, O., and Stoessl, A.J. (2012). Imaging neural correlates of mild cognitive impairment in Parkinson's disease. Lancet Neurol. *11*, 653–655.

Moore, D.J., West, A.B., Dawson, V.L., and Dawson, T.M. (2005). Molecular pathophysiology of Parkinson's disease. Annu. Rev. Neurosci. *28*, 57–87.

Moran, A., Stein, E., Tischler, H., and Bar-Gad, I. (2012). Decoupling neuronal oscillations during subthalamic nucleus stimulation in the parkinsonian primate. Neurobiol. Dis. *45*, 583–590.

Morcom, A.M., and Friston, K.J. (2012). Decoding episodic memory in ageing: A Bayesian analysis of activity patterns predicting memory. NeuroImage *59*, 1772–1782.

Morikawa, H., and Paladini, C.A. (2011). Dynamic regulation of midbrain dopamine neuron activity: intrinsic, synaptic, and plasticity mechanisms. NEUROSCIENCE *198*, 95–111.

Morris, G., Nevet, A., and Bergman, H. (2003). Anatomical funneling, sparse connectivity and redundancy reduction in the neural networks of the basal ganglia. J. Physiol.-Paris *97*, 581–589.

Morris, G., Arkadir, D., Nevet, A., Vaadia, E., and Bergman, H. (2004). Coincident but distinct messages of midbrain dopamine and striatal tonically active neurons. Neuron *43*, 133–143.

Moss, J., and Bolam, J.P. (2008). A Dopaminergic Axon Lattice in the Striatum and Its Relationship with Cortical and Thalamic Terminals. J. Neurosci. *28*, 11221–11230.

Moustafa, A.A., and Poletti, M. (2013). Neural and behavioral substrates of subtypes of Parkinson's disease. Front. Syst. Neurosci. *7*, 117.

Moustafa, A.A., Herzallah, M.M., and Gluck, M.A. (2013). Dissociating the Cognitive Effects of Levodopa versus Dopamine Agonists in a Neurocomputational Model of Learning in Parkinson's Disease. Neurodegener. Dis. *11*, 102–111.

Moustafa, A.A., Herzallah, M.M., and Gluck, M.A. (2014). A model of reversal learning and working memory in medicated and unmedicated patients with Parkinson's disease. J. Math. Psychol. *59*, 120–131.

Moustafa, A.A., Chakravarthy, S., Phillips, J.R., Gupta, A., Kéri, S., Polner, B., Frank, M.J., and Jahanshahi, M. (2016). Motor symptoms in Parkinson's disease: A unified framework. Neurosci. Biobehav. Rev. *68*, 727–740.

Müller, T. (2002). Dopaminergic substitution in Parkinson's disease. Expert Opin. Pharmacother. *3*, 1393–1403.

Müller, T. (2015). Catechol-O-Methyltransferase Inhibitors in Parkinson's Disease. Drugs *75*, 157–174.

Mullinger, K.J., Mayhew, S.D., Bagshaw, A.P., Bowtell, R., and Francis, S.T. (2014). Evidence that the negative BOLD response is neuronal in origin: A simultaneous EEG–BOLD–CBF study in humans. NeuroImage *94*, 263–274.

Nagy, Z., Alexander, D.C., Thomas, D.L., Weiskopf, N., and Sereno, M.I. (2013). Using High Angular Resolution Diffusion Imaging Data to Discriminate Cortical Regions. PLoS ONE *8*, e63842.

Nakano, K. (2000). Neural circuits and topographic organization of the basal ganglia and related regions. BRAIN Dev. *22 Suppl 1*, S5–16.

Nakano, K., Kayahara, T., Tsutsumi, T., and Ushiro, H. (2000). Neural circuits and functional organization of the striatum. J. Neurol. *247 Suppl 5*, V1–15.

Nambu, A. (2004). A new dynamic model of the cortico-basal ganglia loop. In Brain Mechanisms for the Integration of Posture and Movement, (Elsevier), pp. 461–466.

Nambu, A. (2005). A new approach to understand the pathophysiology of Parkinson's disease. J. Neurol. *252*, iv1–iv4.

Nambu, A. (2008). Seven problems on the basal ganglia. Curr. Opin. Neurobiol. *18*, 595–604.

Nambu, A. (2011). Somatotopic Organization of the Primate Basal Ganglia. Front. Neuroanat. *5*, 1–9.

Nambu, A., and Tachibana, Y. (2014). Mechanism of parkinsonian neuronal oscillations in the primate basal ganglia: some considerations based on our recent work. Front. Syst. Neurosci. *8*, 74.

Nambu, A., Tokuno, H., and Takada, M. (2002). Functional significance of the cortico-subthalamo-pallidal "hyperdirect" pathway. Neurosci. Res. *43*, 111–117.

Nandhagopal, R., McKeown, M.J., and Stoessl, A.J. (2008). Invited Article: Functional imaging in Parkinson disease. Neurology *70*, 1478–1488.

Nelson, A.B., and Kreitzer, A.C. (2014). Reassessing Models of Basal Ganglia Function and Dysfunction. Annu. Rev. Neurosci. *37*, 117–135.

Nelson, A.B., Hammack, N., Yang, C.F., Shah, N.M., Seal, R.P., and Kreitzer, A.C. (2014). Striatal Cholinergic Interneurons Drive GABA Release from Dopamine Terminals. Neuron *82*, 63–70.

Nelson, A.J., Blake, D.T., and Chen, R. (2009). Digit-specific aberrations in the primary somatosensory cortex in Writer's cramp. Ann. Neurol. *66*, 146–154.

Nevet, A., Morris, G., Saban, G., Arkadir, D., and Bergman, H. (2007). Lack of Spike-Count and Spike-Time Correlations in the Substantia Nigra Reticulata Despite Overlap of Neural Responses. J. Neurophysiol. *98*, 2232–2243.

Nicola, S.M., Surmeier, J., and Malenka, R.C. (2000). Dopaminergic modulation of neuronal excitability in the striatum and nucleus accumbens. Annu. Rev. Neurosci. *23*, 185–215.

Niethammer, M., Feigin, A., and Eidelberg, D. (2012). Functional Neuroimaging in Parkinson's Disease. Cold Spring Harb. Perspect. Med. *2*, a009274–a009274.

Nili, H., Wingfield, C., Walther, A., Su, L., Marslen-Wilson, W., and Kriegeskorte, N. (2014). A Toolbox for Representational Similarity Analysis. PLoS Comput. Biol. *10*, e1003553.

Nini, A., Feingold, A., and Slovin, H. (1995). Neurons in the globus pallidus do not show correlated activity in the normal monkey, but phase-locked oscillations appear in the MPTP model of parkinsonism. J. Ldots.

Niv, Y., Joel, D., Meilijson, I., and Ruppin, E. (2002). Evolution of reinforcement learning in uncertain environments: A simple explanation for complex foraging behaviors. Adapt. Behav.

Nonnekes, J., Timmer, M.H.M., de Vries, N.M., Rascol, O., Helmich, R.C., and Bloem, B.R. (2016). Unmasking levodopa resistance in Parkinson's disease. Mov. Disord. *31*, 1602–1609.

Norman, D.A., and Shallice, T. (1986). Attention to Action. In Consciousness and Self-Regulation, R.J. Davidson, G.E. Schwartz, and D. Shapiro, eds. (New York, NY: Springer Science & Business Media), pp. 1–18.

Nyholm, D. (2012). Duodopa® treatment for advanced Parkinson's disease: a review of efficacy and safety. Parkinsonism Relat. Disord. *18*, 916–929.

Obeso, J.A., Rodríguez-Oroz, M.C., Rodríguez, M., Lanciego, J.L., Artieda, J., Gonzalo, N., and Olanow, C.W. (2000). Pathophysiology of the basal ganglia in Parkinson's disease. Trends Neurosci. *23*, S8–19.

Obeso, J.A., Rodríguez-Oroz, M.C., Benitez-Temino, B., Blesa, F.J., Guridi, J., Marin, C., and Rodriguez, M. (2008). Functional organization of the basal ganglia: Therapeutic implications for Parkinson's disease. Mov. Disord. *23*, S548–S559.

Obeso, J.A., Rodriguez-Oroz, M.C., Goetz, C.G., Marin, C., Kordower, J.H., Rodriguez, M., Hirsch, E.C., Farrer, M., Schapira, A.H.V., and Halliday, G. (2010). Missing pieces in the Parkinson's disease puzzle. Nat. Med. *16*, 653–661.

Obeso, J.A., Rodriguez-Oroz, M.C., Stamelou, M., Bhatia, K.P., and Burn, D.J. (2014). The expanding universe of disorders of the basal ganglia. The Lancet *384*, 523–531.

O'Doherty, J. (2004). Dissociable Roles of Ventral and Dorsal Striatum in Instrumental Conditioning. Science *304*, 452–454.

O'Doherty, J.P., Buchanan, T.W., Seymour, B., and Dolan, R.J. (2006). Predictive Neural Coding of Reward Preference Involves Dissociable Responses in Human Ventral Midbrain and Ventral Striatum. Neuron *49*, 157–166.

Oguri, T., Sawamoto, N., Tabu, H., Urayama, S., Matsuhashi, M., Matsukawa, N., Ojika, K., and Fukuyama, H. (2013). Overlapping connections within the motor cortico-basal ganglia circuit: fMRI-tractography analysis. NeuroImage *78*, 353–362.

Oizumi, M., Albantakis, L., and Tononi, G. (2014). From the Phenomenology to the Mechanisms of Consciousness: Integrated Information Theory 3.0. PLoS Comput. Biol. *10*, e1003588.

Olman, C.A., and Yacoub, E. (2011). High-field FMRI for human applications: an overview of spatial resolution and signal specificity. Open Neuroimaging J. *5*, 74–89.

Olman, C.A., Pickett, K.A., Schallmo, M.-P., and Kimberley, T.J. (2012). Selective BOLD responses to individual finger movement measured with fMRI at 3T. Hum. Brain Mapp. *33*, 1594–1606.

Oorschot, D.E. (1996). Total number of neurons in the neostriatal, pallidal, subthalamic, and substantia nigral nuclei of the rat basal ganglia: a stereological study using the cavalieri and optical disector methods. J. Comp. Neurol. *366*, 580–599.

O'Reilly, R.C., and Frank, M.J. (2006). Making working memory work: a computational model of learning in the prefrontal cortex and basal ganglia. Neural Comput. *18*, 283–328.

O'Reilly, R.C., Frank, M.J., Hazy, T.E., and Watz, B. (2007). PVLV: The Primary Value and Learned Value Pavlovian Learning Algorithm. Behav. Neurosci. *121*, 31–49.

Pahapill, P.A., and Lozano, A.M. (2000). The pedunculopontine nucleus and Parkinson's disease. Brain *123 (Pt 9)*, 1767–1783.

Palminteri, S., Justo, D., Jauffret, C., Pavlicek, B., Dauta, A., Delmaire, C., Czernecki, V., Karachi, C., Capelle, L., Durr, A., et al. (2012). Critical Roles for Anterior Insula and Dorsal Striatum in Punishment-Based Avoidance Learning. Neuron *76*, 998–1009.

Pan, P.-Y., and Yue, Z. (2013). Genetic causes of Parkinson's disease and their links to autophagy regulation. Parkinsonism Relat. Disord. *20*, S154–S157.

Parent, A., and Hazrati, L.N. (1995a). Functional anatomy of the basal ganglia. I. The cortico-basal ganglia-thalamo-cortical loop. Brain Res. Brain Res. Rev. *20*, 91–127.

Parent, A., and Hazrati, L.N. (1995b). Functional anatomy of the basal ganglia. II. The place of subthalamic nucleus and external pallidum in basal ganglia circuitry. Brain Res. Brain Res. Rev. *20*, 128–154.

Parent, A., Sato, F., Wu, Y., Gauthier, J., Lévesque, M., and Parent, M. (2000). Organization of the basal ganglia: the importance of axonal collateralization. Trends Neurosci. *23*, S20–7.

Parent, M., Lévesque, M., and Parent, A. (1999). The pallidofugal projection system in primates: evidence for neurons branching ipsilaterally and contralaterally to the thalamus and brainstem. J. Chem. Neuroanat. *16*, 153–165.

Parent, M., Lévesque, M., and Parent, A. (2001). Two types of projection neurons in the internal pallidum of primates: single-axon tracing and three-dimensional reconstruction. J. Comp. Neurol. *439*, 162–175.

Parkinson, J. (1817). An Essay on the Shaking Palsy. Lond. Whittingham Rowland.

Parush, N., Tishby, N., and Bergman, H. (2011). Dopaminergic Balance between Reward Maximization and Policy Complexity. Front. Syst. Neurosci. *5*, 22.

Pasupathy, A., and Miller, E.K. (2005). Different time courses of learning-related activity in the prefrontal cortex and striatum. Nature *433*, 873–876.

Pavese, N., and Brooks, D.J. (2009). Imaging neurodegeneration in Parkinson's disease. BBA - Mol. Basis Dis. *1792*, 722–729.

Pelzer, E.A., Melzer, C., Timmermann, L., von Cramon, Y.D., and Tittgemeyer, M. (2016). Basal ganglia and cerebellar interconnectivity within the human thalamus. Brain Struct. Funct.

Penfield, W., and Rasmussen, T. (1950). The cerebral cortex of man; a clinical study of localization of function.

Percheron, G., and Filion, M. (1991). Parallel processing in the basal ganglia: up to a point. Trends Neurosci. *14*, 55–56.

Perlmutter, J.S., and Mink, J.W. (2006). Deep brain stimulation. Annu. Rev. Neurosci. *29*, 229–257.

Pessiglione, M., Guehl, D., Rolland, A.-S., Francois, C., Hirsch, E.C., Féger, J., and Tremblay, L. (2005). Thalamic neuronal activity in dopamine-depleted primates: evidence for a loss of functional segregation within basal ganglia circuits. J. Neurosci. *25*, 1523–1531.

Pessiglione, M., Seymour, B., Flandin, G., Dolan, R.J., and Frith, C.D. (2006). Dopamine-dependent prediction errors underpin reward-seeking behaviour in humans. Nature *442*, 1042–1045.

Pessoa, L. (2014). Understanding brain networks and brain organization. Phys. Life Rev. *11*, 400–435.

Peterson, D.A., Sejnowski, T.J., and Poizner, H. (2010). Convergent evidence for abnormal striatal synaptic plasticity in dystonia. Neurobiol. Dis. *37*, 558–573.

Petzinger, G.M., Fisher, B.E., McEwen, S., Beeler, J.A., Walsh, J.P., and Jakowec, M.W. (2013). Exercise-enhanced neuroplasticity targeting motor and cognitive circuitry in Parkinson's disease. Lancet Neurol. *12*, 716–726.

Plenz, D. (2003). When inhibition goes incognito: feedback interaction between spiny projection neurons in striatal function. Trends Neurosci. *26*, 436–443.

Plow, E.B., Arora, P., Pline, M.A., Binenstock, M.T., and Carey, J.R. (2010). Within-limb somatotopy in primary motor cortex - revealed using fMRI. CORTEX *46*, 310–321.

Politis, M. (2014). Neuroimaging in Parkinson disease: from research setting to clinical practice. Nat. Publ. Group *10*, 708–722.

Posse, S. (2012). Multi-echo acquisition. NeuroImage *62*, 665–671.

Posse, S., Ackley, E., Mutihac, R., Rick, J., Shane, M., Murray-Krezan, C., Zaitsev, M., and Speck, O. (2012). Enhancement of temporal resolution and BOLD sensitivity in real-time fMRI using multi-slab echo-volumar imaging. NeuroImage *61*, 115–130.

Postuma, R.B., and Berg, D. (2016). Advances in markers of prodromal Parkinson disease. Nat. Publ. Group *12*, 622–634.

Price, C.J., and Friston, K.J. (2002). Degeneracy and cognitive anatomy. Trends Cogn. Sci. *6*, 416–421.

Pyatigorskaya, N., Gallea, C., Garcia-Lorenzo, D., Vidailhet, M., and Lehéricy, S. (2013). A review of the use of magnetic resonance imaging in Parkinson's disease. Ther. Adv. Neurol. Disord. 1756285613511507.

Quartarone, A., Morgante, F., Sant'Angelo, A., Rizzo, V., Bagnato, S., Terranova, C., Siebner, H.R., Berardelli, A., and Girlanda, P. (2008). Abnormal plasticity of sensorimotor circuits extends beyond the affected body part in focal dystonia. J. Neurol. Neurosurg. Psychiatry *79*, 985–990.

Quik, M., O'Leary, K., and Tanner, C.M. (2008). Nicotine and Parkinson's disease: Implications for therapy. Mov. Disord. *23*, 1641–1652.

Ramnani, N. (2006). The primate cortico-cerebellar system: anatomy and function. Nat. Rev. Neurosci. *7*, 511–522.

Rascol, O., Payoux, P., Ory, F., Ferreira, J.J., Brefel-Courbon, C., and Montastruc, J.-L. (2003). Limitations of current Parkinson's disease therapy. Ann. Neurol. *53*, S3–S15.

Ray, N.J., and Strafella, A.P. (2012). The neurobiology and neural circuitry of cognitive changes in Parkinson's disease revealed by functional neuroimaging. Mov. Disord. *27*, 1484–1492.

Redgrave, P., and Gurney, K. (2006). The short-latency dopamine signal: a role in discovering novel actions? Nat. Rev. Neurosci. *7*, 967–975.

Redgrave, P., Prescott, T.J., and Gurney, K. (1999). The basal ganglia: a vertebrate solution to the selection problem? NEUROSCIENCE *89*, 1009–1023.

Redgrave, P., Rodriguez, M., Smith, Y., Rodriguez-Oroz, M.C., Lehéricy, S., Bergman, H., Agid, Y., DeLong, M.R., and Obeso, J.A. (2010). Goal-directed and habitual control in the basal ganglia: implications for Parkinson's disease. Nat. Publ. Group *11*, 760–772.

Redgrave, P., Vautrelle, N., and Reynolds, J.N.J. (2011). Functional properties of the basal ganglia's re-entrant loop architecture: selection and reinforcement. NEUROSCIENCE *198*, 138–151.

Reeve, A., Simcox, E., and Turnbull, D. (2014). Ageing and Parkinson's disease: Why is advancing age the biggest risk factor? Ageing Res. Rev. *14*, 19–30.

Reichenbach, J.R., Schweser, F., Serres, B., and Deistung, A. (2015). Quantitative Susceptibility Mapping: Concepts and Applications. Clin. Neuroradiol. *25*, 225–230.

Reynolds, J.N.J., and Wickens, J.R. (2002). Dopamine-dependent plasticity of corticostriatal synapses. Neural Netw. Off. J. Int. Neural Netw. Soc. *15*, 507–521.

Rice, M.E., Patel, J.C., and Cragg, S.J. (2011). Dopamine release in the basal ganglia. NEUROSCIENCE *198*, 112–137.

Rijsman, R.M., Schoolderman, L.F., Rundervoort, R.S., and Louter, M. (2013). Restless legs syndrome in Parkinson's disease. Parkinsonism Relat. Disord. *20*, S5–S9.

Robbins, T.W., and Cools, R. (2014). Cognitive deficits in Parkinson's disease: A cognitive neuroscience perspective. Mov. Disord. *29*, 597–607.

Rodriguez, M., Rodriguez-Sabate, C., Morales, I., Sanchez, A., and Sabate, M. (2015). Parkinson's disease as a result of aging. Aging Cell *14*, 293–308.

Rodríguez-Nogales, C., Garbayo, E., Carmona-Abellán, M.M., Luquin, M.R., and Blanco-Prieto, M.J. (2015). Brain aging and Parkinson's disease: New therapeutic approaches using drug delivery systems. 1–7.

Rodriguez-Oroz, M.C., Rodriguez, M., Guridi, J., Mewes, K., Chockkman, V., Vitek, J., DeLong, M.R., and Obeso, J.A. (2001). The subthalamic nucleus in Parkinson's disease: somatotopic organization and physiological characteristics. Brain *124*, 1777–1790.

Romanelli, P., Esposito, V., Schaal, D.W., and Heit, G. (2005). Somatotopy in the basal ganglia: experimental and clinical evidence for segregated sensorimotor channels. Brain Res. Rev. *48*, 112–128.

Rommelfanger, K.S. (2010). Extrastriatal dopaminergic circuits of the basal ganglia. Front. Neuroanat. *4*.

Root, D.H., Melendez, R.I., Zaborszky, L., and Napier, T.C. (2015). The ventral pallidum: Subregion-specific functional anatomy and roles in motivated behaviors. Prog. Neurobiol. *130*, 29–70.

Ross, C.A., and Pickart, C.M. (2004). The ubiquitin–proteasome pathway in Parkinson's disease and other neurodegenerative diseases. Trends Cell Biol. *14*, 703–711.

Rouault, T.A. (2013). Iron metabolism in the CNS: implications for neurodegenerative diseases. Nat. Publ. Group *14*, 551–564.

Rowe, J.B., Hughes, L.E., Barker, R.A., and Owen, A.M. (2010). Dynamic causal modelling of effective connectivity from fMRI: Are results reproducible and sensitive to Parkinson's disease and its treatment? NeuroImage *52*, 1015–1026.

Rowland, N.C., Sammartino, F., and Lozano, A.M. (2016). Advances in surgery for movement disorders. Mov. Disord.

Rubinov, M., and Sporns, O. (2010). Complex network measures of brain connectivity: Uses and interpretations. NeuroImage *52*, 1059–1069.

Russo, S.J., and Nestler, E.J. (2013). The brain reward circuitry in mood disorders. Nat. Publ. Group *14*, 609–625.

Ryterska, A., Jahanshahi, M., and Osman, M. (2013). What are people with Parkinson's disease really impaired on when it comes to making decisions? A meta-analysis of the evidence. Neurosci. Biobehav. Rev. *37*, 2836–2846.

Sampson, T.R., Debelius, J.W., Thron, T., Janssen, S., Shastri, G.G., Ilhan, Z.E., Challis, C., Schretter, C.E., Rocha, S., Gradinaru, V., et al. (2017). Gut Microbiota Regulate Motor Deficits and Neuroinflammation in a Model of Parkinson's Disease. 1–25.

Sanchez-Gonzalez, M.A. (2005). The Primate Thalamus Is a Key Target for Brain Dopamine. J. Neurosci. *25*, 6076–6083.

Savica, R., Rocca, W.A., and Ahlskog, J.E. (2010). When does Parkinson disease start? Arch. Neurol. *67*, 798–801.

Schapira, A.H.V. (2006). Etiology of Parkinson's disease. Neurology *66*, S10–S23.

Schapira, A.H., and Jenner, P. (2011). Etiology and pathogenesis of Parkinson's disease. Mov. Disord. *26*, 1049–1055.

Schapira, A.H.V., and Gegg, M. (2011). Mitochondrial Contribution to Parkinson's Disease Pathogenesis. Park. Dis. *2011*, 1–7.

Schmidt, L., Lebreton, M., Cléry-Melin, M.-L., Daunizeau, J., and Pessiglione, M. (2012). Neural Mechanisms Underlying Motivation of Mental Versus Physical Effort. PLoS Biol. *10*, e1001266.

Scholz, V.H., Flaherty, A.W., Kraft, E., Keltner, J.R., Kwong, K.K., Chen, Y.I., Rosen, B.R., and Jenkins, B.G. (2000). Laterality, somatotopy and reproducibility of the basal ganglia and motor cortex during motor tasks. Brain Res. *879*, 204–215.

Schroll, H., and Hamker, F.H. (2013). Computational models of basal-ganglia pathway functions: focus on functional neuroanatomy. Front. Syst. Neurosci. *7*, 122.

Schuff, N. (2009). Potential role of high-field MRI for studies in Parkinson's disease. Mov. Disord. *24*, S684–S690.

Schwab, R.S., and England, A.C. (1969). Projection technique for evaluating surgery in Parkinson's disease. In Third Symposium on Parkinson's Disease, F. Gillingham, and I. Donaldson, eds. (Edinburgh: E&S Livingstone), pp. 152–157.

Schwarz, S.T., Abaei, M., Gontu, V., Morgan, P.S., Bajaj, N., and Auer, D.P. (2013). Diffusion tensor imaging of nigral degeneration in Parkinson's disease: A region-of-interest and voxel-based study at 3T and systematic review with meta-analysis. YNICL *3*, 481–488.

Seamans, J.K., and Yang, C.R. (2004). The principal features and mechanisms of dopamine modulation in the prefrontal cortex. Prog. Neurobiol. *74*, 1–58.

Seger, C.A. (2008). How do the basal ganglia contribute to categorization? Their roles in generalization, response selection, and learning via feedback. Neurosci. Biobehav. Rev. *32*, 265–278.

Seger, C.A. (2013). The visual corticostriatal loop through the tail of the caudate: circuitry and function. Front. Syst. Neurosci. *7*, 104.

Seger, C.A., and Peterson, E.J. (2013). Categorization=decision making+generalization. Neurosci. Biobehav. Rev. 1–14.

Seger, C.A., and Spiering, B.J. (2011). A critical review of habit learning and the Basal Ganglia. Front. Syst. Neurosci. *5*, 66.

Seo, M., Lee, E., and Averbeck, B.B. (2012). Action Selection and Action Value in Frontal-Striatal Circuits. Neuron *74*, 947–960.

Sharifi, S., Nederveen, A.J., Booij, J., and van Rootselaar, A.-F. (2010). Neuroimaging essentials in essential tremor: A systematic review. YNICL *5*, 217–231.

Sharma, S., Moon, C.S., Khogali, A., Haidous, A., Chabenne, A., Ojo, C., Jelebinkov, M., Kurdi, Y., and Ebadi, M. (2013). Biomarkers in Parkinson's disease (recent update). Neurochem. Int. *63*, 201–229.

Sharott, A., Gulberti, A., Zittel, S., Tudor Jones, A.A., Fickel, U., Munchau, A., Koppen, J.A., Gerloff, C., Westphal, M., Buhmann, C., et al. (2014). Activity Parameters of Subthalamic Nucleus Neurons Selectively Predict Motor Symptom Severity in Parkinson's Disease. J. Neurosci. *34*, 6273–6285.

Shen, W., Flajolet, M., Greengard, P., and Surmeier, D.J. (2008). Dichotomous dopaminergic control of striatal synaptic plasticity. Science *321*, 848–851.

Sherman, S.M. (2004). Interneurons and triadic circuitry of the thalamus. Trends Neurosci. *27*, 670–675.

Shin, H.-W., Kang, S.Y., Hallett, M., and Sohn, Y.H. (2012). Reduced surround inhibition in musicians. Exp. Brain Res. *219*, 403–408.

Shohamy, D., and Adcock, R.A. (2010). Dopamine and adaptive memory. Trends Cogn. Sci. *14*, 464–472.

Shohamy, D., Myers, C.E., Kalanithi, J., and Gluck, M.A. (2008). Basal ganglia and dopamine contributions to probabilistic category learning. Neurosci. Biobehav. Rev. *32*, 219–236.

Sian-Hülsmann, J., Mandel, S., Youdim, M.B.H., and Riederer, P. (2011). The relevance of iron in the pathogenesis of Parkinson's disease. J. Neurochem. *118*, 939–957.

Sidhu, A., Wersinger, C., Moussa, C.E.-H., and Vernier, P. (2004). The role of alpha-synuclein in both neuroprotection and neurodegeneration. Ann. N. Y. Acad. Sci. *1035*, 250–270.

Smith, Y., Bevan, M.D., Shink, E., and Bolam, J.P. (1998). Microcircuitry of the direct and indirect pathways of the basal ganglia. NEUROSCIENCE *86*, 353–387.

Smith, Y., Raju, D.V., Pare, J.-F., and Sidibe, M. (2004). The thalamostriatal system: a highly specific network of the basal ganglia circuitry. Trends Neurosci. *27*, 520–527.

Smith, Y., Raju, D., Nanda, B., Pare, J.-F., Galván, A., and Wichmann, T. (2009). The thalamostriatal systems: Anatomical and functional organization in normal and parkinsonian states. Brain Res. Bull. *78*, 60–68.

Smith, Y., Galván, A., Ellender, T.J., Doig, N., Villalba, R.M., Huerta-Ocampo, I., Wichmann, T., and Bolam, J.P. (2014). The thalamostriatal system in normal and diseased states. Front. Syst. Neurosci. *8*, 5.

Snijders, A.H., Takakusaki, K., Debû, B., Lozano, A.M., Krishna, V., Fasano, A., Aziz, T.Z., Papa, S.M., Factor, S.A., and Hallett, M. (2016). Physiology of freezing of gait. Ann. Neurol. *80*, 644–659.

Soares, J.M., Marques, P., Alves, V., and Sousa, N. (2013). A hitchhiker's guide to diffusion tensor imaging. Front. Neurosci. *7*, 31.

Solari, V.H., and Rich Stoner, S. (2014). Cognitive consilience: primate non-primary neuroanatomical circuits underlying cognition. 1–23.

Spatola, M., and Wider, C. (2013). Genetics of Parkinson's disease: the yield. Parkinsonism Relat. Disord. *20*, S35–S38.

Spillantini, M.G., Schmidt, M.L., Y, L.V.M., Trojanowski, J.Q., Jakes, R., and Goedert, M. (1997). Alpha-synuclein in Lewy bodies. 1–2.

Sporns, O. (2012). From simple graphs to the connectome: Networks in neuroimaging. NeuroImage *62*, 881–886.

Sporns, O. (2013). Network attributes for segregation and integration in the human brain. Curr. Opin. Neurobiol. *23*, 162–171.

Sporns, O. (2015). Cerebral cartography and connectomics. Philos. Trans. R. Soc. B Biol. Sci. *370*, 20140173–20140173.

Sporns, O., Tononi, G., and Edelman, G.M. (2000). Connectivity and complexity: the relationship between neuroanatomy and brain dynamics. Neural Netw. Off. J. Int. Neural Netw. Soc. *13*, 909–922.

Staempfli, P., Jaermann, T., Crelier, G.R., Kollias, S., Valavanis, A., and Boesiger, P. (2006). Resolving fiber crossing using advanced fast marching tractography based on diffusion tensor imaging. NeuroImage *30*, 110–120.

Staempfli, P., Reischauer, C., Jaermann, T., Valavanis, A., Kollias, S., and Boesiger, P. (2008). Combining fMRI and DTI: A framework for exploring the limits of fMRI-guided DTI fiber tracking and for verifying DTI-based fiber tractography results. NeuroImage *39*, 119–126.

Steece-Collier, K., Maries, E., and Kordower, J.H. (2002). Etiology of Parkinson's Disease: Genetics and Environment Revisited. Proc. Natl. Acad. Sci. U. S. A. *99*, 13972–13974.

Stefanis, L. (2012). α-Synuclein in Parkinson's disease. Cold Spring Harb. Perspect. Med. *2*, a009399.

Stein, E., and Bar-Gad, I. (2013). Beta oscillations in the cortico-basal ganglia loop during parkinsonism. Exp. Neurol. *245*, 52–59.

Stocchi, F., Jenner, P., and Obeso, J.A. (2010). When Do Levodopa Motor Fluctuations First Appear in Parkinson's Disease. Eur. Neurol. *63*, 257–266.

Stocco, A. (2012). Acetylcholine-based entropy in response selection: a model of how striatal interneurons modulate exploration, exploitation, and response variability in decision-making. 1–19.

Stoeckel, M.C., Seitz, R.J., and Buetefisch, C.M. (2009). Congenitally altered motor experience alters somatotopic organization of human primary motor cortex. Proc. Natl. Acad. Sci. U. S. A. *106*, 2395–2400.

Stoessl, A.J. (2009). Functional imaging studies of non-motoric manifestations of Parkinson's Disease. Park. Realt. Disord. *15*, S13–S16.

Stoessl, A.J. (2011a). Neuroimaging in Parkinson's disease: from pathology to diagnosis. Parkinsonism Relat. Disord. *18*, S55–S59.

Stoessl, A.J. (2011b). Neuroimaging in Parkinson's Disease. Neurotherapeutics *8*, 72–81.

Stoessl, A.J., Lehéricy, S., and Strafella, A.P. (2014). Imaging insights into basal ganglia function, Parkinson's disease, and dystonia. The Lancet *384*, 532–544.

Stoodley, C.J., and Schmahmann, J.D. (2009). Functional topography in the human cerebellum: A meta-analysis of neuroimaging studies. NeuroImage *44*, 489–501.

Stoodley, C.J., and Schmahmann, J.D. (2010). Evidence for topographic organization in the cerebellum of motor control versus cognitive and affective processing. CORTEX *46*, 831–844.

Stoodley, C.J., Valera, E.M., and Schmahmann, J.D. (2012). Functional topography of the cerebellum for motor and cognitive tasks: An fMRI study. NeuroImage *59*, 1560–1570.

Strother, L., Medendorp, W.P., Coros, A.M., and Vilis, T. (2012). Double representation of the wrist and elbow in human motor cortex. Eur. J. Neurosci. *36*, 3291–3298.

Sulzer, D. (2007). Multiple hit hypotheses for dopamine neuron loss in Parkinson's disease. Trends Neurosci. *30*, 244–250.

Suri, R.E., and Schultz, W. (1998). Learning of sequential movements by neural network model with dopamine-like reinforcement signal. Exp. Brain Res. *121*, 350–354.

Suri, R.E., and Schultz, W. (1999). A neural network model with dopamine-like reinforcement signal that learns a spatial delayed response task. NSC *91*, 871–890.

Suri, R.E., Bargas, J., and Arbib, M.A. (2001). Modeling functions of striatal dopamine modulation in learning and planning. NSC *103*, 65–85.

Surmeier, J.D., and Graybiel, A.M. (2012). A Feud that Wasn't: Acetylcholine Evokes Dopamine Release in the Striatum. Neuron *75*, 1–3.

Surmeier, D.J., Mercer, J.N., and Chan, C.S. (2005). Autonomous pacemakers in the basal ganglia: who needs excitatory synapses anyway? Curr. Opin. Neurobiol. *15*, 312–318.

Surmeier, D.J., Ding, J., Day, M., Wang, Z., and Shen, W. (2007). D1 and D2 dopamine-receptor modulation of striatal glutamatergic signaling in striatal medium spiny neurons. Trends Neurosci. *30*, 228–235.

Surmeier, D.J., Shen, W., Day, M., Gertler, T., Chan, S., Tian, X., and Plotkin, J.L. (2010). The role of dopamine in modulating the structure and function of striatal circuits. Prog. Brain Res. *183*, 149–167.

Surmeier, D.J., Guzman, J.N., Sanchez-Padilla, J., and Schumacker, P.T. (2011a). The role of calcium and mitochondrial oxidant stress in the loss of substantia nigra pars compacta dopaminergic neurons in Parkinson's disease. NEUROSCIENCE *198*, 221–231.

Surmeier, D.J., Carrillo-Reid, L., and Bargas, J. (2011b). Dopaminergic modulation of striatal neurons, circuits, and assemblies. NEUROSCIENCE *198*, 3–18.

Sutton, R.S. (1988). Learning to predict by the methods of temporal differences. Mach. Learn. *3*, 9–44.

Sveinbjornsdottir, S. (2016). The clinical symptoms of Parkinson's disease. J. Neurochem. *139 Suppl 1*, 318–324.

Svensson, E., Horváth-Puhó, E., Thomsen, R.W., Djurhuus, J.C., Pedersen, L., Borghammer, P., and Sørensen, H.T. (2015). Vagotomy and subsequent risk of Parkinson's disease. Ann. Neurol. *78*, 522–529.

Taha, J.M., Favre, J., Baumann, T.K., and Burchiel, K.J. (1996a). Characteristics and somatotopic organization of kinesthetic cells in the globus pallidus of patients with Parkinson's disease. J. Neurosurg. *85*, 1005–1012.

Taha, J.M., Favre, J., Baumann, T.K., and Burchiel, K.J. (1996b). Functional anatomy of the pallidal base in Parkinson's disease. Neurosurgery *39*, 1164–7– NaN–8.

Takada, M., Tokuno, H., Nambu, A., and Inase, M. (1998). Corticostriatal projections from the somatic motor areas of the frontal cortex in the macaque monkey: segregation versus overlap of input zones from the primary motor cortex, the supplementary motor area, and the premotor cortex. Exp. Brain Res. *120*, 114–128.

Takada, M., Tokuno, H., Hamada, I., Inase, M., Ito, Y., Imanishi, M., Hasegawa, N., Akazawa, T., Hatanaka, N., and Nambu, A. (2001). Organization of inputs from cingulate motor areas to basal ganglia in macaque monkey. Eur. J. Neurosci. *14*, 1633–1650.

Tamburin, S., Manganotti, P., Marzi, C.A., Fiaschi, A., and Zanette, G. (2002). Abnormal somatotopic arrangement of sensorimotor interactions in dystonic patients. Brain *125*, 2719–2730.

Tan, E.K., Lum, S.Y., and Wong, M.C. (2002). Restless legs syndrome in Parkinson's disease. J. Neurol. Sci. *196*, 33–36.

Tanaka, S.C., Doya, K., Okada, G., Ueda, K., Okamoto, Y., and Yamawaki, S. (2004). Prediction of immediate and future rewards differentially recruits cortico-basal ganglia loops. Nat. Neurosci. *7*, 887–893.

Telford, R., and Vattoth, S. (2014). MR Anatomy of Deep Brain Nuclei with Special Reference to Specific Diseases and Deep Brain Stimulation Localization. Neuroradiol. J. *27*, 29.

Tepper, J.M., and Bolam, J.P. (2004). Functional diversity and specificity of neostriatal interneurons. Curr. Opin. Neurobiol. *14*, 685–692.

Tessitore, A., Giordano, A., Russo, A., and Tedeschi, G. (2016). Structural connectivity in Parkinson's disease. Park. Realt. Disord. *22*, S56–S59.

Thenganatt, M.A., and Jankovic, J. (2014). Parkinson Disease Subtypes. JAMA Neurol. *71*, 499.

Theodosopoulos, P.V., Marks, W.J., Christine, C., and Starr, P.A. (2003). Locations of movement-related cells in the human subthalamic nucleus in Parkinson's disease. Mov. Disord. *18*, 791–798.

Thomas, B., and Beal, M.F. (2007). Parkinson's disease. Hum. Mol. Genet. *16*, R183–R194.

Timpka, J., Mundt-Petersen, U., and Odin, P. (2016). Continuous dopaminergic stimulation therapy for Parkinson's disease – recent advances. Curr. Opin. Neurol. *29*, 474–479.

Tinazzi, M. (2006). Pain and motor complications in Parkinson's disease. J. Neurol. Neurosurg. Psychiatry *77*, 822–825.

Titova, N., Padmakumar, C., Lewis, S.J.G., and Chaudhuri, K.R. (2017). Parkinson's: a syndrome rather than a disease? J. Neural Transm. 1–8.

Tomlinson, C.L., Stowe, R., Patel, S., Rick, C., Gray, R., and Clarke, C.E. (2010). Systematic review of levodopa dose equivalency reporting in Parkinson's disease. Mov. Disord. *25*, 2649–2653.

Tononi, G. (2004). An information integration theory of consciousness. BMC Neurosci. *5*, 42.

Tononi, G. (2008). Consciousness as integrated information: a provisional manifesto. Biol. Bull. *215*, 216–242.

Tononi, G., Sporns, O., and Edelman, G.M. (1994). A measure for brain complexity: relating functional segregation and integration in the nervous system. Proc. Natl. Acad. Sci. U. S. A. *91*, 5033–5037.

Tononi, G., Edelman, G.M., and Sporns, O. (1998). Complexity and coherency: integrating information in the brain. Trends Cogn. Sci. *2*, 474–484.

Tononi, G., Sporns, O., and Edelman, G.M. (1999). Measures of degeneracy and redundancy in biological networks. Proc. Natl. Acad. Sci. U. S. A. *96*, 3257–3262.

Tournier, J.-D., Calamante, F., and Connelly, A. (2007). Robust determination of the fibre orientation distribution in diffusion MRI: Non-negativity constrained super-resolved spherical deconvolution. NeuroImage *35*, 1459–1472.

Tournier, J.-D., Yeh, C.-H., Calamante, F., Cho, K.-H., Connelly, A., and Lin, C.-P. (2008). Resolving crossing fibres using constrained spherical deconvolution: Validation using diffusion-weighted imaging phantom data. NeuroImage *42*, 617–625.

Tournier, J.-D., Mori, S., and Leemans, A. (2011). Diffusion tensor imaging and beyond. Magn. Reson. Med. *65*, 1532–1556.

Tournier, J.-D., Calamante, F., and Connelly, A. (2013). Determination of the appropriate b-value and number of gradient directions for high-angular-resolution diffusion-weighted imaging. NMR Biomed. *26*, 1775–1786.

Trapp, S., Schroll, H., and Hamker, F.H. (2012). Open and closed loops: A computational approach to attention and consciousness. Adv. Cogn. Psychol. *8*, 1–8.

Tremblay, L., Worbe, Y., Thobois, S., Sgambato-Faure, V., and Féger, J. (2015). Selective dysfunction of basal ganglia subterritories: From movement to behavioral disorders. Mov. Disord. *30*, 1155–1170.

Tremblay, P.-L., Bedard, M.-A., Langlois, D., Blanchet, P.J., Lemay, M., and Parent, M. (2010). Movement chunking during sequence learning is a dopamine-dependant process: a study conducted in Parkinson's disease. Exp. Brain Res. *205*, 375–385.

Triantafyllou, C., Hoge, R.D., Krueger, G., Wiggins, C.J., Potthast, A., Wiggins, G.C., and Wald, L.L. (2005). Comparison of physiological noise at 1.5 T, 3 T and 7 T and optimization of fMRI acquisition parameters. NeuroImage *26*, 243–250.

Triantafyllou, C., Polimeni, J.R., and Wald, L.L. (2011). Physiological noise and signal-to-noise ratio in fMRI with multi-channel array coils. NeuroImage *55*, 597–606.

Tuch, D.S., Reese, T.G., Wiegell, M.R., Makris, N., Belliveau, J.W., and Wedeen, V.J. (2002). High angular resolution diffusion imaging reveals intravoxel white matter fiber heterogeneity. Magn. Reson. Med. *48*, 577–582.

Tuite, P., Mangia, S., and Michaeli, S. (2013). Magnetic Resonance Imaging (MRI) in Parkinson's Disease. J. Alzheimers Dis. Park. *3*.

Turner, R.S., and Desmurget, M. (2010). Basal ganglia contributions to motor control: a vigorous tutor. Curr. Opin. Neurobiol. *20*, 704–716.

Tykocki, T., Mandat, T., and Nauman, P. (2011). Pedunculopontine nucleus deep brain stimulation in Parkinson's disease. Arch. Med. Sci. AMS *7*, 555–564.

Ulla, M., Bonny, J.M., Ouchchane, L., Rieu, I., Claise, B., and Durif, F. (2013). Is R2* a New MRI Biomarker for the Progression of Parkinson's Disease? A Longitudinal Follow-Up. PLoS ONE *8*, e57904.

Updyke, B.V. (1993). Organization of visual corticostriatal projections in the cat, with observations on visual projections to claustrum and amygdala. J. Comp. Neurol. *327*, 159–193.

Urbain, N., Gervasoni, D., Soulière, F., Lobo, L., Rentéro, N., Windels, F., Astier, B., Savasta, M., Fort, P., Renaud, B., et al. (2000). Unrelated course of subthalamic nucleus and globus pallidus neuronal activities across vigilance states in the rat. Eur. J. Neurosci. *12*, 3361–3374.

Utter, A.A., and Basso, M.A. (2008). The basal ganglia: An overview of circuits and function. Neurosci. Biobehav. Rev. *32*, 333–342.

Vaillancourt, D.E., Schonfeld, D., Kwak, Y., Bohnen, N.I., and Seidler, R. (2013). Dopamine overdose hypothesis: Evidence and clinical implications. Mov. Disord. *28*, 1920–1929.

Valadas, J.S., Vos, M., and Verstreken, P. (2014). Therapeutic strategies in Parkinson's disease: what we have learned from animal models. Ann. N. Y. Acad. Sci. *1338*, 16–37.

Veazey, C., Aki, S.O.E., Cook, K.F., Lai, E.C., and Kunik, M.E. (2005). Prevalence and treatment of depression in Parkinson's disease. J Neuropsychiatry Clin Neurosci *17*, 310–323.

Vila, M., Ramonet, D., and Perier, C. (2008). Mitochondrial alterations in Parkinson's disease: new clues. J. Neurochem. *107*, 317–328.

Vitay, J., and Hamker, F.H. (2010). A computational model of Basal Ganglia and its role in memory retrieval in rewarded visual memory tasks. Front. Comput. Neurosci. *4*.

Voon, V., Fernagut, P.-O., Wickens, J., Baunez, C., Rodriguez, M., Pavon, N., Juncos, J.L., Obeso, J.A., and Bezard, E. (2009). Chronic dopaminergic stimulation in Parkinson's disease: from dyskinesias to impulse control disorders. Lancet Neurol. *8*, 1140–1149.

Voon, V., Mehta, A.R., and Hallett, M. (2011). Impulse control disorders in Parkinson's disease. Curr. Opin. Neurol. *24*, 324–330.

Wagle Shukla, A., and Okun, M.S. (2013). Surgical Treatment of Parkinson's Disease: Patients, Targets, Devices, and Approaches. Neurotherapeutics *11*, 47–59.

Wall, N.R., De La Parra, M., Callaway, E.M., and Kreitzer, A.C. (2013). Differential Innervation of Direct- and Indirect-Pathway Striatal Projection Neurons. Neuron *79*, 347–360.

Wang, A.Y., Miura, K., and Uchida, N. (2013). The dorsomedial striatum encodes net expected return, critical for energizing performance vigor. Nat. Publ. Group *16*, 639–647.

Webb, J.T., Ferguson, M.A., Nielsen, J.A., and Anderson, J.S. (2013). BOLD Granger Causality Reflects Vascular Anatomy. PLoS ONE *8*, e84279.

Wei, L., Zhang, J., Long, Z., Wu, G.-R., Hu, X., Zhang, Y., and Wang, J. (2014). Reduced Topological Efficiency in Cortical-Basal Ganglia Motor Network of Parkinson's Disease: A Resting State fMRI Study. PLoS ONE *9*, e108124.

Weingarten, C.P., Sundman, M.H., and Hickey, P. (2015). Neuroimaging of Parkinson's disease: Expanding views. Neurosci. Biobehav. Rev. *59*, 16–52.

Weiskopf, N., Suckling, J., Williams, G., Correia, M.M., Inkster, B., Tait, R., Ooi, C., Bullmore, E.T., and Lutti, A. (2013). Quantitative multi-parameter mapping of R1, PD(*), MT, and R2(*) at 3T: a multi-center validation. Front. Neurosci. *7*, 95.

Whitacre, J.M. (2010). Degeneracy: a link between evolvability, robustness and complexity in biological systems. Theor. Biol. Med. Model. *7*, 6.

Wichmann, T., and DeLong, M.R. (1996). Functional and pathophysiological models of the basal ganglia. Curr. Opin. Neurobiol. *6*, 751–758.

Wichmann, T., and Dostrovsky, J.O. (2011). Pathological basal ganglia activity in movement disorders. NEUROSCIENCE *198*, 232–244.

Wickens, A.P. (2001). Ageing and the free radical theory. Respir. Physiol. *128*, 379–391.

Wider, C., Ross, O.A., and Wszolek, Z.K. (2010). Genetics of Parkinson disease and essential tremor. Curr. Opin. Neurol. 1.

Wiestler, T., and Diedrichsen, J. (2013). Skill learning strengthens cortical representations of motor sequences. eLife *2*, e00801–e00801.

Williams, D.R., and Litvan, I. (2013). Parkinsonian syndromes. Contin. Minneap.

Williams, Z.M., Neimat, J.S., Cosgrove, G.R., and Eskandar, E.N. (2005). Timing and direction selectivity of subthalamic and pallidal neurons in patients with Parkinson disease. Exp. Brain Res. *162*, 407–416.

Winklhofer, K.F., and Haass, C. (2010). Mitochondrial dysfunction in Parkinson's disease. BBA - Mol. Basis Dis. *1802*, 29–44.

Wolpert, D.M., and Landy, M.S. (2012). Motor control is decision-making. Curr. Opin. Neurobiol. *22*, 996–1003.

Wood-Kaczmar, A., Gandhi, S., and Wood, N.W. (2006). Understanding the molecular causes of Parkinson's disease. Trends Mol. Med. *12*, 521–528.

Wu, Y., Le, W., and Jankovic, J. (2011). Preclinical biomarkers of Parkinson disease. Arch. Neurol. *68*, 22–30.

Wymbs, N.F., Bassett, D.S., Mucha, P.J., Porter, M.A., and Grafton, S.T. (2012). Differential Recruitment of the Sensorimotor Putamen and Frontoparietal Cortex during Motor Chunking in Humans. Neuron *74*, 936–946.

Xiong, Q., Znamenskiy, P., and Zador, A.M. (2015). Selective corticostriatal plasticity during acquisition of an auditory discrimination task. Nature *521*, 348–351.

Yael, D., Vinner, E., and Bar-Gad, I. (2015). Pathophysiology of tic disorders. Mov. Disord. *30*, 1171–1178.

Yarkoni, T., Poldrack, R.A., Nichols, T.E., Van Essen, D.C., and Wager, T.D. (2011). Large-scale automated synthesis of human functional neuroimaging data. Nat. Methods *8*, 665–670.

Youdim, M.B.H., Edmondson, D., and Tipton, K.F. (2006). The therapeutic potential of monoamine oxidase inhibitors. Nat. Publ. Group *7*, 295–309.

Zecca, L., Youdim, M.B.H., Riederer, P., Connor, J.R., and Crichton, R.R. (2004). Iron, brain ageing and neurodegenerative disorders. Nat. Publ. Group *5*, 863–873.

Zhang, H., Schneider, T., Wheeler-Kingshott, C.A., and Alexander, D.C. (2012). NODDI: Practical in vivo neurite orientation dispersion and density imaging of the human brain. NeuroImage *61*, 1000–1016.

Zheng, T., and Wilson, C.J. (2002). Corticostriatal combinatorics: the implications of corticostriatal axonal arborizations. J. Neurophysiol. *87*, 1007–1017.

Zhuang, X., Mazzoni, P., and Kang, U.J. (2013). The role of neuroplasticity in dopaminergic therapy for Parkinson disease. Nat. Publ. Group *9*, 248–256.

Zrinzo, L., Zrinzo, L.V., Tisch, S., Limousin, P.D., Yousry, T.A., Afshar, F., and Hariz, M.I. (2008). Stereotactic localization of the human pedunculopontine nucleus: atlas-based coordinates and validation of a magnetic resonance imaging protocol for direct localization. Brain *131*, 1588–1598.

van der Zwaag, W., Jorge, J., Butticaz, D., and Gruetter, R. (2015). Physiological noise in human cerebellar fMRI. Magma N. Y. N.

Harrison, L. and Friston, K.J. (2004). Effective Connectivity. In Human Brain Function (Second Edition), R.S.J. Frackowiak, K.J. Friston, C.D. Frith, R.J. Dolan, C.J. Price, S. Zeki, J.T. Ashburner, and W.D. Penny, eds. (Burlington: Academic Press), pp. 1019–1047.